Shifting Tides: Modelling How Sea-level and Tidal Dynamics Shape Coral Connectivity on the Great Barrier Reef

Katherine Charlotte Lee

Doctor of Philosophy

University of York

Department of Environment and Geography

July 2025

Abstract

The Great Barrier Reef (GBR) is the world's largest coral reef, stretching 2000 km along Australia's northeast continental shelf, where it experiences complex and intricate tidal dynamics. Despite being one of the most studied reef systems, the role of hydrodynamics in shaping coral connectivity remains poorly understood.

This thesis examines how sea-level and tidal dynamics influence coral connectivity across the GBR, focusing on larval self-seeding. High-resolution hydrodynamic modelling and Lagrangian particle tracking are used to assess connectivity across three timeframes: present-day wind and tidal interactions; tidal regimes during the Holocene initiation; and projected tidal changes under future sea-level rise scenarios in 2100.

Results show that tides, particularly tidal ellipses, play a critical role in larval retention and self-seeding. During the Holocene initiation, rising sea levels enhanced tidal dynamics and increased self-seeding, supporting the initiation of the modern GBR. In the future, sea-level under all three Shared Socioeconomic Pathways (SSPs) is predicted to amplify tidal range, further enhancing self-seeding but also fragmenting connectivity networks.

These findings provide new insight into the physical drivers of coral connectivity, with implications for understanding reef resilience, forecasting connectivity and informing management. They also highlight the importance of incorporating sea-level change and tidal change into connectivity modelling and management frameworks.

Declaration

The work presented in this thesis is original and my own, composed solely by myself and has not been submitted, either in whole or in part, for any other award or professional qualification. Appropriate credit has been given within the thesis where reference has been made to the work of others. This research was funded by the Natural Environment Research Council (NERC) through the Adapting to the Challenges of a Changing Environment Doctoral Training Programme (ACCE DTP).

Chapter 2: I am the sole author.

Chapter 3: I am the sole author.

Chapter 4: I am the sole author.

Chapter 5: I am the sole author. The analysis and interpretation were conducted independently. However, Isaac Abbott contributed code to assist with a principal component analysis (PCA) test used as part of the analysis. All final processing, implementation, and interpretation of the PCA results were carried out by the author.

Acknowledgments

First and foremost, I want to give the biggest thank you in the world to my supervisor Jon Hill for the incredible support, patience, encouragement and time he provided me. Thank you for taking on a Masters student with no relevant background, only enthusiasm, and getting me to this point. Secondly, huge thank yous to my co-supervisors: Jon Pitchford for the time, energy and patience you put into teaching me the mathematics behind dynamical systems and providing me with so much confidence in my work; and Jody Webster, for also being there since my Masters, and having so much enthusiasm and knowledge to provide me with. Thank you also to Fiona Hibbert for assisting me with finding palaeo sea-levels curves for the time periods I needed. An enormous thank you also to Ana Vila-Concejo, who served as a mentor and enabled my incredible trip to Sydney and to One Tree Island research station, which provided me with invaluable experience, contacts and understanding of the Great Barrier Reef. Thank you to everyone in Australia who made that trip so incredible. Thank you as well to Lauren Rawlins for letting me base the formatting of my thesis on her beautiful work.

I would also like to acknowledge the Natural Environment Research Council's Adapting to the Challenges of a Changing Environment Doctoral Training Partnership (ACCE DTP) for funding this PhD.

I am very grateful to have had the opportunity to undertake a placement with the National Oceanography Centre in Liverpool. While not contributing to my thesis, the experience was invaluable with instilling confidence in myself in modelling, and developing new skills and knowledge. I'd like to thank the whole Coastal Systems Modelling group, especially Lucy Bricheno.

Thank you to the wonderful ENV group: Isla Thorpe, Ale Bouzas Monroy, Zheng Fang, Isabel Navarro Law, Nahum Ashfield, Harriet Sleight and Katie Plaisted. Thank you for the support, pub trips and laughs. Thank you also to the best of ACCE: my 2021 cohort Edd Page and Josh Thurston, thank you for both the fun and laughter, and the support. Thank you also to the EMRG group: Zoe Mackay and Jenny Cudmore, representing the numerical modellers!!

I couldn't have done this without my friends who provided the most wonderful distractions from the PhD: Ollie Martin, Molly Brown, Nikki Paterson, Mary Taylor-Lewis, Hanan Golabi, Victoria Wynters, Lydia Barder and Vivian Ng for the love, support and endless opportunities to escape off into nature. To Mags Gwynne for living with me for four years and for the countless number of times you picked me up off the floor, always without question, and cheered me up.

Of course, an enormous thank you to Jake, for your endless love, support and adventures, for guiding me through the PhD, especially this end part, and also for taking over all brain activity outside of the PhD for the last few months. Thank you also to the Anderson family, Amanda, Shaun, Chloé and Sam for their love, understanding and support.

For my family: a big thank you to my brothers, Matthew, Johnny and Benjamin, providing distractions, keeping me humble but also believing in me and keeping me going. Thank you to my grandparents for their support, enthusiasm and love. Finally, and most importantly, an absolutely enormous thank you to mum and dad for your absolute unwavering support throughout – not only this PhD – but my entire education. Your belief in me got me past every single hurdle, and boy were there a lot! I couldn't have gotten this far without you.

Contents

1 Introduction 1

1.1 Introduction to coral reefs 1

1.1.1 Climate Change and coral reefs 4

1.1.2 Conservation Attempts 6

1.2 Coral Reproduction and Connectivity 7

1.2.1 Definitions of Connectivity 8

1.2.2 Larval Dispersal Process 8

1.2.3 Swimming Behaviour 11

1.3 Physical drivers of dispersal 11

1.3.1 Ocean Currents 13

1.3.2 Wind Stress 16

1.3.3 Tidal dynamics 17

1.3.4 Larvae dispersal models 18

1.4 Introduction to the Great Barrier Reef - the study site 20

1.4.1 Management and importance of the GBR 21

1.4.2 Oceanographic Setting 25

1.4.3 Annual Mass Spawning Event 31

1.4.4 Development history 31

1.5 Sea-level change and tidal dynamics 36

1.5.1 Holocene sea-level rise and tidal changes 37

1.5.2 Projections of sea-level rise 39

1.5.3 Effects of sea-level rise on connectivity 41

1.6 Numerical modelling in Coral Reef Studies 42

1.6.1 Global ocean circulation models . . . 43
1.6.2 Coastal models . . . 44
1.6.3 High resolution GBR models . . . 48
1.6.4 Limitations and uncertainty . . . 49
1.7 Knowledge Gaps . . . 49
1.8 Thesis Research Aims, Questions and Objectives . . . 50
1.9 Thesis Structure . . . 51
1.9.1 Chapter 2 - Methodological Overview . . . 51
1.9.2 Chapters 3 - 5 - Results . . . 52
1.9.3 Chapter 6 - General Discussion . . . 53

2 Methodologies 54
2.1 Numerical Modelling . . . 55
2.1.1 Mesh generation . . . 57
2.1.2 Model Setup Data . . . 62
2.1.3 Validation . . . 63
2.2 Larvae transportation . . . 64
2.2.1 Resolution testing . . . 68
2.2.2 Particle Numbers . . . 70
2.3 Summary . . . 71

3 Winds Vs Tides - What drives coral larvae dispersal on the GBR? 73
3.1 Introduction . . . 74
3.1.1 Mass spawning event . . . 74
3.1.2 Tidal dynamics . . . 75
3.1.3 Influence of winds and tides on larvae dispersal . . . 76
3.1.4 Research Questions . . . 77
3.2 Methods . . . 78
3.2.1 Study Site . . . 78
3.2.2 Simulation set-up . . . 78

3.2.3 Larvae transportation 81
3.2.4 Analysis 81
3.3 Results 86
3.3.1 Transport 86
3.3.2 Connectivity 92
3.4 Discussion 100
3.4.1 Transport 100
3.4.2 Connectivity 103
3.4.3 Summary of key results 106
3.4.4 Limitations, Implications and Future Work 107
3.5 Conclusion 109

4 Tidal dynamics driving the Holocene Great Barrier Reef initiation 111
4.1 Introduction 112
4.1.1 Research Questions 114
4.2 Methods 115
4.2.1 Study Site 115
4.2.2 Sea-Level Reconstructions 115
4.2.3 Palaeo Reef Locations 118
4.2.4 Larvae Transport 119
4.2.5 Changing tidal dynamics 119
4.2.6 Connectivity 119
4.3 Results 120
4.3.1 Morphological evolution 121
4.3.2 Tidal dynamics 121
4.3.3 Connectivity 132
4.4 Discussion 135
4.4.1 Summary of key findings 138
4.4.2 Changes in tidal dynamics 138
4.4.3 Connectivity 145

4.4.4 Summary . . . 147
4.4.5 Implications, limitations and Future Work . . . 147
4.5 Conclusion . . . 150

5 Future Sea-level shaping coral reef connectivity 152
5.1 Introduction . . . 153
5.1.1 Climate Change . . . 153
5.1.2 Research Questions . . . 156
5.2 Methods . . . 156
5.2.1 Study Site . . . 156
5.2.2 Future Sea-Level Constructions . . . 157
5.2.3 Model Setup . . . 158
5.2.4 Larvae Transport . . . 159
5.2.5 Tidal Dynamics . . . 159
5.2.6 Connectivity . . . 159
5.3 Results . . . 160
5.3.1 Tidal Changes . . . 161
5.3.2 Connectivity . . . 170
5.4 Discussion . . . 174
5.4.1 Summary of key results . . . 174
5.4.2 Tidal dynamics . . . 174
5.4.3 Connectivity . . . 181
5.4.4 Summary . . . 182
5.4.5 Implications and Limitations . . . 183
5.5 Conclusion . . . 185

6 Discussion 187
6.1 Synthesis . . . 187
6.1.1 Summary of key research findings . . . 189
6.2 Wider Implications . . . 192

6.3 Limitations 194
6.4 Directions for future research 196
6.5 Conclusions 199

List of Figures

1.1 Locations of global reefs 3
1.2 Map of gene flow of coral reefs in the South China Sea based on predictions from genetic sequencing 9
1.3 Coral larvae: from gametes to recruits 12
1.4 Major currents of the Pacific Ocean 14
1.5 Simple schematic of a shelf sea 17
1.6 Map of the Great Barrier Reef 22
1.7 Zoning of the Great Barrier Reef Marine Park as of 2004 24
1.8 Influential currents of the Coral Sea 27
1.9 Coral reef during spawning event 32
1.10 Diagram of annual mass spawning event 33
1.11 Evolution of GBR across 30,000 years of sea level change 35
1.12 The five Shared Socioeconomic pathways 40
1.13 Example of a simple finite element mesh 44

2.1 Work flow of developing GBR tidal model and integrating with Parcels tracking software 58
2.2 Map of model bathymetry and domain 59
2.3 Unstructured mesh shown at different distances 62
2.4 Thetis model validation against observations of tidal constituents . 64
2.5 Validation of Thetis model against AusTides tidal gauges 65
2.6 Example of reef shapefiles in Cairns sector with some particle trajectories 67
2.7 Violin plots of levels of sinuosity variation across raster resolutions 69

2.8 Violin plot of self-seeding percentage for varying particle numbers released per km^2 71

3.1 Map of 11 sectors with 3 chosen sectors highlighted 79
3.2 Vorticity of entire GBR for winds vs. tides 87
3.3 Vorticity for each sector for winds vs tides 88
3.4 ERA5 wind data plotted for the area of interest across four time steps of the 48 hour annual mass spawning window 89
3.5 Tidal ellipses sample from each sector 90
3.6 Map of a sub-sample of trajectories released from Cairns reefs from each model 91
3.7 Sinuosity violin plots for winds vs tides 92
3.8 Map of self-seeding reefs within each sector 94
3.9 Reordered connectivity matrices following stochastic transformation 95
3.10 γ parameter sensitivity analysis results of tides-only model of Cairns 98
3.11 Map of network clusters generated by Constant Potts Model 99

4.1 Palaeo relative sea-level curve 118
4.2 Map of how bathymetry of the GBR has changed across nine thousand years 122
4.3 Modern day tidal dynamic diagrams 123
4.4 Graph of tidal elevation across the GBR 124
4.5 Map of differences in M2 amplitude between the present day and each palaeo-model 125
4.6 Map of difference in tidal range between the present day and each palaeo-model 126
4.7 Average velocity long term changes between the present day and each palaeo-model 128
4.8 Average bed shear stress long term differences between the present day and each palaeo model 129

4.9 Average L_2 Norm vorticity measurements across each palaeo time interval . . . 130
4.10 Sinuosity value violin plots of palaeo models . . . 131
4.11 Palaeo model density curve plot of self-seeding rates . . . 136
4.12 Maps of reef community clusters from Constant Potts Model for each model and sector . . . 137

5.1 Map of future sea level change of SSP 585 . . . 158
5.2 Map of tidal dynamics of the present day Great Barrier Reef . . . 162
5.3 Mean measurements of tidal dynamic variables . . . 163
5.4 Map of differences in M2 amplitude between present day and future sea-levels . . . 163
5.5 Maps of difference in tidal range between modern and future sea-level . . . 165
5.6 Map of difference in average velocity between present day and future sea-level . . . 166
5.7 Map of differences in average bed shear stress between present day and future sea-level . . . 168
5.8 Graph of average L_2 Norm across each sea-level scenario . . . 169
5.9 Sinuosity violin plot for each future sea-level projection . . . 170
5.10 Maps of reef community clusters from Constant Potts Model for each sea-level scenario . . . 172
5.11 PCA graph for network style changes across sea-level projections . 173

List of Tables

1.1 Full list of tidal constituents and their respective period and speed 29

2.1 Table of data used for methods 63
2.2 Tidal constituent validation using Pearson correlation analysis . . . 64

3.1 Table showing simulation setup 80
3.2 Sinuosity mean for each model 92
3.3 Table of settled particles for each sector and model 96
3.4 Diagonal mean values of particles self-seeding 96

4.1 Relative sea-level curve data between 15 - 4 thousand years ago . . 117
4.2 Diagonal mean values of particles self-seeding and percentage of self-seeding reefs 134
4.3 Number of communities calculated from the Constant Potts Model 136

5.1 Diagonal mean values of particles self-seeding for the present day (Modern) and the three future scenarios for each sector 171

Chapter 1

Introduction

This chapter aims to give an overview of the current understanding of the biophysical processes and tools behind coral reef connectivity. Particular focus is first given to coral reef ecology and the role of oceanography in coral connectivity. Research which has explored biophysical processes on the Great Barrier Reef (GBR) is then addressed in detail, leading to addressing how palaeo-climate change affected the GBR and, therefore, what is expected in the future to the best of knowledge at this point in time. Finally, biophysical numerical modelling tools are detailed, and the best choices to answer the questions posed in this thesis are considered.

1.1 Introduction to coral reefs

Tropical coral reefs are some of the most biodiverse ecosystems across the globe (see figure 1.1), directly supporting numerous species and human populations (Good and Bahr 2021). The Asia-Pacific reefs in particular are responsible for providing economical value of over $25 billion through fisheries and tourism as well as protecting shorelines from erosion and cyclones (Bartelet, Barnes, and Cumming 2024; Cesar, Burke, and Pet-Soede 2003; Reguero et al. 2018). Tropical

coral reefs are found between 31°40'S and 32°50'N (Hori 1977). Benthic composition is made up of rock, rubble, sand, macroalgae and assortments of massive, branching hard corals and soft corals, the proportions of these varies across reef locations (Wilson, Graham, and Polunin 2007). At the latitudinal limits the benthic composition changes; reefs are dominated by coral and coralline algae in tropical waters and are replaced by an assemblage of foraminifera and molluscs outside of the latitudinal limits (Maragos and Williams 2011). Coral reefs begin as coral and/or coralline algae communities on existing substrate near the surface, such as from submerged volcanoes or continental islands, and then grow depending on environmental conditions (Maragos and Williams 2011).

These resulting reef substrates can take the form of multiple different geomorphologies, the most common being fringing reefs, barrier reefs and atolls (Ladd 2012). Fringing reefs are coral reefs which grow from shorelines of volcanic or continental island, these reefs will grow upwards until they meet the sea surface and will then grow laterally until all available space is taken (Kennedy and Woodroffe 2002). Barrier reefs are linear reefs separated from the shore by a lagoon of over 10 m depth (Kennedy and Woodroffe 2002; Toomey, Ashton, and Taylor Perron 2013). Atoll reefs are found in the mid-ocean, they are ring shaped with a central lagoon and the reefs reach sea level (Woodroffe and Biribo 2011). Submerged reefs are also commonly mentioned, these are reefs established during pre-existing sea levels, they lie at lower depths than most tropical coral reefs, below 20 m depth, with living reefs on the top of the ancient reef structure (Macintyre 1972).

Most tropical corals are confined to a very narrow range of environmental conditions (Kleypas, Mcmanus, and Meñez 1999), a temperature change of 1°C above long-term monthly average can lead to mortality (Goreau and Hayes 1994), but the exact range varies by location, corals in the Persian Gulf can tolerate 35°C whilst corals in the cooler waters of South Africa faced mortality at 28°C (Riegl 2003). A decrease in temperature can also be catastrophic to corals, many reefs

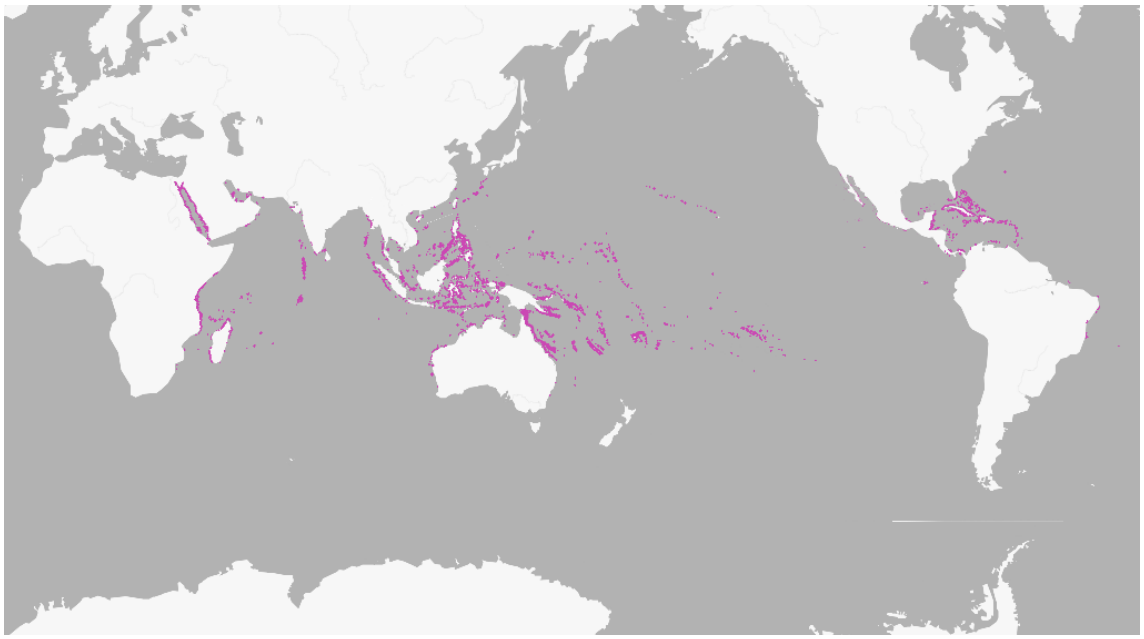


Figure 1.1: Location of coral reefs (pink points) around the globe. Dataset from UNEP-WCMC, WorldFish Centre, WRI, TNC (2021). Global distribution of coral reefs, compiled from multiple sources including the Millennium Coral Reef Mapping Project. Version 4.1. Data DOI: https://doi.org/10.34892/t2wk-5t34

have a long-term limit of tolerating 15-16°C (Kleypas, Mcmanus, and Meñez 1999), but corals in the Arabian Gulf have been found to tolerate 11.5-14°C for up to 30 days (Coles and Fadlallah 1991). Tolerance to light and salinity is also a narrow range (Kleypas, Mcmanus, and Meñez 1999). Coral reefs can occur in areas of salinity much higher than the global average, salinity tolerance is a range of 25 - 42 PSU but exposure to 20 PSU for 1 day can be fatal (Coles and Jokiel 2018). Corals require light in order to photosynthesise, the tolerance range is usually found to be between 50 -450 $\mu Em^{-2}s^{-1}$ (Chalker 1981; Chalker et al. 1988). Low levels of light caused by turbidity, such as in surf zones, limit photosynthesis and can lead to mortality (Storlazzi et al. 2011). As effects of climate change increase, coral reef environmental limits are pushed to the extremes (Hoegh-Guldberg et al. 2007; DeFilippo et al. 2022; McWhorter et al. 2022a).

1.1.1 Climate Change and coral reefs

Global marine environments are under significant threat from anthropogenic changes (Crain et al. 2009; Gissi et al. 2021; Priya et al. 2023). Coral reefs with their narrow environmental limits are one of the most fragile ecosystems on Earth (Goreau and Hayes 2021). Threats vary from meter scale localised threats such as damaging fishing practices (Saila, Kocic, and McManus 1993; Valderrama Ballesteros, Matthews, and Hoeksema 2018), overfishing (Valentine and Heck 2005; Milne, Bauch, and Anand 2022; Jackson et al. 2001) and tourism (Suryawan et al. 2025; Aldyan et al. 2023); to catastrophic global damage from climate change leading to mass bleaching (Mellin et al. 2024; Woesik et al. 2022; Wolanski et al. 2017; Goreau and Hayes 2021), acidification (Pandolfi et al. 2011; Hoegh-Guldberg et al. 2007), disease (Priya et al. 2023; Mumby, Hastings, and Edwards 2007), stronger storms (Bozec, Alvarez-Filip, and Mumby 2015; Carter et al. 2022; Dixon et al. 2022), eutrophication (Dubinsky and Stambler 1996; Devlin and Brodie 2023; Lesser 2021) and sea-level rise (SLR) (Woodroffe and Webster 2013; Storlazzi et al. 2011; Masselink, Beetham, and Kench 2020).

Temperature change is the most pressing challenge reefs are facing, with mass bleaching events becoming more common, wider spread and more fatal to tropical coral reefs. Bleaching results from thermal stress, normally an increase of > 2°C more than the monthly average (Mellin et al. 2024), breaking the symbiotic relationship between coral and zooxanthellate microalgae, leaving the coral physiologically damaged and unable to obtain nutrients (Glynn 1984). Recovery from bleaching is more likely if the period of increased temperature is short, not followed by further bleaching events and the amount of bleached corals was limited (Baker, Glynn, and Riegl 2008), however prolonged periods of bleaching tends to leads to high levels of coral mortality (Glynn 1984; Berkelmans et al. 2004). Corals that recovered fastest after bleaching events are encrusting and massive coral morphologies, such as *Porites* and *faviids*, as well as *Acropora* colonies <

5 cm, these were found to be thermally tolerant and not dependent on symbionts (Grottoli, Rodrigues, and Palardy 2006); the most successful colonies 10 years after bleaching events were found to be thermally tolerant species, surviving fragments of coral which rapidly regrew and colonies which were able to recruit externally from the damaged reef (Woesik et al. 2011). As average global temperatures increase, bleaching events from increasing marine heatwaves are expected to become more regular, limiting recovery time and degrading resilience to thermal stress (Rodrigues et al. 2025; Nunn et al. 2025).

As well as generating higher frequency and more intense marine heatwaves, climate change will also generate more consistent cyclones, causing severe destruction to coral reefs (Carter et al. 2022). Impacts of cyclones on coral reefs are from large waves and increased currents leading to hydrodynamic dislodgement and coral rubble instability (Madin et al. 2014; Harris and Vila-Concejo 2013; Vila-Concejo et al. 2013). Due to breakage of corals and over-turning of massive taxa (Woodley et al. 1981; Rogers, Suchanek, and Pecora 1982; Hubbard et al. 1991), reef community composition can be radically altered (Mumby, Hastings, and Edwards 2007; Roff et al. 2015). However, from breakage, colonies can expand through reproduction from coral fragments (Viehman et al. 2018; Highsmith 1982), although rubble instability prevents high coral recruitment (Viehman et al. 2018; Fox et al. 2019).

Rising sea levels are predicted to lead to increased wave energy and suspended sediment concentrations (Ogston and Field 2010). Increased sediment causes stress to corals by limiting photosynthesis through the blockage of light, hinders feeding and wastes energy from having to clear settled sediment (Bak 1978). Increased sea level will also contribute to more interaction with offshore water and higher levels of erosion, generating resuspension and transport of sediment on fringing reefs (Ogston and Field 2010). Hydrodynamics affected by rising sea level will also have ecological consequences by altering conditions such as temperature, velocity and depth: such as nutrient uptake (Perris et al. 2024), coral

bleaching due to flushing times (Carruthers et al. 2024) and species distribution (Sebens and Johnson 1991). RSL would generate larger waves and currents, both contributing to the ability of moving larger sediment by generating higher bed shear stress levels and leads to much lower residency time on reefs (Storlazzi et al. 2011). Increased turbidity contributes to unstable rubble substrate, leading to lower levels of settlement of coral recruits (Liu, Callaghan, and Baldock 2025), and also limits light available for photosynthesis (Piniak and Storlazzi 2008). Addressing and mitigating against these hydrodynamic stressors requires proactive intervention, and a variety of reef conservation tools are now in use globally (Good and Bahr 2021).

1.1.2 Conservation Attempts

Coral reefs require protection from human impact (Williams 2025). To limit and assist recovery from anthropocentric stressors, conservation attempts have been in practice for decades (Rinkevich 2005). Localised efforts have developed techniques of coral transplantation (Pelasula et al. 2023), coral nurseries (Ishida-Castañeda et al. 2020), artificial reefs (Higgins, Metaxas, and Scheibling 2022) and substrate stabilisation (Ceccarelli et al. 2020; Birkeland et al. 2013). Larger scale conservation efforts are the assignment of marine protected areas (Botsford et al. 2009; Marcos et al. 2021; Hays et al. 2020), however the largest scale protection needs to be reducing climate change (Goreau and Hayes 2021; Good and Bahr 2021; Mulà et al. 2025).

Coral transplantation and coral nurseries are used to reintroduce large amounts of corals to damaged communities by taking advantage of coral asexual propagation from fragmentation (Shafir, Van Rijn, and Rinkevich 2006), although this is one of the most favoured methods of restoration, there is growing evidence that there is little success (Mulà et al. 2025; Boström-Einarsson et al. 2020). These projects have struggled with a lack of clear objectives, appropriate monitoring and being poorly designed (Boström-Einarsson et al. 2020), as well as focusing

on areas close to human coastal settlements where heavy stressors, such as increased sedimentation and temperature change, are present and in areas of frequent bleaching events (Williams 2025). Overall, these projects have been seen to detract from mitigating climate change (Hughes et al. 2017; Bruno and Valdivia 2016).

The damage caused by storms and cyclones can lead to substrate rubble instability (Ceccarelli et al. 2020). To reintroduce stability in reef structures, simple rock piles placed on top of reefs has been used (Ceccarelli et al. 2020), or unstable rubble is removed and displaced corals are returned using cement (Pennisi 2005), the most popular method has been using meshes or netting over rubble to prevent further movement (Ceccarelli et al. 2020). Moreover, reduced structural complexity leads to limited recruitment of new larvae and corals reaching maturity (Madin et al. 2014; Harris and Vila-Concejo 2013; Vila-Concejo et al. 2013; Fox and Caldwell 2006).

Larger scale protection and restoration can be generated using marine protected areas (MPA), allowing extensive and diverse reef habitats and feeding groups, having a fundamental role in improving ocean health if the MPA is large enough (Hays et al. 2020). MPAs have been found to be extremely successful in increasing biodiversity and biomass (Lester et al. 2009; Ballantine 2014) as well as social benefits, such as well being, food security (Ban et al. 2019; Mascia, Claus, and Naidoo 2010). Large MPAs and networks of MPAs are also vital for protecting communities of reefs, connected through larvae dispersal (Botsford et al. 2009; Lu et al. 2023; Roberts et al. 2021).

1.2 Coral Reproduction and Connectivity

Coral reproduction is vital for population growth and regenerating damaged reefs (Woesik et al. 2011). Reefs which receive the highest rates of larvae will be the healthiest and recover faster than reefs which are not well connected or able to

retain their larvae.

1.2.1 Definitions of Connectivity

Coral reefs can be physically, demographically or genetically connected (Almany et al. 2009). Physical connectivity of corals can be defined as the exchange of individuals between populations via dispersal of larvae through networks, driven by ocean currents (Almany et al. 2009; Ani et al. 2024; Cowen and Sponaugle 2009; Limer, Bloomberg, and Holstein 2020). Genetic connectivity is the study of the movement of genes through dispersal, and can be used to show spatial distribution of genetic variation, demonstrating the effects of physical connectivity (Underwood et al. 2007; Kendrick et al. 2017). The benefit of using genetics to investigate connectivity is that field observations of larvae dispersal are difficult and therefore rare, leading to indirect and interpretative studies to establish connectivity (Largier 2003; Raitsos et al. 2017), whereas using DNA sequencing has enabled empirical approaches (Thorrold et al. 2002; Huang et al. 2018; Underwood et al. 2007). Demographic connectivity refers to the degree of interaction between geographically separated reefs and overall population dynamics (Figueiredo et al. 2021; Hock et al. 2014; Hock et al. 2017; Kendrick et al. 2017). Coral larvae connectivity is considered a function of larval behaviour, such as spawning times, settlement and competency periods; and physical connectivity (Ani et al. 2024).

1.2.2 Larval Dispersal Process

Coral reefs grow and are regenerated sexually from internal or external fertilisation of gametes, or asexually from fragments of coral (Soong and Chen 2003). Coral larvae dispersal and recruitment are vital for coral reef growth, resilience and regeneration. Corals are either brooding, where fertilization takes place internally within the coral before larvae are released at varies stages of advanced development and capable of settling immediately (Fadlallah and Pearse 1982;

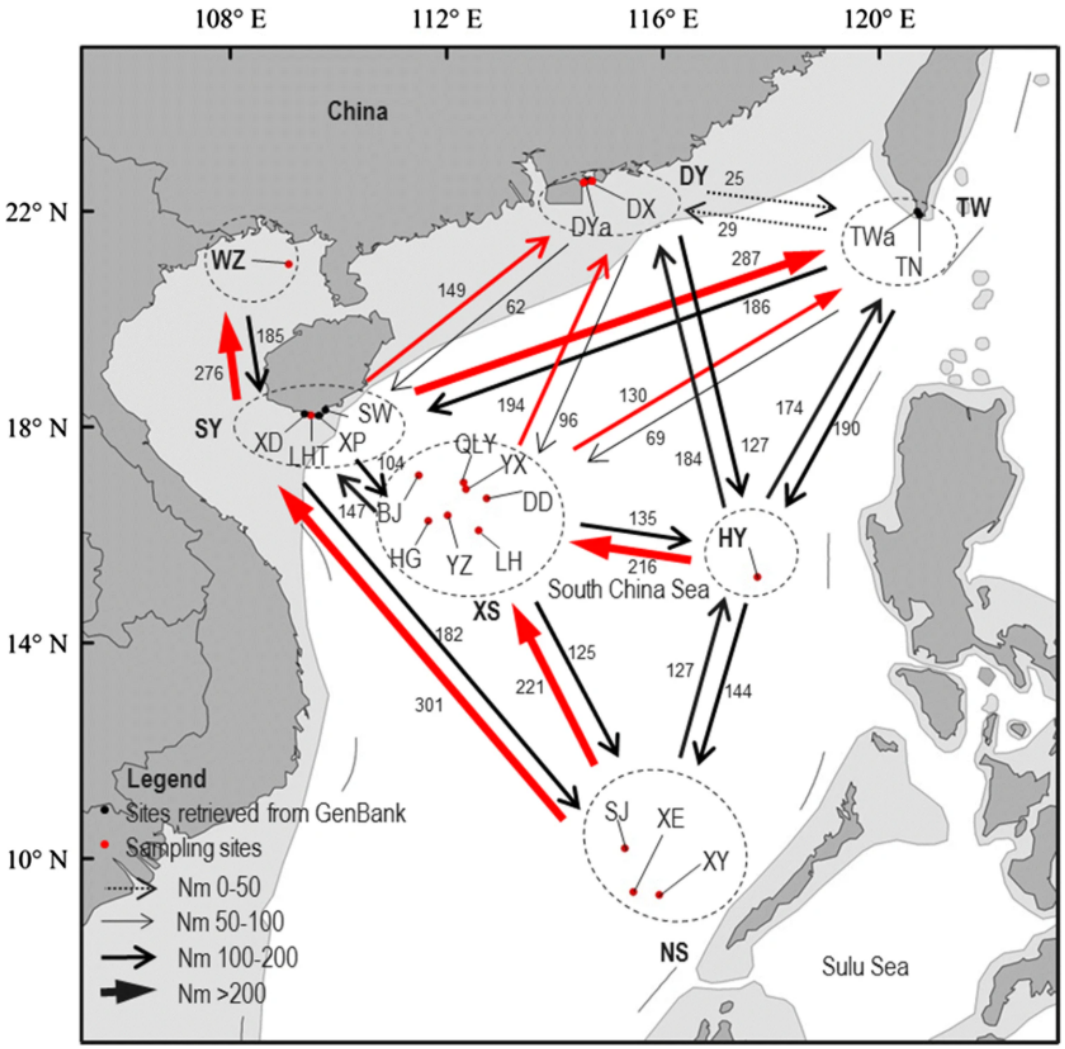


Figure 1.2: Map of gene flow of coral reefs in the South China sea based on predictions from genetic sequencing. Red arrows represent asymmetrical northward gene flow and direction and values of the effective number of migrants per generation are shown as arrows with different widths. After Huang et al. (2018).

Harrison and Wallace 1990); or broadcasting, where gametes are ejected into the water column to fertilize before sinking to settle on a reef. Broadcast external fertilization is the most common fertilization method in tropical corals (Babcock et al. 1986). There are also a large number of species which partake in a hybrid method of releasing only sperm into the water column and then internally brooding fertilised larvae (Gleason and Hofmann 2011).

As most brooding corals release their larvae directly onto the natal reef and the larvae are ready to settle quickly (see Figure 1.3), there is therefore a higher chance that the larvae will settle onto the natal reef (Sammarco and Andrews 1988; Hughes et al. 1999). Brooding coral larvae are found to be capable of swimming into the water column or crawling along the substrate until settling (Warner, Willis, and Oppen 2016). Crawling rates differ across species of corals as well as temporally: rates of crawling have been recorded to be highest in the first hour (Harii et al. 2002). Brooding coral larvae, such as *Pocillopora damicornis*, are also capable of swimming vertically and are capable of dispersing widely away from the parent reef over 103 days (Richmond 1987). Broadcast coral larvae have longer planula periods (period of time active in the water column) than brooding coral larvae, as the gametes need to fertilize and reach competency (the ability settle and metamorphose (Richmond 1997)) in the water column first before settling, a longer planula period leads to larger larvae dispersal ranges (Wilson and Harrison 1998). Broadcast larvae have a typical minimum development period of 4-6 days to reach competency and a maximum of 26 - 78 days depending on species of broadcast corals (Wilson and Harrison 1998; Harrison and Wallace 1990). Although brooded larvae is able to settle faster than broadcast larvae, species such as *P. damicornis* are able to take 103 days to settle due to their much larger energy reserves (Wilson and Harrison 1998; Richmond 1997). Swimming larvae of tropical corals is thought to provide ecological benefits from larvae travelling away from the parent reef, thereby reducing competition and chances of inbreeding as well as increasing genetic diversity amongst neighbouring reefs (Miller and

Mundy 2003).

1.2.3 Swimming Behaviour

Coral larvae are capable of controlling their vertical direction of travel in the water column, allowing them to orient towards suitable settlement areas (Babcock et al. 1986). Navigation has been found to be based on the sounds (Vermeij et al. 2010), chemical cues (Deshpande et al. 2025) and pressure changes (Stake and Sammarco 2003) of nearby reefs. Larvae are weak swimmers and cannot swim against currents (Chia, Buckland-Nicks, and Young 1984), therefore the fate of larvae is determined by ocean physical forces (Thompson et al. 2018). Generally, coral larvae with a short competency phase or produced directly onto the natal reef, such as brooding coral larvae, will settle on the natal reef, which is termed self-seeding (Crimp and Braddock 1993). Self-seeding is linked with short time frames of larval competency, whereas dispersal to neighbouring reefs or further afield is carried out by larvae capable of longer competency periods to survive being transported by ocean currents. The impact of larvae dispersal has been the subject of controversy (Stake and Sammarco 2003): reefs may be dependent upon networks of neighbouring reefs for larval recruits (Harrison et al. 1984; Babcock et al. 1986) or that reefs rely upon their own larvae being retained on the natal reef (Sammarco and Andrews 1988; Black 1993; Wolanski, Burrage, and King 1989). However, both short and local dispersal can take place simultaneously (Sammarco 1994; Sammarco and Andrews 1988).

1.3 Physical drivers of dispersal

As coral larvae are passive floaters for the majority of their competency time, currents will have the dominant effect on where long-range larvae settle (Thompson et al. 2018), whereas tides and wind will drive local dispersal between reefs (Wolanski and Spangnol 2000; Roberts 1997).

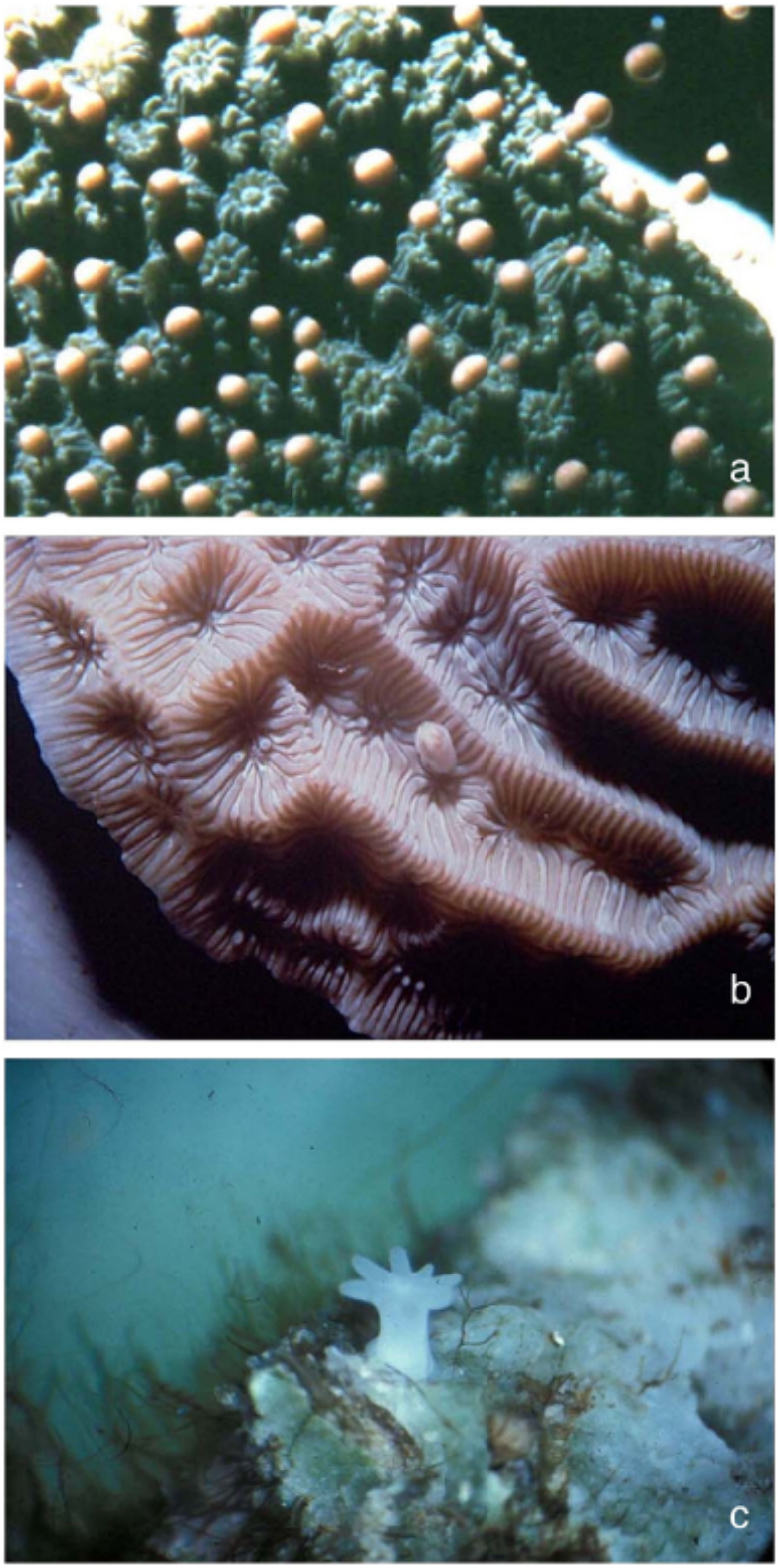


Figure 1.3: (a) broadcasting gamete bundle from *Montastraea faveolata*, containing both eggs and sperm, (b) planula larva from brooding coral *Agaricia agaricites* being expulsed, (c) *Heteroxenia fuscescens* polyp recruited onto a coral skeleton. After Gleason and Hofmann (2011)

.

1.3.1 Ocean Currents

Marine organism dispersal is directly related to the direction, timing and speed of oceanic currents, as well as competency periods of the larvae (Richmond 1990). The Pacific tropics are influenced by the North Equatorial Countercurrent (NECC), the South Equatorial Current (SEC), the North Equatorial Current (NEC) and the South Pacific Gyre (SPG) (fig. 1.4). The NECC flows eastward from May through to December before dissipating in January, when the intertropical convergence moves northwards away from the equator in May, the NECC re-establishes. The SEC is strong surface current which enables weak dispersal connections between the Central Tropical Pacific and the Eastern Tropical Pacific (Romero-Torres et al. 2018). The SEC comes in contact with the NECC, when this countercurrent comes to the surface the SEC flows eastwards but the majority of the time transport is westward. For the majority of the annual cycle, the SEC forms a barrier to south-north dispersal, however during May the eastward flow of the NECC commences, and water from the Southern Hemisphere is able to cross the barrier to the northern Pacific (Richmond 1990). The NEC is north of the NECC and flows westward however the NEC also varies across the seasons, between July and December the NEC is fed by the NECC and between March and June water enters the NEC through the California Current (Richmond 1990). The Southern Oscillation Index (SOI) is also a dominating driver of transport around the Coral Triangle and affects the SEC, it is a measure of air pressure difference across the Pacific Ocean which is used to track and predict changes to the Walker Circulation (WC), an atmospheric wind system of great importance and prominence (Power and Kociuba 2011).

El Niño heavily influences anomalies of oceanic currents, sea surface patterns and weather patterns (Enfield 1989). The SEC is heavily under the influence of the El Niño-Southern Oscillation (ENSO) (Gordon and Fine 1996; Bray et al. 1996), a powerful driver of current circulation patterns and climatic variability in the tropical Pacific Ocean. Southern hemisphere eastern Pacific waters are pushed

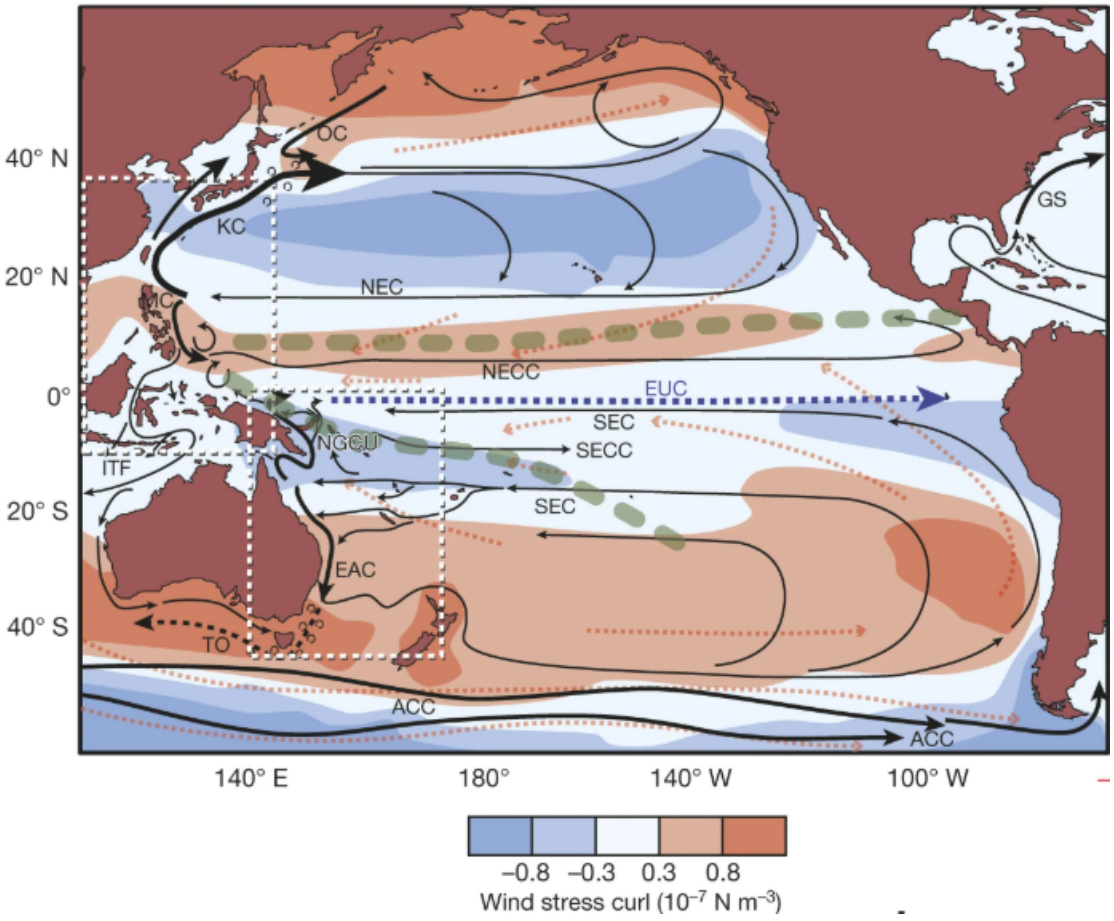


Figure 1.4: Schematic of major currents of the Pacific, as well as wind stress curl. Green-dashed lines indicate the Intertropical Convergence Zone and SOuth PAcific Convergence Zone. Abbreviations: OC, Oyashio Current; KC, Kuroshio Current; NEC, North Equatorial Current; MC, Mindanao Current; NECC, North Equatorial Counter Current; NEC, North Equatorial Current; EUC, Equatorial Undercurrent; NGCUC, New Guinea Coastal Undercurrent; ITF, Indonesian Throughflow; SECC, South Equatorial Counter Current; SEC, South Equatorial Current; EAC, East Australian Current; TO, Tasman Outflow; ACC, Antarctic Circumpolar Current; GS, Gulf Stream. After Hu et al. (2015).

across the equator by south easterly winds into the Northern Indo-West Pacific, the extent of current deviation from normal conditions depends upon the force and duration of these winds (Richmond 1990). Shifts in currents caused by sea level changes and the following Kelvin Wave indicating the beginning of an El Niño period cause eastward displacement of water and therefore planktonic organisms to the eastern Pacific (Richmond 1990). Dispersal of marine larvae is also influenced by annual shifts in ENSO due to the effect of temperature change on currents (Cheal et al. 2007). For example, when the SOI is increased during La Niña years, the Leeuwin Current (an ENSO influenced current) is stronger and sea surface temperatures are higher, leading to higher densities of planktonic dispersal (Wilson et al. 2018).

During normal current conditions, not during El Niño periods, dispersal from the east Pacific to west Pacific is blocked by the Eastern Pacific Barrier (Briggs 1961), but in rare dispersal events, the barrier can be breached, with the Eastern Tropical Pacific as the source and the Central Tropical Pacific as the sink (Romero-Torres et al. 2018). During normal conditions, the only route from Central Pacific to the eastern Pacific is via the NECC, however traversing this current from the Line Islands, in the centre of the Pacific slightly north of the Equator, to the Galapagos takes 155 days with mean current velocity of 0.39 ms^{-1} (Richmond 1990). Only larvae with competency times over 155 days could make this journey. To cross the north south divide, such as between Hawaii and Polynesia, larvae would need to travel from the central Pacific all the way to the east or west to enter the north Pacific, a longer journey than long competency coral larvae could endure (Newman 2017).

During El Niño periods, a direct south to north pathway across the equator exists, allowing planula larvae to be swept into the NEC (Hasson et al. 2018). Many coral larvae dispersal anomalies like this can be explained by ENSO variation, corals of the genus Acropora have a limited distribution in the central Pacific due to larvae only having a competency period of < 25 days (Richmond 1997). However

several colonies of Acropora have been found in an area of Columbia, as they are of similar size and age they most likely were dispersed there through an El Niño oceanic anomaly (Von Prahl and Mejía 1985).

1.3.2 Wind Stress

Winds disperse larvae away from natal reefs (Willis and Oliver 1988). For example prior to the Monsoon season, high concentrations of larvae are found around coastal areas of the Indian Ocean, during and after the Monsoon larvae concentrations are depleted due to winds dispersing larvae (Gaonkar et al. 2012). As well as driving oceanic surface currents, wind also drives more local dynamics: reefs depend on the wind for developing interconnections between reefs for larvae and nutrient transportation (Wolanski and Spangnol 2000; Roberts 1997). The best studied coral larvae regional dispersal via wind is on the GBR. In windy conditions (> 10 knots and < 20 knots), Langmuir circulations can be formed around the GBR reefs. These are shallow counter-rotating vortices on the surface which are aligned with the wind (Kingsford, Wolanski, and Choat 1991). These Langmuir cells can gather larvae into slicks and influence the direction and distance of their dispersal (Kingsford, Wolanski, and Choat 1991; Willis and Oliver 1990). These slicks can be 5 km in length and 10 m in width, and last until the larvae lose their positive/neutral buoyancy, typically after 48 hours from release (Oliver and Willis 1987). However, slicks created during the annual mass spawning event can be broken up and dispersed by waves if wind speeds reach above 20 knots (Oliver and Willis 1987). Whilst high winds have been observed to typically break up slicks and disperse larvae widely around the area, low wind conditions allow larvae to remain within the reef lagoon (Willis and Oliver 1988). Studies on Bowden Reef in the Central GBR have determined that wind is the dominant factor for coral larvae dispersal (Wolanski, Burrage, and King 1989).

Due to the disruptive nature of wind on larvae dispersal, it is thought that corals time their spawning to match weak wind conditions to keep the larvae around

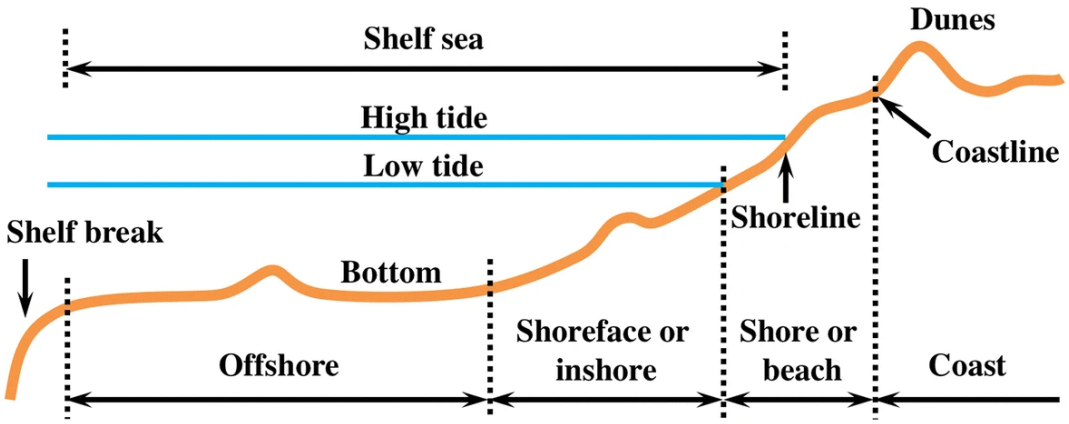


Figure 1.5: Simple schematic of a shelf sea. After Swart and Yuan (2019)

the adult colonies (Gleason and Hofmann 2011; Woesik 2010). Globally, corals tend to spawn during periods of calm wind, leading to retention of coral larvae around reef systems which has been shown by areas with long periods of calm wind, such as Kenya, corals spawn for months at a time. Whereas locations, such as the Great Barrier Reef, with very short periods of calm wind host reefs which have a tightly coupled spawning period (Woesik 2010).

1.3.3 Tidal dynamics

Most coral areas are situated on the shallow waters of shelf seas, high energy bodies of shallow water between 0-200 m deep, which extend from the shoreline to the edge of a continental shelf (Swart and Yuan 2019; Hoeksema, Giyanto, and Suharsono 2019; Simpson and Sharples 2012) (fig. 1.5). The edge of the continental shelf tends to steeply drop down to the abyssal ocean, this abrupt change in depth generates complex tidal dynamics (Simpson and Sharples 2012). Shelf seas with strong tidal currents capable of moving and transporting sediments are classified as tidally-dominated (Molen, Gerrits, and Swart 2004). These areas experience complicated and variable dynamics: biological, sedimentation and thermal balance are all heavily impacted by the vertical mixing rates of these shelf environments (Prandle 1997).

High energy shelf seas lead to various drivers of larvae retention and dispersal

(Robins et al. 2013). The production of eddies from interactions between hydrology and bathymetry can lead to concentrations of larvae (Mace and Morgan 2006). Fine scale tide driven flows dominate coral atoll hydrodynamics: tidal oscillations increase larvae retention (Grimaldi et al. 2024), even finer scale hydrodynamic processes such as wave-driven flows, channels and lagoons all affect dispersal patterns of reef systems (Tartinville, Deleersnijder, and Rancher 1997; Rogers, Suchanek, and Pecora 1982). Lagoons separated from open sea by narrow channels can cause phase lags between water levels of within and outside of the lagoon, leading to slow flushing rates of the lagoon, therefore retaining larvae within it (Dumas et al. 2012). Waves play a key role in transporting larvae in and out of lagoons and atolls, washing larvae over coral walls (Grimaldi et al. 2024).

1.3.4 Larvae dispersal models

As already stated, studying larvae dispersal and reef connectivity is difficult due to large scales, visibility, oceanic conditions etc. Examining genetic data assisted with this problem and enables a jigsaw puzzle of connected reefs to be put together, however it is not able to help with understanding the mechanisms behind dispersal, retention and connection. To best capture the interaction of biology and physics during larvae dispersal, biophysical numerical models are required (e.g. Cowen, Paris, and Srinivasan 2006; Figueiredo et al. 2021; Assis et al. 2025; Page et al. 2019; Raitsos et al. 2017) etc. Biophysical models can be used across a range of scales, from investigating connectivity of global oceans (Assis et al. 2025; Feng et al. 2016; Wood et al. 2014), to fine scale intra-reef connectivity (Rogers et al. 2017; Grimaldi et al. 2024).

Biophysical models are developed in two stages: the first stage is to develop a model of oceanic and wind forcings in the area of interest. For large scale oceanic models the resolution will be coarse, likely on the kilometre scale and built on structured meshes (a mesh made up on equal sized squares) (Danilov 2013). Sin-

gular reef scale models will have a resolution of 10's of meters, and generally developed using an unstructured mesh (a mesh made up of differing sized elements, smaller elements capture areas of higher interest, large elements capture deep off-shore features with less detail) (Rappaz, Bellet, and Deville 2010). More information on numerical models is detailed below in section 1.6. Once a model of the physical processes exists, it is coupled with a Lagrangian particle tracking model, such as Parcels (Delandmeter and Sebille 2019), where high numbers of tracer particles can be released from sites of interest and are tracked through hydrodynamic fields for an extended amount of time using a volumetric flow measurement technique (Schröder and Schanz 2023; Lange and Sebille 2017). These models are successful in capturing how ocean currents, tidal features and wind transport coral larvae as long as the appropriate resolution is used for the study (Saint-Amand et al. 2023; Carruthers et al. 2024).

The traced particles in these models can represent larvae, as well as plastic pollution (Garrard et al. 2024; Mansui, Molcard, and Ourmières 2015), water parcels (Yang et al. 2023) and sediment (Allison et al. 2017), as the particle trajectories can be analysed for flow and velocity fields to investigate dispersal characteristics and transit times (Defne and Ganju 2015), as well as connectivity between areas. Some Lagrangian codes are capable of incorporating 'behaviour' of particles to enable some active dispersal such as swimming or sinking (Lange and Sebille 2017). Using these models has helped to understand the role oceanic currents have on connectivity between far separated regions (Romero-Torres et al. 2018), as well as weather systems such as El Niño periods have on connectivity anomalies (Hasson et al. 2018), to how reef flushing times effect the dispersal of larvae (Dumas et al. 2012) and how waves are a route in and out of enclosed reef atolls (Tartinville, Deleersnijder, and Rancher 1997).

Biophysical models are limited to how well they can replicate reality, such as uncertainty of oceanographic and ecological processes; the biggest challenge is resolution of models due to balancing computational time and power (Choukroun

et al. 2024). Larvae dispersal is often driven by fine scale hydrodynamic features such as tidal eddies around reefs, as well as transported by oceanic currents. Large scale oceanic models are often have high vertical resolution, necessary for modelling varying depth of larvae (Assis et al. 2025), whereas fine scale models with high horizontal resolution tend to have poor vertical resolution, most often being depth-averaged which loses all detail of vertical migrations and transport of larvae (Saint-Amand et al. 2023; Lambrechts et al. 2008). However, these models tend to be used in shallow areas where the water is well mixed in the vertical, so vertical processes are less important (Steinberg 2007; Greenwood et al. 2025). To capture small scale eddies across reefs, a resolution of under 100 m would be necessary (Wolanski et al. 2024a), however the computational power and time necessary for such a fine scale restricts modellers to modelling a single reef (Rogers et al. 2017; Grimaldi et al. 2024). Compromises have to be made.

1.4 Introduction to the Great Barrier Reef - the study site

The Great Barrier Reef (GBR) is the world's largest coral reef ecosystem (fig. 1.6), it stretches along the 2,000 km continental shelf edge of east Australia within the Coral Sea and has over 2,500 individual coral reefs made up of five different varieties of coral island: fringing, atoll, barrier and platform reefs (Fairbridge 1950; Hopley 2006; Hughes et al. 1999). The GBR hosts over 120 species of scleractinian corals, all of which have evolved to depend on water circulation to maintain gene flow, nutrients, and temperature (Andutta, Kingsford, and Wolanski 2012; Raitsos et al. 2017; Babcock et al. 1986).

Like all tropical coral reefs, the GBR is experiencing the effects of climate change. The first mass bleaching was recorded in the early 1980s and these events have become increasingly common as time has passed: a coral cover loss of 50% was

recorded on the GBR between 1985 and 2012 De'ath et al. 2012. During the 2016 bleaching event, Australia's north eastern waters reached 30 °C, with some reef areas reaching 32 °C for over two months (Hughes et al. 2017). Although this bleaching event was experienced on coral reefs across the world, research on the GBR during this time was able to show oceanography of surrounding seas to be responsible for amplifying the thermal effect (Wolanski et al. 2017). Up to that point, the northern GBR had been assumed to be unlikely to be affected by heat stress because of it being in a pristine state (Brodie and Pearson 2016). During the 2015/16 El Niño event, the North Queensland Coastal Current, responsible for flushing and cooling the Northern Coral Sea, shutdown; alongside this, warm water from the Gulf of Carpentaria moved southwards through the Torres Strait over the northern GBR (Wolanski et al. 2017). Since 2016, mass bleaching events on the GBR were recorded for 2017 and 2020 and 2022, with 2022 being the first bleaching event to happen during a La Niña year (Richards et al. 2024). The cumulative impact of recent bleachings may have reduced larval supply by 71%, reducing the reefs ability to regenerate itself after bleaching events. (Cheung et al. 2021). As corals recover and regenerate through reproduction, this poses a significant problem (Hock et al. 2019).

1.4.1 Management and importance of the GBR

The GBR sits inside the world's largest marine park (GBRMP), covering an area of approximately 345,000 km^2, it was established in 1975 and is managed by the GBR Marine Park Authority. Management strategies were developed to protect the reef from human impacts, including permits, education, management plans and zoning (Day 2002). Zoning is a spatial planning tool used to define areas of the reef which have a range of protective strategies, rights and responsibilities bespoke to that particular area of reef (Day et al. 2019), the GBR is considered the world's best working example of marine zoning (Ruckelshaus et al. 2008). Zones range from general use zones, allowing fishing, cruise ships, collecting with a per-

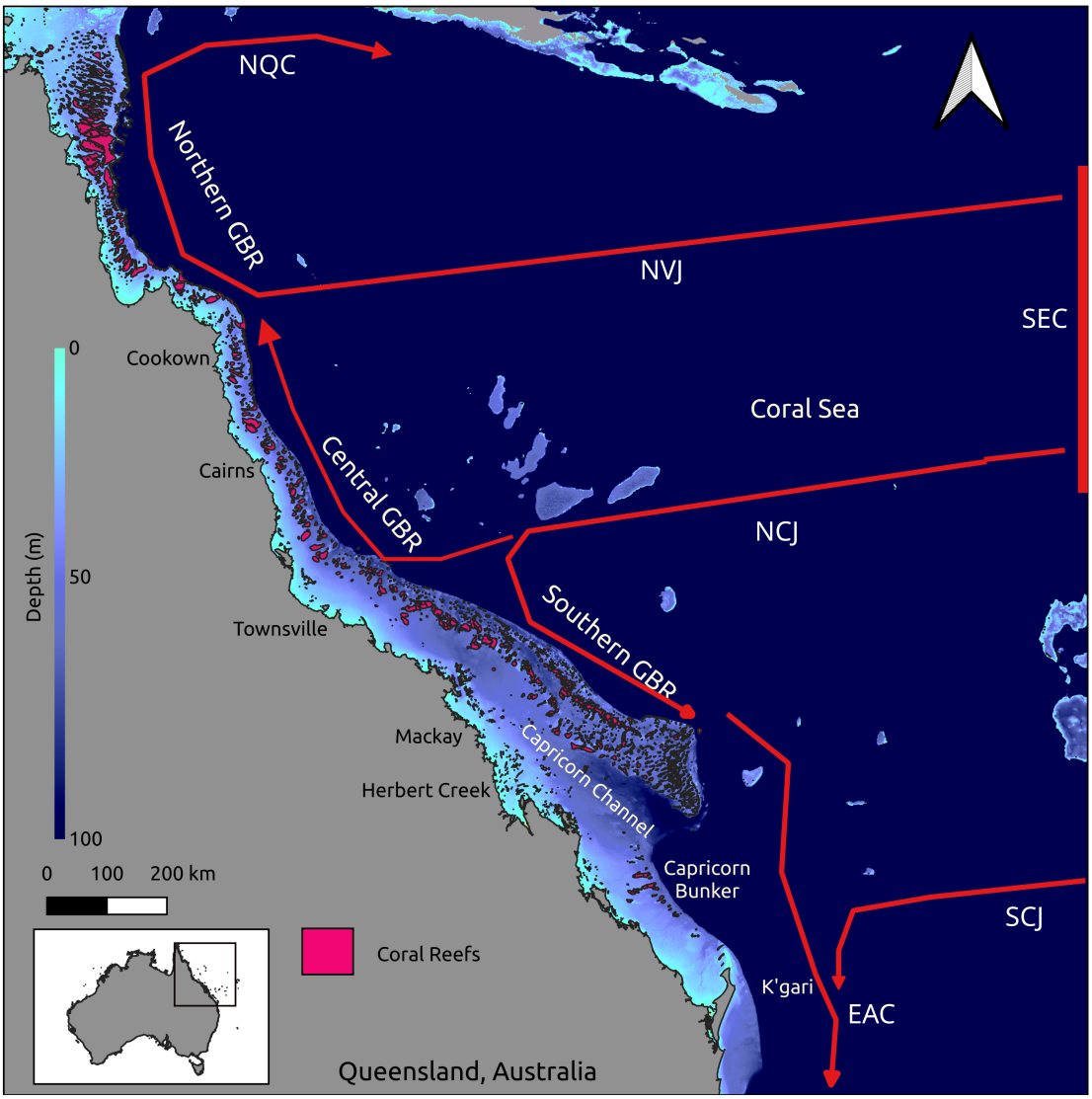


Figure 1.6: Map of the Great Barrier Reef showing locations of reefs, currents and bathymetry of the shelf and Coral Sea. The major currents of the GBR are presented, those which reach the GBR come from divisions of the South Equatorial Current (SEC). One of these is the north Vanuatu jet (NVJ), which eventually becomes the North Queensland Current (NQC). The NQC is also fed by the north Caledonian jet (NCJ), this current splits north and south, the southern section eventually feeds into the East Australian Current (EAC). The EAC is also fed by the southern Caledonian jet (SCJ).

mit and even trawling; conservation park zones which allow access but only the least destructive forms of fishing; to preservation zones, disallowing any human access (Day 2002) (fig. 1.7). Re-zoning took place in 2004 to take significant action on fishing and trawling, although effective action did not take place until 2008, as part of the Australian Government Reef Rescue initiative (Brodie and Waterhouse 2012). Although overall coral cover has declined across the GBR (Brodie and Waterhouse 2012), no-take zones within the GBR have been successful in protecting coral cover, cover has remained consistent in newly allocated no-take zones, and increased in well established no-take zones (Fraser et al. 2019). Proactive management of the GBRMP have been found to reduce the chronic stressors of climate change impacts on hard corals in no-take zones, and should lead to higher resistance and recovery, simply by reducing local stressors introduced by fishing, leading to increased biodiversity, less disease and more grazing fish to control algae populations (Ceccarelli et al. 2020).

For marine zones to fully benefit reproduction of marine species which use dispersal, such as corals and fish, the zones need to be twice the size of the maximum larvae dispersal distance, and separate marine zones should be within the dispersal range distance to allow connectivity and migration between zones (Green et al. 2015). Genetic studies of coral and fish connectivity within protected areas of the GBR showed that as these zones become more established, they form highly connected networks and are responsible for replenishing larvae to fished zones both near (200 m - 50 km) and far ($\sim$ 250 km) from the protected zones (Williamson et al. 2016).

Protection of the GBR is not only necessary for ecological protection, but also for local and global cultural and economic importance, which can lead to better protection of the GBR, as well as global reef systems (Marshall et al. 2016). It was global public affinity with the reef which led to the creation of the GBRMP, followed by the GBR being listed as a World Heritage Area in 1981 in recognition of its “outstanding universal values” (Marshall et al. 2018). The GBR holds immense

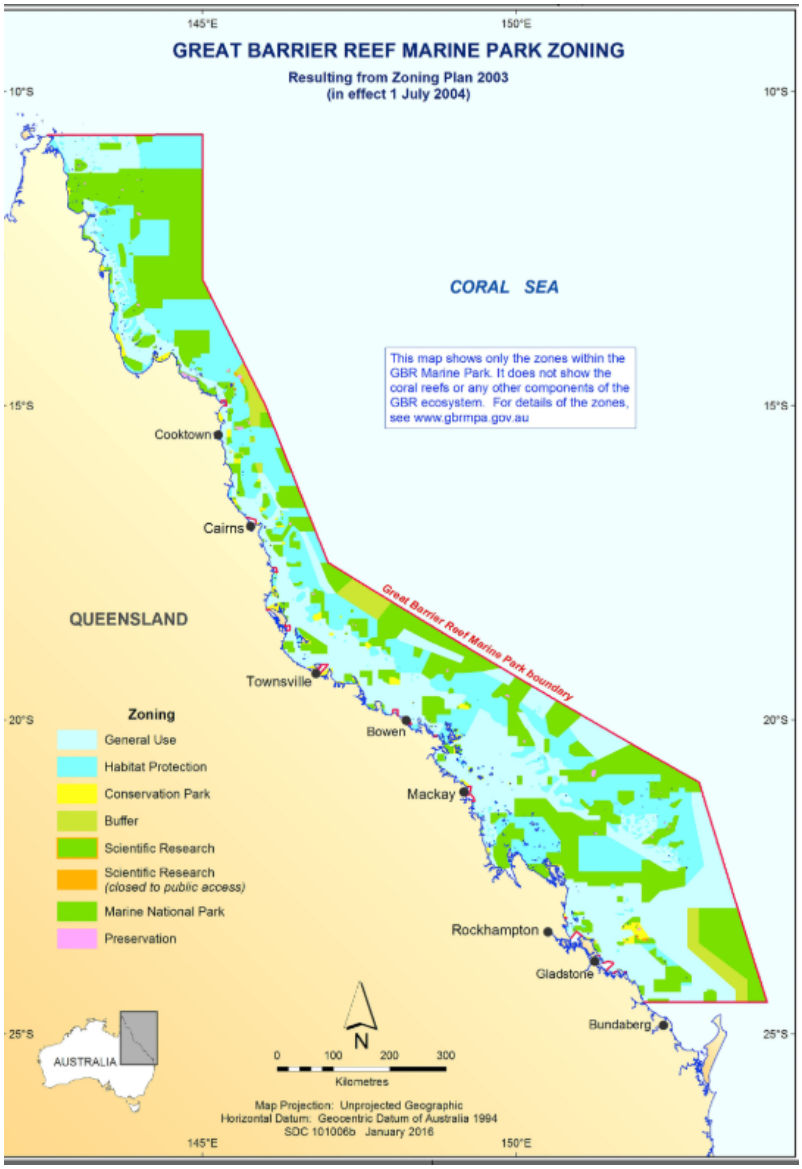


Figure 1.7: Zoning of the Great Barrier Reef Marine Park as of 2004. After Day et al. (2019).

cultural importance to First Nations people who have held deep spiritual connections with the GBR for thousands of years (Reef 2050 Traditional Owner Steering Group. 2022) In a study on local residents near the GBR, it was found that coral cover, healthy reef fish and iconic marine species are considered more important to quality of life than their jobs and incomes (Larson et al. 2015). Another study found that people from a range of industries, such as fishing and tourism on the GBR are heavily dependent financially on the GBR, as well as culturally dependent due to their age, years spent in the region and industry and their lack of education (Marshall et al. 2017). A study carried out by Stoeckl et al. (2014) estimated the GBR to be worth between $15 and 20 billion AUS per annum, however later studies found that placing an economical value on the GBR is incredibly difficult because of the range of values and global reach (Rolfe and De Valck 2021; De Valck and Rolfe 2022).

1.4.2 Oceanographic Setting

The GBR extends from the subtropics (24°S) to the deep tropics (10°S), along the edge of the Coral Sea (see figure 1.6) (Richards et al. 2024). The southern GBR is made up of the Capricorn Bunker and Swain Reef, a large dense areas of reef system on a wide section (over 200 km) of the continental shelf. Swain and the Capricorn Bunker sit at the mouth of the Capricorn Channel (CC), which runs between the coastline and the GBR southern and central GBR. Ribbon reefs sit along the southern section of the CC, forming a barrier between the channel and the Coral Sea (Wolanski et al. 1988). The Central GBR sits on the narrowest section of the continental shelf. Further up the coastline, the shelf begins to widen again before the GBR finishes at the Torres Strait. In the northern GBR, ribbon reefs and true barrier reefs are found (Wolanski et al. 1988).

The GBR is influenced by the SEC and the East Australian Current (EAC) (see fig. 1.8). The EAC is fed by the SEC and flows polewards along the outer edge of the continental shelf in the southern Coral Sea (Ridgway and Dunn 2003), the

EAC is the western boundary current of the South Pacific subtropical gyre and therefore plays a key role in the southwestern Pacific Ocean's circulation (Boland and Church 1981). The majority of the EAC remains outside of the GBR, separated by the continental shelf, however a lagoonal current flows from the EAC onto the narrow central GBR ($\sim$ 18-19°S) and exits from the CC (Benthuysen et al. 2022). The EAC is thought to be responsible for generating the Capricorn Eddy, a mescoscale eddy in the southern GBR, the EAC generates frictional effects on the shallow sea floor as it flows along the continental shelf, a lee is created by Swains Reefs topography, the lee exerts a cyclonic torque on turbulent momentum and the offshore current (Weeks et al. 2010). The Capricorn Eddy is a transient feature, it tends to only appear between late September and late October, due to sea surface temperatures being affected by monsoonal weather patterns, summer solar heating and seasonal fluctuations of the strength of the EAC (Mao and Luick 2014).

1.4.2.1 Tides

Transport of tidal water through the GBR is controlled by the Coral Sea, circulation across the continental shelf is dominated by tidal constituents: M2, S2, N2, O1 and K1, which affect both the lagoon and reef areas (Andrews and Bode 1988; Lambrechts et al. 2008; Wolanski 1983). Tidal constituents are unique harmonic frequencies which contribute to the tide-generating force, predominantly from the moon or the sun, however harmonic frequencies are also detected from planetary gravitational pulls (Thomson and Emery 2014) (see table 1.1 for full list). Each constituent has a specific amount of time which is required to separate its from other constituents, named the Rayleigh Criterion. M2 is the semidiurnal principle lunar constituent with a period of 12.421 hours, S2 is the semidiurnal principle solar constituent (12 hour frequency) and N2 is the semidiurnal lunar elliptical; O1 is diurnal principle lunar constituent and K1 is diurnal lunar-solar declinational, each constituent has its specific tidal period while amplitude and

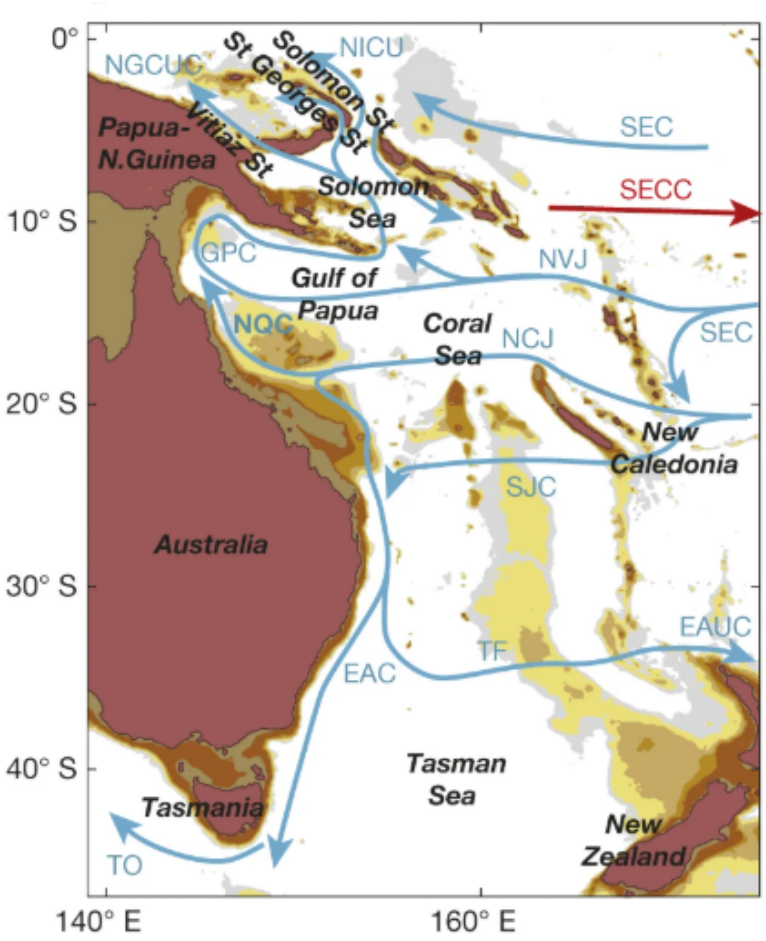


Figure 1.8: Schematic of currents of the west Pacific, focusing on influential currents of the east coast of Australia. Colours refer to bottom depth, dark = shallower, lighter = deeper. Abbreviations are as follows: NGCC, New Guinea Coastal Current; NEUC, NICU, New Ireland Coastal Current; NVJ, North Vanuatu Jet; NCJ, North Caledonia Jet; SCJ, South Caledonia Jet; NQC, North Queensland Current; GPC, Gulf of Papua Current; TF, Tasman Front; EAUC, East Auckland Current; TO, Tasman Outflow. After Hu et al. (2015).

phase vary by location. The lagoon and reef areas on the continental shelf are an average depth of 20 m while the shelf edge has a depth of ∼100 m before dropping to 1500 m in the Coral Sea (Wolanski 1983). The complex bathymetry created by the dense matrix of reefs cause cross-shore gradients in radiation stress by sitting higher than the seabed and tend to reach the surface, occasionally being exposed, leading to complex and ever changing paths for tides to flow through (Andutta, Kingsford, and Wolanski 2012). The hydrodynamics of the GBR is incredibly sensitive to spatial heterogeneity created by bathymetry and reef matrices (King and Wolanski 1996; Taebi et al. 2011). The GBR experiences mixed semidiurnal tides as well as semidiurnal tides, being semidiurnal south of Cairns, to being mixed semidiurnal north of Cairns. The northern GBR is made up of dense and closely packed together reefs which form a barrier between the GBR lagoon and the Coral Sea. However, even this area is permeable to the semidiurnal tides (Wolanski 1983). Tidal range on the GBR differs with location. Around Herbert Creek estuary, the tidal range can be up to 8 meters, whereas in Northern Queensland is 2 meters and in South Queensland, around 4 meters (Andrews and Bode 1988).

Due to the shallow nature of the continental shelf reefs, tidal flow is diverted by the abrupt change in bathymetry and tidal eddies occur in the recirculating flow of the lee of reefs and islands (Burgess, Kingsford, and Black 2007). These eddies occur typically 10's of meters in size and exist for only a few hours during reversing tidal flows, named phase eddies. As the tide begins to move in the opposite direction, the eddy dissipates and generally an eddy will then form at the other end of the reef (Black and Gay 1987). These eddies are able to transport material around the reef with each tidal cycle, and therefore have a significant role in retaining larvae (Williams, Wolanski, and Andrews 1984; Black 1993). Wolanski (1994) coined the term "Sticky Water" to refer to the phenomenon of these phase eddies reducing flushing times of tidal flow due to high numbers of eddies forming less permeable waters around dense areas of reefs. This phenomenon steers currents

Name	Symbol	Period (h)	Speed (° /h)
Higher Harmonics			
Shallow water overtides principle lunar	M4	6.2103	57.96
Shallow water overtides of principle lunar	M6	4.1402	86.95
Shallow water terdiurnal	MK3	8.1771	44.03
Shallow water overtides of principle solar	S4	6	60
Shallow water quarter diurnal	MN4	6.2691	57.42
Shallow water overtides of principle solar	S6	4	90
Lunar terdiurnal	M3	8.2804	43.48
Shallow water terdiurnal	2"MK3	8.38639	42.927
Shallow water eighth diurnal	M8	3.1051	115.936
Shallow water quarter dirurnal	MS4	6.1033	58.98
Semi-diurnal			
Principle lunar semidiurnal	M2	12.42	28.98
Principle solar semidiurnal	S2	12	30
Larger lunar elliptic semidiurnal	N2	12.6583	28.4397
Larger lunar evectional	υ 2	12.626	28.51
Variational	MU2	12.8718	27.968
Larger lunar elliptic semidiurnal second-order	2"N2	12.9053	27.895
Smaller lunar evectional	λ2	12.2218	29.456
Larger solar elliptic	T2	12.0164	29.959
Smaller solar elliptic	R2	11.9835	30.041
Shallow water semidiurnal	2SM2	11.607	31.016
Smaller solar elliptic semidiurnal	L2	12.1917	29.528
Lunisolar semidiurnal	K2	11.9672	30.082
Diurnal			
Lunar diurnal	K1	23.9344	15.0410
Lunar diurnal	O1	25.8193	13.9430
Lunar diurnal	OO1	22.3061	16.1391
Solar diurnal	S1	24	15
Smaller lunar elliptic diurnal	M1	24.8412	14.492
Smaller lunar elliptic diurnal	J1	23.0985	15.5854
Larger lunar evectional diurnal	ρ	26.7230	13.4715
Larger lunar elliptic diurnal	Q1	26.8684	13.3987
Larger elliptic diurnal	2Q1	28.0062	12.854
Solar diurnal	P1	24.0659	14.959
Long period			
Lunar monthly	Mm	661.311	0.544
Solar semiannual	Ssa	4383.076	0.082
Solar annual	Sa	8766.153	0.0411
Lunisolar synodic fortnightly	Msf	354.367	1.016
Lunisolar fortnightly	Mf	327.8599	1.098

Table 1.1: Full list of tidal constituents and their respective period and speed. After M. Lopes and Tenreiro Machado (2017).

away from the region during spring tides and also forms a barrier for connectivity between high-density and low-density areas of reefs as the high-density areas retain larvae (Wolanski and Spangnol 2000).

1.4.2.2 Wind

Wind travelling across the GBR is generally either southwest-ward or northwest-ward (Wolanski and Pickard 1985), with dominant strong winds from the South East (Larcombe et al. 1995). Low-frequency longshore currents are wind driven (Schlaefer et al. 2018; Wolanski and Pickard 1985), wind stress over the GBR causes long-term residual currents due to the GBR lagoon being so shallow (less than 50 m) (King and Wolanski 1992). Both wind and tides generate vertical mixing within the water column and the wind drives flushing of the GBR into the Coral Sea by generating wind-driven currents (Andutta, Ridd, and Wolanski 2013). Wind is responsible for wave creation which also drive sea surface currents; the high and consistent South-Easterly trade winds over the midshelf generate long wavelength swell within the GBR lagoon. These long wavelength swells contribute to high sea surface currents due to producing high oscillatory velocities on the seabed and carry nutrients to reefs (Larcombe et al. 1995).

Wind generated currents transport material around the GBR, strong winds of 15-20 knots will lead to low concentrations of larvae following release due to higher levels of vertical mixing and larger spatial dispersal (Willis and Oliver 1988). Even light winds of 5 - 15 knots will disrupt slicks of larvae and retention around reefs (Oliver and Willis 1987). Winds are weakest near the November and December full moon, which coincides with the annual mass spawning event, it is thought that the GBR corals have evolved to synchronise with this time to avoid larvae being washed out to the Coral Sea by wind (Woesik 2010). In contrast, other species capitalise on the winds, such as Snapper fish, to enable larvae to be dispersed far via surface currents (Schlaefer et al. 2018).

1.4.3 Annual Mass Spawning Event

The GBR undergoes an annual mass spawning event which 105 species of coral partake in (Willis et al. 1985; Babcock et al. 1986) (fig. 1.9). The annual mass spawning event happens at around midnight following the November full moon, a neap tide, generating the lowest levels of water volume and movement of the year, giving an advantage to fertilization and settlement of new recruits (Babcock et al. 1986; Keith et al. 2016; Willis et al. 1985). The larvae are observed to float up to the surface and remain there forming vast slicks kilometres long in length, and around 10 m in width, for 48 hours before sinking down to the substrate to settle (Oliver and Willis 1987) (fig. 1.10). Babcock et al. (1986) observed these larvae do not become mobile until 36 hours after joining the water column, which is a slightly shorter time for larvae settlement than seen elsewhere in the world. Larvae in the water column have their transportation controlled by tidal dynamics (Wolanski, Burrage, and King 1989). The tidal phenomenon on the GBR mentioned previously, which Wolanski (1994) coined "the sticky water effect", collect coral larvae during the spawning event and retain them above the parent reef, preventing them from being washed away and lost (Andutta, Kingsford, and Wolanski 2012). Mass-spawning events have been found to be connected to lunar phases and restricted to specific seasons, observed to be connected to ideal tidal systems and temperature for highest success rate of larvae settlement (Babcock et al. 1986; Willis et al. 1985). Corals reach competency in a very short space of time on the GBR, $\sim$ 48 hours (Miller and Mundy 2003), possibly to match the short window of calm wind driven currents (Van Dongeren et al. 2013).

1.4.4 Development history

The present day GBR is known as the Holocene reef; it is the fifth iteration of the GBR over the last 30,000 years and is thought it have began growth around 8000 years ago following 2000 years of dormancy after the death of previous the reef

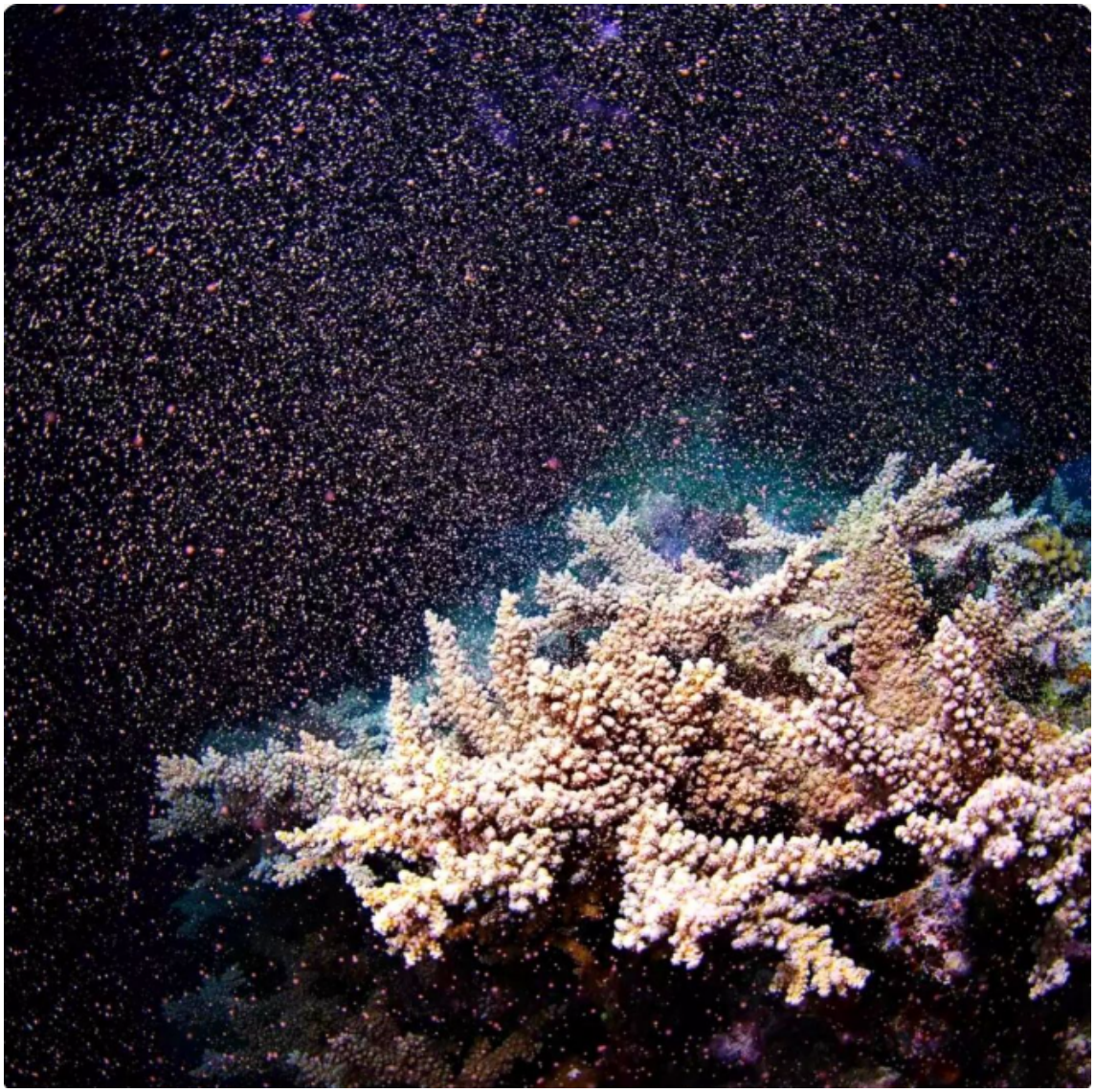


Figure 1.9: Coral reef following the release of larvae during the annual mass spawning of the Great Barrier Reef. Photo courtesy of Flora and Fauna (2022, January 21) https://www.floraandfauna.com.au/blogs/ecohub/successful-coral-spawning-event-brings-new-hope-for-the-great-barrier-reef



Figure 1.10: Diagram of annual mass spawning event, gametes are released and fertilised into the water column with the first larvae settling after 48 hours.

structure (reef 4), caused by increased sediment flux onto the reef (Webster et al. 2018). The continental shelf which hosts the GBR was once completely terrestrial, as sea levels rose ∼ 452 ka following a glacial period, corals were able to establish themselves in the new shallow waters (Hopley, Smithers, and Parnell 2007). The shelf is now made up of corals building on top of submerged and drowned reefs; the antecedent topography (Hopley, Graham, et al. 1997).

The first records of the GBR date back to ∼ 452 ka (Braithwaite et al. 2004), during the Pleistocene period, however some areas of the GBR are younger than others, for example One Tree Island in the south GBR has a difference of > 10,000 yr to other reefs (Marshall and Thom 1976), and northern GBR initiated earliest as it reached tropical temperatures first (Marshall and Davies 1988). The reason for this is that SLR was not uniform across the GBR. Typically reef growth on the outer shelf began earlier than reef growth on the inner shelf (Webster and Davies 2003). Pleistocene sea level has fluctuated with glacial shifts, during interglacial periods sea level was high, ∼ 125 ka will have experienced similar sea level to the present day, followed by a steep reduction of sea level as glacial maximum periods began, exposing reefs to air and leading to a mass death (Bryant 1992; Fairbanks 1989). Following meltwater pulses, sea level would then rise rapidly and lead to mass drowning events as corals struggled to keep up with sea level (Chappell et al. 1996), this cycle over the last 100,000 years has developed the GBR into the structure we see today (Hopley, Smithers, and Parnell 2007).

During 28-27 ka , the GBR initiated reef growth along the narrow shelf edge following the global mean sea level (GMSL) fall which led to the death of the first reef (Webster et al. 2018) (fig. 1.11). Across the GBR, sea level was lowest by ∼ 20.7 - 20.6 ka as GMSL reached ∼ 125 - 130 metres below sea level during the Last Glacial Maximum (LGM) (Yokoyama et al. 2018), considerable seaward migration of the GBR by ∼0.25 - 1 m within 2 kyr during the LGM showed that the GBR was a robust ecosystem before aerial exposure led to the second mass death at 22 ka (Webster et al. 2018). The deglaciation of the LGM ∼ 17 - 16.5 ka led to the initiation

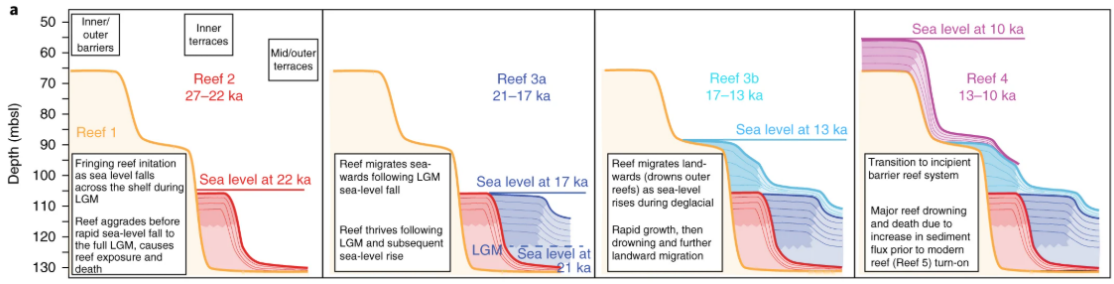


Figure 1.11: Simplified model of sea level change and evolution of the GBR across 30,000. Each panel shows the formation of a key stage and facies relationships of shelf-edge reef development. After Webster et al. (2018).

of reef 3 which migrated landwards in shallow water assemblages and vertical accretion rates of up to 20 mm yr-1 at 15.5-15.0 ka, the highest recorded accretion rates of the GBR and allowed the reef to keep up with accelerating SLR for a while (Felis et al. 2014). However, the sustained rapid SLR eventually drowned reef 3 $\sim$ 13.72 ka (Webster et al. 2018). Reef 4 closely followed reef 3, initiation began at 13 ka with fast growing *Acropora-Isopora* reef framework (Felis et al. 2014), the reef drowned between 10.31 - 10.14 ka due to a flux of sediment which is thought to have smothered the reef (Page and Dickens 2005). Finally, the present day GBR (reef 5) began $\sim$ 9 ka as sea levels rose to $\sim$ 10 - 20 mbsl.

A study using numerical modelling was carried out to reconstruct past GBR sea levels going back to 16.8 ka, where sea levels were 96 m below present, the study found that sea level changes significantly changed the tidal dynamic regime and that ooids could be formed in the GBR by stronger tidal currents at 16 ka (Lee et al. 2022). It was also found that S2 and M2 amplitude have generally increased in strength as sea levels have risen, and changes in bed shear stress (BSS) were found due to difference in depth around the Capricorn Channel. Data captured by drill cores and models has enabled us to see that sea-levels heavily impacted the tidal environment of corals around this time through changes in wave and tidal energy, direction and sediment transportation (Hopley, Smithers, and Parnell 2007; Lee et al. 2022). As the hydrodynamics of the GBR are incredibly sensitive to spatial heterogeneity created by bathymetry and reef matrices (King and

Wolanski 1996; Taebi et al. 2011), SLR over the Holocene has led to a large change in tidal dynamics (Yokoyama et al. 2006; Hinestrosa, Webster, and Beaman 2016).

Quantification of past sea levels is possible using corals as they are a robust measurement of sea level due to their vertical growth being dependent on reaching the sea surface (Dutton et al. 2015; Humblet and Webster 2017). From these records, coral assemblages and response to sea level can also be derived, for example the rapid increase of SLR between 8.2 and 8 ka lead to fast growing, clear-water and shallow reef assemblages, followed by a shift to deeper, slower growth between 8 and 7 ka and then a return to fast growing, shallow and clear water growth as the reef caught up with sea level, during this time delicate branching corals begin to appear, indicating calm water (Sanborn et al. 2019). By understanding how sea level affected tidal dynamics and the GBR, we can begin to anticipate how the present GBR will respond to future sea level change (Bryant 1992).

1.5 Sea-level change and tidal dynamics

Global sea level has already increased throughout the twentieth Century by 1.7 $\pm$ 0.3 mm yr^{-1} (Church and White 2006; Priya et al. 2023; Thompson et al. 2018), linked to the melting of ice sheets and glaciers, and ocean thermal expansion as global temperature increases (Hay et al. 2015; Vermeer and Rahmstorf 2009). Shallow coastal and shelf systems bearing the worst of the effects of SLR (Idier et al. 2017). Shallow water tropical coral reefs are in a vulnerable position, already being impacted by increased temperatures and storms, they are also at risk from being outpaced by rising sea level and becoming more susceptible to damage from increasingly turbulent waters and tidal range (Rasheed et al. 2021). In coastal areas the impact of tides is seen in coastal morphology (Rodrigues et al. 2021), species distribution (Stumpf and Haines 1998) and saline intrusion (Bricheno, Wolf, and Islam 2016). Tidal levels (the depth defined by the rise and fall of

astronomic tides), currents and range (the difference in height between spring and neap tides) vary on a range of scales, from the daily oscillations to inter-annual variations based on the positions of the Moon, Sun and Earth (Pugh and Woodworth 2014). However, as sea levels have risen, tides have been observed to be changing across all time scales, due to reasons other than astronomical forcing (Woodworth 2010; Haigh et al. 2020).

Tides are one of the most predictable phenomenons in the ocean due to their astronomical origin, leading to the assumption that tides are stationary and stable (Cartwright 2000; Rose, Rohith, and Bhaskaran 2022). Measurements such as sea surface elevation can be accurately predicted as long as relevant topographic and non-tidal sea state conditions, such as wind and wave swell, remain constant (Zahel 2005). Ocean tides are affected by depths, coastal tidal dampening, continents, shoreline position, ocean stratification, ice sheet coverage and astronomical forcing (**wilm**; Arbic, Karsten, and Garrett 2009; Müller, Arbic, and Mitrovica 2011); the tidal spectrum in the open ocean is represented by well defined diurnal and semidiurnal astronomical frequencies (Andersen et al. 2006).

1.5.1 Holocene sea-level rise and tidal changes

The response of the ocean to tidal forcing over millennia has been found to have been impacted by sea level change, in particular this leads to large changes being simulated in S2 and M2 amplitudes (Müller, Arbic, and Mitrovica 2011), affected by depth and frictional energy loss (Haigh et al. 2020). Increase of amplitude from SLR may be caused, at least over short times scales, by changes in phase of the internal tide leading to changes in amplitude and phase change of the surface tide (Colosi and Munk 2006).

During the LGM (26.5 - 19 kyr BP), mean sea level (MSL) was 120 - 130 m lower than present day, caused by oceans having retreated into ice sheets which covered most of the Northern Hemisphere (Clark et al. 2009). MSL decrease and ocean

basin shape change increased M2 tidal amplitude in the North Atlantic by several meters, as well in the South Atlantic (Wilmes and Green 2014). K1 changed little throughout the LGM in open-ocean but diurnal tides increased along margins of the South China Sea, Sea of Okhotsk and Antarctica (Griffiths and Peltier 2009; Wilmes and Green 2014). Meltwater from ice sheets reduced salinity and affected the oceanic Meridional Overturning Circulation (Green et al. 2009). These changes to stratification lead to alterations in eddy viscosity and bottom friction, which in turn can affect barotropic transport, deep ocean circulation and changes to tides (Müller 2012).

As the de-glacial period (19 - 16 kyr BP) began, MSL increased by $\sim$ 5 m/kyr, during which time, shelf areas were slow to flood (Peltier, Argus, and Drummond 2015), and there was little change from LGM amplitude values except around the European shelf (Uehara et al. 2006). High rates of global MSL (15 m/kyr) took place between 16 - 8 kyr (Stanford et al. 2011), during this time, all major shelf seas were flooded along with increased tidal amplitudes.

The continental shelf of east Australia underwent 76 m of SLR rise been 19.8 - 10 ka, leading to amplification of M2 and S2 as the shelf flooded (Lee et al. 2022). Tidal range originally decreased between 16.8 - 15 ka but then increased between 12.5 - 10 ka. In the north Atlantic, between 10 and 8 ka, open-ocean amplitudes dissipated with melt water and with the opening of Hudson Strait, European shelf tidal amplitudes increased to a maximum of 4.5 m at 10 ka (Uehara et al. 2006; Wilmes and Green 2014; Ward et al. 2016). An increase in amplitude occurred in the northwest Atlantic, also around 9 ka, with a smaller increase of amplitude in the Gulf of Mexico (Hill et al. 2011). However, M2 amplitude decreased between 10-8 ka on the European Shelf (Uehara et al. 2006). Few changes to tidal amplitude took place globally between 7 ka and the present day, with conditions similar to those observed in the present day (Wilmes and Green 2014; Hill et al. 2011) but localised effects did occur on shelf areas showing increases in tidal range such around the Bay of Fundy and Gulf of Maine (Scott and Greenberg 1983; Gehrels

et al. 1995).

The tidal range increase in the Bay of Fundy and Gulf of Maine continued to $\sim$ 5 ka, when it is thought that these areas became strongly resonant (Hill et al. 2011). Tidal resonance effects play a role in amplifying tides when the length of the shelf is 1/4 of the wavelength of the tidal constituent, (Green 2010), when the natural frequency of oscillations of a body of water, such as a bay or gulf, match the tidal frequency, an amplification of tides occurs (Green et al. 2009; Godin 1993). The increase of tidal amplitude in the Bay of Fundy was not actually due to change of depth within the Bay, but instead to depth variation on Georges Bank along the outer edge of the bay (Scott and Greenberg 1983).

1.5.2 Projections of sea-level rise

Over the last 30 years, global temperature has increased by $\sim 0.2^{\circ}$ per decade (Goreau and Hayes 2024; McCulloch et al. 2024). Global sea level has increased throughout the twentieth Century by 1.7 ± 0.3 mm yr^{-1} (Church and White 2006; Priya et al. 2023; Thompson et al. 2018), linked to the melting of ice sheets and glaciers, and ocean thermal expansion as global temperature increases (Hay et al. 2015; Vermeer and Rahmstorf 2009). Already the consequence of greenhouse gases on global mean sea level will last centuries through ocean thermal expansion and loss of land ice (Mengel et al. 2018). Moreover, the trajectory of global temperature and SLR relies heavily upon on our socioeconomic decisions and meeting climate goals laid out by the Paris Agreement (Matemilola, Fadeyi, and Sijuade 2023). One popular method of predicting the impact of these decisions has been termed Shared Socioeconomic Pathways (SSP) (O'Neill et al. 2014) (see Figure 1.12) and have been used to develop climate scenario predictions (Ebi et al. 2014; Vuuren et al. 2014; Kriegler et al. 2014). The pathways range from the ideal green route, cutting all greenhouse emissions, prioritising human health and education and accepting a slower economic growth (SSP 1), to a middle ground where there is no marked shift from historic patterns but a slow movement to-



Figure 1.12: The five Shared Socioeconomic pathways showing their respective positions along axes representing challenges of adaptation and mitigation. After O'Neill et al. (2017).

wards a more sustainable future (SSP 2) and then SSP 5 which sees no action being taken to shift towards sustainability, prioritising capital over health and well-being (O'Neill et al. 2017). Sea levels over the next 100 years heavily depends on the scenario pathway society takes, SSP scenarios have been converted to sea level rise by IPCC AR6 (Garner et al. 2021; Intergovernmental Panel on Climate Change (IPCC) 2023; Kopp et al. 2023): for example, best case scenario SSP 1 1.9, corresponding to 0.45 m mean sea level rise by 2100 and worst case scenario SSP 5 8.5, corresponds to 0.87 m mean sea level by 2100. These sea level conversions are achieved by taking the radiative trajectories of each SSP, which correspond to change in energy balance from greenhouse gases. IPCC develop ocean models which simulate the Earth's response to different radiative forcing levels considering contributions from thermal expansion, glacier ice melt and land water storage changes, from which sea level projections are derived.

Over the next 1 m of SLR on the East Australian continental shelf, M2 amplitude is expected to decrease as sea level increases (Mawson, Lee, and Hill 2022). Another study on sea level rise around Australia also found non-linear changes to tidal constituents, the largest change in M2 amplitude being 15% of the SLR sig-

nal south of Papua New Guinea and smaller changes shown in K1 (Harker et al. 2019; Schindelegger et al. 2018). The impacts of this is increased turbulence and benthic velocity (Harris, Vila-Concejo, and Webster 2014); this is in fact beneficial up to a limit, assisting with recovery from thermal stress, nutrient influx and waste removal (Sandin et al. 2022; Page et al. 2019; Page et al. 2021; Nakamura, Yamasaki, and Woesik 2003; Sebens et al. 1998; Sebens et al. 2003). Elsewhere, such as across the European shelf, sea level will effect tides by modifying bed friction, reflection and resonance properties, leading to changes in tidal amplitude (Idier et al. 2017), and flooding of estuaries and Dutch coastlines (Pelling and Mattias Green 2013); changes have already been recorded in the Gulf of China where it decreases (Li et al. 2016) and an increase in M2 amplitude in the Gulf of Maine and Bay of Funday (Gehrels et al. 1995).

One of the most studied consequences is tidal damping. Tidal amplitude is half of the tidal range, increased sea levels lead to changes in tidal amplitude: decrease in amplitude, induced by dissipation, is referred to as tidal damping and increase of amplitude is called tidal amplification (Friedrichs, Aubrey, and Speer 1990). Amplitude damping is predominantly experienced around estuaries due to the complex relationship between SLR and increased levels of estuary infill from sedimentation (Palmer, Watson, and Fischer 2019). Tidal amplification is likely to increase on shelf coasts. However, tidal amplification is only expected to be problematic during storm surges, as it affects the total water level (Rose, Rohith, and Bhaskaran 2022).

1.5.3 Effects of sea-level rise on connectivity

On a global scale, it is predicted that changes to ocean currents from will affect coral connectivity in terms of supply and survival rate (Munday et al. 2009), but the impact of changing tidal dynamics on coral connectivity is not well understood. Coral reef populations greatly depend upon connectivity for growth and resilience, so it is important that we are able to predict what will happen with ris-

ing sea levels (Caley et al. 1996; Armsworth 2002). On a global scale, changes to poleward-flowing currents may continue to strengthen, such as the South Equatorial Current, impacting global and local current patterns (Steinberg 2007; Cai et al. 2005). Future projections of changes to Australian tides have shown shown non-linear changes in M2 amplitude depending on region, and reduction of K1 amplitude when the Gulf of Carpentaria becomes flooded (Harker et al. 2019), and a local study of the GBR predicted general damping of M2 but an increase of S2 with SLR, and is likely to lead to changes in connectivity (Mawson, Lee, and Hill 2022). Further studies are required to understand what changes coral larvae dispersal are going to undergo from sea level rise and changes of tidal dynamics, these studies will need to employ biophysical numerical modelling tools to simulate and predict future changes.

1.6 Numerical modelling in Coral Reef Studies

Numerical modelling is a widely applied tool in ocean and tidal dynamics (e.g. Colberg et al. 2019; Paris et al. 2013; Chen et al. 2006; Mansui, Molcard, and Ourmières 2015). Numerical modelling enables complex or inaccessible physical systems to be simulated across large spatial and temporal scales by solving equations such as the shallow water equation or Navier-Stokes equations (Lambrechts et al. 2008; Wallwork et al. 2024). Numerical modelling solves systems of equations across the domain by discretising the equations onto discrete elements, in the form of a model mesh or grid (Rappaz, Bellet, and Deville 2010). The mesh of a numerical model can either be structured or unstructured, depending on the scale of the model and the resolution required, structured meshes divide the mesh into equal sized squares, allowing all mesh cells to be calculated using the same resolution (Danilov 2013). These meshes are commonplace in oceanic modelling, as large spatial scales are being modelled at degrees of latitude (e.g. 1/1°) due to fine bathymetry features not needing to be captured, these meshes tend

to follow coordinate systems (Wood et al. 2014; Assis et al. 2025; Lyard et al. 2006). Their advantage is that the memory arrangement in computers is structured, like the grid, such that information flow is predictable and the data can be cached and loaded onto the processor ahead of being needed, increasing efficiency.

Unstructured meshes are made up of triangles, or other geometric shapes, varying in size (fig. 1.13). Large triangles are used in deep water, for example, away from areas of particular interest, whilst the smallest triangles, handling the highest resolution calculations, are used for the areas of interest (Piggott et al. 2008). Unstructured meshes are often used for coastal and shelf modelling, as areas of very fine bathymetry resolution is necessary to pick up important bathymetric features, such as shelf-edges, lagoons and bays (Danilov 2013). The benefit of the unstructured mesh with varying resolution over a structured mesh of the same area at equal highest resolution is the reduction of computational power, as unstructured meshes using varying resolution, modelled areas surrounding the key locations of interest can be solved at a much coarser resolution without sacrificing accuracy (Danilov 2013). However, their unstructured nature means that data access is not predictable, unstructured mesh models are generally slower than their structured counterparts. Accuracy of simulations also depends on a number of factors such as mesh resolution (Avdis et al. 2018); boundary conditions (Weaver and Sarachik 1991); parameters and parametrisations (Chandra et al. 2019); and the equations solved (Kärnä et al. 2018).

1.6.1 Global ocean circulation models

The most published oceanic models are NEMO (Nucleus for European Modelling of the Ocean) (Gurvan et al. 2017), and ROMS (Regional Ocean Modelling System) (Kerry et al. 2016). Ocean models are primarily used to understand large scale global processes, such as biogeochemical processes such as the carbon cycle (Fennel et al. 2022), ocean acidification (Jiang et al. 2023) and ocean deoxygenation (Takano et al. 2023); atmospheric interactions to inform large-scale climate

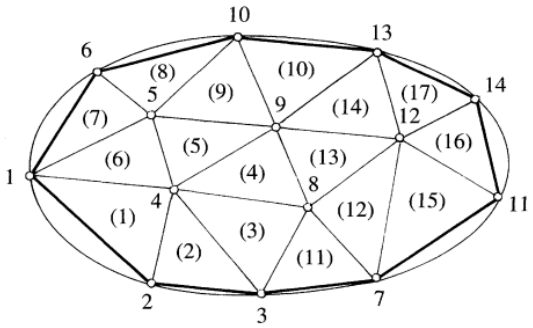


Figure 1.13: Example of how a geometric domain is divided into finite elements to generate an unstructured mesh. Numbers in brackets label the element and numbers without brackets label the nodes. After Rappaz, Bellet, and Deville (2010).

predictions (Seo et al. 2023) and impacts from oceanic currents (Wang et al. 2022). Global ocean circulation simulate daily ocean currents, which can be constrained using data from from services such as the Global Ocean Physics Reanalysis (GLORYS12V1 (Cmems 2023), https://doi.org/10.48670/moi-00021), provided by the EU Copernicus Marine Service (https://marine.copernicus.eu), the hybrid coordinate ocean model HYCOM (Chassignet et al. 2007), which can then be used to integrate with Lagrangian particle tracking software such as Parcels (Delandmeter and Sebille 2019), or the Connectivity Modelling System (Paris et al. 2013), to develop biophysical models to trace marine connectivity (Wood et al. 2014; Assis et al. 2025), as discussed earlier. Most of these models use the finite difference method (FDM). FDM discretizes the domain into a grid and solves difference equations at each point on the grid or on the tie-lines between grid point (Bode and Stark 1983).

1.6.2 Coastal models

Unstructured mesh models are used for coastal and shallow shelf modelling because of their ability to be high resolution and capable of solving complex bathymetry interactions. They are generally discretised using either the finite volume method (FVM): such as FVCOM (Chen et al. 2006) or the finite element method (FEM), such as Thetis (Kärnä et al. 2018). Finite volume refers to discretiz-

ing the model domain into volumes and then applied the conservation laws of mass, momentum and energy to each volume, this is a popular method in fluid flow simulations where conservation of mass, momentum and energy is vital to the simulation, however FVM is challenging to use with complex geometries, such as a complex bathymetry. FEM discretizes the domain into elements, such as triangles, and solves each element using partial differential equations such as the Shallow Water Equation (Kärnä et al. 2011; Woodroffe et al. 2023; Lambrechts et al. 2008). FEM is efficient in solving flow calculations on complex geometries because of its flexible mesh. Some examples of coastal models that are commonly used in both research and practical applications are described below.

1.6.2.1 SLIM

SLIM (Second-generation Louvain-la-Neuve Ice-ocean Model) (Lambrechts et al. 2008) is a Discontinuous Galerkin (DG) element method model and is well published due to its accuracy for complex coastlines and bathymetry. SLIM has been designed to handle 1D, 2D simulations by solving depth-averaged shallow water equations; and 3D simulations by solving hydrostatic equations under the Boussinesq approximation. SLIM was first used as a high-resolution model of the entire GBR for the purpose of explicitly illustrating the benefit of using a unstructured mesh to capture fine scale hydrodynamics rather than a structured mesh. Since 2008, SLIM has been used to accurately model river suspended sediment (Le et al. 2020), liquid motion of lakes on Titan (Vincent et al. 2019), oil spills (Verhofstede et al. 2023) and multiscale ocean modelling (Hanert et al. 2023). SLIM has also been developed with its integrated Lagrangian particle tracking software which has been used to track plastic particles (Li et al. 2018), connectivity of ecosystems across the GBR (Wildermann et al. 2017; Grech et al. 2018; Schlaefer et al. 2018), including coral (Figueiredo et al. 2021; Saint-Amand et al. 2023; Thomas et al. 2014; Thomas et al. 2015), as well as Indonesia (Faryuni et al. 2024) and Florida (King et al. 2023).

1.6.2.2 FVCOM

FVCOM (Finite Volume Community Ocean Model) (Chen et al. 2006) is a finite volume three-dimensional model, designed specifically for coastal use and is capable of solving momentum, temperature, density, salinity and continuity equations (primitive Navier-Stokes under Boussinesq and hydrostatic assumptions). FVCOM was designed to improve upon FDMs ability to capture better residual currents and tidal elevation around tidal creeks and islands; and has been successfully applied to coastal applications, such as effects of mangroves on tides (Li et al. 2012); impacts of typhoons on shelf mixing (Cong et al. 2023); saline intrusion in deltas (Bricheno, Wolf, and Islam 2016); and temperature change in the Persian Gulf (Ramak, SoyufJahromi, and Akbari 2023). FVCOM can be linked to the Integrated Compartment Water Quality Model (ICM) to add capabilities of modelling biogeochemical processes, such as eutrophication (Jiang et al. 2015), acidification (Bianucci et al. 2018) and phytoplankton dynamics (Sun, Kang, and Xia 2024).

1.6.2.3 DELFT3D-FM

One of the most well known numerical models is Delft3D (Lesser et al. 2004), Delft3D is a FDM solving 2D and 3D shallow-water equations with the option to include baroclinic flows to model rivers, coastal systems, waves and estuaries particularly for coastal erosion and sediment transportation purposes (Storlazzi et al. 2011; Elahi et al. 2020), including coastal engineering and impact assessments (Mirdan et al. 2024). However, Delf3D is a structured grid model and therefore resolution is limited by computational power, which is why DELF3D-FM (Flexible Mesh) (http://oss.deltares.nl/web/delft3dfm), an unstructured mesh FVM, was then developed. DELFT3D-FM was been popular for modelling reef atolls due to the capacity to handle complex bathymetry at a high resolution with accuracy and robustness, as well capable of being integrated with wave model SWAN (Simulating WAves Nearshore) (Booij, Ris, and Holthuijsen 1999), capturing fine scale hydrodynamics (Green, Lowe, and Buckley 2018), and can be coupled with

Lagrangian transport equations to capture hydrodynamic drivers of connectivity (Grimaldi et al. 2022).

1.6.2.4 Thetis

Thetis (Kärnä et al. 2018) is a finite element, unstructured mesh model. Developed specifically for the use of coastal ocean modelling, Thetis is capable of simulating 3D baroclinic flows and 2D depth-averaged models with greater control of diffusion, leading to high accuracy and lower computational cost than previous unstructured grid models (Shi et al. 2017). It is implemented using Firedrake – a framework for solving Partial Differential Equations via the finite element method using sophisticated code generation (Goss et al. 2019). Thetis has been used to study a variety of coastal phenomena, including the links between tidal regimes and sediment flow (Rasheed et al. 2021), ancient tsunamis (Bateman et al. 2021; Hill et al. 2023; Sharrocks and Hill 2024), tracer transportation (Wallwork et al. 2022), impacts of tidal turbines (Zhang et al. 2022; Baker et al. 2020; Goss et al. 2021; Mackie et al. 2021; Wallwork et al. 2024), as well as palaeo-sediment transport (Lee et al. 2022) and future tidal dynamics in the Great Barrier Reef (Mawson, Lee, and Hill 2022). It has advanced capabilities such as using adjoint methods to quantify uncertainty or optimise parameters (Warder, Horsburgh, and Piggott 2021).

In this thesis, Thetis is the chosen numerical model. The benefit of Thetis over the other models comes down to the infrastructure of Firedrake, which automates finite element discretisation and is highly optimised for high-performance computing, outperforming models such as Delft3D and FVCOM which are based on older code such as Fortran. The Discontinuous Galerkin method available in Thetis is able to handle sharp numerical gradients and complex advection better than continuous FEM. SLIM also uses DG but as Thetis and Firedrake are being actively developed, it makes it a more flexible and scalable choice than SLIM.

1.6.3 High resolution GBR models

Using numerical models to understand hydrodynamic processes on the GBR has a long history. A numerical model paper was published in 1993 investigating the importance of local retention and inter-reef dispersal (Black 1993), one in 1991 modelling Langmuir circulations around coral reefs (Kingsford, Wolanski, and Choat 1991) and another in 1983 on simulating tides and currents (Bode and Stark 1983). Models such as these used FDM and were written in Fortran with coarse resolution due to computational limitations at that time. Today's models of the GBR are typically FEM or FVM, for example SLIM was specifically developed to study shelf processes of the GBR (Lambrechts et al. 2008). Since then, SLIM has been widely used for modelling hydrodynamics as well as connectivity across the GBR (Thomas et al. 2014; Thomas et al. 2015; Munday et al. 2009; Figueiredo et al. 2021; Wildermann et al. 2017; Schlaefer et al. 2018; Andutta, Ridd, and Wolanski 2013; Andutta, Kingsford, and Wolanski 2012). Iterations of Delft3d have also been used for conducting simulations of reef hydrodynamics (Green, Lowe, and Buckley 2018) and thermal stress (Baird et al. 2020). Thetis has also been used for modelling future tidal dynamics (Mawson, Lee, and Hill 2022) and palaeo-sea level influences on tides (Lee et al. 2022).

Modelling the GBR requires high resolution as tidal dynamics are heavily influenced by bathymetry (King and Wolanski 1996), meaning that if a model captures bathymetry coarsely or misses bathymetric features, incorrect assumptions will be made (Seifi, Deng, and Andersen 2019; Harker et al. 2019). The current highest resolution for the entire GBR is 250 m (Saint-Amand et al. 2023), but ideal resolution should be less than 100 m in order to capture the reef scale dynamics such as eddies and jets (Wolanski et al. 2024a). However a resolution that high is computationally expensive, most high resolution simulations are restricted to at most a handful of reefs (Andutta, Kingsford, and Wolanski 2012; Thomas et al. 2014; Greenwood et al. 2025).

1.6.4 Limitations and uncertainty

The most difficult limitation for modellers to overcome is resolution, there is a payoff between resolution and computational power: if the resolution is too low, important bathymetric features get missed which leads to inaccurate simulations but if the resolution is too high it will be computationally expensive, slow and unstable (Choukroun et al. 2024; Saint-Amand et al. 2023; Wolanski et al. 2024a; Seifi, Deng, and Andersen 2019). Infrastructure such as DG and Firedrake assist with pushing the limit of resolution further, by creating more robust and agile solvers and increasing computational efficiency (Goss et al. 2019; Goss et al. 2021).

Ensuring boundary conditions are accurately defined can be challenging, doing so incorrectly can lead to instability and inaccuracy of the model (Marsaleix, Auclair, and Estournel 2006). In a similar theme, parametrizing models can lead to uncertainty due to translating empirically derived processes from one small area, such as turbulence and bottom drag, and applying them to much larger scales using methods such as Bayesian inference (Chandra et al. 2019). Forcing data such as atmospheric pressure or river input can also be inadequate for model calibration if it has come from observations or reanalysis (Simmons et al. 2017).

1.7 Knowledge Gaps

Previous studies on GBR connectivity differ in concluding whether wind or tides are the dominant force responsible for coral larvae transportation (Willis and Oliver 1988; Williams, Wolanski, and Andrews 1984; Andutta, Kingsford, and Wolanski 2012; Miller and Mundy 2003), and what is the physical mechanism behind self-seeding (Wolanski, Burrage, and King 1989; Schlaefer et al. 2018; Sammarco and Andrews 1988; Black 1993). Field studies rely on empirical observations typically carried out on a handful of reefs (Wolanski, Burrage, and King 1989; Willis and Oliver 1988; Willis et al. 1985). Local field observations are unlikely to capture

large-scale trends, and it is also difficult to separate the effects of wind from tides in field observations. Tidal dynamics have changed with sea level over time, as shown by Lee et al. (2022) in a study across the Holocene. As they have changed in the past, tidal dynamics will continue to change into the future with SLR. It is not currently understood what tidal dynamics conditions were present during the Holocene initiation (Webster et al. 2018), other than sea-level, sediment levels, turbidity and temperature becoming optimal (Sanborn et al. 2024; Dechnik et al. 2015). By understanding critical points of how the relationship between sea level and tidal dynamics shaped coral reef connectivity, we will be able to predict how the GBR will respond the SLR in the future. Following on from this, the implication of SLR on future coral reef connectivity across the GBR is currently unknown, meaning that management strategies are currently unguided on how to best protect the GBR as sea-levels rise, using network protection.

1.8 Thesis Research Aims, Questions and Objectives

In this thesis I examine the interaction between sea-level and tidal dynamics, and the role they have on shaping coral connectivity across the GBR. I provide novel information on the physical drivers behind coral larvae dispersal and retention, how tidal dynamics may have been responsible for the initiation of the modern day GBR 8,000 years ago and and finally how future will impact coral connectivity on the GBR depending on which shared socioeconomic pathway (SSP) the world takes. To do this, finite element numerical models using Thetis were developed of the GBR to simulate a variety of sea level scenarios. These sea level scenarios consisted of the present day, palaeo sea level reconstructions of up to 17 m below present sea level, and future of up to an average of 0.87 m above present sea level. For each sea level scenario throughout the thesis, bespoke bathymetry and reef location reconstructions were created, taking into account depth change and position of reefs. These models were then used for tidal analysis, and inte-

grated with Lagrangian particle tracking software, Parcels, to investigate changes to connectivity driven by tidal dynamics.

To examine how sea level change has impacted the relationship between tidal dynamics and coral reef connectivity across the GBR from 9 thousand years ago to 2100, three research questions and their respective sub-questions are outlined below:

1. **What are the differing effects of wind and tides on coral larvae transportation?**
    1.1. What is the mechanism behind self-seeding behaviour?
2. **What tidal dynamics were present during the Holocene GBR initiation around 8 ka and how are they different to the present day?**
    2.1. How has connectivity changed throughout the Holocene initiation?
    2.2. How did tidal dynamics affect coral connectivity during the Holocene initiation?
3. **How is self-seeding behaviour affected by future sea level rise across different Shared Socioeconomic Pathways?**
    3.1. How are tidal dynamics affected in 2100 by each SSP sea level rise scenario?
    3.2. How does using a higher resolution model of the entire GBR and relative sea level rise improve predictions to tidal dynamics?

1.9 Thesis Structure

1.9.1 Chapter 2 - Methodological Overview

Chapter 2 outlines the methodology used for numerical modelling of the Great Barrier Reef (GBR) and particle tracking within each subsequent chapter. This

chapter covers the numerical model used throughout the thesis, the Lagrangian particle tracking software, including all validation and parametrisation which were carried out.

1.9.2 Chapters 3 - 5 - Results

Chapters 3, 4 and 5 are each stand alone results chapters that respond to the research questions outlined above. The methodological overview written in chapter 2 is the foundation of the methods used in chapters 3 - 5, each of these chapters is also presented with additional or bespoke methods for requirements of the questions being addressed.

Chapter 3 addresses research question 1 by modelling three different forcing scenarios: tidal forcing only, wind forcing only and combined wind and tidal forcing. Each of these models were integrated with Lagrangian particle tracking software Parcels to simulate coral larvae transport in order to compare results of differing effects of wind and tides on larvae transportation and explore the mechanism behind self-seeding behaviour. Chapter 4 is a study using three palaeo-tidal reconstructions of the Holocene initiation of the GBR around 8,000 years ago, these simulations are used to investigate the tidal dynamics present during the Holocene and how these may have affected coral connectivity during this time. These models are also integrated with Parcels in order to study connectivity. Finally, chapter 5 builds three models developed of GBR future sea-level in 2100 based on three different SSP to investigate how tidal dynamics and self-seeding behaviour will be affected by future SLR. The main purpose of this final chapter is to provide GBR management strategies with better insight into how the GBR will respond to future sea level.

1.9.3 Chapter 6 - General Discussion

The general discussion provides a synthesis of the thesis and key findings from each chapter. Wider implications from findings are explained, connecting each of the chapters together and demonstrating how they have built upon one another. Limitations of the thesis are addressed along with considerations of how these feed into future work. This section is then finished with concluding remarks.

Chapter 2

Methodologies

This chapter outlines the methodology used for numerical modelling of the Great Barrier Reef (GBR) and particle tracking within each subsequent chapter. The workflow, illustrated in Fig. 2.1, begins with obtaining bathymetric data for the study area at an appropriate resolution. This data is processed in spatial analysis software to define the model domain boundaries. Next, the bathymetry and boundary domain undergo pre-processing to prepare them for mesh generation. Once the mesh is created, it – along with the bathymetry – is input into the selected numerical model, which simulates tidal dynamics over a specified period, generating outputs for velocity, elevation and vorticity. Following completion of the numerical simulations, Lagrangian particle tracking software is implemented to model the transportation of coral larvae between reefs. The velocity outputs need to first be converted to a compatible format for the particle tracking software, which uses this data to track particles transportation. Verification experiments were conducted to calibrate the particle tracking parameters. Once simulations are complete, the start and end points of particle trajectories are recorded, allowing for the extraction of path data and the generation of connectivity matrices. Finally, these connectivity matrices are used in network analysis to assess how connectivity varies across different model scenarios. I will first de-

tail the tidal numerical modelling, including validation. The particle tracking is detailed before showing the validation results from that section of the workflow.

2.1 Numerical Modelling

Numerical modelling is widely applied in a number of scientific disciplines, including engineering (e.g. (e.g. Lee et al. 2021; Rappaz, Bellet, and Deville 2010; Kyvelou, Buchanan, and Gardner 2022; Liu et al. 2022)), atmospheric physics (e.g. (Sadourny 1975; Amores et al. 2022; Beaurepaire et al. 2021)) and ocean dynamics (e.g. (Colberg et al. 2019; Paris et al. 2013; Chen et al. 2006; Mansui, Molcard, and Ourmières 2015)). Numerical modelling solves systems of equations, by discretising the equations onto discrete finite elements. For ocean modelling systems, equations such as the shallow water equation or Navier-Stokes equations are solved (Lambrechts et al. 2008; Wallwork et al. 2024). Accuracy of simulations depends on a number of factors such as mesh resolution (Avdis et al. 2018); boundary conditions (Weaver and Sarachik 1991); parameters and parametrisations (Chandra et al. 2019); and the equations solved (Kärnä et al. 2018).

Throughout this thesis, Thetis (Kärnä et al. 2018) is employed to develop high-resolution numerical models of the GBR. Thetis is a finite element, unstructured mesh model. It is implemented using Firedrake – a framework for solving Partial Differential Equations via the finite element method using sophisticated code generation (Goss et al. 2019). Developed specifically for the use of coastal ocean modelling, Thetis is capable of simulating 3D baroclinic flows and 2D depth-averaged models with greater control of diffusion, leading to high accuracy and lower computational cost than previous unstructured grid models (Shi et al. 2017). Thetis has been used to study a variety of coastal phenomena, including the links between tidal regimes and sediment flow (Rasheed et al. 2021), ancient tsunamis (Bateman et al. 2021; Hill et al. 2023; Sharrocks and Hill 2024), tracer transportation (Wallwork et al. 2022), impacts of tidal turbines (Zhang et al. 2022; Baker et al.

2020; Goss et al. 2021; Mackie et al. 2021; Wallwork et al. 2024), as well as palaeo-sediment transport (Lee et al. 2022) and future tidal dynamics in the Great Barrier Reef (Mawson, Lee, and Hill 2022). Here, Thetis is used to solve the 2D shallow water equation (eqs. 2.1 and 2.2), with wetting and drying capability enabled – the ability to handle exposure and submersion of the seabed, or coral reefs, capturing the difference in flow during sequential tidal cycles (Kärnä et al. 2011).

$$A(H)\frac{\partial \eta}{\partial t} + \nabla \cdot (\tilde{H}\mathbf{u}) = 0, \tag{2.1}$$

$$\frac{\partial \mathbf{u}}{\partial t} + \mathbf{u} \cdot \nabla \mathbf{u} + f\mathbf{u}^{\perp} + g\nabla\eta + \nabla\frac{p_a}{\rho_0} = \frac{\tau_s - \tau_b}{\rho\tilde{H}} + \nabla \cdot (\nu(\nabla\mathbf{u} + \nabla\mathbf{u}^T)), \tag{2.2}$$

where $A(H)$ is the wetting and drying formulation (see below), $\tilde{H}$ is the total fluctuating depth given by $\tilde{H} = \eta + h$, where $\tilde{h}$ is the function of elevation and static bathymetry (eq. 2.3), $\mathbf{u}$ is the depth-averaged velocity vector and ν is the kinematic viscosity of the fluid. Wind stress, τ_s, can be applied via a number of forcing formulations, along with atmospheric pressure (p_a). $f\mathbf{u}^{\perp}$ represents the Coriolis term, where $\mathbf{u}^{\perp}$ is the velocity vector rotated counter-clockwise over 90^o. Note that the continuity equation (eq. 2.1) has been further developed by $\frac{\partial \eta}{\partial t} + \frac{\partial \tilde{h}}{\partial t} = A(H)\frac{\partial \eta}{\partial t}$, where $\tilde{h}$ is defined by:

$$\begin{aligned} \tilde{h}(\eta, h) &= h + f(H), \\ f(H) &= \frac{1}{2}(\sqrt{H^2 + \alpha^2} - H) \end{aligned} \tag{2.3}$$

where $f(H)$ ensures redefined total depth remains positive, via the wetting and drying parameter, α, η is the free surface height and h is the original static bathymetry depth. Finally, $f = 2\Omega\sin\zeta$ with ζ the latitude and Ω corresponding to the angular frequency of the Earth's rotation. Bed shear stress (τ_b) effects are represented through the Manning's n formulation as:

$$\frac{\tau_b}{\rho} = gn^2 \frac{|\mathbf{u}|\mathbf{u}}{H_d{}^{\frac{1}{3}}} \tag{2.4}$$

where n is the Manning's friction coefficient and ρ is the density. A discontinuous Galerkin finite element discretisation (DG-FEM) is implemented in Thetis using the $P_{1DG} - P_{1DG}$ velocity-elevation finite element pair. All model runs use parallel computation via spatial domain decomposition, which is handled automatically by Thetis using the MPI library.

Thetis uses a Diagonally Implicit Runge-Kutta (DIRK22), an implicit timestepping scheme for temporal discretisation used for stability for the wetting and drying algorithm (Kärnä et al. 2011). In this thesis, all models used a timestep of 90 s with an output generated every 900 s. The Manning's coefficient, n, was set to 0.025, matching GBR Thetis parameters by Mawson, Lee, and Hill (2022) and Lee et al. (2022). The wetting and drying parameter was set using an automatic α, a function of resolution and slope: minimum α was set to 0.5 (allowing smooth transition between wet and dry states) and maximum α was set to 75.0 (controlling the resistance to drying in very steep areas). This maintains numeric stability whilst accounting for the steep slopes within the bathymetric data. Parameters were checked during the validation process, and modified if outputted tidal elevation and phase lags did not well match tidal gauge data: see validation section.

2.1.1 Mesh generation

Thetis requires a mesh on which to solve the equations, capable of handling fine resolution required for capturing fine-scale bathymetric complexities around coral atolls, and coarse resolution for deep open water. This requires a spatially varying mesh, allowing high resolution only in areas of interest. The whole of the GBR is modelled (see Fig. 2.2), the most southern point of the domain is K'gari and the most northern point is Somerset, Queensland. Bathymetry was taken from AusBathyTopo250m (Beaman 2023), the most recent 250 m resolution

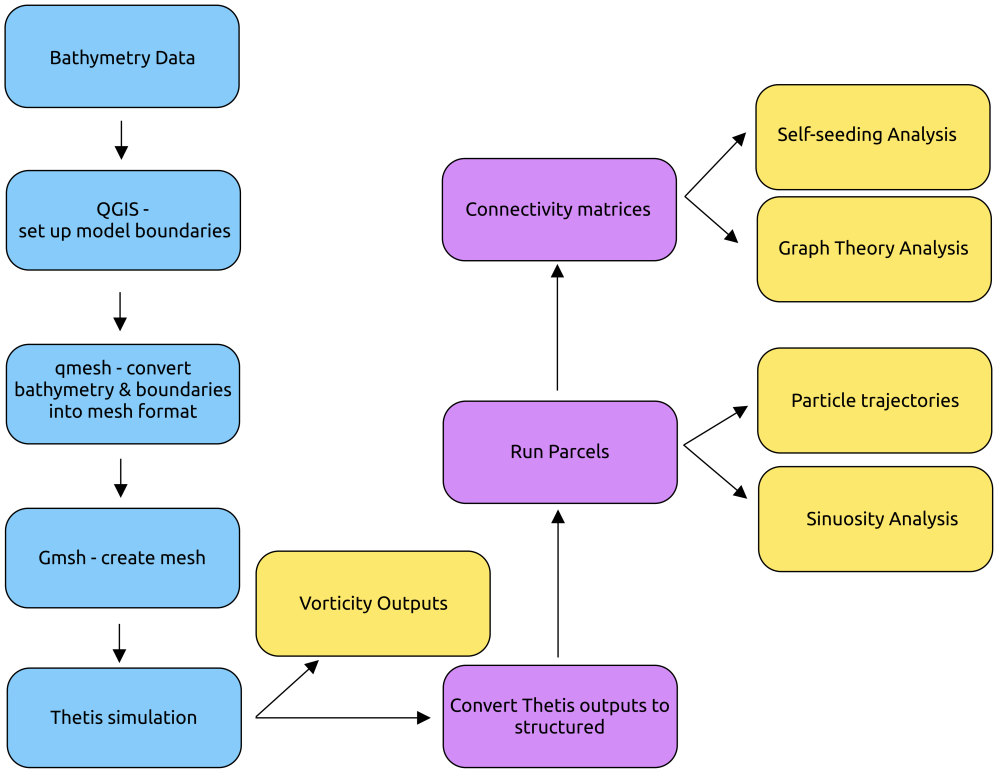


Figure 2.1: Work flow of developing GBR tidal model and integrating with Parcels tracking software. Blue icons represent the process of setting up the Thetis simulation, purple icons represent the process of running the Lagrangian particle tracking software to generate connectivity matrices, and yellow icons represent final outputs.

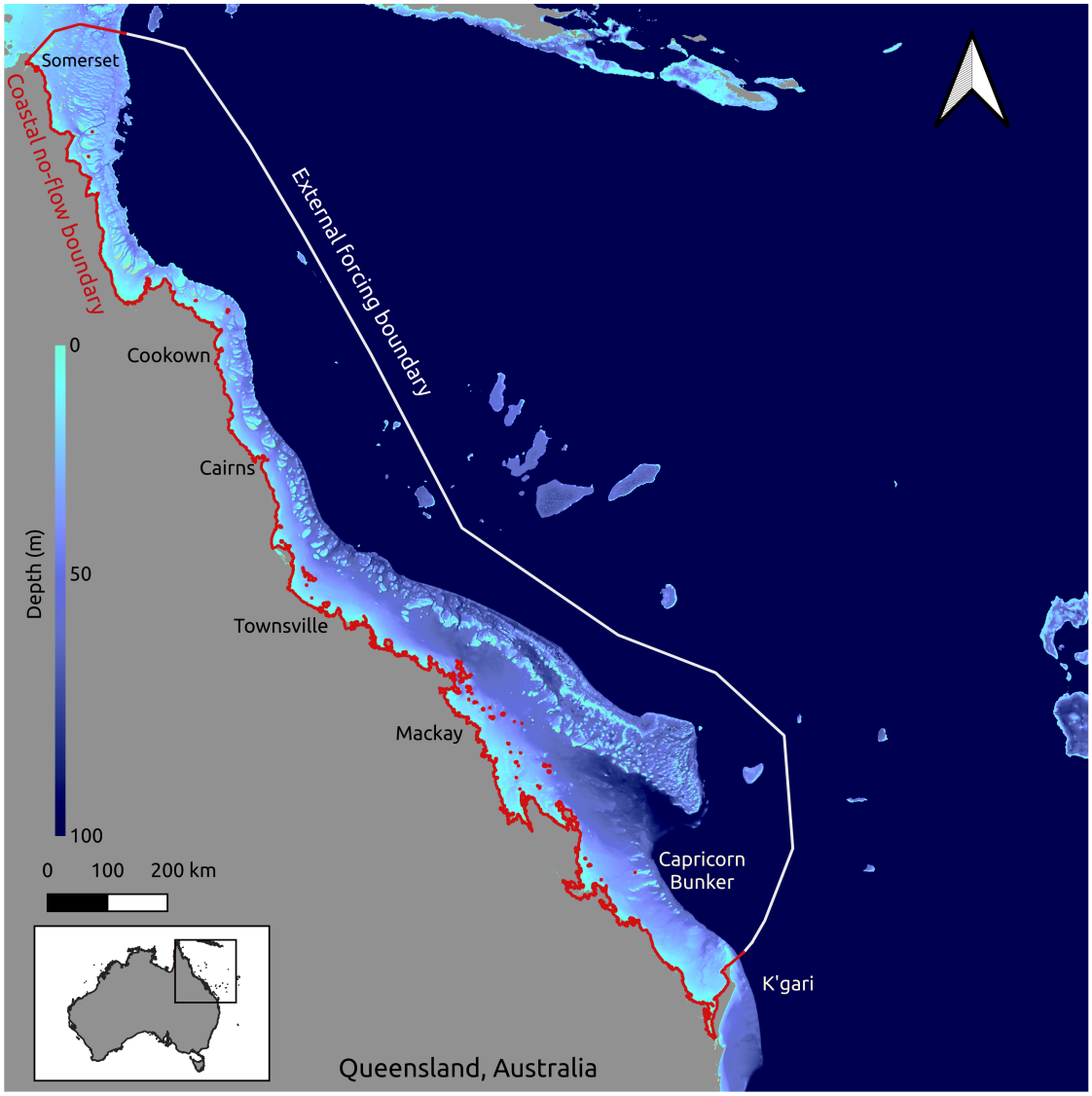


Figure 2.2: Model bathymetry and domain showing external forcing boundary in white and coastal no-flow boundary in red.

bathymetric data of Australia.

QGIS 3.12 (QGIS.org, 2020) was used to develop and modify the model domain. A 10 m contour line was extracted for the “coastline” boundary. This allows space for wetting and drying during the tidal cycle without boundary effects becoming an issue. It also allows for sea-level rise simulations without altering the mesh (see chapter 5). Small inlets along the coast smaller than 250 m (minimum resolution) were closed to prevent model instability. The external boundary was drawn from 10.19° S at the northern extent to 24° S at the southern extent and between 72,000 m and 250,000 m away from the shelf edge, to allow sufficient

space to generate accurate tidal forcing on the shelf without inefficient use resources simulating areas outside of interest. Within the model domain, small islands under 5000 m in perimeter were removed to prevent errors during mesh generation, as recommended by Avdis et al. (2018).

The model domain data is translated by $qmesh$ (Avdis et al. 2018) to the structure required by the mesh generator software $Gmesh$ (Geuzaine and Remacle 2009). $qmesh$ defines mesh elements of controlled shape and size using QGIS boundary and depth data. Once $qmesh$ has created a *Gmsh* input file from the QGIS data, $Gmsh$ generates a mesh according to a set of mesh metrics which control element size (see below) to create a spatially varying mesh resolution, covering spatial distances of hundreds of kilometres, as well as small coastal inlets only a few hundred meters wide. Mesh element size is defined as minimum 250 m and maximum 2 km, the size of each mesh element is controlled by the mesh metrics: element sizes will be smallest along coastlines and in shallow water, these are areas which require the highest resolution modelling for small-scale bathymetric features as well as any areas of interest (Fig. 2.3).

Mesh resolution is determined by four factors: depth from bathymetry, Ω_β; the gradient of bathymetry, Ω_g; distance from the coastlines, $\Omega_{\delta\epsilon}$ and distance from the boundary, $\Omega_{\delta\omega}$. The final mesh resolution, Ω, is the minimum of the four factors:

$$\Omega = \min\left(\Omega_\beta, \Omega_g, \Omega_{\delta\epsilon}, \Omega_{\delta\omega}\right) \tag{2.5}$$

Bathymetric depth was controlled by:

$$\Omega_\beta = \cosh\left(\frac{\beta}{\gamma}\right) \tag{2.6}$$

where β is the topographic height. For modern meshes γ was 17. For palaeo-simulations, γ was 15 (see chapter 4).

The gradient term was based on a simple finite element gradient ($\Delta\beta$) with a difference step of 10 km. The gradient was then modified to produce a edge-length metric based on:

$$\Omega_g = 750 \cdot \sinh\left(\frac{-\Delta\beta + 0.3}{0.05}\right) \tag{2.7}$$

A linear increase in mesh size from the coastline boundary was defined as:

$$\Omega_{\delta\epsilon}(d) = \begin{cases} L_{min} & 0 \leq d \leq d_0 \\ L_{min} + (L_{max} - L_{min})\left(\frac{d-d_0}{d_1-d_0}\right) & d_0 < d < d_1 \\ L_{max} & d > d_1 \end{cases} \tag{2.8}$$

where d is the distance to coastline, L_{min} is the minimum edge-length required, L_{max} is the maximum edge length required, d_0 is the minimum distance and d_1 is the maximum distance. In the modern and future models, resolution L_{min} is set to 500, increasing to L_{max} 15,000 linearly, to the distance of d_1 = 20,000, with the first d_0 = 1000 m fixed to L_{min}. In the palaeo-models L_{min} is set to 750, L_{max} is set to 15,000, d_0 is set to 1500 and d_1 is set to 25,000, these different metric parameters were used to reduce the higher number of elements in the palaeo meshes to a more tractable number (4 million elements).

Similarly, resolution increased as a function of distance from the external boundary, calculated using:

$$\Omega_{\delta\omega}(d) = \begin{cases} L_{\text{min}} & 0 \leq d \leq d_0 \\ L_{\text{min}} + (L_{\text{max}} - L_{\text{min}})\left(\frac{d-d_0}{d_1-d_0}\right) & d_0 < d < d_1 \\ L_{\text{max}} & d > d_1 \end{cases} \tag{2.9}$$

For the external boundary, both modern, future and palaeo model resolution increased from L_{min} = 7500 m to L_{max} = 15,000 m linearly to a distance of d_1 =

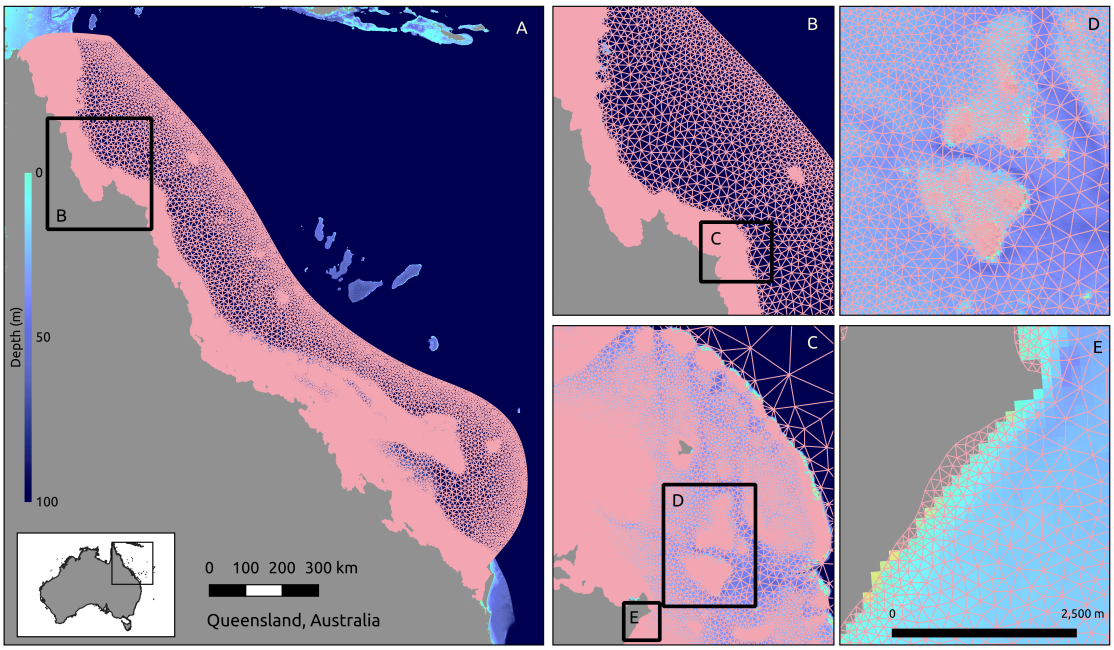


Figure 2.3: Unstructured mesh shown at different distances. A. shows the whole domain with resolution ranging from 250 m to 2000 m resolution. B. shows the resolution different between reefs along the coastline and the external boundary. C. zooms in further to show the seamless changes in high resolution between reefs. E. shows the wetting and drying area where the mesh has covered part of the coast

15,000 m away from the boundary, with the nearest d_0 = 7550 m fixed at L_{min}.

2.1.2 Model Setup Data

The present day tidal model used for validation in this chapter underwent a spin-up of 5 days before being run for a further 30 days to capture the full spring-neap cycle and ensure correct diagnostics of the four principal tidal constituents (M2, S2, K1, and O1) according the Rayleigh Criterion, which dictates the minimum amount of time needed to separate tidal constituents from each other, typically 14.7 days is required to separate M2 and S2. The 30 days of simulation ensured two full tidal cycles were captured for validation. The annual mass spawning event simulated here matches the 17-19th November 2000 annual mass spawning, as recorded by McCormick 2003, beginning at midnight of the 17th and lasting

Data	Use	Reference
AusBathyTopo250	Model bathymetry	Beaman 2023
TPXO	Tidal forcing data	Egbert and Erofeeva 2002
AHO AusTides	Tidal Gauge data model for validation	https://www.hydro.gov.au/prodserv/publications/ausTides/tides.htm
ERA5	Wind and atmospheric pressure forcing data (see chapter 3)	Hersbach et al. 2023
Great Barrier Reef (GBR) Features	GBR reef shapefiles	GBRMPA, 2014

Table 2.1: Table of data used for methods

for 48 hours. This spawning event took place under normal weather conditions with no reported anomalies, and can therefore be used to assess general trends in transportation. The model ran from the 12th November 2000 to allow time for spin-up before capturing the mass spawning event. Finally, tidal boundary conditions for tide-only models throughout the thesis are applied via TPXO (Egbert and Erofeeva 2002) (see table. 2.1) to the elevation. Tidal forcing data used here does not include temperature or salinity. Wind forcing can be applied. A no-flow boundary condition is used on the "coastal" boundary (Fig. 2.2). Details of data used throughout this thesis can be found in table 2.1.

2.1.3 Validation

Thetis outputs are validated by comparing elevation from an entire lunar cycle (30 days) against AHO AusTides data (https://tinyurl.com/3a9swx4c). The four major tidal constituents S2, M2, O1 and K1 were compared against AHO tidal observations amplitude measurements at 126 tidal gauge locations, as done in Lee et al. 2022; Mawson, Lee, and Hill 2022. A sample of five tidal gauge locations and their respective tidal elevation comparisons are shown in Fig. 2.5, capturing the northern, central, southern sectors of the GBR, as well as the Capricorn Bunker. The figure shows well-matched comparisons of tidal elevation, with Thetis slightly under-predicting elevation of the neap tide at Triangle Reed and Tideway Reef.

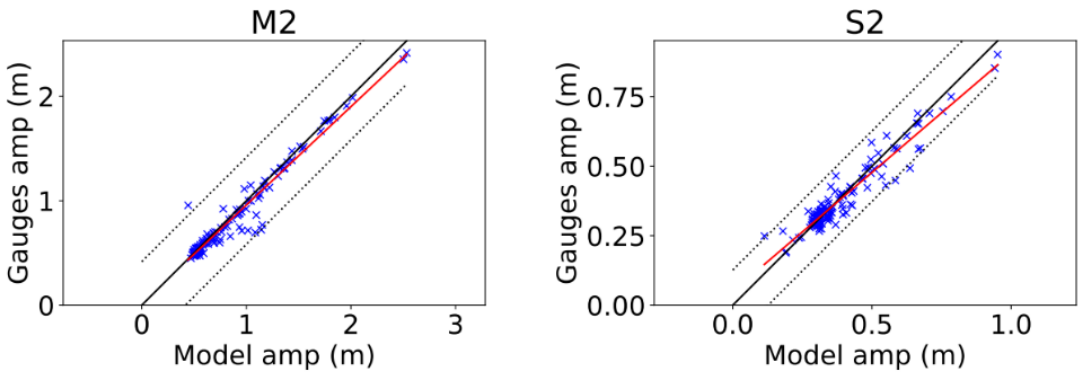


Figure 2.4: Cross plots for Thetis vs. observations for tidal constituents M2 and S2

Table 2.2 shows tidal constituents results: M2 and S2 are the two most significant constituents on the GBR and were those most accurately predicted by Thetis (standard error 1.9 cm and 2.3 cm respectively). O1 performed least well (standard error 8.8 cm). All tidal constituent amplitude measurements predicted by Thetis are acceptable for validation as they show strong agreement with tidal gauge data and are statistically significant ($p < 0.01$). Crossplots of constituent M2 and S2 amplitudes (Fig. 2.4) were generated to compare estimates by Thetis compared to observed tidal amplitudes. Thetis shows an excellent fit with observed amplitude for M2 constituent, as well as a good prediction for S2 amplitude, indicating a similar trend to elevation predictions by Thetis.

Constituent	r	p value	Std. error (m)
M2	0.975	< 0.01	0.019
S2	0.958	< 0.01	0.023
K1	0.860	< 0.01	0.054
O1	0.780	< 0.01	0.090

Table 2.2: Tidal constituent validation using Pearson correlation analysis.

2.2 Larvae transportation

To track coral larvae, Lagrangian particle tracking software Parcels (Probably A Really Computationally Efficient Lagrangian Simulator) v2.0 (Delandmeter and Sebille 2019) was used. Parcels is an open-source framework for Lagrangian passive and active particle tracking, which was paired with tidal velocity rasters gener-

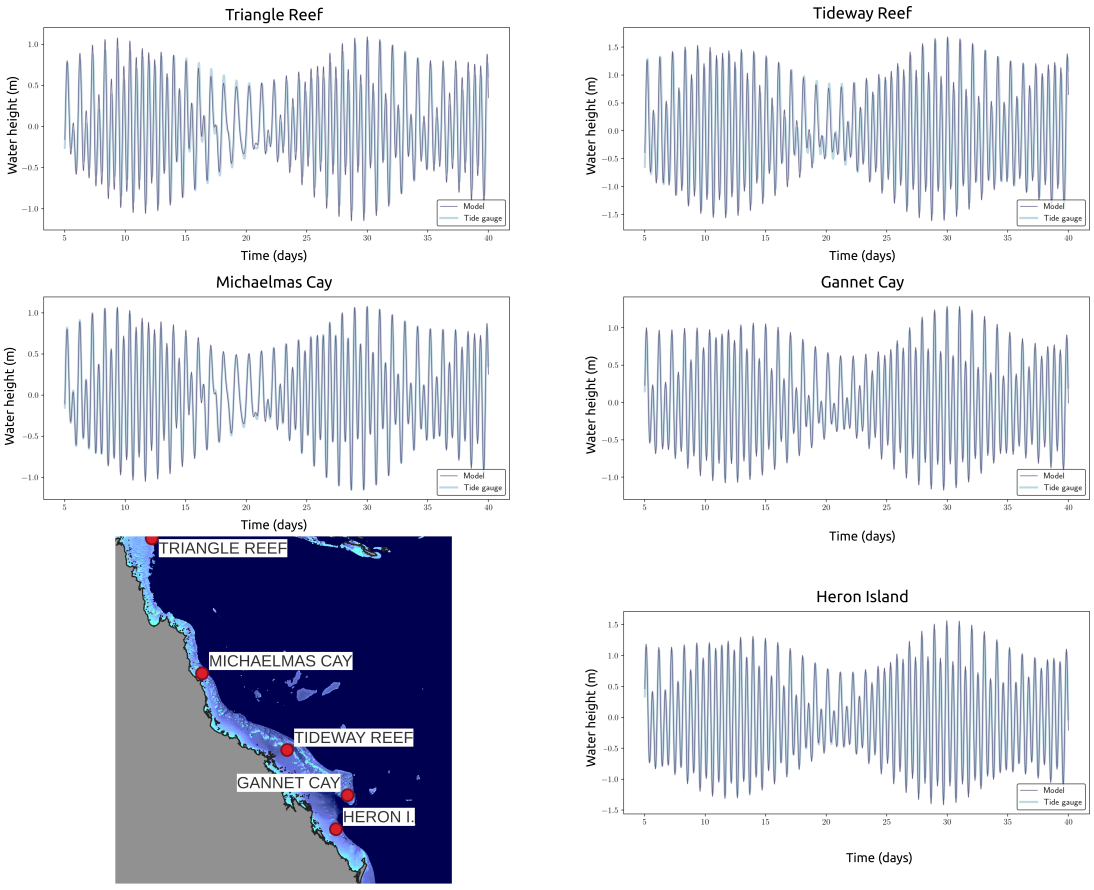


Figure 2.5: Validation against AusTides tidal gauges, showing 5 of the 125 tidal gauge locations used in validation. Tidal elevation graphs show Thetis elevation predictions compared to the AusTides data. Locations of these tidal stations are shown in the map.

ated by Thetis tidal and wind models. Parcels uses an advection algorithm to compute Lagrangian trajectories:

$$\mathbf{X}(t + \Delta t) = \mathbf{X}(t) + \int_{t}^{t+\Delta t} \upsilon(x, \tau) + \Delta \mathbf{X}_b(t) \tag{2.10}$$

where t is the current time, Δt is the timestep, $\mathbf{X}$ is the three-dimensional position of a particle (note only two-dimensional data was used here), $\Delta \mathbf{X}_b(t)$ is a change in position due to behaviour, such as from downward velocity in the 3D model, diffusion, or swimming, and $\upsilon(x, \tau)$ is the three-dimensional velocity field at that location from the model. Equation 2.10 is time-stepped using a forth-order Runge-Kutta scheme. A 10 minute time-step was used, with outputs generated every 30 minutes.

In this thesis, particles are simulated via two-dimensional surface velocities, ideal for simulating surface movement of larvae slicks (Thomas et al. 2014; Oliver and Willis 1987; Willis and Oliver 1990; Wolanski, Burrage, and King 1989). Parcels is capable of particle diffusion using stochastic differential equations to introduce random displacement of particles to produce sub-grid scale effects. However diffusion is not included in Parcels simulations used in this thesis, as this is only relevant in large-scale ocean modelling where effects of mesoscale eddies have not been captured by coarse velocity fields. In this thesis, velocity fields are high resolution and as a coastal region is being simulated, mesoscale eddies do not need to be taken into consideration for particle diffusion. Although coral larvae are capable of swimming, the dominant mechanism of transport is passive (Vermeij et al. 2010; Carlon and Olson 1993; Vogt-Vincent et al. 2024; Thomas et al. 2014), therefore Lagrangian modelling of larvae in this thesis will be passively modelled.

After a tidal simulation is completed, the model domain is divided into 11 sections matching the Australian Institute of Marine Science (AIMS) reef monitoring sectors of the GBR. Three sectors were selected to carry out Lagrangian particle

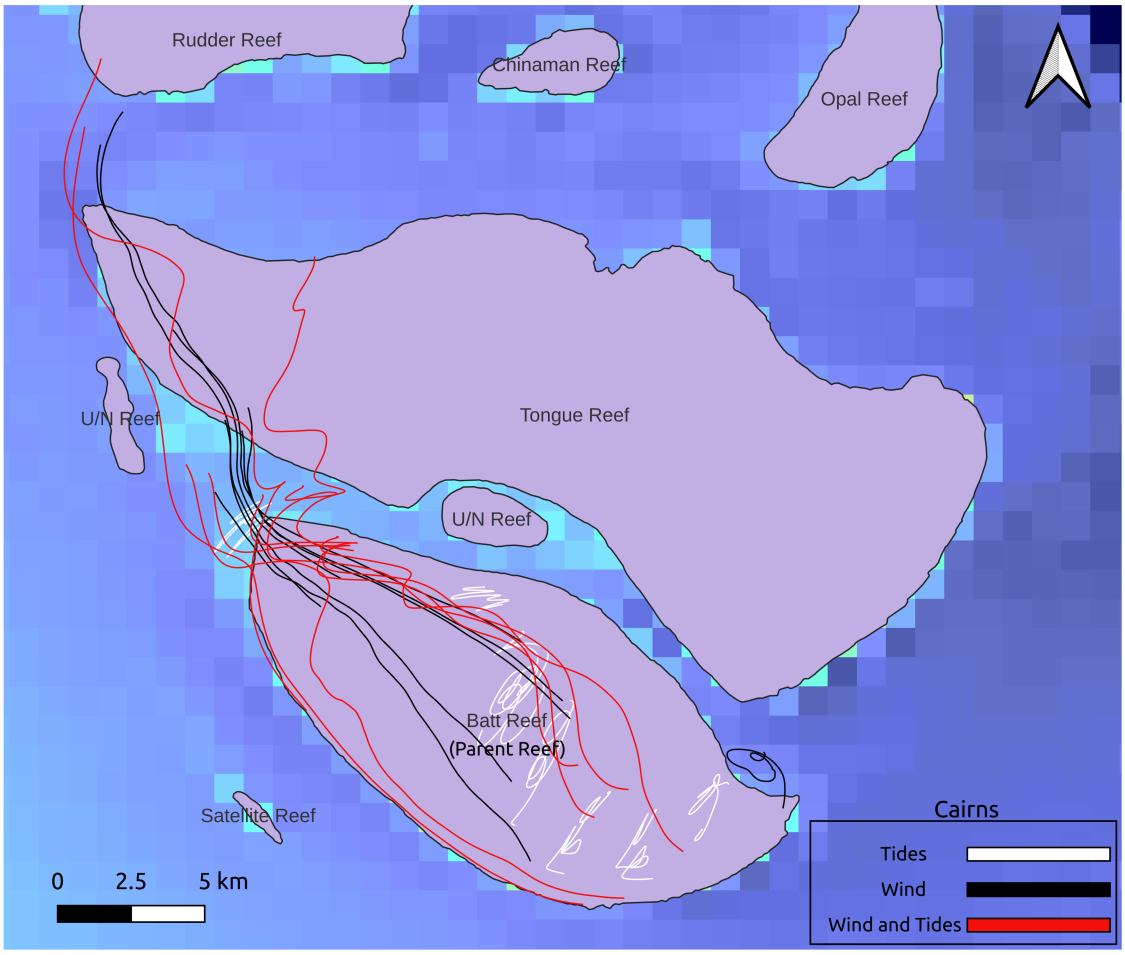


Figure 2.6: Example of Reef shapefiles in Cairns sector released from Batt Reef, illustrating start and end position of released particles within different models. Colours of trajectories indicate which model was used. Blue shows water depth. Purple areas are reef polygons used for releasing and receiving particles.

tracking: Swain Area (20°, 151° S to 23°, 153° S), Cairns (15°, 145° S to 16°, 145° S) and Cape Grenville (10°, 142° S to 12°, 143° S) to represent the southern, central and northern GBR respectively. Particles were released and captured from present day GBR reef location shapefile derived from eAtlas Great Barrier Reef Features (Hammerton and Lawrey 2024) (table 2.1). For each model throughout this thesis, particles were released from reefs at midnight of the 17th November 2000 and tracked for 48 hours (Fig. 2.6).

2.2.1 Resolution testing

Parcels requires a structured mesh to calculate particle tracking. However, as Thetis uses an unstructured mesh, the unstructured data needs to be interpolated onto a structured mesh. Velocity rasters are used by Parcels to calculate surface movement, therefore velocity is extracted from the unstructured mesh outputs and interpolated onto a structured mesh. However, the resolution of the unstructured triangular mesh varies in resolution from 250 m to 20,000 m, therefore the most efficient resolution for these structured rasters needs to be determined. Seven tests were performed to compare resolutions: 6000 m, 5000 m, 4000 m, 2500 m, 1250 m, 750 m and 500 m. Simulations were carried out in the Swain area with 100 particles released per 1 km^2 of reef area (see next section), reefs smaller than 1 km^2 in size had the same number of particles released as a reef 1 km^2 in size, as in Mayorga-Adame, Batchelder, and Spitz (2017). For each raster resolution, particles were tracked for 48 hours and used to generate particle trajectory shapefiles (Fig. 2.6), which could be analysed for differences in sinuosity (ζ, eq. 3.3) to show if resolution affects particle trajectories. Sinuosity values of 1 are a straight line, the larger the value the more curvature the trajectory contains. A sinuosity value of infinity would be a complete circle. This test examines when sinuosity values stabilise, ensuring that the chosen resolution does not unduly influence particle trajectories. Sinuosity is calculated as:

$$\zeta = \frac{\Phi}{\Psi} \tag{2.11}$$

where ζ is sinuosity, Ψ is straight distance of trajectory and Φ is length of trajectory.

Statistical differences between velocity raster resolutions were observed following using a Wilcoxon test to compare the median sinuosity values across the seven velocity raster resolutions: $X_2(6)$ = 15,862, $p < 0.0001$ (Fig. 2.7). A Dunn's

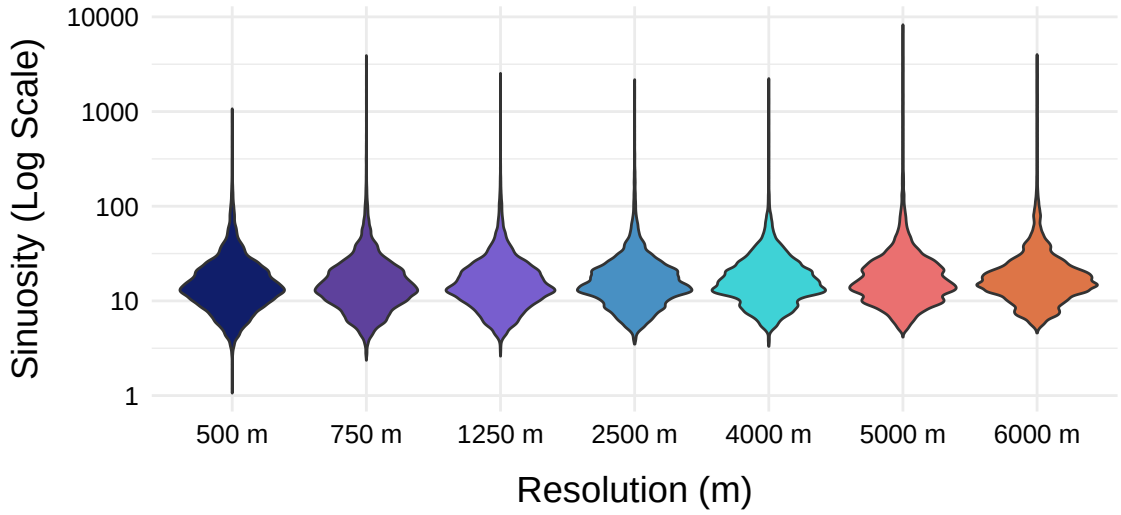


Figure 2.7: Violin plots of levels of sinuosity variation across 7 different velocity raster resolutions.

post-hoc test was conducted, revealing significant difference between all groups ($p < 0.0001$, Bonferroni corrected). For example, sinuosity at 500 metres was significantly lower than 750 meter resolution ($Z = -4.85, p < 0.0001$), and significantly lower than at 6000 meters ($Z = -89.69, p < 0.0001$). Cohen's d effect size was calculated for each comparison, effect sizes were small between all resolution pairs ($d < 0.2$), indicating minimal practical differences in resolution despite statistical significance. This indicated that despite different resolution leading to statistically different median sinuosity values, using 6000 m resolution rasters would not create practical differences to 500 m resolution rasters for sinuosity values. This was surprising given the range between minimum and maximum resolutions tested, however this finding is supported by a study done by Saint-Amand et al. (2023) where resolution does not cause variation in dispersal within 48 hours of release, resolution was found to only affect particle transportation weeks after release in the GBR. Figure 2.7 also shows that lower values of sinuosity reduce as resolution becomes coarser, this may be due to particles becoming stuck (such as if released in a dry area) more frequently at a higher resolution.

2.2.2 Particle Numbers

Releasing particles per km^2 means that all reefs are scaled appropriately for their size (Thomas et al. 2014). To determine the minimum number of particles to release from each reef per 1 km^2 to produce stable self-seeding simulation, four convergence tests were run. The first test released 1 particle per km^2 across all reefs (2160 particles total), reefs under 1 km^2 had 1 particle released, reef size is rounded up, matching work by Mayorga-Adame, Batchelder, and Spitz (2017) and Vogt-Vincent and Mitarai (2020). The second test released 10 particles per 1 km^2 (21,600 particles total), the third test released 100 particles per 1 km^2 (216,100 particles total) and the final test released 1000 particles per 1 m^2 (2,161,000 particles total). Each test used a 500 m velocity raster across the Swain Area. Following each of these simulations, a diagonal analysis of connectivity matrices and statistical tests were performed to find convergence points of stability.

Particles were tracked for 48 hours and were considered settled onto a reef at the end of 48 hours if the particle was within a reef, or within 10 m of a reef (Mayorga-Adame, Batchelder, and Spitz 2017), as Acropora larvae are capable of sensing a reef from 10 m due to their ability to hear reefs (Vermeij et al. 2010; Baird et al. 2014). For each simulated larva, start and end points were analysed to produce a connectivity matrix to show seeding behaviour. As the connectivity matrix is a uni-partite adjacency matrix, values on the diagonal of the connectivity matrix correlate to self-seeding reefs. Diagonal values were extracted from the matrices and compared against the different particle number tests using a non-parametric Kruskal-Wallis test.

Diagonal element analysis was carried out on the four particle number experiments, using a Kruskal-Wallis non-parametric test showed there was statistically different variation among the four tests $X_2(3) = 80.57$, $p < 0.001$. The statistical difference was found by a Pairwise Wilcoxon rank-sum test to be between 1 particle per km^2 and all other groups ($p < 0.001$). Releasing particle numbers between 10

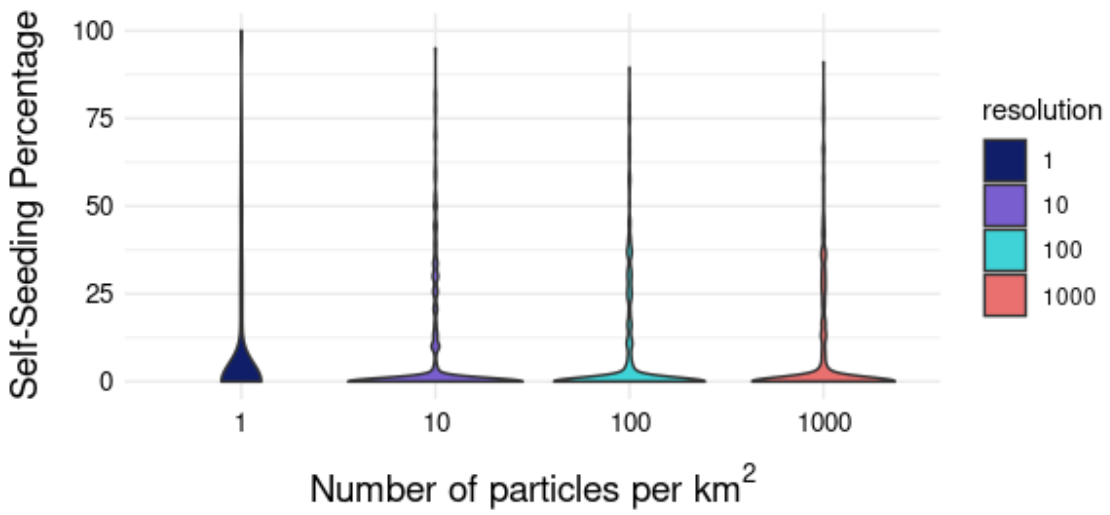


Figure 2.8: Violin plot of self-seeding percentage for varying particle numbers released per km^2

and 1000 per km^2 would not produce statistical differences in self-seeding behaviour (Fig. 2.8). Releasing 1 particle per km^2 created a statistically different result due to the consequence of rounding up the number of particles released per km^2: in small sample sizes, such as 1 particle per km^2, the rounding effect is large, whereas when more particles are released, the sample size difference is more approximated.

2.3 Summary

In summary, Thetis was used to develop finite element models of the GBR using an unstructured mesh, with minimum resolution set to 250 m, and the models were validated using AHO AusTides. Models were set up with boundary conditions to be forced with tidal data, from TPXO, and with wind data from ERA5, in preparation for a subsequent chapter. Following completion of tidal models, velocity outputs were extracted and converted to structured raster format in order to be compatible with Lagrangian particle tracking software Parcels. Parametrization of resolution and number of particles released underwent testing for calibration, the tests showed that 10 or more particles needed to be released per km^2 of reef to provide stable outputs, and that the velocity raster resolution could be 500 m

to 6000 m without affecting results of self-connectivity. Here, 500 m resolution was chosen for the subsequent chapters. The methodology detailed in this chapter will be used in each subsequent chapter, with alterations made to bathymetry, depending on what sea-levels are being investigated; boundary conditions, depending on whether wind or tides are being modelled; and reef location, again depending on what sea-levels are being investigated.

Chapter 3

Winds Vs Tides - What drives coral larvae dispersal on the GBR?

This chapter investigates the difference physical drivers make to the transportation of coral larvae and self-seeding behaviour. Three numerical models are developed of the Great Barrier Reef to simulate tidal and wind dynamics, both separately and together, which are used for tidal analysis and integrating with Lagrangian Particle Tracking software. Throughout three sections in the south, central and northern GBR, particles representing coral larvae are released from reef polygons and tracked for developing connectivity matrices. Self-seeding reefs are defined as a reef which receives the larvae it produces, levels of self-seeding are assessed using connectivity matrices produced by each of the three models. This information is extracted from connectivity matrices using diagonal analysis and used to assess changes to self-seeding behaviour. The findings of this chapter will be used to answer "what are the differing effects of wind and tides on coral larvae transportation when modelled separately?" and "what is the mechanism behind self-seeding behaviour?". Finally, as this study focuses on the present day GBR, the findings will be used to inform work in subsequent chapters on past and future sea-levels.

3.1 Introduction

3.1.1 Mass spawning event

The Great Barrier Reef (GBR) is the world's largest coral reef, hosting approximately 2,500 individual reefs and reaching 2000 km on the north-east continental shelf of Australia where it experiences complex and intricate tidal dynamics (Hughes et al. 1999). The GBR hosts over 120 species of scleractinian corals, all of which have evolved to depend on water circulation to maintain gene flow, nutrients, and temperature (Andutta, Kingsford, and Wolanski 2012; Raitsos et al. 2017; Babcock et al. 1986).

Once a year, 105 species of coral collectively spawn on the spring full moon of November, causing huge concentrations of gametes to enter the tidal system (Willis et al. 1985; Babcock et al. 1986). Broadcast corals release their gametes into the water column for fertilisation, these float on the surface for 48 hours before sinking to the substrate for settlement (Miller and Mundy 2003; Oliver and Willis 1987). For some broadcast larvae, such as from *Platygyra daedalea* and *Goniastrea favulus*, it can take less than 2 days to settle after being released, with all remaining larvae settled 60 - 66 hours after release (Miller and Mundy 2003; Randall et al. 2024). There have been a few species of *Acropora* larvae found able to survive for up to 90 days, enabling long distance transport (Harrison et al. 1984). Following release large slicks can form on the surface, sometimes up to 5 km in length and 10 m wide, preventing larvae from being washed into the Coral Sea, and enable self-seeding – where the reef which released the larvae, receive it back (Sammarco and Andrews 1988; Kingsford, Wolanski, and Choat 1991; Wolanski, Burrage, and King 1989). The timing of the GBR mass spawning event is believed to be synchronised with the smallest neap tide of the year, a difference of 0.5 m between high and low tide, which results in a long period of little tidal movement (Babcock et al. 1986). The timing is also consistent with a calm period

of regional wind fields, leading to weak wind-driven currents, preventing long distance dispersal (Woesik 2010). Therefore, during the annual mass spawning event, the two main dispersal mechanisms are both at their weakest.

3.1.2 Tidal dynamics

Tidal constituents Transport of water through the GBR is controlled by the Coral Sea and five dominant tidal constituents: M2, S2, N2, O1 and K1, it is also affected by complex bathymetry and wind throughout the lagoon and reef areas (Andrews and Bode 1988; Lambrechts et al. 2008). The lagoon and reef areas on the continental shelf are an average depth of 20 m while the shelf edge has a depth of ∼100 m before dropping to 1500 m in the Coral Sea (Wolanski 1983). The complex bathymetry is created by a dense matrix of reefs, causing cross-shore gradients in radiation stress by sitting higher than the seabed, reefs also often reach the surface, occasionally being exposed, leading to complex and ever changing paths for tides to flow through (Andutta, Kingsford, and Wolanski 2012).

Water circulation is also heavily impacted by wind as trade and local winds generate currents across the whole GBR (Lambrechts et al. 2008). Wind also drives vertical mixing, influencing sediment transportation and producing Langmuir circulations (Wolanski et al. 1988). Light winds (5-15 knots) during the mass spawning event have been observed to assist with transporting larvae slicks across the sea surface but stronger winds have been recorded to break up the slicks and lead to far distribution, resulting in low concentrations of coral larvae around the parent reef (Willis and Oliver 1988). Records have shown that slicks can generally persist in winds up to 20 knots and waves 1.5 m in height but those same conditions present during spawning may impede slick formation (Oliver and Willis 1987). Wind has been observed to determine the direction and distance of larvae transport, even in calm conditions (Willis and Oliver 1990).

3.1.3 Influence of winds and tides on larvae dispersal

On the GBR, the combination of wind, tides and bathymetry control connectivity between networks of reefs (Wolanski et al. 1988). GBR connectivity studies differ in concluding whether wind or tides are the dominant force responsible for coral larvae transportation (Willis and Oliver 1988; Williams, Wolanski, and Andrews 1984; Andutta, Kingsford, and Wolanski 2012; Miller and Mundy 2003), and what is the physical mechanism behind self-seeding (Wolanski, Burrage, and King 1989; Schlaefer et al. 2018; Sammarco and Andrews 1988; Black 1993). The spawning event is timed to the least windy time of year (Woesik 2010), as well as during the smallest neap tide of the year (Babcock et al. 1986), proposed to be a strategy to have the highest chance of retaining larvae, resulting in self-seeding (Wolanski et al. 1988). However, as larvae float on the surface, even light winds disperse larvae away from parent reefs (Williams, Wolanski, and Andrews 1984; Wolanski, Burrage, and King 1989).

Tidally driven motions are correlated with self-seeding behaviour, although presence of longshore currents can transport larvae downstream (Wolanski, Burrage, and King 1989). An example of tidally driven retention is a tidal phenomenon called 'Sticky Water' (Wolanski 1994), a process where regions of high-reef density become less permeable to currents during spring tides, leading to water becoming trapped in these regions (Wolanski and Spagnol 2000). Eddies produced in the lee of islands have been found to have a significant impact on the ecosystem due to retaining coral and fish larvae around the reef (Kingsford, Wolanski, and Choat 1991; Wolanski et al. 1988; Thompson et al. 2018). In general, self-seeding only happens on short time frames (Miller and Mundy 2003), such as during the annual mass spawning event where the lifespan of the gamete is short; when the lifespan is longer, larvae are able to travel further and do not self-seed (Thompson et al. 2018; Sammarco and Andrews 1988).

Field studies rely on empirical observations typically carried out on a handful of

reefs used for research observations (Wolanski, Burrage, and King 1989; Willis and Oliver 1988; Willis et al. 1985), typically these are fairly close to the coast and in the central GBR, therefore unlikely to provide the trend of the entire GBR. Local field observations are unlikely to capture large-scale trends, it is also difficult to separate the effects of wind from tides in field observations.

In previous studies of GBR connectivity, numerical modelling has been employed for simulating tidal dynamics and connectivity of the GBR, due to the ease of investigating large spatial scales (Thomas et al. 2014; Andutta, Kingsford, and Wolanski 2012; Schill et al. 2015; Hock et al. 2017). However, numerical models have not yet been used to compare the effects of wind and tides separately to study the effects of transportation of coral larvae following the annual mass spawning event. Nor have studies yet explored self-seeding mechanisms, as studies so far have looked at time frames of weeks or months (Hock et al. 2017; Hock et al. 2019; Thomas et al. 2014), which miss short-term self-seeding behaviour (Miller and Mundy 2003; Sammarco 1980; Sammarco and Andrews 1988). In this study, numerical modelling will be used to investigate whether tides or wind have greater impact on coral larvae transportation and connectivity during annual mass spawning events. In particular, mechanisms behind self-seeding behaviour will be examined.

3.1.4 Research Questions

The key questions of this study are:

1. **What are the differing effects of wind and tides on coral larvae transportation?**
2. **What is the mechanism behind self-seeding behaviour?**

3.2 Methods

Chapter 2 contains all general information on creating and running numerical models along with integrating Lagrangian particle tracking to simulate the movement of coral larvae.

3.2.1 Study Site

The whole of the GBR is modelled in this study, however only three sectors are studied for coral connectivity: Swain Reef Area (Southern GBR), Cairns (Central GBR) and Cape Grenville (Northern GBR) (Fig. 3.1) (see chapter 2 for more information). From henceforth, Swain Area sector will be referred to as Swain, Cape Grenville will be referred to as Grenville and Cairns will continue to be referred to as Cairns. The annual mass spawning event simulated here matches the 17-19th November 2000 annual mass spawning (McCormick 2003). The mass spawning event began at midnight of the 17th November 2000 and lasted for 48 hours with no weather anomalies.

3.2.2 Simulation set-up

One unstructured mesh is created to run three models with the finite element model Thetis (Kärnä et al. 2018) (see methods section) to investigate the effect tides and wind have on coral larvae transportation: 1) a model containing tidal forcing only, 2) another containing wind forcing only and 3) a model of wind and tidal forcing together (Table 3.1). A simulation with neither tides nor winds was inappropriate in this case, as the simulation would be stagnant with no significant diffusion. From henceforth, the tidal forcing only model will be referred to as TO, the wind forcing only model will be referred to as WO and the tidal and wind forcings combined model will be referred to as WT. When referring to a specific sector and model run, sector models will be referred to as the name of the

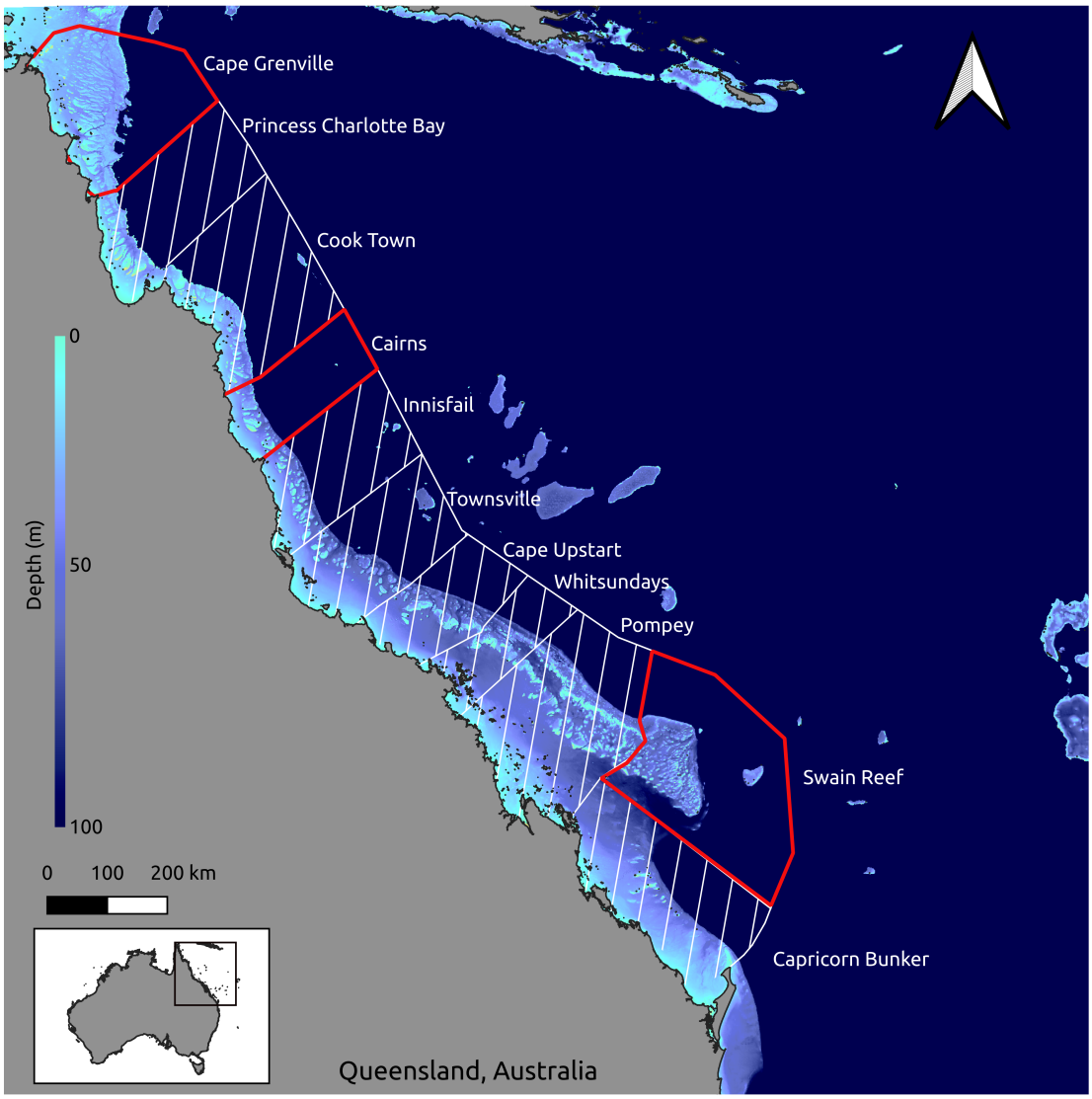


Figure 3.1: Map of model domain separated into 11 sectors. 3 sectors of interest are highlighted in red.

sector with the model acronym as subscript, for example, Cairns TO model will be referred to as $\text{Cairns}_{\text{TO}}$. Tidal forcing is described in the methods chapter. Hourly wind forcing data was extracted from ERA5 Copernicus Climate Change Service (C3S) (Hersbach et al. 2023) for the chosen time period and forced the velocity via wind stress. Surface pressure from ERA5 was also used, forcing the surface elevation across the whole modelled domain (see figure 3.4). ERA5 data is transferred to the ocean surface in Thetis by computing wind stress and added to the velocity as shown in Equation 3.1:

$$\tau_w = C_D \rho_{air} \|\mathbf{U}_{10}\| \mathbf{U}_{10} \tag{3.1}$$

where C_D is the drag coefficient, ρ_{air} is the density of air and U_{10} is wind speed 10 m above the sea surface (Kärnä et al. 2018). The drag coefficient, C_D was formulated following Large and Yeager (2009).

Simulation	Tides	Wind
Tides Only	×	
Wind Only		×
Wind and Tides	×	×

Table 3.1: Table showing simulation setup

The TO model underwent a spin-up of 5 days before being run for a further 30 days to capture the spring-neap cycle, spin-up time is not used in model analysis. The model was started from the 12th November 2000 in order to capture data across the mass spawning event following the spin-up period (see chapter 2 for more information). WO and WT models were simulated for 5 days of spin-up followed by 48 hours to capture the annual mass spawning event. Wind models were not validated against observed tidal data, raw tidal data for Australia containing wind is not attainable, especially for the simulated time. Instead, it is widely accepted that ERA5 wind data has been extensively used in validated models (Garrard et al. 2024; Vogt-Vincent, Mitarai, and Johnson 2023; Richards et al. 2024) and as Thetis has also been extensively used and validated, it can be assumed that models

containing wind forcing are correct.

3.2.3 Larvae transportation

To track particle larvae transportation via TO, WO and WT, Parcels (Delandmeter and Sebille 2019) was run with each of the three GBR sectors for each simulation, producing nine particle tracking simulations in total (see chapter 2). A total of 256 particles per km^2 from each reef were released for 48 hours, resulting in 1,813,504 particles released in Grenville, 269,312 in Cairns and 580,352 in Swain. These numbers are in line with particle number testing (see chapter 2 for more information), and matching particle numbers released in previous work done by (Vogt-Vincent and Mitarai 2020; Vogt-Vincent, Mitarai, and Johnson 2023; Vogt-Vincent et al. 2024; Mayorga-Adame, Batchelder, and Spitz 2017; Thomas et al. 2014) . After 48 hours, particles whose end point was within a reef polygon or within 10 m of a reef polygon were recorded along with the parent reef ID. Tracking locations of particles at the end of 48 hours allows the capture of the earliest settling larvae from broadcasting corals, such as *Platygyra daedalea* (Miller and Mundy 2003; Randall et al. 2024), brooding coral larvae is able to settle immediately following release (Fadlallah and Pearse 1982; Harrison and Wallace 1990). As self-seeding is linked to shorter periods of time in the water column (Crimp and Braddock 1993), and also linked to coral slicks which only last 48 hours after release (Oliver and Willis 1987; Wolanski, Burrage, and King 1989), tracking particles for 48 hours was deemed appropriate for monitoring self-seeding mechanisms.

3.2.4 Analysis

3.2.4.1 Transport

To explore the mechanisms behind larvae retention and dispersal, average vorticity measurements were extracted from each sector within the Thetis simulations as a metric for the amount of eddies occurring (equation 3.2). As vorticity is a

measurement of the curl of velocity, it is expected that self-seeding reefs are in areas of high vorticity with larvae circling the parent reefs, if this is shown to be the case, vorticity can be linked to particle retention.

$$w = -v_x - v_y, \tag{3.2}$$

for a velocity field, $\mathbf{u} = (u, v)$. The calculation is carried out in $\mathbb{P}1$ space (linear continuous Galerkin).

Along with vorticity, sinuosity, (equation 3.3) is also used to quantify circular motion linked with retention. Values closer to 1 correspond to a straight trajectory, whereas trajectories which are more circular in shape will have a higher sinuosity value. It is expected that areas of high vorticity will have areas of high sinuosity values for particle trajectories, which would also be expected to correspond to areas with high rates of self-seeding. Trajectory shapefiles of particles were extracted from Parcel outputs and analysed for length of trajectory and straight line distance between start and end point to solve equation 3.3:

$$\zeta = \frac{\Phi}{\Psi} \tag{3.3}$$

where ζ is sinuosity, Ψ is straight distance of trajectory and Φ is length of trajectory. Statistical analysis is carried out using a Kruskal-Wallis test, to determine whether there are significant differences in sinuosity for WO, TO and WT within the three sectors. For significant results found by the Kruskal-Wallis test, η^2 was used to measure effect size for each sector.

3.2.4.2 Connectivity

To compare differences between self-seeding behaviour throughout three sectors, depending on whether they had been forced using TO, WO or WT, a combination of approaches looking at connectivity were carried out. Adjacency con-

nectivity matrices were created from Parcels outputs to record the number of particles transferred between reefs, along with the name of sink and source reefs. Larvae which has self-seeded, is recorded on the diagonal of the matrix (Duan et al. 2023). Visual assessment of connectivity matrices is difficult due to their sparseness, therefore the connectivity matrices will be used for statistical analysis and network analysis (Zalesky, Fornito, and Bullmore 2012; Jacobi and Jonsson 2011).

Firstly, the R package Vegan (Oksanen et al. 2019) was used to perform Hierarchical Clustering, a method of cluster analysis grouping data into clusters based on similarity of connections, used to reorder the matrices based on reefs with similar connectivity, where connected reefs are next to each other on the axis (Frost et al. 2012; Kool et al. 2011). By reordering the matrix, visibility of community structure is improved. Reordered matrices were then converted to stochastic matrices, where each column (source reef) sums to 1. This transformation provides a clearer view of potential connectivity strength between reefs, including self-recruitment, and offers greater insight into the likelihood of a reef receiving or dispersing larvae (Botsford et al. 2009; Cowen, Paris, and Srinivasan 2006). These converted matrices are used for visualisation purposes only.

Analysis on connectivity-matrices were carried out on raw data, rather than stochastic transformations. To extract self-seeding information from the connectivity matrices, diagonal analysis was performed by extracting all values on the diagonal and comparing each model within each sector (e.g. $\text{Cairns}_{\text{TO}}$ was only compared against $\text{Cairns}_{\text{WO}}$ and $\text{Cairns}_{\text{WT}}$), using Kruskal-Wallis tests to check if there were statistical differences between the amount of self-seeding created by each forcing model. Following this, a post-hoc Dunn's test was run on each sector to identify which groups are significantly different from each other.

Using a non-parametric bootstrapping approach, Confidence intervals (CI) are also calculated from diagonal values to provide a measure of uncertainty around

self-seeding predictions, helping assess the reliability and precision of the estimated mean values of each variable. For each model, 100 bootstrap interactions were performed with a resample size equal to 50% of the original dataset. The mean of each bootstrap sample was calculated and stored. From the distribution of bootstrap means for each model, the 95 percent CI is calculated by identifying the 2.5th and 97.5th percentiles of the bootstrap distributions. These intervals indicate the range within which the true mean self-seeding value is likely to fall, with 95% confidence.

3.2.4.3 Network Analysis

Change in connectivity was also quantified by calculating community structure from connectivity matrices using R package iGraph (Csárdi et al. 2025) and visualised using ggraph (Pedersen 2024). Here, the Leiden algorithm (Traag, Waltman, and Eck 2019) with the Constant Potts Model (CPM) (Traag, Van Dooren, and Nesterov 2011) as the objective function is used to identify community structure within the each sector (equation 3.4). The Leiden algorithm optimizes CPM by improving robustness upon the earlier Louvain algorithm, enduring communities are well-connected and providing higher quality necessary for real-life networks.

CPM is defied as:

$$H = \sum_{c} [e_c - \gamma(\frac{n_c}{2})] \tag{3.4}$$

where e_c is the total edge weight within community c, n_c is the number of nodes in community c, γ is the resolution parameter. The resolution parameter is set depending on the edge weights in the data and the question being asked. Using a low resolution finds larger but fewer and weakly connected communities – answering questions regarding where connectivity barriers are, such as the northern GBR being a separate community to the southern GBR. In contrast, using a high resolution parameter results in many smaller communities in higher detail and

can reveal localised dispersal barriers, such as reef communities on the continental shelf being separate from communities on the mid-shelf (Traag, Waltman, and Eck 2019). This happens because intra- connectivity is identified when the average connection strength between members of the same community is greater than γ, and inter- connectivity is identified when average connection strength between any two reefs in different communities is less than γ. To match CPM analysis done by Thomas et al. 2014, the weighted adjacency matrix is normalised to avoid large reefs being assigned higher edge weights than smaller reefs, as large reefs produce more particles than small reefs due to particle release scaling. "Edge" refers to connections between reefs, and weight of the edge is assigned from the connection strength between two reefs, denoted as X_{ij}, where i is the source reef and j is the sink reef. Normalising the matrix makes it "non-dimensional", which is done by dividing X_{ij} by the total number of particles released at reef i, denoted by T_i and gives the normalised edge weight $N_{ij} = X_{ij}/T_i$.

A sensitivity analysis is then run on a range of possible γ values for each matrix to identify stabilising in the the number of communities and inter/ intra-community changes over the range of γ values. For example, Cairns TO normalised matrix has a minimum edge weight of 0, maximum edge weight of 0.9 and a mean of 0.005, therefore the γ range used was 0.00001 - 0.1 in 50 steps. The chosen γ must be more than the mean inter-density and less than the mean intra-density. To obtain detailed community structure, a high resolution with high intra-connectivity but communities become overly fractured is prioritised, the most robust γ values ideally are represented as a plateaus.

3.3 Results

3.3.1 Transport

3.3.1.1 Vorticity

Average vorticity measurements were examined in three stages. Firstly across the entire GBR domain for a full moon cycle (30 days) of TO, beginning on the first day of the annual mass spawning event (17th November 2000 at 00:00 am) (fig. 3.2 A.). General trends of average vorticity throughout the entire tidal cycle show the spawning event takes place when vorticity is around mid-level (30 - 55 L_2 Norm). Then, the 48 hours of 17 - 19th November 2000 velocity was examined for effects of wind and tides across the entire GBR (fig. 3.2 (B.)). TO produce much more variation in average vorticity than WO, winds keep a consistent level of vorticity between 16 - 18 L_2 Norm throughout the 48 hours. WT produces the same trend in average vorticity fluctuations as TO, but L_2 Norm is increased slightly during some low tides. This enhancement to L_2 Norm is also present in two of the individual sectors, Swain and Grenville (fig.3.3). Finally, vorticity across three separate sectors were compared for TO, WO and WT (fig. 3.3): WO is more similar to minimum TO/WT L_2 norms in individual sectors, for example in Grenville, TO and WO create the same L_2 norm of 0.9 s^{-1}/km^2 immediately after day 0.75. Cairns has a very unique trend: TO create the weakest vorticity levels and WT is most similar to WO. Grenville experiences the highest levels of vorticity and Swain experiences the lowest.

3.3.1.2 Trajectories

Trajectory visualisation in fig. 3.6 shows that WO models produce particle trajectories that travel mostly in a consistent direction away from the parent reef, following the direction of the wind. However, some trajectories (fig. 3.6 A.1.) are very circular in shape, following cyclonic wind momentum (see fig. 3.4). Trajec-

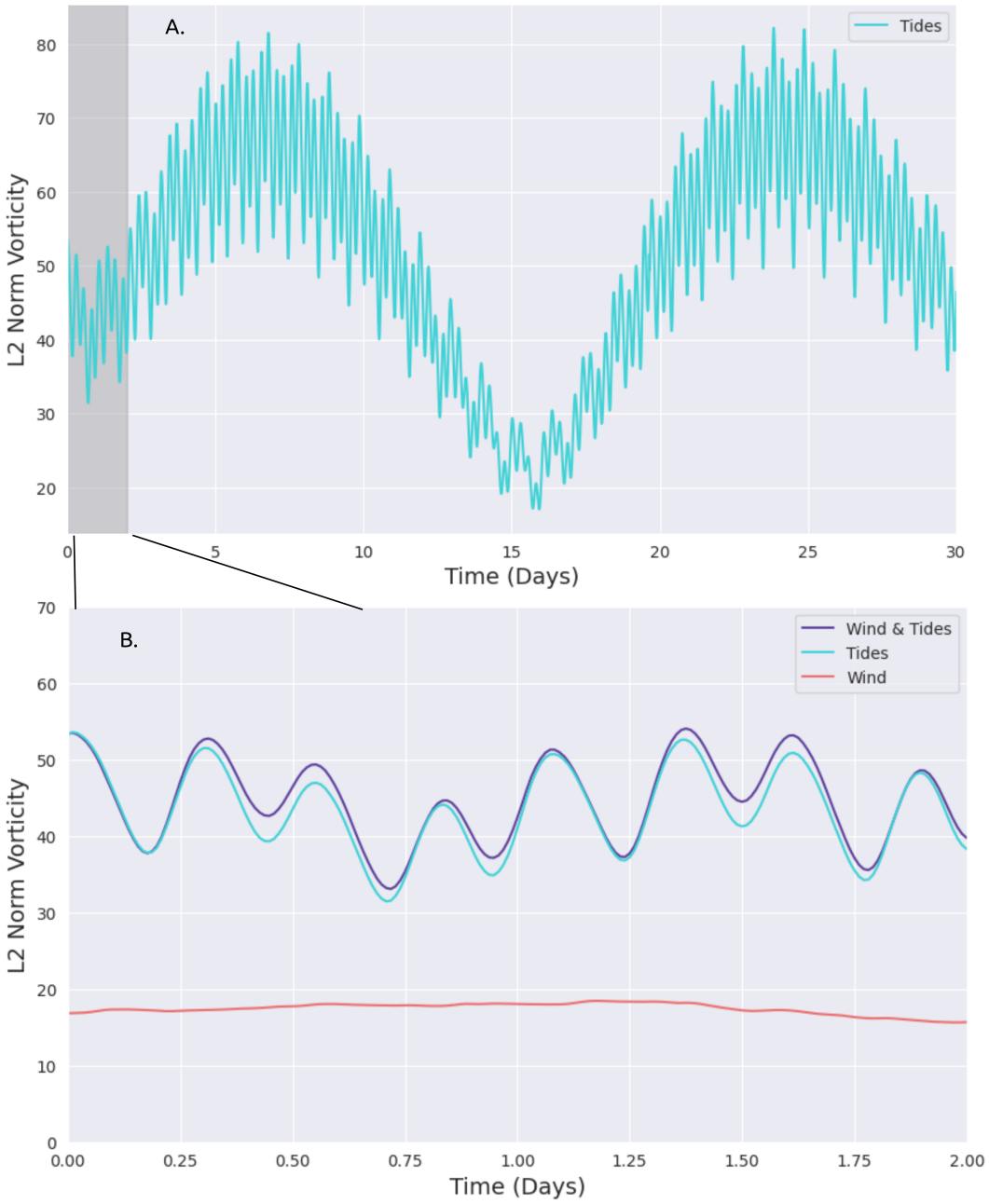


Figure 3.2: (A.) Vorticity across entire GBR domain for a full moon cycle (30 days). Duration of annual mass spawning event is shown by the shaded dark grey. (B.) Vorticity across entire GBR for 48 hours of mass spawning event. The three physical forcing simulations are compared.

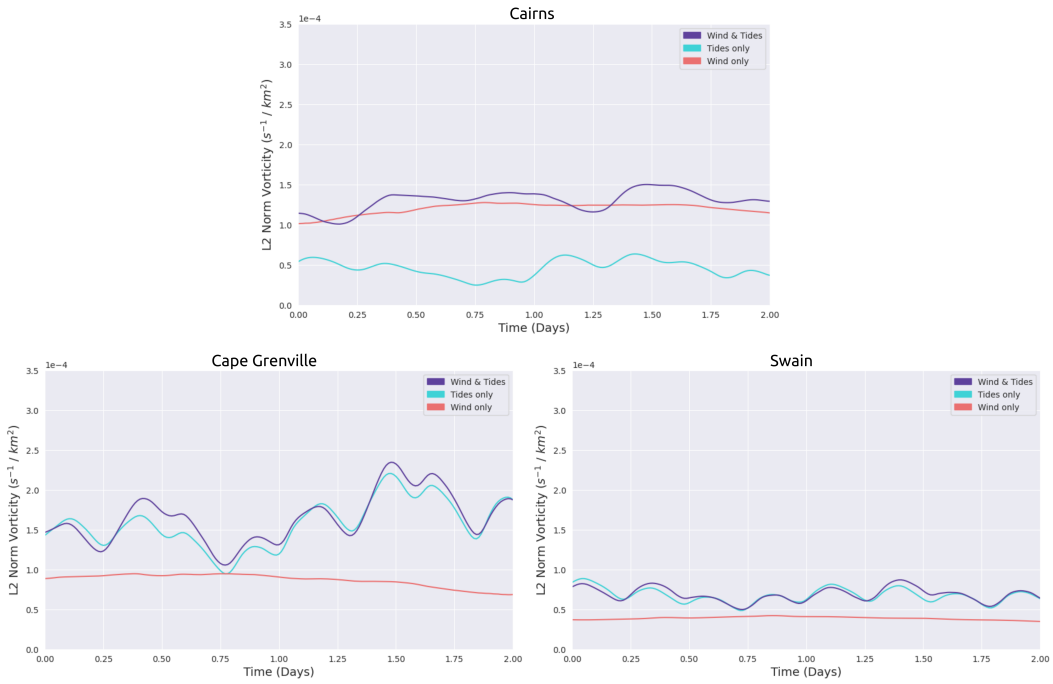


Figure 3.3: Vorticity per unit area across all three sectors and all three physical forcing simulations.

tories from TO models contain indirect paths away from reefs and involve oval, back-and-forth trajectories (fig. 3.6 B.1), these match the shape shown of tidal ellipses in figure 3.5. Trajectories formed by WT have varying effects: most trajectories are similar to WO but some trajectories, such as those with higher sinuosity values (fig. 3.6 C.1) contain some back and forth oscillations, similar to TO. Trajectories with a value of 1 or near 1, such as fig. 3.6 A.2, are surprisingly straight and may be an incorrect anomaly generated by ERA5 resolution (see discussion).

3.3.1.3 Sinuosity

Sinuosity was calculated for each particle trajectory for each model and sector, the mean sinuosity values for each model are shown in table 3.2. TO models have the highest values of sinuosity (mean range of 8.51 - 30.8 across sectors), WO models generated the lowest levels of sinuosity (mean range of 1.12 - 1.22 across sectors), whilst WT generates sinuosity means higher than WO but lower than TO (mean range of 1.44 - 9.90 across sectors).Throughout all the models, Cape Grenville has the highest sinuosity mean while Cairns has the lowest. Distribution

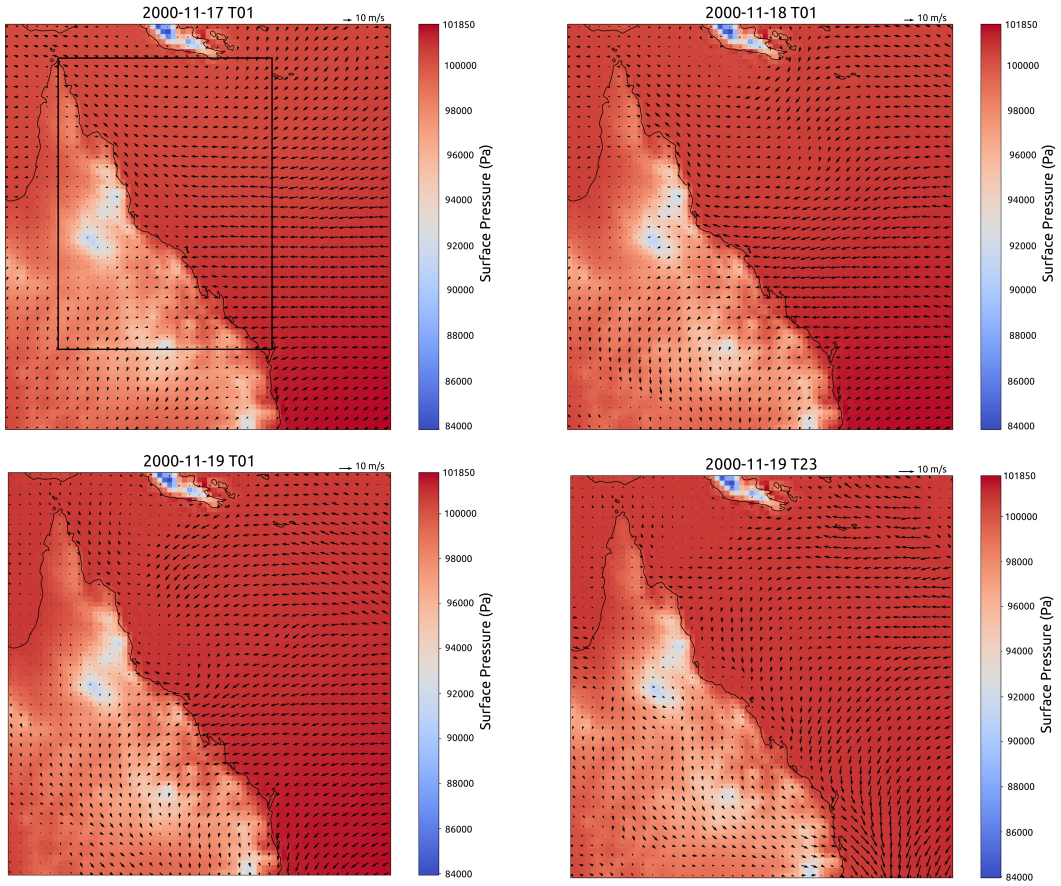


Figure 3.4: ERA5 wind data plotted for the area of interest across four time steps of the 48 hour annual mass spawning window. Vectors indicate wind speed (m/s) and colour represents pressure (Pa).

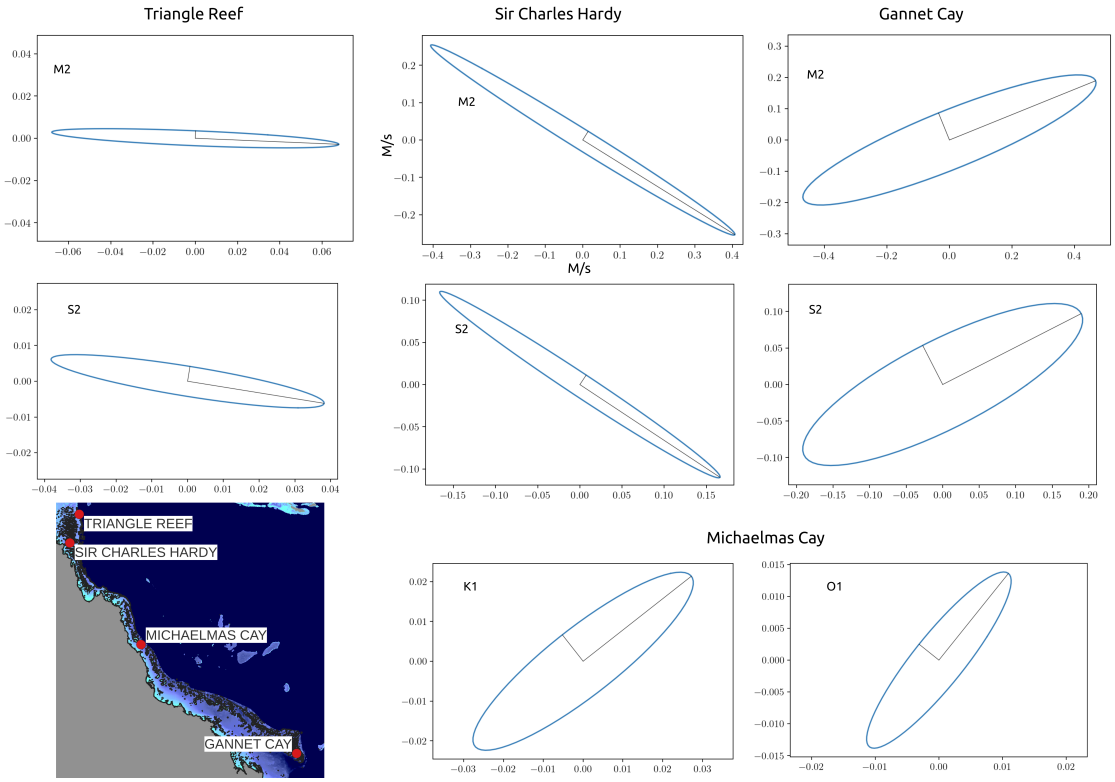


Figure 3.5: Tidal ellipses plots from tide gauge locations within each of the three sectors across the GBR. M2 and S2 constituents are shown for Triangle Reef and Gannet Cay, where tides are diurnal (Grenville is mixed-semidiurnal but M2 and S2 are dominant) and O1 and K1 constituents are shown for Michaelmas Cay, which is semidiurnal. Ellipses plots represent direction and speed changes throughout a tidal cycle. Narrow plots represent very directional tides, a back and forth movement.

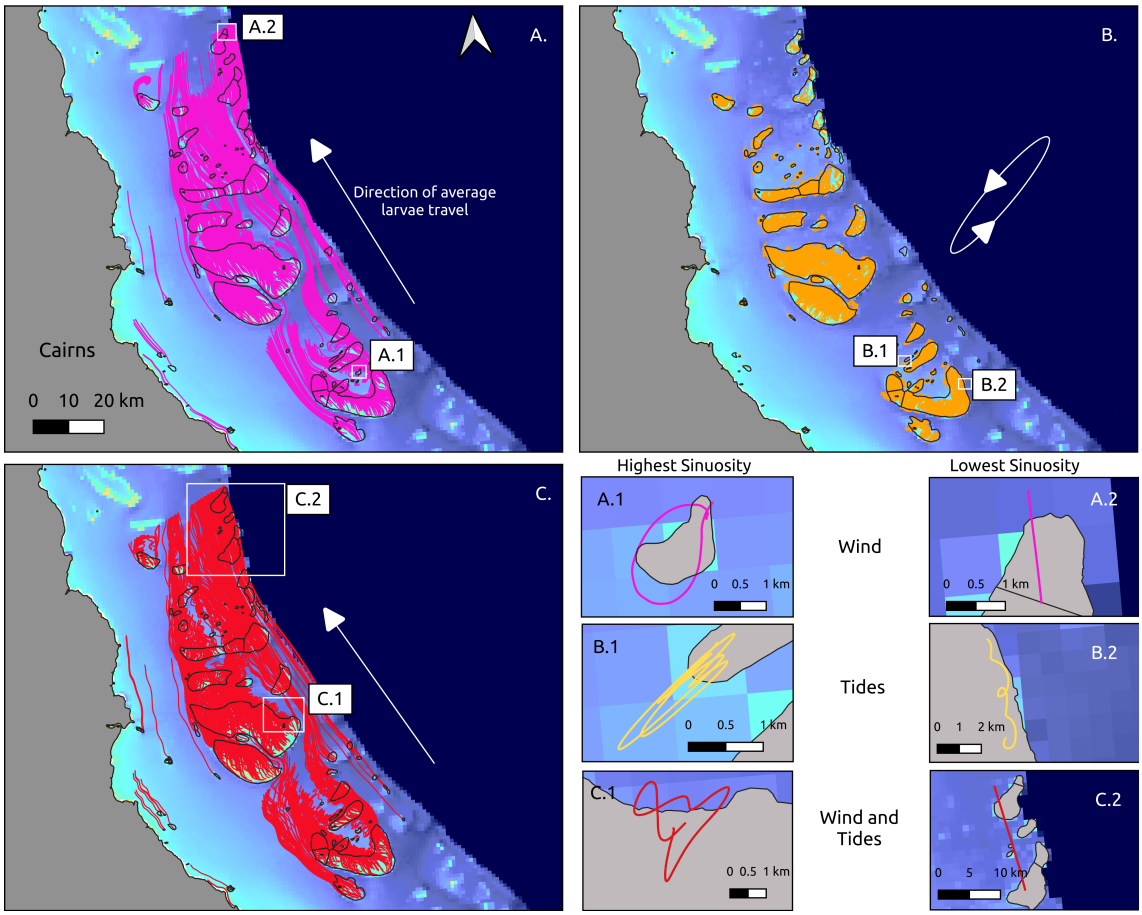


Figure 3.6: Map of a sub-sample of trajectories released from Cairns reefs from each model. A. represents trajectories transported by wind only. B. represents trajectories transported by tides only. C. represents trajectories transported by both wind and tides. An example of a trajectory from each model representing either highest sinuosity (A.1., B.1. and C.1.), all of which are recorded as self-seeding, and lowest sinuosity (A.2., B.2., and C.2.). Blue represents bathymetry depth, grey in A-C represents the coastline, in A.1 - C.1 and A.2 - C.2. grey represents a reef polygon. Transparent shapes in A - C represent reefs. Sinuosity of A.1: 17.52, A.2: 1, B.1: 69.02, B.2: 1.63, C.1: 32.9, C.2: 0.00025.

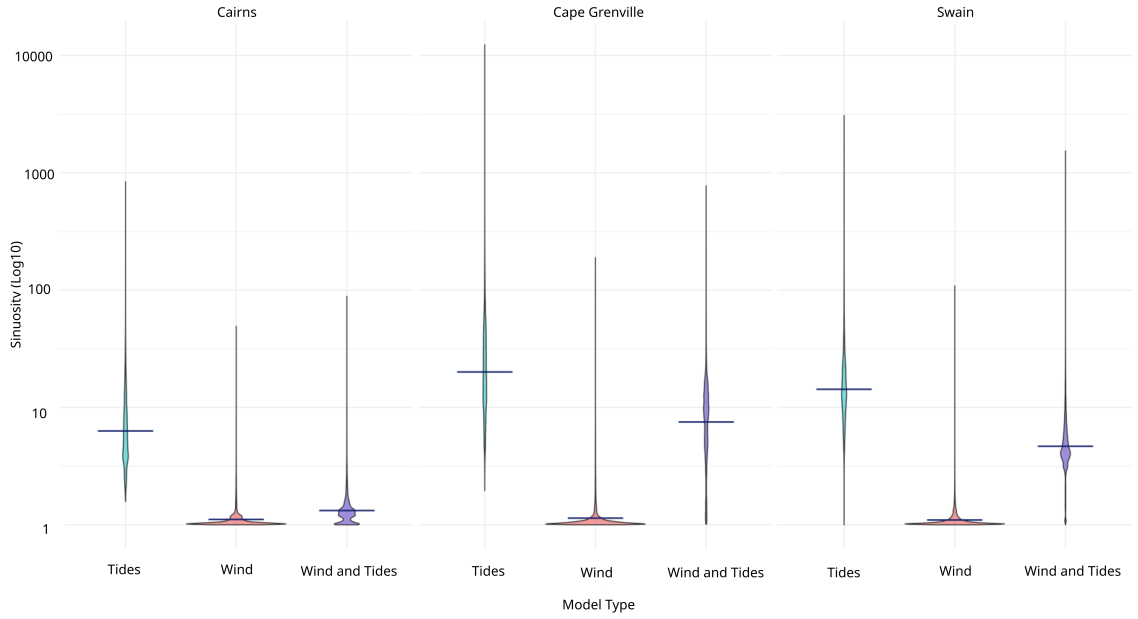


Figure 3.7: Violin Plots of distributions of sinuosity across all models

of sinuosity values are largest for TO sectors (fig. 3.7, whereas distribution is limited in WO models, with most values being around 1.

Statistical analysis revealed significant differences within the three models. Cairns: $X_2(2) = 563494$, $p < 0.001$, Grenville: $X_2(2) = 2314226$, $p < 0.001$ and Swain: $X_2(2) = 1407383$, $p < 0.001$. To assess the strength of these differences, η^2 was calculated for each sector to measure effect size: Cairns $\eta^2 = 0.697$, Cape Grenville $\eta^2 = 0.722$ and Swain $\eta^2 = 0.808$, indicating that model type strongly influences sinuosity across all sectors, the effect is most pronounced in Swain.

Model	Cape Grenville	Cairns	Swain
Tides	30.8	8.51	18.6
Wind	1.22	1.15	1.12
Tides and Wind	9.9	1.44	5.5

Table 3.2: Sinuosity mean for each model

3.3.2 Connectivity

Connectivity matrices were created for each sector throughout each of the three simulation variations (WO, TO, WT) (fig. 3.9). From the connectivity matrices, values of settled particles were obtained (table 3.3). Overall, $\text{Cairns}_{\text{TO}}$ led to the high-

est percentage of particles successfully settling (78.85%), and self-seeding reefs (75%), whilst $Swain_{WT}$ had the lowest percentage of settled particles (10.43%) and the lowest percentage of self-seeding reefs (5.93%). Of settled particles which had also self-seeded, $Grenville_{TO}$ had the highest value (94.15%) and $Swain_{WO}$ had the lowest level of self-seeding (9.03%). Across all three forcing models, TO led to the highest level of settling (57.82%) and highest rates of self-seeding (87.45%). WT had the lowest level of settled particles (21.44%) and WO had the lowest level of self-seeding behaviour (26.73%).

Spatial patterns of self-seeding behaviour are shown in figure 3.8 for each model across the three sectors. TO self-seeding occurs in the high majority of reefs in each sector, covering reefs on the outer, mid and inner shelf. $Swain_{TO}$ indicates several reef patches which were not recorded to self-seed, these are mostly in the densest sections of Swain in the centre and in the southern tip, and on the southern shelf-edge. WO self-seeding is seen to greatly reduce across all sectors compared with TO. Grenville retains a lot of self-seeding in the mid-shelf but reefs on the shelf-edge do not self-seed, this is also seen in Cairns. Swain observes the opposite trend, where only reefs on the shelf-edge self-seed. WT generates spatial patterns of self-seeding differently again. Grenville regains self-seeding from WO in some of the shelf-edge reefs and more self-seeding is seen on the mid/inner shelf compared to WO. Cairns experiences a minor increase of self-seeding reefs only on the inner-self and Swain's inner shelf reefs experience more self-seeding than WO.

3.3.2.1 Diagonal Analysis

Diagonal analysis was carried out on the connectivity matrices to extract the mean, as a measure of self-recruitment strength. Table 3.4 shows how different simulations impact the proportion of particles self-seeding in each sector. Across all the sectors, the TO model leads to the greatest number of self-seeding particles and WT leads to the least particles self-seeding. To investigate whether

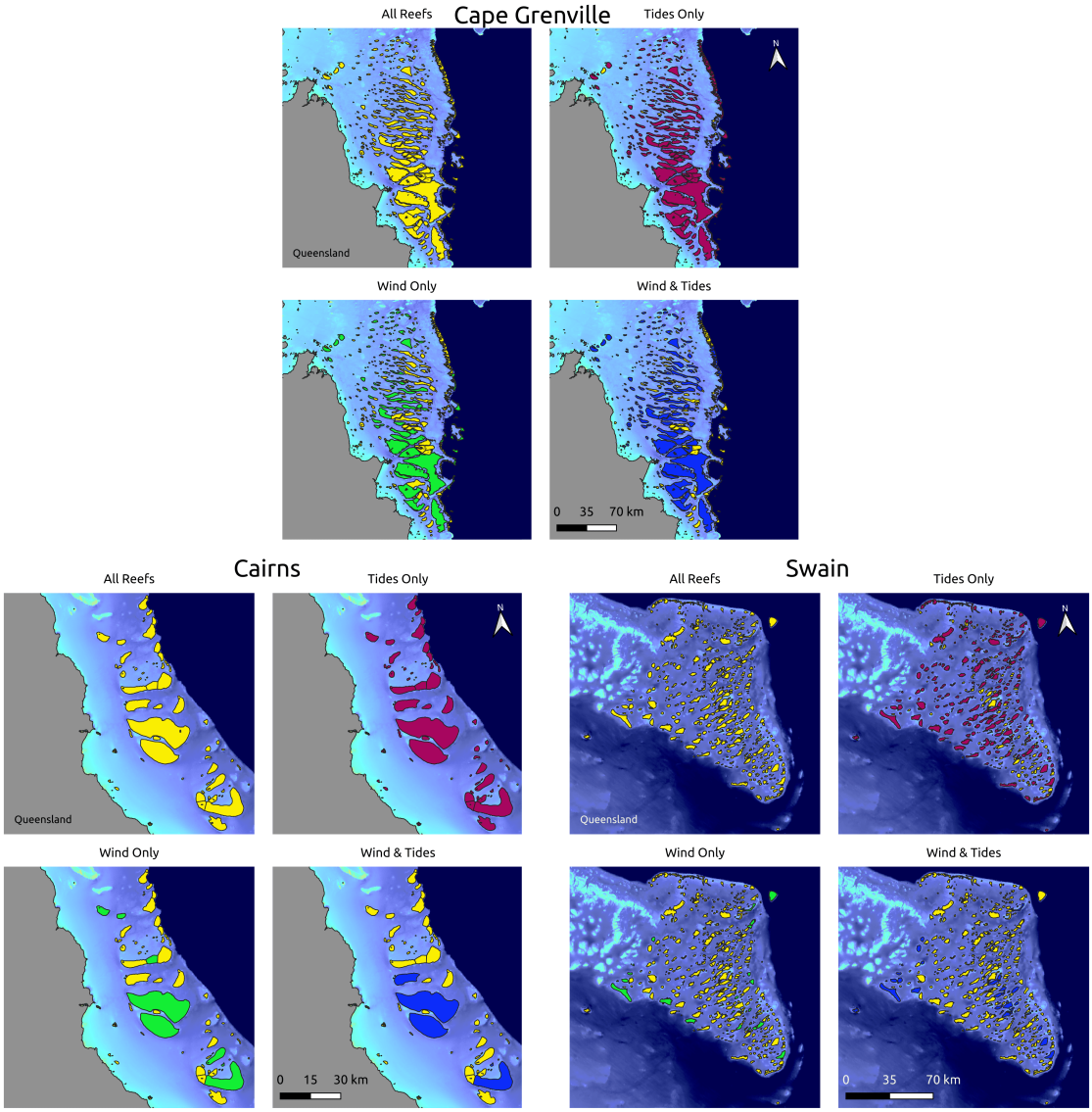


Figure 3.8: Self-seeding behaviour shown by coloured reef polygons across each sector and model. Yellow represents all reefs of the sector and is shown in each filtered reef polygon map to show spatial distribution of reefs.

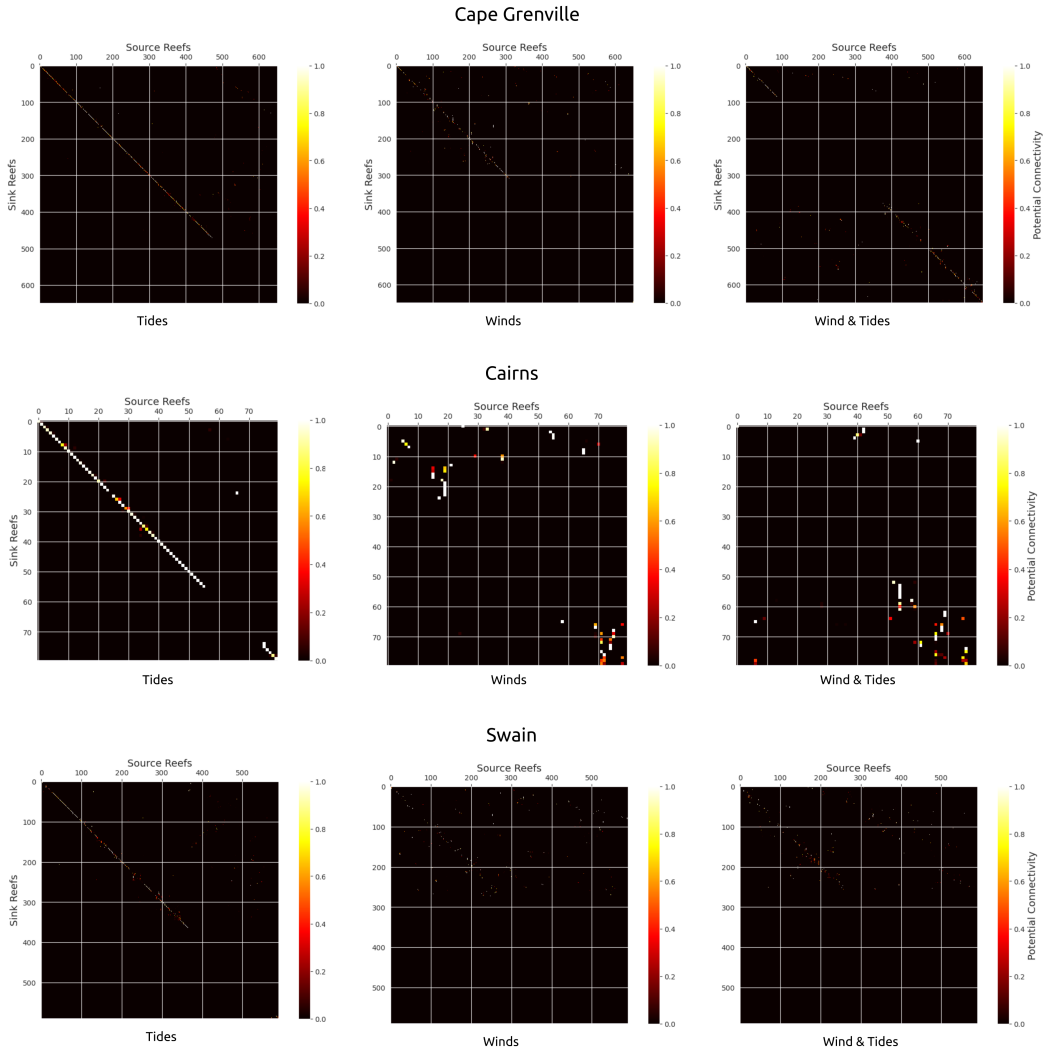


Figure 3.9: Reordered connectivity matrices of all 3 sectors and each 3 simulations following stochastic transformation to show potential connectivity.

Swain					
Model	TS	% of S	TSS	% of SSS	% of SRR
Tides	159462	27.48	110648	69.39	38.64
Wind	65875	11.35	5946	9.03	3.89
Wind and Tides	60535	10.43	7649	12.64	5.93

Cape Grenville					
Model	TS	% of S	TSS	% of SSS	% of SRR
Tides	1217160	67.12	1145965	94.15	68.61
Wind	647624	35.71	283060	43.71	17.69
Wind and Tides	721380	39.78	430275	59.65	23.23

Cairns					
Model	TS	% of S	TSS	% of SSS	% of SRR
Tides	212364	78.85	209852	98.82	75
Wind	56381	20.94	15477	27.45	11.12
Wind and Tides	37999	14.11	10905	28.70	8.75

Table 3.3: Table of settled particles for each sector and model. Abbreviations: % of S: percentage of settled particles, TSS: total of settled particles which have self-seeded, % of SSS: percentage of settled particles which have self-seeded, % of SRR: percentage of self-recruited reefs

Model	Swain	Grenville	Cairns
Tides	188	1763	2623
Wind	10.1	435	193
Wind and Tides	13	662	136

Table 3.4: Diagonal mean values of particles self-seeding

the differences seen in each sector between models is significant or not, Kruskal-Wallis tests were run for each sector. All sectors experienced statistically significant differences between each simulation (p = < 0.001). The post-hoc Dunn's test showed Grenville had significant differences between all three models (p = < 0.001), however both Cairns and Swain showed no statistical difference between WO and WT (p = 1) but statistical difference between TO and wind models (p = < 0.001).

3.3.2.2 Network Analysis

Sensitivity analysis of the γ parameter for CPMs were conducted on each TO model. $\text{Cairns}_{\text{TO}}$ (see fig. 3.10) resulted in a stable plateau of inter- (dark blue) and

intra - (light blue) community and number of communities (green) around 0.0015. Sensitivity analysis on $\text{Grenville}_{\text{WT}}$ and Swain_{TO} did not result in any plateaus, suggesting sensitivity to γ values. Therefore the same γ value of 0.0015 is used for these sectors as it allows cross comparison. The γ value 0.0015 is also the final resolution before steep increases in inter-community values, which ideally are kept to a low value. To allow comparison across each model, the same γ 0.0015 is used for WO and WT.

CPM were run for each connectivity matrix to partition reefs into reef communities. Community networks are shown in figure 3.11 and display the changes the different models make to community structure. $\text{Grenville}_{\text{TO}}$ has many more clusters than WO and WT, both on the mid/inner shelf and the outer shelf, the clusters of $\text{Grenville}_{\text{WT}}$ are horizontally arranged. $\text{Grenville}_{\text{WO}}$ generates a large cluster across the whole of the lower and middle mid-shelf, with reefs on the northern mid-shelf, shelf-edge and inner shelf forming small or singular clusters. $\text{Grenville}_{\text{WT}}$ form large and well-defined clusters, with each area of the shelf separate to the others.

$\text{Cairns}_{\text{TO}}$ clusters are in East-West formations, similar to $\text{Grenville}_{\text{WT}}$, as the shelf is much narrower here, reefs on the shelf edge are part of the same clusters as the reefs on the mid-shelf. $\text{Cairns}_{\text{WO}}$ mid-shelf reefs form more North-South clusters, with larger clusters on the mid-shelf and reefs along the shelf-edge forming small or singular clusters. Cairns_{WT} clusters are very similar to $\text{Cairns}_{\text{WO}}$.

The size of Swain makes visual assessment of clusters difficult, but a large cluster in the centre is present across all three models, and is at its largest in WT. Clusters in Swain_{TO} are slightly more circular in shape compared to Swain_{WO}, where clusters form vertical ribbons across the area. Swain_{WT} clusters have a more random appearance than Swain_{TO} and Swain_{WO}, however, the northern section of Swain contains many smaller and singular clusters compared to the southern section, which has larger and well defined clusters.

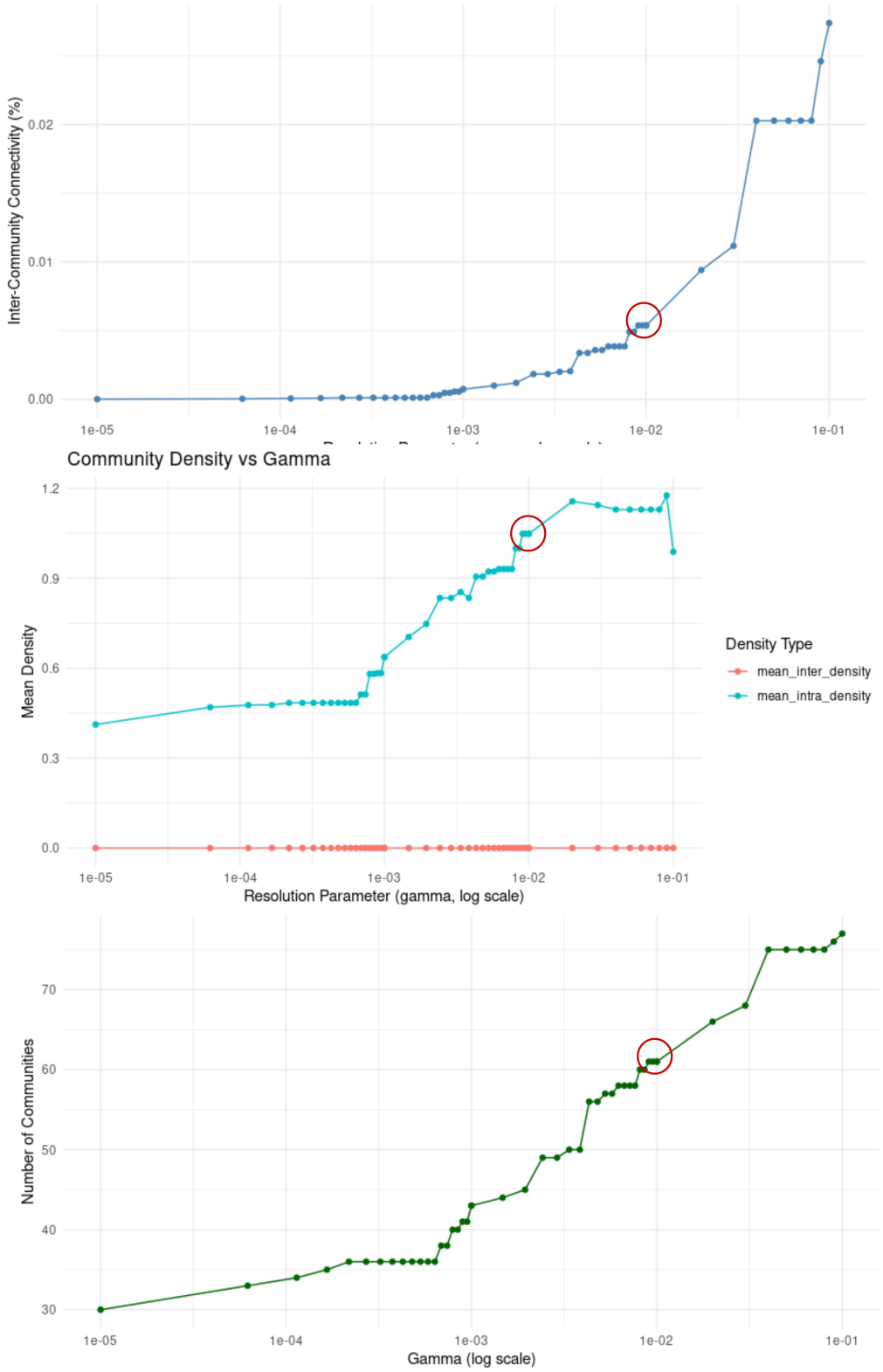


Figure 3.10: γ parameter sensitivity analysis results of $\text{Cairns}_{\text{TO}}$. Chosen γ shown in red circles. The analysis produces a graph which shows curves and plateau's corresponding to jumps and stable connection of inter-community increasing as γ is increased. Each jump illustrates a significant change to the community partitions.

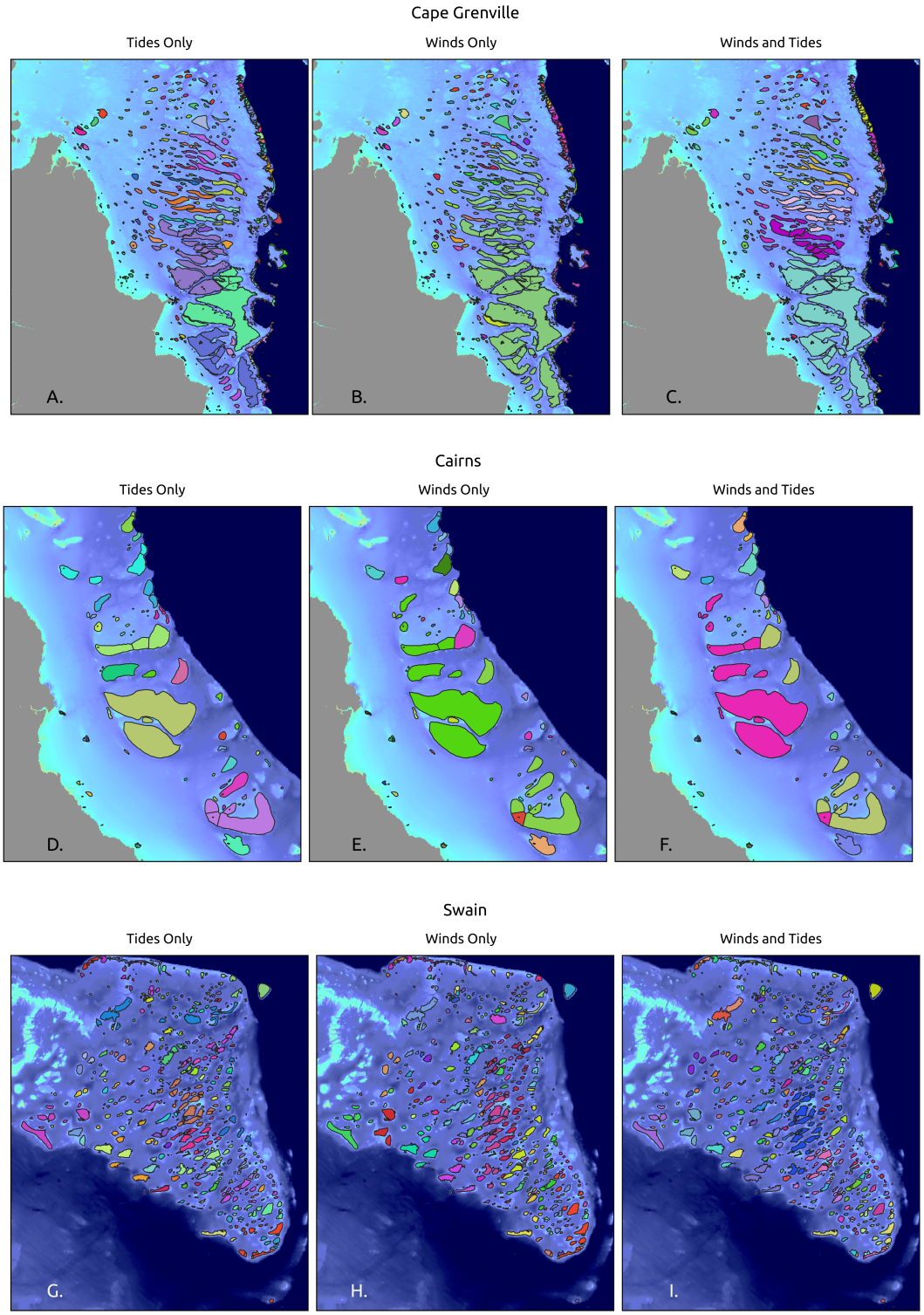


Figure 3.11: Clusters generated by CPM across all models within each sector. Different colours represent different clusters. Cluster colours are allocated randomly in each panel, therefore colours should not be compared across sectors, only groupings.

3.4 Discussion

3.4.1 Transport

3.4.1.1 Vorticity

Vorticity results showed that tides are dominant drivers of vorticity. As vorticity is a measurement of "spinny-ness", tides generate more eddies than wind does, and subsequently more velocity. WT showed an increase of vorticity from TO measurements, tides remained dominant over vorticity shown by the continued following of tidal oscillations. The increased vorticity indicate eddies were still being generated by tidal movement but the wind was then transporting the eddies, leading to higher levels of vorticity. The only sector where this was not the case is Cairns, where winds drive the highest L_2 Norm of vorticity, and tides generate the lowest L_2 Norm. The reason for this shift in dominant drivers may be due to Cairns being the point along the East Australian coast where tides change from being semidiurnal south of Cairns, to being mixed semidiurnal north of Cairns. During a study by Sammarco and Andrews (1988), of Helix Reef in the Central GBR, tides were recorded to be semidiurnal before spawning and then became diurnal during the spawning event, reducing the neap reduction in tidal amplitude. In Cairns, the results suggest eddies were not being generated by the weak tidal movement.

When looking at sector differences in vorticity, Grenville experiences the highest levels of vorticity, this may be due to having the highest population of reefs, including ribbon reefs which create more bed shear stress during tidal movement (Marshall and Davies 1988; Hopley 2006). High density of reefs has also been shown to lead to the "Sticky Water Effect" (Wolanski and Spangnol 2000), which could lead to higher levels of vorticity from increased number of eddies. Swain generates the lowest levels of vorticity, this may be due to the sector being large, containing a lot of open ocean around Swain which may have affected how the

L_2 Norm was calculated. Another reason could also be due to reefs being far from the coast, meaning that area experiences less tidal range/ tidal impact than Cairns and Grenville.

This particular experiment aims to partly answer research question 1 (as listed in section 3.1.4). Vorticity is associated with retention, tides are shown to be responsible for generating higher levels of vorticity than wind. WT results show that different areas of the GBR experience different levels of vorticity due to tidal strengths: either due to tidal convergence zones, such as Cairns; being further away from the coast, such as Swain; and the impact of reef density, such as in Grenville. In regards to question 2, tide-driven-vorticity is likely to be a mechanism for self-seeding behaviour but further discussion will take place before this conclusion is drawn.

3.4.1.2 Trajectories

Trajectories created by Parcels showed clear distinctions of pathways depending on TO, WO or WT. Trajectories of self-seeding corals had high values of sinuosity and showed back-and-forth trajectories across and away from the reef, the patterns are characteristic of tidal ellipses and tidal signal, as shown in figure 3.5. Trajectories caught in eddies would be circular and found in the lees of reefs. In areas such as Cape Grenville or Swain there is a strong tidal signal (Wolanski 1983), creating these large tidal oscillations. Whereas in Cairns being in the tidal convergence zone, there are only very small tidal ellipses (Sammarco and Andrews 1988; Church, Andrews, and Boland 1985; Williams, Wolanski, and Andrews 1984). Oscillating trajectories in models containing tidal data suggest that the particles are kept close to the reef via tidal ellipses. Retention of coral larvae is correlated to the strength of the tidal signal. Research question 1 (3.1.4) is addressed here by demonstrating the difference wind and tides separately make to the pathways of particles: wind carried particles away from the parent reef whereas tides keep particles close to the parent reefs; when modelled

together, the strength of the tides and the density of the reefs impact whether wind or tides are the dominant driver of transportation. This experiment partly answers research question 2, it suggests that the mechanism behind self-seeding behaviour will be driven by tides.

3.4.1.3 Sinuosity

Sinuosity was measured to show the impact physical drivers have on particle transportation. Findings from the sinuosity analysis found that across all locations, sinuosity values were higher for all TO models and lowest for WO models, confirming circular movement of particles correlate to the strength of tidal ellipses. WT models for Swain and Cape Grenville have high values of sinuosity, suggesting that tides are responsible for generating tight-serpentine trajectories, even when wind is present. $Cairns_{WT}$ generated low levels of sinuosity, similar to sinuosity generated by $Cairns_{WO}$; suggesting that particle transportation is strongly dominated by winds in this sector, consistent with findings of low vorticity. These findings suggest that wind carries larvae away, and tides lead to retention. Sinuosity shows tides drive trajectories with high sinuosity values, even when wind is present, as eddies are also being transported by wind. The sinuosity values near 1 are probably generated due to the low spatial and temporal resolution of the ERA5 data (see fig. 3.4), these are anomalies, as shown by the majority of trajectories in fig. 3.6 having some form of slight curvature. Circular trajectories generated by WO are likely caused by mild cyclonic wind momentum, as can be seen in fig. 3.4 during 2000-11-19 T01.

Regarding trajectory pathways, research question 1 is addressed by demonstrating the difference in sinuosity between winds and tides. Wind generates very low levels of sinuosity whereas tides generate high levels of sinuosity, correlating with sinuosity values expected of oscillating and spiralling pathways. When WT are modelled, the results show that location on the GBR greatly affects whether wind or tides are dominant in transportation. For research question 2, the high levels

of sinuosity driven by tides suggest that the mechanism behind self-seeding is connected to tidal ellipses.

3.4.2 Connectivity

3.4.2.1 Self-seeding reefs

Locations of self-seeding reefs differs greatly depending on which model was used. For TO models, self-seeding is uniform and consistent across the entire shelf of Grenville and Cairns. In Swain the centre of the area and the southern toe does not self-seed. The difference may be due to Grenville and Cairns having higher levels of vorticity than Swain does, leading to higher levels of retention. As Swain is away from the coast, tidal influence will be limited, but even more-so in the centre of the reefs, as tidal energy is lost due to interaction with the outer reef (Perris et al. 2024). Another reason could be that the reefs are extremely close to neighbouring reefs in the centre, leading to larvae easily being caught by other reefs. The non-self seeding reefs in the southern toe of Swain are particularly small, meaning that retention may be harder as the larvae are less likely to land back on a small reef, compared with larger reefs. WO models massively reduce the amount of self-seeding reefs across all sectors, any which do self-seed are typically large, suggesting that the larvae didn't have time to clear off the parent reef. Other self-seeding reefs may also be sheltered from wind, as suggested by reefs which have not self-seeded are isolated or on the edge of the sectors. WT leads to less self-seeding than TO but more than WO, suggesting that tides protect some reefs from having larvae washed away by winds. Self-seeding is still carried out mostly by large reefs and those in a goldilocks position of being in a dense area of reefs, providing retention, but not too near other reefs for their larvae to easily be caught. This study shows the difference in amount and location of self-seeding across the sectors; and also suggests that reefs are retaining spores by being large and being in a fairly dense area of reefs.

3.4.2.2 Diagonal Analysis

Patterns of self-connectivity from analysing Parcels outputs show clear differences between whether models have been forced with wind or with tides. It is clear from table. 3.4 and from the connectivity matrices that TO models lead to self-seeding as the dominant connectivity trend. Across all sectors, at least double the amount of larvae successfully settle on a reef with TO than when modelled with WO and almost all of those TO settled larvae have self-seeded. This indicates tides keep larvae close to the parent reef, allowing larvae to have higher chances of reaching a reef to settle. However, when wind is present, even when only a light breeze, it is found to disrupt the self-seeding behaviour and chances of settling on a reef, as observed by Willis and Oliver (1990).

When wind is simulated alone or with tides in Swain and Cairns, self-seeding is at least three times lower than TO, highlighting the strong disruptive influence wind has on connectivity. Self-seeding behaviour happening in Swain and Cairns with wind present is likely to be occurring due to larvae not having time to pass clear off a large parent reef, or larvae have got trapped in areas sheltered from wind, such as in the lee of islands. Grenville is not impacted as strongly by wind as Cairns and Swain, self-seeding is only 1.5 times lower with wind than TO, this could be due to the large area of reefs in the Grenville sector, preventing larvae from being transported away from the reef within 48 hours: only larvae released close to the edges of reefs will be dispersed off the reef. Another reason could be the morphology of these reefs are barrier reefs, which could prevent a lot of circulation and flushing experienced in the more exposed parts of the GBR. It is important to note, that studies which observe wind transporting coral larvae far from parent reefs are conducted around Bowden Reef in the central GBR near the Cairns sector (Wolanski, Burrage, and King 1989; Wolanski, Doherty, and Carleton 1997; Willis and Oliver 1988; Willis et al. 1985; Kingsford, Wolanski, and Choat 1991), which could be heavily influenced by wind more-so than in other areas. These

findings show that field studies do need to be cautious with their findings of general GBR trends, as location does determine the likely-hood of self-seeding due to the strength of local tides.

3.4.2.3 Network analysis

The CPM clustering maps show the patterns of connectivity based on which model has been used in each sector. The maps show the different shapes of clusters depending upon this. For example, Grenville_{WT} clusters are long horizontal clusters, matching the shape and size expected from tidal ellipses. Clusters generated by wind tend to be in a long vertical line, following the direction of wind which follows the coastline. When winds and tides are generated together, the clusters are a much more rounded shape, illustrating the different directions particles are flowing in depending on whether they are being transported by winds or tides.

Grenville and Cairns both sit on the shelf, reaching from the shelf edge all the way to the coast. The clusters in these sectors show that there is a connectivity gap between the shelf-edge, the middle shelf and the inner shelf, which remains throughout the three simulations – suggesting that there are larger variables present which keep these three areas separate to each other, either because of spatial distance or fine scale tidal dynamics not captured in this chapter. Swain does not experience this same separation as it does not sit so closely between shelf-edge and coast, however the outer reefs do remain separate from the inner reefs, suggesting that there is a tidal phenomenon present which only affects the reefs along the outside of the sector. As these separations across the sectors aren't effected by the presence or absence of wind and tidal forcing, it suggests that the difference is caused by something constant, most likely bathymetry, which is well known to be the keystone variable in tidal dynamics (Wolanski 1983; Saint-Amand et al. 2023; Seifi, Deng, and Andersen 2019).

In response to research question 1 (3.1.4), the differing effects of wind and tides

make to larvae transportation is demonstrated by the differing levels of self-seeding behaviour. Models containing tides lead to higher levels of self-seeding than wind does: tides drive self-seeding behaviour whereas wind disrupts it. Results from the CPMs show that tides generate more clusters, generated in a rounded shape, demonstrating that tides drive local retention, either for individual reefs or small networks of neighbouring reefs. CPM results of wind show larger and fewer clusters, with clusters forming in horizontal groups representing the direction of wind, networks are local but with further reach than tidal driven networks. The response from this connectivity study to research question 2 is that the mechanism behind self-seeding behaviour is tidally driven and connected to the tidal ellipses, based on the shape of the clusters.

3.4.3 Summary of key results

Here, the results of each study will be combined to give a comprehensive answer to the two research questions (3.1.4). The key findings were:

- Tides drive self-seeding behaviour.
- Wind disrupt self-seeding behaviour and drive dispersal.
- Vorticity is found to be driven by tides.
- High values of vorticity correlate with high levels of particle trajectory sinuosity and self-seeding behaviour.
- Particle trajectories show pathways generated by tidal movement follow the shape of tidal ellipses.
- The location of the GBR heavily dictates whether tides or wind are the dominant driver of larvae transportation. This is due to differing strengths of tides along the shelf.

Research question 1: The differing effects of wind and tides on coral larvae transportation is that winds disperse larvae away from the parent reef, most of this

larvae does not make it to another neighbouring reef. Tides retain coral larvae near the parent reef, larvae is moved back and forth from the parent reef with the tidal ellipses, leading to higher retention than wind. When wind and tides are modelled together, the effect of wind was controlled by the strength of tides in particular regions: Cairns has very weak tides, therefore wind was the dominant driver of transportation, leading to self-seeding only being seen on large reefs where particles had not cleared the parent reef within 48 hours. Swain and Grenville had stronger tidal effects, due to their positions on the shelf and the density of the reefs, therefore there was still self-seeding behaviour when modelled with wind and tides.

Research question 2: The mechanism behind self-seeding behaviour is driven by tides. Results showed highest levels of vorticity in TO models and WT combined. Trajectory sinuosity showed highest values with tides only, the circling trajectories correlated well with the high levels of vorticity. Trajectory pathways showed the particles were moving back and forth with the tidal ellipses. These results together, suggest that the mechanism behind self-seeding behaviour is tidal ellipses. The strength of the effect depends upon the density of the reefs and the location of the reefs in regard to tidal strength. To investigate further into the mechanisms of retention, such as the "Sticky Water Effect", a finer resolution of under 100 m would be required (Wolanski et al. 2024a).

3.4.4 Limitations, Implications and Future Work

A limitation of this study is that the EAC was also not included in these models, which may be expected to have an effect on dispersal in the southern section of the GBR, however as this chapter is focusing solely on tidal dynamics and wind dynamics, including current forcing would have distorted the results. This study uses one of the highest resolution so-far used for the entire GBR, yet 250 m will still miss small scale tidal dynamics which operate at 10's of m scale, such as the "sticky water phenomenon" (Wolanski et al. 2024a). However the computational

cost of doing ∼50 m resolution for a sector of the GBR is large and not feasible at this point in time and 250 m is currently the highest resolution for simulating the entire GBR. Finer resolution could be used but only for very small areas of reef.

The implications from this study are that coral larvae retention relies heavily upon the strength of tides across the GBR, with rising sea level tides are expected to weaken in some areas (Mawson, Lee, and Hill 2022) which will lead to less larvae being retained. The negative consequence of this is that more larvae may be lost, leading to a decline in population growth on the GBR. However, a positive consequence may be that reefs begin to form larger networks, thereby improving resilience by damaged reefs being replenished by healthy reefs, and assisting with the southward migration to cooler waters – which has already been seen by corals appearing off the coast of Sydney (Davies et al. 2023).

Another useful study would be to model the SLR the GBR has already undergone since the Holocene initiation around eight thousand years ago. This would allow insights into how connectivity has changed throughout SLR. Work carried out in this study will be important for both of these modelling studies: predicted wind data for the past and future is not available in the scope of the projects, meaning that only tides can be modelled. As shown by this project, there are significant differences in connectivity depending on whether wind is present in the tidal models, therefore modelling without wind does not provide a realist prediction on connectivity patterns. However, tides have been shown to lead to maximum connectivity which is still a useful metric when it is understood that winds will disrupt this. It will be understood that lower measurements of tidal strength will mean that maximum connectivity generated by tides will be disrupted more than in the present day.

3.5 Conclusion

Throughout this study, three numerical models were built of the GBR to simulate tides only, winds only and tides and winds combined, these models were used to generate velocity rasters for Lagrangian particle tracking software Parcels, to track coral larvae transportation to inform connectivity analysis. Outputs of velocity, sinuosity and connectivity matrix analysis were used to gain insight into the dominant drivers of coral larvae transportation and connectivity trends of the GBR. Results showed TO models exhibited the highest levels of self-seeding behaviour, along with the highest levels of vorticity and particle trajectory sinuosity through tidal ellipses. In contrast, weak tides – such as those observed at Cairns, produce minimal vorticity, allowing larvae to be more readily transported away from parents reefs by wind. The particle trajectories in tidal models revealed that tidal ellipses, rather than sporadic tidal eddies, are primarily responsible for larvae retention. However finer resolution modelling of the whole GBR is required to investigate smaller scale dynamics (under 100 m).

WO models produced minimal self-seeding, low vorticity and trajectory sinuosity of particle trajectories. In these scenarios, larvae were carried away from parent reefs, and any observed self-seeding occurred only because some parent reefs were too large for the larvae to clear before settling. WT models resulted in intermediate levels of self-seeding – less than TO models but more than WO models – indicating that tides promote self-seeding while wind tends to disrupt it. Size of a reef and surrounding reefs influence whether self-seeding is protected from wind or not.

Simulations around Cairns further emphasised that self-seeding patterns are not uniform across the GBR. In this region, wind dominates over tidal influence, leading to low self-seeding even in the presence of tides. Consequently, caution is needed when generalising findings from field studies: those conducted in weak-tide regions like Cairns are more likely to observe wind-driven dispersal and lim-

ited self-seeding. The results suggest that inconsistencies in the literature may stem from the geographic focus of fieldwork. As TO models show maximum self-connectivity, findings from this study will allow subsequent tidal studies on the effects of past and future sea-levels on coral connectivity.

Chapter 4

Tidal dynamics driving the Holocene Great Barrier Reef initiation

This chapter investigates the tidal dynamics present during initiation of the Great Barrier Reef around 8,000 years ago (8 ka) during the early Holocene (Hopley, Smithers, and Parnell 2007). Three numerical models were developed of the Great Barrier Reef across three thousand years: representing sea level at 9 ka (17 m below present sea level), 8 ka (7 m below present sea level) and 7 ka (1.7 m below present sea level). For each of these models, bespoke bathymetry and reef location reconstructions were created for each palaeo-sea level taking into account depth change and position of reefs. These models were then used for tidal analysis, and integrated with Lagrangian particle tracking in order to investigate whether tidal dynamics at 8 ka were responsible for increased larvae retention that may have contributed to regional reef initiation. Throughout, three sectors in the south, central and north of the GBR were selected to study. From each sector, particles representing coral larvae are released from reef polygons and tracked to calculate connectivity matrices. A self-seeding reef is defined as a reef which receives back at least some of the larvae it produces. Levels of self-seeding are assessed using the connectivity matrices produced by each of the

three models using diagonal analysis. The findings of this chapter will be used to answer three key questions: "What tidal dynamics were present during the Holocene GBR initiation around 8 ka and how are they different to the present day?", "How has connectivity changed throughout the Holocene initiation?" and "How did tidal dynamics affect coral connectivity during the Holocene initiation?". Finally, findings from this chapter will be used to inform predictions of changes to self-seeding behaviour in the future as sea levels continue to rise and how this could impact future management in the GBR.

4.1 Introduction

The present day Great Barrier Reef (GBR), known as the Holocene Reef, initiated coral growth around 8 thousand years ago (hereby abbreviated to 8 ka), coinciding with a large meltwater pulse following the Last Glacial Maximum (LGM), during the LGM between 21 - 19 ka sea level was approximately around 125 m lower than the present day (Yokoyama et al. 2018). As sea level rose and the GBR reefs established themselves, tidal dynamics are likely to have undergone significant changes, as sea levels and bathymetry interacted with each other. These changes have been shown by a numerical modelling study reconstructing past sea levels on the GBR, showing that tidal amplitude from M2 and S2 tidal constituents have increased since 16.8 ka, along with increased velocity, tidal range and bed shear stress measurements (Lee et al. 2022). Prior to 9 ka, sea level sat below the continental shelf of Australia: at this time the GBR lagoon was only a small inlet. Around 9 ka, as sea levels rose to 17 m below present day sea-level, the shelf slowly became submerged, forming complex bathymetry for tides to navigate. Sea level continued to rise and reached 3.5 m below present between 8.3 and 8 ka, with present sea level being reached around 7.9 and 7.7 ka (Sloss, Murray-Wallace, and Jones 2007). During this increase of sea level, the shallow waters establishing in the southern shelf were able to begin hosting corals which

appeared quickly between 8.2 and 8 ka; growth then slowed down between 8 and 7 ka and corals appeared in deeper, more turbid waters before tidal conditions changed to allow clear-water, enabling rapid growth to catch-up with sea level and the appearance of branching corals (Sanborn et al. 2019). Some areas of the GBR initiated growth earlier, for example the central GBR initiated around 9.5 ka (Webster et al. 2018).

The relationship between coral reef growth and sea level since the Holocene initiation have been studied so far using two different approaches. The first is taking core samples throughout the GBR, which provide data on community structure, stratigraphical and chronological data (Humblet and Webster 2017; Montaggioni et al. 1997; Marshall and Davies 1982). This method has been used to show coral community structure and facies over timespans of 100-kyr (Humblet and Webster 2017) and the effect of sea level on coral growth and death through accumulation of reef limestone and interruption of limestone accumulation when sea level falls (Hopley, Smithers, and Parnell 2007; Webster et al. 2018). Borehole core analysis has been able to map out reef community across the continental shelf for different sea-level scenarios, during low sea level throughout glacial periods where reefs were restricted to a narrow band on the edge of the continental shelf (Yokoyama et al. 2011). It is these studies that established that the present day Holocene reef initiated around 8000-7000 years ago, appearing first on the edge of the shelf. This was followed by a delay before the inner-shelf reef developed, when the reef moved seaward through the mid-Holocene to form reef flats covering the submerged shelf (Ryan et al. 2018). It is believed that the present day GBR reef positions were in place by around 7 ka, and that present day sea-level was reached between 8-7 ka (Lewis et al. 2013).

Studies have shown that the GBR initiated when sea-level, sediment levels, turbidity and temperature became optimal (Sanborn et al. 2024; Dechnik et al. 2015), but it is not yet understood how the GBR initiated itself in the Holocene in terms of larval supply and connectivity (Webster et al. 2018). Predictions about turbidity

caused by tidal dynamics can be made from the type and amount of sediment found in cores, but little is known about how coral ecology has been impacted by tidal dynamics on centennial-to-millennial temporal scales (Sanborn et al. 2024). Attempts have been made by coupling ecological models with stratigraphic forward models, such as pyReef (Salles et al. 2018), used to look at changes such as sea-level and temperature, rather than the impact of tidal dynamics on coral ecology. Modelling the development of tidal dynamics requires much more detailed and realistic algorithms than stratigraphic modelling allows. The relationship between tidal dynamics and rapid sea level rise (SLR) is expected to have influenced how coral reefs connected to each other based on previous studies on coral larvae transportation, and understanding how the GBR initiated and adapted to sea level increase and changing tidal dynamics is important for informing predictions into the future (Corrège 2006; Pandolfi et al. 2011; De'ath et al. 2012; Sanborn et al. 2019).

Here, numerical modelling, coupled with Lagrangian passive tracers, is employed to construct past sea-level scenarios between 7000 - 9000 years ago and the impact increasing sea level has on reef connectivity. This study will explore tidal dynamics before, during and after the initiation, to begin to pinpoint the critical tidal dynamics required both for initiation and for the survival of the GBR and to generate insight to how the GBR will respond to continuing sea-level rise.

4.1.1 Research Questions

The research questions being addressed in this section are:

1. What tidal dynamics were present during the Holocene GBR initiation around 8 ka and how are they different to the present day?
2. How has connectivity changed throughout the Holocene initiation?
3. How did tidal dynamics affect coral connectivity during the Holocene initiation?

4.2 Methods

Chapter 2 contains all general information on creating and running numerical models along with integrating Lagrangian particle tracking to simulate the movement of coral larvae. The same atmospheric forcings are used in this study, as although global palaeo-tide forcings have been generated before (Egbert, Ray, and Bills 2004; Wilmes et al. 2023), they are not used for this study. However, present day forcings have been used for palaeo-tide studies beforehand (Lee et al. 2022). For each model, configurations are as follows: viscosity was set to 1.0, mannings drag was set as 0.025 and the wetting and drying alpha was set to minimum of 0.5 and maximum of 75.0. The selected timestep was 90 seconds, with outputs generated every 900 seconds. The models were forced with tidal forcing from TPXO (Egbert and Erofeeva 2002) and no atmospheric forcings were used.

4.2.1 Study Site

The same study sites as chapter 3 are used in this study: The whole of the GBR is simulated with tidal forcing and analysis is carried out on both the entire GBR and the three subsections: Cape Grenville (north), Cairns (central) and Swain (south). Using the same study locations allows comparison between the sites, which is necessary for showing how reef connectivity has been impacted by rising sea-levels. It is noted that the sector of Grenville is close to the model boundary, which in theory could affect accuracy of tidal forcing, however the model validation carried out in chapter 2 showed that the tidal gauge in Grenville matched the tidal outputs of Thetis well.

4.2.2 Sea-Level Reconstructions

Palaeo relative sea level curves were taken from Lin et al. (2023) across the entire GBR between 15 - 4 ka (see table 4.1 and figure 4.1). This study used a version of the

ANU ice model (Lin 2019), used to reflect early global mean sea-level and matches sea level curve findings by Yokoyama et al. (2018). The mean sea-level from three locations across the central GBR (Missionary Bay (south central), Fantome Island (south central), Magnetic Island (south central)), was used to generate the past sea-level reconstructions across the entire GBR, data from other locations of the GBR were not available for the timeslices analysed in this chapter. To create palaeo-bathymetries, Beaman (2023) 250 m resolution bathymetry was used as the starting bathymetry with Holocene reefs stripped off the bathymetry (Salles et al. 2018; Maxwell and Swinchatt 1970). QGIS was used to raise the modern day bathymetry up by the correlating palaeo-sea level drop, for example, a sea-level of -1.7 metres below present was generated by raising the modern bathymetry elevation by 1.7 metres. This was done for 7 ka, 8 ka and 9 ka in order to capture the Holocene initiation in 8 ka, the modern day reef establishing in 7 ka and the sea-level prior to initiation in 9 ka.

- 9 ka is equivalent to 17 m below present sea level
- 8 ka is equivalent to 7 m below present sea level
- 7 ka is equivalent to 1.7 m below present sea level

Tidal models were forced with TPXOv9 (Egbert and Erofeeva 2002) data from the 5th November 2000 for an initial 5 days spin-up before continuing for 14 days to capture the spring and neap cycle. Although global palaeo-tidal forcing does exist (Wilmes et al. 2023), palaeo-models are constructed using present day tidal forcings with reconstructed palaeo-bathymetry, using the same methods as published in Lee et al. 2022. Simulations were carried out using Thetis, following methods outlined in chapter 2.

Year (ka)	NOG	Missionary Bay	Fantome Island	Magnetic Island	HYD	Mean
4		1.2	1.4			1.3
5		2	1.4	1.6		1.666666667
6		2	1	1.2		1.4
7		**-1**	**-3.4**	**-1**		**-1.8**
8		**-7**				**-7**
9		**-17**				**-17**
10	-40				-40	-40
11	-48				-48	-48
12	-58				-56	-57
13	-62				-60	-61
14	-72				-80	-76
15	-92				-92	-92

Table 4.1: Relative sea-level curve data taken from Lin et al. 2023, showing meters below present sea-level for available data. Abbreviations: NOG is Noggin Pass; HYD is Hydrographers Passage

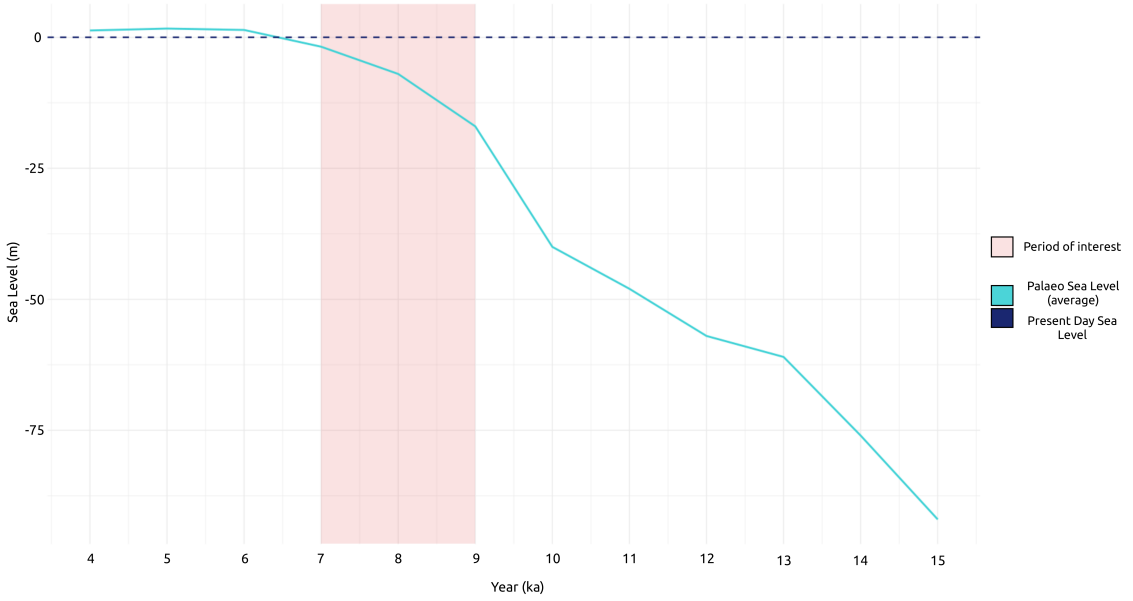


Figure 4.1: Average relative sea level curve plotted between 4 ka and 15 ka with period of interest (7 ka -9 ka) highlighted. Relative sea level came from Nogging Pass (north central), Missionary Bay (south central), Fantome Island (south central), Magnetic Island (south central), and Hydographers Pass (southern GBR)

4.2.3 Palaeo Reef Locations

Palaeo-reef positions across the entire GBR are not known, the scale of the GBR means confirming palaeo reef location using borehole cores across the entire shelf is impossible, instead, the shapefile polygons used in chapter 2 and chapter 3 will be modified to only contain reefs which are in optimal depth at each model sea level. Most reefs on the GBR are found at a depth between 3 meters and 30 on the GBR (Woesik and Done 1997; Gleason and Wellington 1995; Fabricius et al. 2023), we assume that corals between 7 - 9 ka required the same environmental conditions. Average depths were calculated for each polygon when positioned on the altered palaeo bathymetry, any reefs which had an average depth outside of 3 to 30 m were removed from the shapefile. The output is a shapefile only containing reefs which are at an appropriate depth for each model.

4.2.4 Larvae Transport

Coral larvae transportation is modelled using Parcels. Particles are released from the same point of the tidal cycle as they were released on the 11th November 2000 and tracked for 48 hours in each of the three sectors for each palaeo-model. Particle release from each reef polygon is scaled in the same method used in chapter 3, where 256 particles per km^2 from each reef were released. Although this meant that fewer particles overall were released across the model compared to in chapter 3, this method allowed for easier comparison between palaeo and modern day simulations.

4.2.5 Changing tidal dynamics

To understand how palaeo-tidal dynamics impacted the initiation of the Holocene GBR, the dominant tidal constituent M2 is modelled to capture tidal cycles (12.42 hours to complete a tidal cycle) and is analysed to extract data on tidal range, tidal velocity, elevation, amplitude and phase shift, as well as bed shear stress. Vorticity and sinuosity are also analysed using the same methods as chapter 2, to allow comparison of retention quantification, i.e. eddies and tidal ellipses. Tidal elevation from each model, including the modern day, is extracted from one location within each sector. The location was chosen from the bathymetry of 9 ka to ensure that the tidal gauge location would remain in the water across all palaeo-models.

4.2.6 Connectivity

From the Parcel simulations, trajectory start and end positions were recorded, all particles which landed on or were within 10 m of a reef polygon were considered to have landed on that reef polygon. They were then recorded in connectivity matrices for each sector, producing nine connectivity matrices in total. These connectivity matrices are used to extract the self-seeding information and per-

form network analysis. Self-seeding data comes from diagonal analysis, which follows the same methods as in chapter 3. Here, the self-seeding data is used to examine how self-seeding behaviour changed throughout large shifts in sea-level across the Holocene initiation. Self-seeding will be examined before, during and after the Holocene initiation and also compared with present day self-seeding behaviour from chapter 3 to provide scale to the changes. The mean is extracted from each diagonal as well as a non-parametric Kruskal-Wallis test to compare medians for significant differences.

4.2.6.1 Network analysis

To give greater dimension to understanding the changes to tidal dynamics and self-seeding behaviour, network analysis using iGraph Constant-Potts-Model (CPM) with Leiden algorithm will be conducted in the same way as chapter 3, but here to explore how networks have changed over nine thousand years of SLR. The same γ parameter of 0.005, as used in chapter 3, will be used in order to be able to compare differences of community structure.

4.3 Results

This section will cover the results of location of possible palaeo reefs, changes to tidal dynamics and changes to connectivity shown by connectivity matrices and CPM analysis. The research questions being addressed are listed below with their respective results location:

The research questions being addressed in this section are:

1. What tidal dynamics were present during the Holocene GBR initiation around 8 ka and how are they different to the present day?
2. How has connectivity changed throughout the Holocene initiation?
3. How did tidal dynamics affect coral connectivity during the Holocene initi-

ation?

4.3.1 Morphological evolution

Three palaeo-bathymetric reconstructions were made, the changes to bathymetry and coral reef locations are shown in figure 4.2. Bathymetry in 7 ka is not dissimilar to the present day, most reef locations are the same apart from the shallowest reefs of the present day – these are located in the southern GBR, along the Capricorn Channel and Swain. Depth of the 8 ka bathymetry is visibly shallower than 7 ka throughout the shelf and many reefs were removed from the inside of the shelf, depth along the edge of the shelf has remained more stable. A clear difference in depth can be seen between 8 ka and 9 ka, where most of the shelf is less than 20 m deep, the northern GBR is particularly shallow, around 5 metres deep. There are much fewer locations available for reefs in 9 ka, most present day reef locations are exposed permanently as islands at this time, palaeo-reef locations are almost exclusively on the edge of the shelf.

4.3.2 Tidal dynamics

Changes to tidal dynamics are analysed from each of the palaeo-sea level models and differences are compared with the modern day M2 amplitude, tidal range, average velocity and average BSS (see fig. 4.3).

4.3.2.1 Tidal elevation

Tidal elevation in Grenville, Swain and Cairns were visualised across 7 days following the larvae release date for the modern day and each palaeo-model (fig. 4.4). Overall, palaeo-tides follow the same tidal cycles as observed in the present day but of varying elevation height depending on location within the GBR. Tidal elevation in Cairns has not changed since 9 ka, there is a slight reduction in elevation since 9 ka to the present day, but the changes are not considered significant.

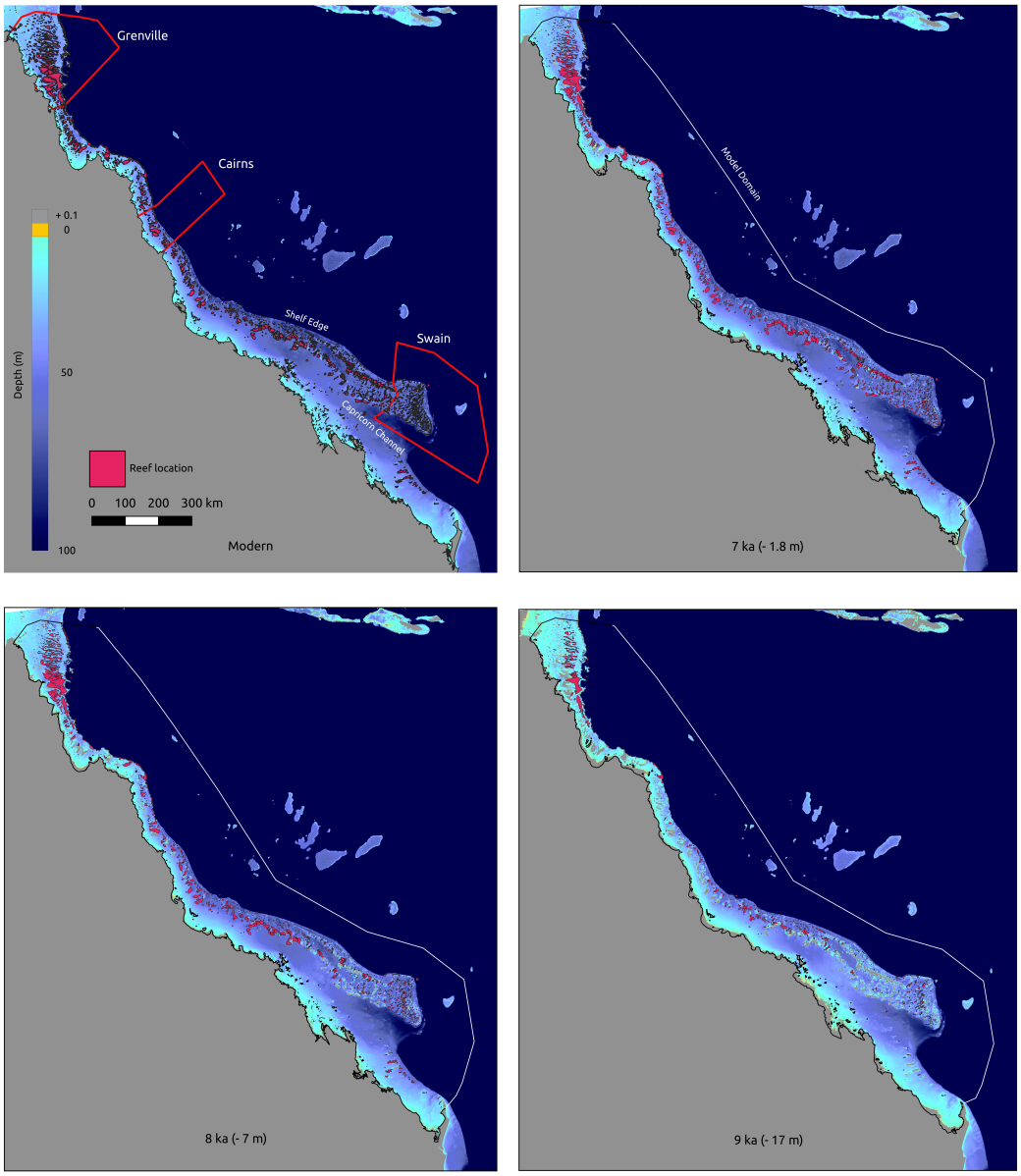


Figure 4.2: Bathymetric changes for 7 ka, 8 ka and 9 ka created by increasing the height of the modern bathymetry using QGIS. Reef locations for each model are shown in red and represent modern day reefs which are in suitable locations of depth in each of the model sea levels, modern reefs which have an average depth outside of tropical reef tolerance are removed. Black line along coast and top of GBR, and the white line represent the simulation boundary.

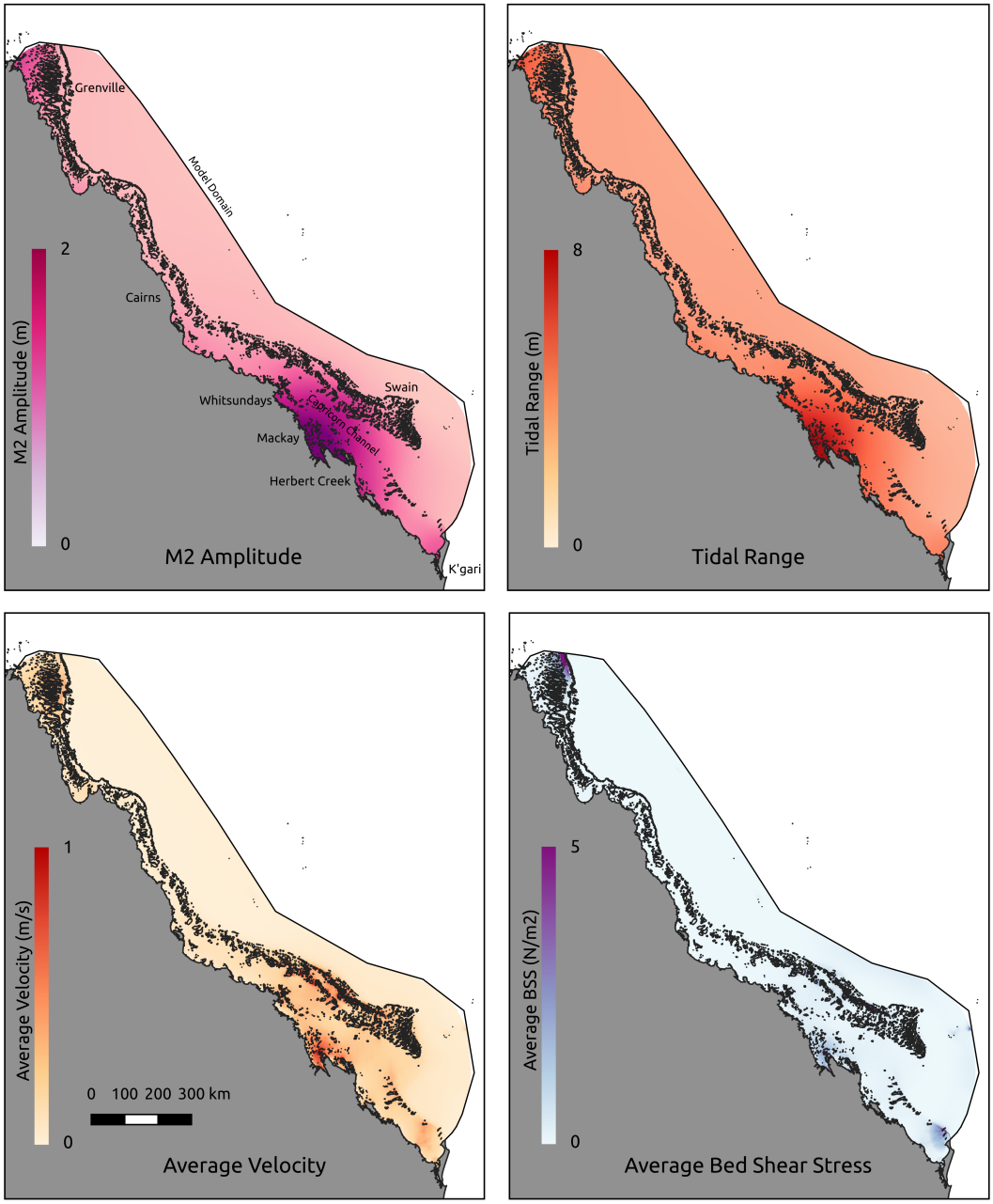


Figure 4.3: Tidal dynamics of the modern day for M2 amplitude, tidal range, average velocity and average bed shear stress. This figure is for assisting with later figures showing changes to tidal dynamics between the specified timestep and the modern day.

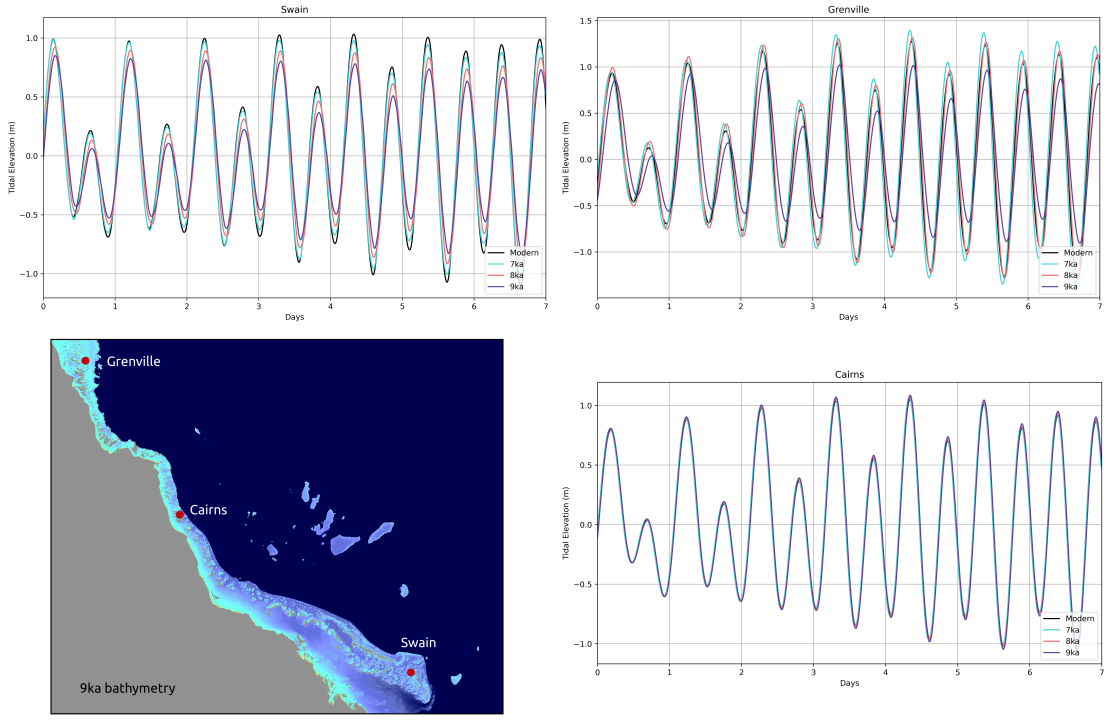


Figure 4.4: Tidal elevation taken from three locations across the GBR, locations are specified by red dots in the map view. Tidal elevation is generated for the entire model domain, and then extracted from the location of each dot, representing each sector. Tidal gauge locations were kept central in each sector.

Both Swain and Grenville experience clear shifts in tidal elevation amplitude between 9 ka and the present day. Tidal elevation at 9 ka is at its lowest across both sectors. At the Swain gauge location, the tidal elevation amplitude is greatest in the modern model and sea-level rise is consistent with increased tidal elevation. In contrast, Grenville records the highest elevation in 7 ka. At Grenville, tidal elevation amplitude increases from 9 ka to 8 ka; however, tidal elevation amplitude at 7 ka is then found to be higher than 8 ka around the spring tide, while 8 ka produces higher tidal elevation amplitude than 7 ka around the neap tide. The modern elevation is most similar to the tidal elevation during 8 ka.

In Swain and Grenville, tidal phase has slightly shifted since 9 ka; in Grenville spring and neap tides occur around an hour earlier today than they did in 9 ka, whereas in Swain the time difference is less than Grenville at around 30 minutes.

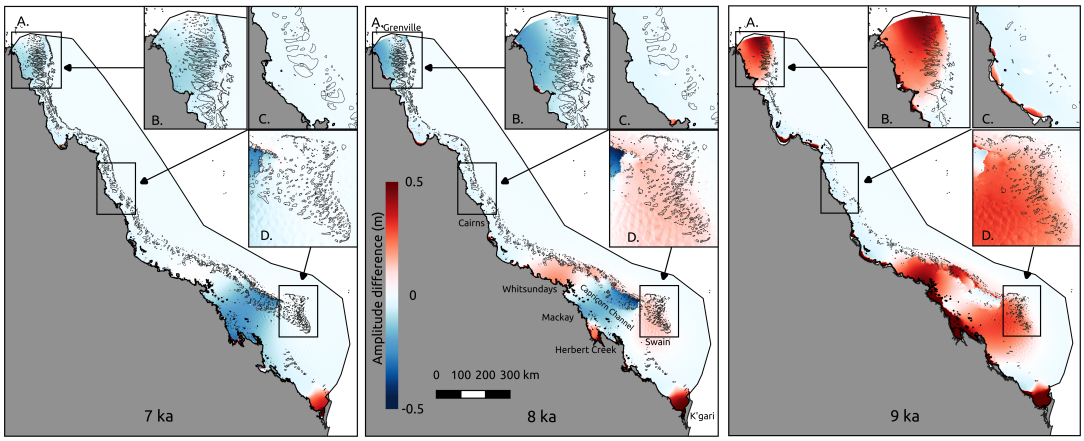


Figure 4.5: Difference in M2 amplitude between the present day and each palaeo-model (calculated by modern raster minus the palaeo raster). The figures (A) show the entire GBR with zoomed in sections (B - D) for each sector of interest.

4.3.2.2 Change in M2 amplitude

The dominant tidal constituent, M2, has shifted in amplitude over the last 9 thousand years (fig. 4.5). Since 9 ka, tidal amplitude has increased across the majority of the GBR, in particular around the southern GBR, including Swain, and the northern-most GBR at Grenville. However, M2 amplitude has reduced since 9 ka in the central GBR, around Cairns. Since 8 ka, areas of M2 change are different to 9 ka: Swain, the northern Whitsundays and the inlets of K'gari and Herbert Creek still increase as sea levels rose to the present day, while M2 amplitude has reduced throughout the entire northern and central GBR, as well as north of Swain in the widest section of the Capricorn Channel. Grenville undergoes a large change between 9 ka and 8 ka: where at 9 ka M2 amplitude is over 0.5 m lower than found in the present day, it then increases to 8 ka where it is then ~0.3 m higher than the present day. A convergence zone between increased and decreased M2 has appeared at the Whitsundays in this model. Since 7 ka, M2 amplitude has decreased across the entire GBR, apart from around K'gari, most reduction is found in Grenville and in the Capricorn Channel around Herbert Creek. Although Swain has reduced slightly in amplitude since 7 ka, M2 amplitude is mostly the same as it is now.

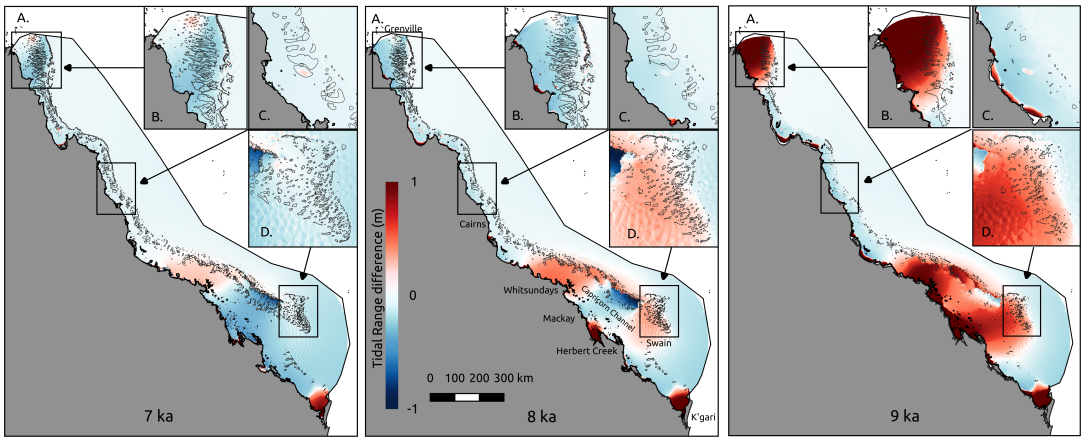


Figure 4.6: Difference in tidal range between the present day and each palaeo-model (calculated by modern raster minus the palaeo raster). The figures (A) show the entire GBR with zoomed in sections (B - D) for each sector of interest.

4.3.2.3 Tidal range

Palaeo-sea level constructions experienced different tidal range to the present day (fig. 4.6). Since 9 ka, tidal range has increased across most of the GBR, particularly in the southern GBR and the northern GBR. The reefs in the north east of Swain and the south of Grenville have undergone a reduction in tidal range since 9 ka, while the rest of the reef areas have increased in tidal range. Since 8 ka, most of the southern GBR has increased in tidal amplitude, particularly in Swain, K'gari and Herbert Creek. The central and northern GBR tidal range has reduced since 8 ka, this includes the sectors of Cairns and Grenville. In both of these areas, tidal range has reduced most between the coast and reefs. Like with M2 amplitude, Grenville undergoes a large change between 9 ka and 8 ka: where at 9 ka M2 amplitude is over 1 m lower than found in the present day, it then increases to 8 ka where it is then ~0.5 m higher than the present day. Since 7 ka, tidal range has continued to mostly reduce across the GBR to the present day. There has been an increase in tidal range in the south-central reef and north of K'gari. Swain and Cairns have only reduced in tidal range very slightly as sea level continued to rise, whereas Grenville has experienced a much larger reduction in tidal range since 7 ka.

4.3.2.4 Velocity

Changes to tidally-average velocity demonstrate long term velocity trends across a tidal cycle, figure 4.7 illustrates how average velocity has changed across M2 cycles since 9 ka. Note that this velocity is from the neap to spring cycle, rather than a full tidal cycle. Changes in average velocity since 9 ka are fragmented across the GBR, with areas that have undergone the greatest increase in velocity since 9 ka are within the reefs of the Capricorn Channel and along the coast near Herbert Creek. The Swain area has mostly reduced in velocity since 9 ka, particularly within the shelf edge reefs, however there has been some increase in velocity within the southern reefs. Average velocity in Cairns has mostly decreased along the shelf since 9 ka, some small areas have increased in velocity which become reefs in 8 ka and 7 ka. Grenville has reduced in velocity since 9 ka along the shelf edge and across the shelf, areas which have increased in velocity are along the coast. Since 8 ka, trends of velocity change mirror 9 ka but the magnitude of change is higher, for example, Swain and Grenville contain more areas which have reduced in velocity by at least 0.5 m/s, while north of Swain increases in velocity by at least 0.5 m/s. Since 7 ka, the GBR has mostly experienced a reduction in average velocity but the changes to velocity are much less than the changes since 8 ka and 9 ka. Swain has mostly reduced in velocity since 7 ka, with some reefs in the south of the sector increasing in velocity as sea level rose. Velocity has also increased on reefs in Cairns, while the shelf has slightly reduced in velocity. Grenville has reduced in velocity mostly along the barrier reefs sitting on the shelf edge, while the mid shelf and southern reefs have increased in velocity as sea levels have increased. Overall since 7 ka, the central GBR, where the shelf is at its narrowest has not changed in velocity.

4.3.2.5 Bed Shear Stress

Similar to changes in velocity, average bed shear stress across the GBR has mostly reduced since 9 ka (fig. 4.8). Magnitude of changes to BSS are highest in the

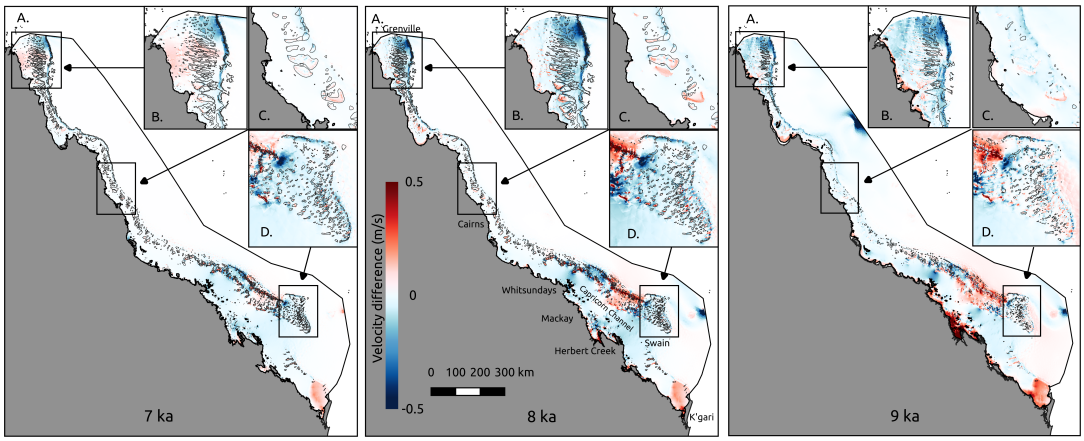


Figure 4.7: Long term changes (across a spring-neap cycle) in average velocity between the present day and each palaeo-model (calculated by modern raster minus the palaeo raster). The figures (A) show the entire GBR trends with zoomed in sections (B - D) for each sector of interest.

southern and northern GBR. Since 9 ka, increases of BSS are located in Herbert Creek, north of Swain and in the north of Grenville. Behind the northern barrier reefs, Grenville has increased in BSS since 9 ka and has reduced in BSS across the rest of the shelf in the sector. Swain and Cairns have both reduced in bed shear stress. For Swain and Grenville, BSS increased between 9 ka and 8 ka before reducing the BSS of the present day, this is seen from the difference between 9 ka and the present day, is smaller than the difference between 8 ka and the present day. From 7 ka, BSS in Swain and the majority of Grenville continued to reduce to levels of the present day, northern Grenville continued to increase in BSS. The central GBR has only experienced a slight reduction in BSS since 9 ka, Cairns has undergone very little change in BSS since 8 ka. Since 7 ka, the BSS change trend is the same as the other sectors, but in smaller intensity. Grenville experiences almost the same BSS across the mid-shelf as the present day, but the present day experiences higher BSS in the north east of the sector.

4.3.2.6 Vorticity

Average L_2 Norm of vorticity was calculated for each palaeo-model and the present day across each sector (figure 4.9). Palaeo-vorticity levels have decreased across

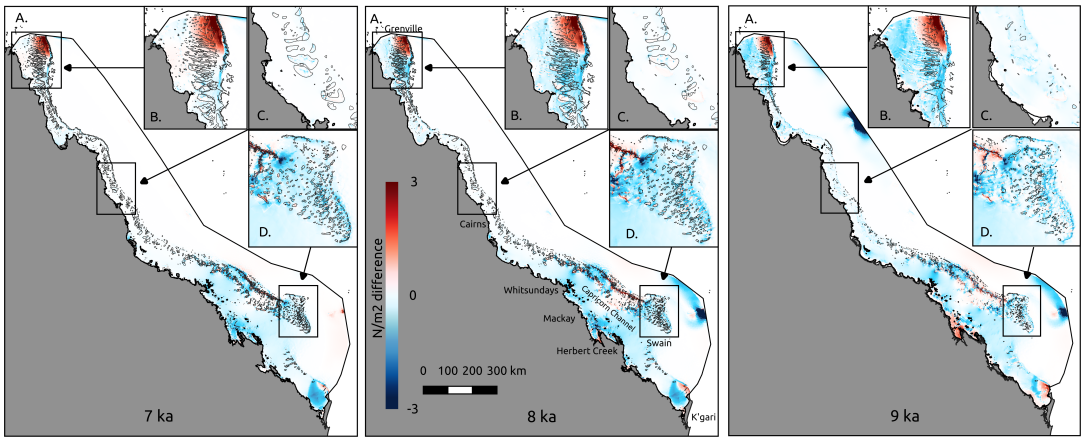


Figure 4.8: Long term difference (across a spring-neap cycle) in average bed shear stress between the present day and each palaeo model (calculated by modern raster minus the palaeo raster). The figures (A) show the entire GBR with zoomed in sections (B - D) for each sector of interest.

all sectors since 9 ka as sea levels rose. The highest vorticity levels are generated by the 8 ka model for each sector. The smallest changes across the models is in Cairns, where vorticity increases from 9 ka to 8 ka, it then reduces at 7 ka almost back to 9 ka L_2 Norm levels, before reducing again to the modern model, which shows the lowest L_2 Norm. The Swain area undergoes slightly more change but follows the same trend: vorticity increases from 9 ka to 8 ka where the L_2 Norm is highest, before reducing in 7 ka back to similar L_2 Norm as 9 ka, modern vorticity is again the lowest of the models. Large changes in vorticity are seen in Grenville, vorticity increases from 9 ka to 8 ka: the minimum vorticity in 8 ka is equivalent to the maximum L_2 Norm in 9 ka, before reducing back to 9 ka L_2 Norm levels in 7 ka. Modern L_2 Norm is overall lower than 7 ka and 9 ka, but there is overlap with modern maximum and palaeo minimum L_2 Norm values.

4.3.2.7 Sinuosity

Mean sinuosity values fluctuate across sectors and time (see figure 4.10). Cairns 9 ka had a mean value of 11.9, which decreased with sea level to 9.16 in 8 ka, before increasing slightly to 9.43 in 7 ka and reducing again to 8.51 in the present day. Sinuosity in Grenville remained stable between 9 ka and 7 ka (19.7 - 19.9) before

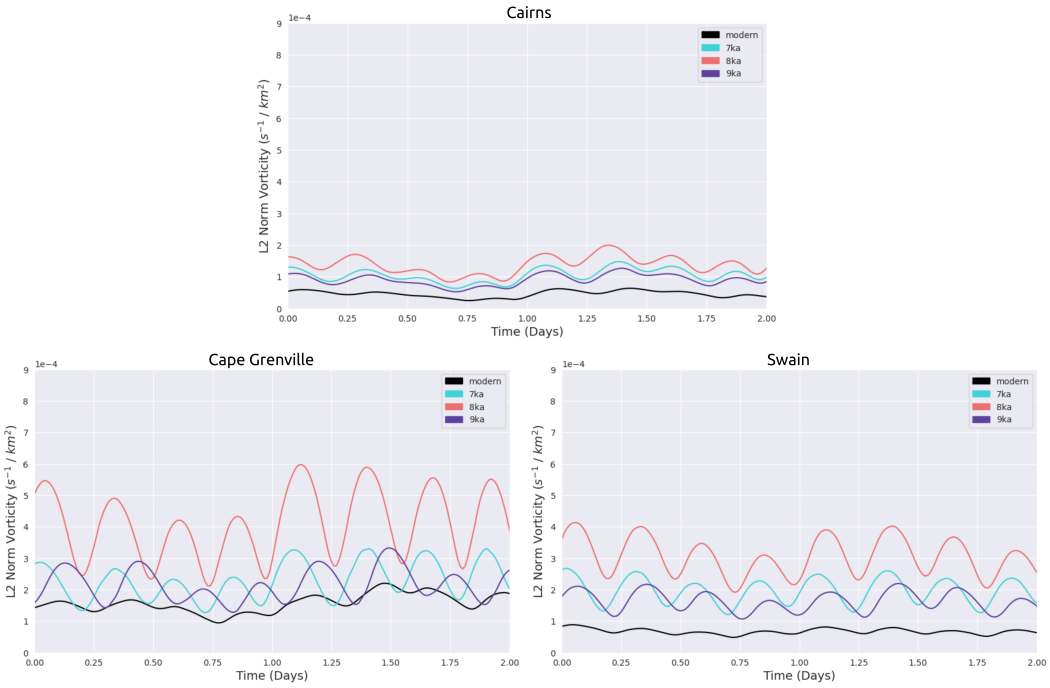


Figure 4.9: Average L_2 Norm vorticity measurements plotted across the anticipated 48 hour window of annual mass spawning events for each palaeo-model. Vorticity was calculated for each sector individually and the 48 hour window captures the annual mass spawning event. L_2 Vorticity underwent a logscale 10 to show the differences between each of the measurements. Modern vorticity averages are included for comparison against palaeo results.

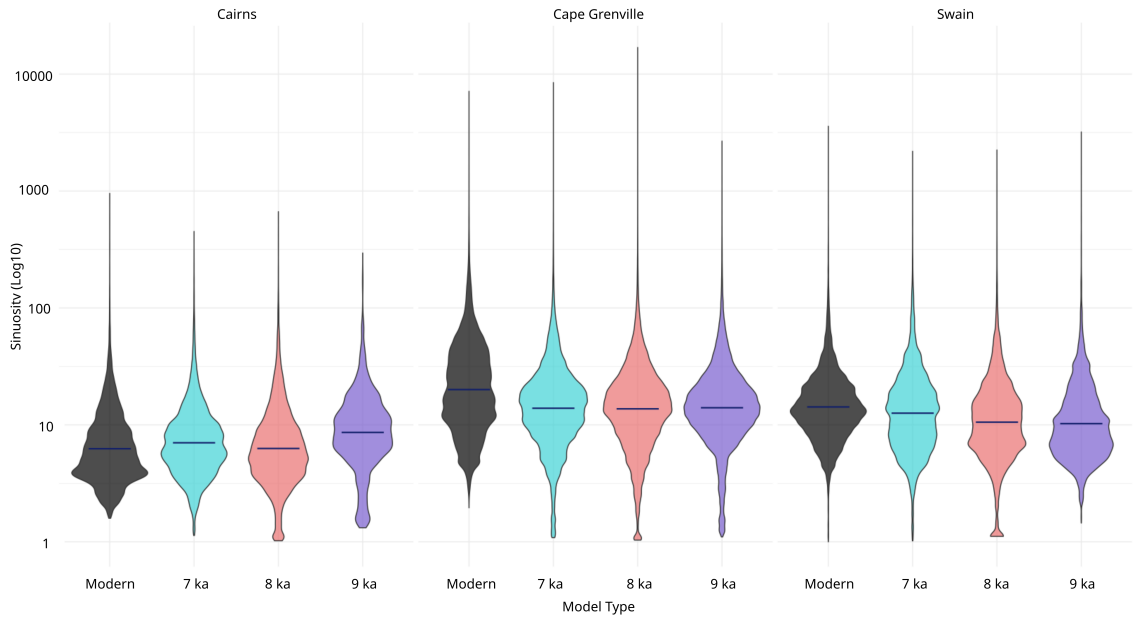


Figure 4.10: Violin plots of sub-sampled data of sinuosity values for each model in each sector. Sinuosity values of 1 translate to a straight line, the larger the sinuosity score the more curvature is contained in the particle trajectories. Trajectories with high curvature are associated with stronger tidal dynamics.

increasing to 30.8 in the modern. Swain increased slightly between 9 ka and 8 ka from 14.1 to 15.2, before increasing to 18.5 in 7 ka, increasing slightly to 18.6 in the modern day. Grenville has the highest mean in sinuosity across the time steps, it also had the highest mean vorticity of the sectors. Cairns experienced the lowest sinuosity, as well as the lowest mean vorticity.

Non-parametric Kruskal Wallis statistical tests were ran on all models to indicate if there are significant differences within each sector across the time steps. Significant differences were found within each sector (p = < 0.001). Effect-size was calculated using eta-squared (η^2) for assessing practical use of the significant differences due to the large dataset. Results of the effect-size for palaeo models showed there were small practical differences within each sector, Cairns is (η^2) = 0.01), Swain is ((η^2) = 0.03), and Grenville is (η^2) = 0.03.

4.3.3 Connectivity

4.3.3.1 Self-Seeding Behaviour

Following tracking particle transport between reefs with Parcels for 48 hours, connectivity matrices were generated. Self-seeding reefs are recorded on the diagonal of the connectivity matrix, the diagonal was extracted and analysed for each model to explore how self-seeding behaviour has changed in each sector across the Holocene initiation. Firstly, during the extraction of the diagonal values the percentage self-seeding reefs are recorded in table **??**. The percentage of self-seeding reefs has slowly increased since 9 ka, with the biggest increase seen in Cairns between 9 and 8 ka (increase of 32.14% points over 1000 years), taking place around the Holocene initiation. During the same time, Grenville increased by 11.51% points and Swain an increase of 12.72% points. Self-seeding percentage increases continue after 8 ka to 7 ka but at a smaller scale: Cairns increased by 2.11% points, Grenville by 5.59% points and Swain decreased in self-seeding reefs by 2.92% points. Self-seeding continues to increase from 7 ka to the present day, Cairns increases by 22.89% points, Grenville by 13.93% points and Swain by 4.06% points. Mean diagonal value has also increased since 9 ka (table **??**), representing an increase in the number of reefs as well as the percentage of self-seeding reefs. The largest increase happens in Cairns between 9 and 8 ka with an increase of 1559 in mean diagonal value, the smallest difference in mean is 19 in Swain also between 8 and 9 ka. Swain diagonal mean increases by 57.1 between 8 ka and 7 ka. Grenville increases by 22 and Cairn's by 2.11 in the same period.

The distribution of self-recruitment values, as shown in figure 4.11, shows Cairns has the highest frequency of low self-recruitment values in 9 ka, frequency of non-self-seeding reefs decreases with SLR. The distribution in Cairns for 7 ka and 8 ka are similar to each other, both showing a shift towards higher self-recruitment. The modern distribution exhibits the highest frequency mean self-recruitment. In 9 ka, Grenville also has the highest frequency of low self-recruitment

values, followed by an increase of self-recruitment values in 8 ka. Similar to Cairns, 8 and 7 ka similar, with the modern distribution showing the highest overall self-recruitment, consistent with patterns observed in Cairns. In contrast, Swain shows the highest frequency of low self-recruitment values at 8 ka. However 9 ka has the lowest mean self-recruiting overall. The 7 and 8 ka distributions are similar, while the modern distribution again shows the highest frequency of high self-recruitment values. Overall, as sea level has increased since 9 ka, reefs have increased in self-recruitment values.

Kruskal-Wallis tests were conducted to detect significant differences in median values within each sector for the models. Significant differences were found within all sectors (p = < 0.001), therefore a post-hoc Dunn's test was carried out to detect which models a significant difference existed between. There was no significant difference detected in Swain and Cairns between 7 ka and modern, there is a significant difference in Grenville between 7 ka and modern (p = 0.003). Grenville has significant differences between all model combinations apart from between 8 ka and 9 ka (p = 0.27). For Cairns, no significance was found between 7 ka and modern (p = 0.1) and 8 ka and modern (p = 0.059), but significant differences were found for all other model combinations (p = < 0.05). Swain also had no significant differences between 7 ka and modern (p = 0.09) and 7 ka and modern (p = 0.27).

Model	Swain		Grenville		Cairns	
	Mean	Self-seeding reef %	Mean	Self-seeding reef %	Mean	Self-seeding reef %
Modern	188	38.64	1763	58.62	2623	75
7ka	116	34.58	1270	44.69	2133	52.11
8ka	58.9	37.5	1248	39.1	1682	50
9ka	39.9	24.78	1174	27.59	123	17.86

Table 4.2: Diagonal mean values of particles self-seeding and percentage of self-seeding reefs in each sector.

4.3.3.2 Network Analysis

Network analysis conducted by CPM produced maps of clusters across each palaeo-sea level reconstruction (see fig. 4.12 and table 4.3). Care has to be taken with comparing clusters across models in each sector, as there is a reduction in available reefs within each model, altering how clusters are able to form. Table 4.3 shows that there is a fluctuation in number of communities across the time steps, number of communities reduced between 9 ka and 7 ka in Swain and Cairns, but increased between 9 ka and the modern day in Grenville. Grenville shows clusters of reefs in 7 ka and 8 ka, particularly in the southern section; 9 ka shows very fragmented reefs, almost all of which form their own independent cluster. The clusters increase in size between 8 ka and 7 ka: nearby reefs to 8 ka clusters become recruited in 7 ka. Cairns has only a handful of small reefs in the 9 ka model, most of which form their own clusters. By 8 ka, more and larger reefs have been able to establish themselves and clusters have began to form, the largest cluster holding more than 8 reefs. By 7 ka, the clusters have fragmented slightly, there are more clusters, however they contain fewer reefs and are generally much more localised to neighbouring reefs. As Swain's number of reefs increased with SLR, so did the number of clusters. In 9 ka reefs are located in the northern section of Swain, primarily in the centre, the central clusters are large and widely spread across the Swain area, whereas clusters around the edge of Swain are much more fragmented. 8 ka holds many more reefs, forming smaller clusters in the centre than found in 9 ka; edge reefs have began to form clusters. 7 ka sees another increase in number of reefs and the number of clusters, these are kept to immediate neighbouring reefs.

4.4 Discussion

The discussion will firstly cover changes to tidal dynamics across the past 9,000 years, examining how and why changes occurred between the present day and

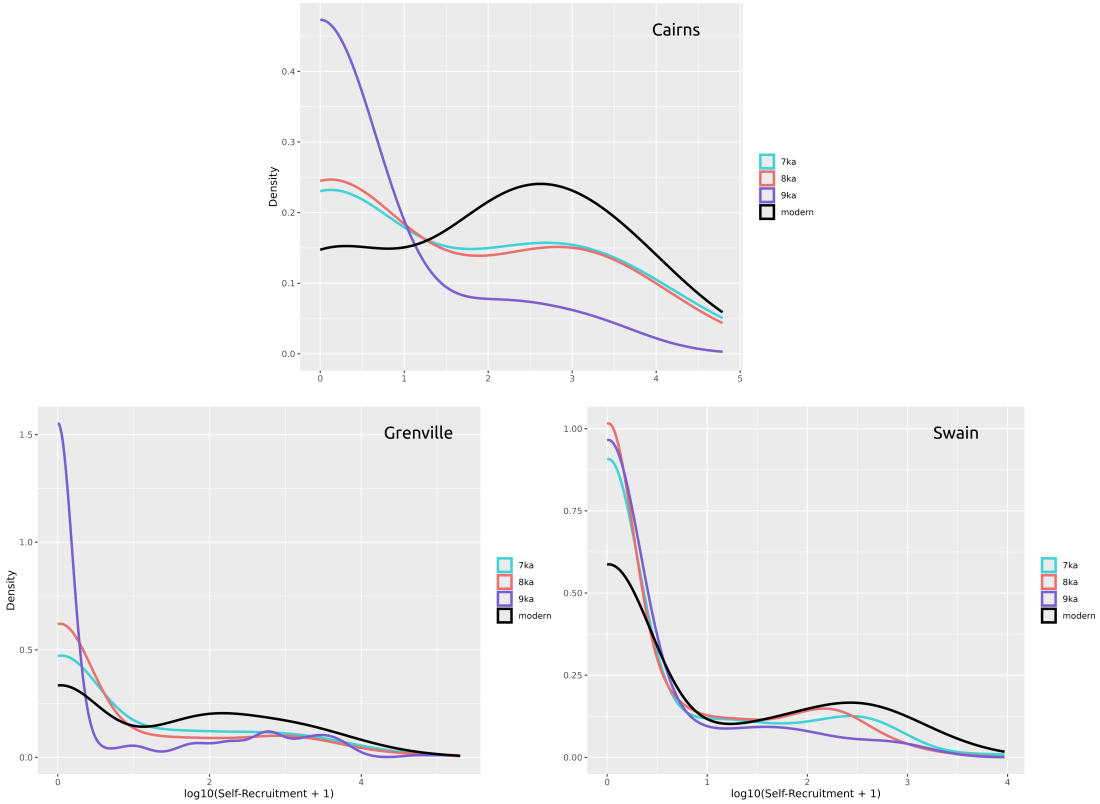


Figure 4.11: Density curves of self-seeding mean generated from connectivity matrices for each sector across each model. Modern density curves are included for comparison of the modern day versus palaeo mean.

Model	Swain		Grenville		Cairns	
	No. of Communities	No. of available reefs	No. of Communities	No. of available reefs	No. of Communities	No. of available reefs
7ka	111	402	111	537	20	71
8ka	113	416	97	468	19	62
9ka	130	335	93	232	22	28

Table 4.3: Number of communities calculated from the CPM, and the total number of available reefs for each timestep.

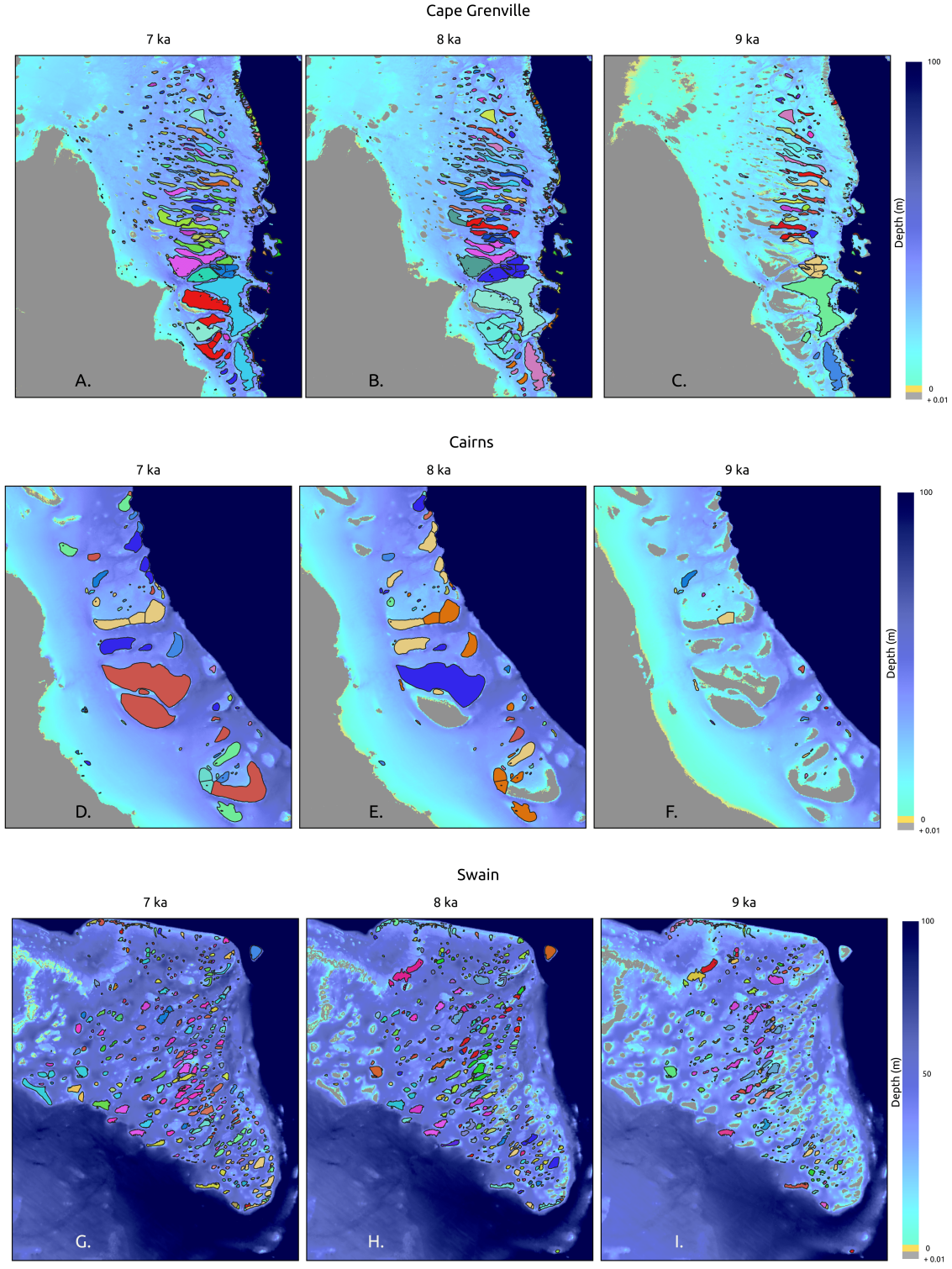


Figure 4.12: Maps of reef community clusters from CPM model for each model and sector. Each CPM model had the parameter γ set to 0.0015. Colours of clusters do not correlate to each other across maps: only shape and size of clusters should be compared.

the past, with particular attention paid to changes at 8 ka. Following on from this, coral connectivity changes will be examined to explain how connectivity is the present day evolved across the Holocene initiation. Once these two areas have been examined, they will be combined to find patterns and reasons for changes: how tidal dynamics may have influenced coral connectivity, and how increased coral growth may have influenced tidal dynamics. Finally, limitations and implications of the research will be addressed.

4.4.1 Summary of key findings

The key findings of study in response to the three research questions 4.1.1 were:

- Self-seeding reefs increased as sea levels rose.
- Shelf areas away from the coastline were affected by rising sea level later than shelf areas close to the coast.
- The peak of tidal dynamic strength was between 8 ka and 7 ka, depending on location on the GBR.
- High levels of velocity, BSS and vorticity indicated greater presence of eddies and tidal oscillation – these are attributed to coral larvae retention and hence the increase in self-seeding behaviour.
- Sea level in 8 ka also created more areas for reefs to establish and develop into large reefs.

4.4.2 Changes in tidal dynamics

4.4.2.1 Tidal elevation

Changes in tidal elevation over the last 9 thousand years varied across the GBR. For example, Cairns does not experience large tidal changes across the four time slices; Cairns is in the central GBR and sits on the narrowest section of the shelf,

therefore SLR will have affected this area first and quickly, establishing similar tidal regime to the modern model much earlier than other shelf areas. Swain area undergoes an increase in tidal elevation alongside SLR: Swain sits in the southern GBR, is far from the coast and is the deepest of the sectors. The increase in tidal elevation suggests that sea level intruded this area uniformly and was not restricted by dense reef matrices. In contrast to Swain, Grenville increases and decreases in tidal elevation over the 4 models. Grenville is a large area sitting on a wide shallow area of the shelf, it has true barrier reefs sitting along the shelf edge, blocking incoming tides from the Coral Sea and restricting flushing from the shelf (Wolanski et al. 1988). Across the mid-shelf the reefs are increasingly dense and large southwards, the northern reefs sit far from the coast and the southern reefs are very close to the coast. This complex morphology in Grenville controls rising sea level intrudes the sector at different points in time and compared to other locations along the GBR (Wolanski 1983), the highest tidal elevation being in 7 ka suggests a delay in SLR affecting Grenville. In response to the research questions (4.1.1), tidal elevation during the Holocene initiation varied across the GBR, tidal elevation was higher than the present day in Grenville, similar to the present day in Cairns and lower than the present day in Swain.

4.4.2.2 M2 amplitude and tidal range

The M2 amplitude was the lowest in 9 ka, and it has since increased with sea level to 8 ka. The theory behind non-uniformity of M2 amplitude change will be the same as for tidal elevation: the shelf width, depth and proximity to the coastline along with density of reefs and proximity of those to the coastline will affect the magnitude and timing of SLR effects. For example, resonance effects may play a role in amplifying tides when the length of the shelf is 1/4 of the wavelength of the tidal constituent (Green 2010). The narrow shallow central GBR shelf around Cairns has not experienced much change throughout the 9 thousand years because it will have been impacted by rising sea level at an earlier stage (Hopley

2006). M2 amplitude in 8 ka is the least consistent across the GBR, the decrease in M2 amplitude since 8 ka in Grenville and the Capricorn channel suggest that M2 amplitude was at its highest during 8 ka. Areas which have increased in M2 ampltiude since 8 ka, such as Swain, the Whitsundays, the outer-reefs of the Capricorn Channel, Herbert Creek and K'gari, which are all protected by dense areas of reefs and the Capricorn Channel. Herbert Creek and K'gari increased in M2 amplitude as both are inlets and water becomes trapped, this could also be an example of possible tidal resonance. The large change Grenville undergoes between 9 ka and 8 ka is likely due to bathymetry. As mentioned in 4.4.2.1, the depth, size and morphology of reefs appears to be blocking tidal wave propagation into the area in 9 ka, the morphology then traps the tidal wave within the sector in 8 ka. By 7 ka, Swain area has reached the same M2 amplitude as the present day, whereas M2 amplitude is still higher within the Capricorn Channel and Grenville than in the present day. The reason for this may also be due to dense reefs causing a lag in the timing of the tidal wave passing through and preventing the flushing of a spike in SLR (Wolanski 1994). The Capricorn Channel around Mackay has also been shown to be sensitive to SLR (Mawson, Lee, and Hill 2022).

Tidal range was lowest in 9 ka: the present day experiences a tidal range over 1 m higher than recorded in the 9 ka model. The same trends in location of changes are found across tidal range as M2 amplitude. The greatest changes in tidal range occur in the southern section of the GBR, within the Capricorn Channel, whilst the central GBR is similar to but slightly higher than the present day. Grenville experiences the same changes in tidal range as experienced in M2 amplitude between 9 ka and 8 ka, supporting the idea that the tidal wave is blocked by bathymetry/morphology in 9 ka and trapped in 8 ka. Inlet areas such as Herbert Creek and K'gari increase with SLR due to water being trapped, the same as found in M2 amplitude. Tidal range in 7 ka was higher than recorded in the present day, this may be due to the increased density of reefs in the present day blocking tidal

waves.

Overall, tidal elevation, range and M2 amplitude have all changed over the last 9 thousand years to the present day. The results have shown that different areas of the GBR are influenced by rising sea level in different directions and at different times. Cairns has remained very similar to tidal dynamics in 9 ka but tidal activity has reduced slightly over this time, suggesting that this area is robust during SLR but tidal dynamics will continue to reduce in intensity as sea level continues to increase. Swain increases in tidal activity between 9 ka and 7 ka during SLR, however tidal dynamics between 7 ka and the present day are very similar, with tidal range and M2 amplitude reducing between 7 ka and the present day, suggesting that tidal dynamics reached their peak strength around 7 ka and 8 ka. Grenville recorded highest tidal elevation during 7 ka for spring tides and 8 ka during neap tides, this was also found for M2 amplitude and tidal range, suggesting that Grenville also experienced tidal dynamic peak around 8 ka. In response to the research questions, the results so far suggest that the initiation took place during higher levels of tidal elevation, range and M2 amplitude than experienced in the present day.

4.4.2.3 Average velocity and bed shear stress

Exploring velocity and bed shear stress change across 9 thousand years assists with establishing what conditions were present during the 10 m rapid increase of sea level. Velocity in Swain, Grenville and Cairns was higher in 9 ka than recorded in the present day. However, 8 ka records velocity of 0.5 m/s faster in Swain and Grenville than the present day, whereas in the same areas in 9 ka, velocity difference was found to be < 0.5 m/s, suggesting velocity was highest in 8 ka. Velocity values are slightly lower in 7 ka than in 8 ka. Areas of high increases in average velocity are around areas of dense reefs, such as the edge of Swain and the barrier reefs on the shelf edge within Grenville, this suggests that sea level was having the greatest effect on the shelf-edge, or that as reefs began to congregate

in denser matrices, higher velocity was generated. As reefs require high levels of velocity (**Mawson2025-un**; Drake et al. 2025; King and Wolanski 1992; Hopley 2006), it is difficult to distinguish whether reefs developed in these areas due to high velocity or whether velocity increased because the shallow edge was able to host corals. For findings in this study, reef locations in this study are based on depth rather than velocity, it can be assumed that reefs established there due to depth and contributed to causing higher levels or velocity on the already shallow edge. Overall, increased velocity on the GBR from 9 ka and reaching a peak in 8 ka will be due to sea level reaching a height it can flood the shelf in increasing magnitude, however there will be a balance for sea level being high enough to flood the shelf but shallow enough to reach high levels of velocity. Turbidity is considered to be a major factor in coral reef "turn-ons" (Buddemeier and Smith 1988). Sea levels in 8 ka will have been high enough to generate stronger tidal oscillations across the shelf, as seen from tidal range and elevation, as sea levels continued to increase the strength of tidal oscillations have decreased (Lee et al. 2022).

Bed shear stress across the majority of the GBR has reduced from palaeo-levels, with highest levels recorded in the 8 ka model for the southern and northern GBR. The reason for this will be connected to the increase in velocity in these areas during the same time, which could be due to sea level reaching a balance of height and tidal oscillation strength. As more reefs appeared, higher levels of BSS will have been generated from eddies and tidal jets forming around reefs (Wolanski et al. 1988). There is a relationship between water depth and bed shear stress, with shallow water generating more bed shear stress for a given velocity (Pascolo, Petti, and Bosa 2018). BSS has increased since 9 ka in Grenville behind barrier reefs as well as north of Swain, which is also around barrier reefs. The reason for this may be that barrier reefs were blocking the tide in these areas, water will have had to seep into these areas from other routes, such as through the Capricorn Channel and weaving through the southern Grenville reefs. This

may also be the reason why the barrier reefs of the Capricorn Channel also have increased in velocity since 9 ka. High levels of velocity are recorded in the palaeo-models in the same location as BSS is seen to increase throughout the palaeo-models. The reason for this could be depth, as high velocity over deep water will have a smaller impact on BSS than the same velocity in shallow water (Zou, Bowen, and Hay 2006). Another possibility is that it could be that velocity was due to the barrier reefs creating eddies and jets, which will have dissipated in energy once past the barrier reefs, creating a lagoon behind the reefs (Munday et al. 2009). The reason may be a combination, the second idea is supported by BSS being recorded along the barrier reefs, which slowly reduces to where figure 4.2 shows slightly deeper water free of reefs, here BSS would be expected to be less than in the shallower depths surrounding it.

Overall, velocity and BSS both increased in strength from 9 ka to 8 ka where tidal dynamic strength peaked, 7 ka velocity and BSS were both still higher than the present day but began to reduce. This finding suggests that the sea level of 7 m below present was the optimal sea level for maximum velocity and BSS and co-coincided with the Holocene initiation. Tidal intrusion into the GBR during low levels of sea level were blocked by barrier reefs and dense areas of reefs. In response to the research questions: during the Holocene initiation, BSS and velocity were both higher than in the present day and in 9 ka.

4.4.2.4 Vorticity and Sinuosity

Vorticity describes the local rotation motion and is used here to detect circular motion created by eddies or oscillations from tidal flow. Across the three sectors, 8 ka has the highest levels of vorticity, indicating the highest amount of tidal activity is being generated here. This supports the findings of previous tidal dynamic change described above: 8 ka generated the highest tidal energy of the last 9 thousand years. Vorticity from tidal oscillations and eddies measured here will generate the BSS described above. Vorticity is highest in Grenville, this could

be due to reef matrices being densest in this sector. Grenville also experiences the largest difference in vorticity across time, suggesting that SLR has a large effect on tidal dynamics in this area, this could be because depth in Grenville has changed the most throughout the ∼17 m of SLR (figure 4.2). Swain also undergoes a large change in vorticity across time, most likely also related to large changes in depth change. Cairns experiences the lowest levels of vorticity, which correlates to Cairns having a small tidal range, therefore small amounts of tidal movement is being generated. Cairns also had the smallest difference in vorticity across the 9 thousand years to the present day, this correlates to small differences being found in Cairns for other tidal dynamics across time: Cairns appears to be stable throughout SLR, as the narrow shelf only undergoes small depth change throughout time.

Sinuosity was used to quantify change in particle trajectory paths across SLR. It is perhaps surprising to find that SLR did not make significant differences to sinuosity levels. However, sinuosity is highest in Grenville which is also where vorticity was highest, Cairns generated trajectories with the lowest sinuosity which correlates to Cairns also generating the lowest levels of vorticity. Therefore it can be assumed sinuosity is being influenced by vorticity. However, sinuosity is not directly equal to vorticity, as is shown by sinuosity in Grenville not changing despite large changes in vorticity. A possible reason for this is that sinuosity is not directly equal to vorticity. Particles may have followed the mean flow rather than being affected by local eddies and turbulence. For example, particles were being transported by tidal movement and were not impacted by the increasing number of small scale eddies.

Overall, vorticity increased with SLR to 8 ka, before reducing to levels found in the present day, suggesting more eddies and tidal oscillations were generated during 8 ka. Sinuosity did not undergo significant changes with changes in vorticity, however sinuosity trends follow sectors where vorticity is generated highest. In response to the research questions, levels of vorticity were highest during the

Holocene initiation but the effect on sinuosity of particle trajectories was not significantly different to the present day.

4.4.3 Connectivity

4.4.3.1 Diagonal analysis and network analysis

Connectivity matrices were generated from each model and their diagonals were extracted to analyse self-seeding reefs to explore how self-seeding changed in each sector across 17 metres of SLR. The percentage of self-seeding reefs has increased as sea levels rose. Cairns and Grenville increased in percentage of self-seeding reefs the most between 9 ka and 8 ka, however Swain has the smallest increase in self-seeding reefs during the same time – Swain undergoes the largest increase in self-seeding reefs between 8 ka and 7 ka. This indicates that sea level affected Cairns and Grenville around 1000 years earlier than Swain. Tidal range in Swain was found to still be around 0.5 m lower in 8 ka than the present day, whereas at the same point in time, tidal range in Cairns and Grenville is around 0.3 m higher than in the present day, also showing a lag in the southern GBR. By 7 ka, tidal range in Swain has surpassed the present day, matching the point in time where self-seeding rapidly increases. It is surprising that the largest increase in percentage of self-seeding reefs is in Cairns, as the sector does not undergo large changes in sea level or tidal dynamics. The reason may be that there is a large increase in both the amount and the size of reefs in Cairns between 9 ka and 8 ka: large reefs are more likely to self-seed than small reefs because of the time taken for a particle to clear a large reef.

Results indicate that self-seeding behaviour increased at the same time that tidal dynamics peaked. Once sea level increased by 10 m between 9 ka and 8 ka, the effect on self-seeding stabilised in Cairns and Grenville, this was also shown by the stabilisation in tidal dynamics between 8 ka and 7 ka. Self-seeding continued to increase to the modern day in Grenville and Cairns, however Cairns experienced

a larger increase in diagonal mean values in the modern day, this may have also been due to more large reefs establishing themselves in Cairns between 7 ka and the modern day. Swain recorded the least self-seeding reefs in 8 ka, however there is a large difference between 8 ka and 7 ka, suggesting that the SLR lag was responsible for this. This is supported by a study by Sanborn et al. (2024) and Salas-Saavedra et al. (2022), where water quality in the southern GBR improved $\sim$ 7 ka, which may have been driven by higher tidal velocities flushing the reef system. Although these studies are focused on the Capricorn Bunker, Swain area is likely to have had similar conditions due to also sitting on the widest section of the continental shelf. Diagonal mean increases in 8 ka and is similar to 7 ka, as found in Grenville and Swain. The modern day density curve is a slight increase from 7 ka. Overall, SLR has been shown to increase the amount of self-seeding, both in the number of reefs self-seeding and also in the mean number of particles being retained.

Network analysis using CPM showed that as sea levels rise, reefs have formed more and larger clusters. During lower sea levels in 9 ka reefs were fragmented from each other, this could be due to reefs also being physically further from each other and also tidal dynamics such as velocity, not being strong enough in Cairns and Grenville to connect reefs together. Swain has a large cluster of reefs in the centre forming a vertical line, this may have been due to water being trapped within the reef matrices from low sea level and therefore low tidal range and velocity. As sea level increased, more clusters appeared and they gained size, suggesting that even as tidal dynamics became stronger, flushing was slow.

Overall, as sea levels increased, the amount of self-seeding reefs also increased. This was a combination of more suitable depths for coral establishment, larger reefs and changes in tidal dynamics. Levels of self-seeding were lowest during 9 ka, where tidal dynamics were weak.

4.4.4 Summary

Research question 1: Tidal dynamics which were present during the Holocene initiation in 8 ka were very different to the present day GBR, tidal range, M2 amplitude, velocity, BSS and vorticity were all higher than the present day, this would have created a much higher energy GBR than found today. As sea level continued to increase following 8 ka, velocity, BSS and vorticity all reduced, suggesting there is a small ideal window of sea level which produces the conditions modelled in 8 ka.

Research question 2: Connectivity has changed between 9 ka and 7 ka by reefs becoming more self-seeding as sea levels increase, a large difference was found in the amount of self-seeding between 9 ka and 8 ka, whereas only a small difference is shown between 8 ka and 7 ka.

Research question 3: the 10 m of sea-level rise between 9 ka and 8 ka generated higher levels of tidal dynamics in 8 ka than found before or after, this increase in tidal energy coincided with a sharp increase in the amount of self-seeding reefs, suggesting that increased eddies and stronger tidal ellipses led to more coral larvae retention. As sea level rose from 9 ka, tidal range increased along with the strength of M2 tidal constituent. The effect of this was that higher levels of velocity, BSS and vorticity were generated around 8 ka and 7 ka. During this time was when self-seeding increased, suggesting that these three products of tidal dynamics assisted with the Holocene initiation. The increase in sea level also created more locations for coral reefs to establish and as reefs became larger, they will have been able to retain more larvae.

4.4.5 Implications, limitations and Future Work

The implications of this study are that self-seeding levels increased with SLR, and that during the Holocene initiation, sea level reached an ideal height to generate

much stronger tidal energy than experienced in the present day. This suggests that as sea level continues to rise in the future, reefs on the GBR may increase in self-seeding. The mechanisms behind this would be increased tidal oscillations and vorticity, driving circular momentum of the water, retaining larvae close to the parent reef. The consequence of this is that although some reefs will benefit from retaining more of their larvae, reef communities will become more fragmented from each other and damaged reefs will struggle to rely on healthy neighbouring reefs to regenerate them. This will also make management more difficult as the entire GBR will need protection rather than targeted highly connected reefs.

Palaeo reef locations were found based on a simple metric of modern day reef polygons having a suitable palaeo average depth, as average depth was calculated for each polygon, some areas of these polygons may be areas of inappropriate depths for reefs yet had larvae particles released from them. The method of establishing reef locations also did not include establishing possible areas where modern reefs are no longer found. More complex methods of establishing palaeo reef positions were attempted, generating rasters of appropriate depth and bed shear stress without the use of the modern reef polygons, however these methods were not suitable to the scale required and appropriate reefs were not generated. For example, in the Capricorn Bunker the collection of reefs were modelled as one single reef, of which there is no hard evidence for. Also, enormous areas were considered suitable for reefs by this method along with innumerable pixel sized reefs, this result was also deemed inappropriate for use. Finally, the simplest and most likely to be correct method was decided upon, of using the present day reef polygons and removing those which were in areas too deep to host tropical corals.

Another limitation is that wind was not included in the model, chapter 3 showed that a combination of tides and wind drives dispersal on the GBR and so connectivity driven only by tides will not capture a realistic result. To include wind data in these models, a palaeo climate model would need to be integrated with

the work developed here. Palaeo climate models do exist which could have provided wind data, such as the Paleoclimate Modelling Intercomparison Project (PMIP). However it was not deemed necessary to include wind in this study, as the work was focusing on changes to tidal dynamics generated by changing sea levels, including wind data would have extended the project aims considerably. For a future study or extension on this work, including palaeo climate model data would be valuable to understand past wind and tide interaction. Using present day wind would have also provided an additional potential of error to the results. chapter 3 showed that using tides only to model larvae dispersal resulted in maximum connectivity, therefore it was deemed best to only model maximum connectivity of palaeo reefs, with the understanding that wind would, in reality, disrupt local retention and self-seeding.

Ideally waves would also be included in larvae transportation models, as they play a key role in transporting larvae in and out of enclosed atoll lagoons (Grimaldi et al. 2024), as well as dispersing larvae which have congregated together on the surface (Oliver and Willis 1987). However, including waves at this spatial scale and resolution was not possible for this study, but running smaller models at finer resolution integrated with wave models such as SWAN (Simulating WAves Nearshore) (Booij, Ris, and Holthuijsen 1999) in the future would be highly beneficial to understanding small scale transportation of larvae.

A further limitation is that the CPM resolution parameter for each sector was set and remained as the appropriate resolution parameter for the modern day model despite the number of reefs reducing in each time step, potentially leading to unstable clusters being found. The reason for this was to allow comparison across each model, if the resolution parameter was adjusted for each time step, any changes would likely be invisible and not comparable. Also the benefit of the CPM is that the resolution parameter should be fairly robust, therefore maintaining it across the timesteps was deemed appropriate.

If the study was to be repeated with further resources and time, developing a global palaeo-tidal model to force the GBR would be conductive to more accurate results, as this does not yet exist for use on the GBR. This would mean implementing the South Equatorial Current and the East Australian Current into the model which may also improve accuracy. Finally, by running further models around 8 ka, such as using smaller timesteps or including 10 ka and 6 ka, the tipping point of sea level driving such high levels of tidal dynamics could be pinpointed. If also paired with systematic geological investigations, such as community structure and geochemical proxies, the relationship between tidal dynamics and coral ecology could be unveiled in much further detail, answering why the tidal dynamics present led to the initiation of the GBR on such a huge scale.

4.5 Conclusion

In this study, three models were built of palaeo-sea level reconstructions to study the GBR in 7 ka, 8 ka and 9 ka, representing 1.7 m, 10 m and -17 m of sea level drop respectively. These models were used to investigate changes to tidal dynamics throughout time, looking at M2 amplitude, tidal elevation and range, velocity, BSS and vorticity. Velocity rasters from the models were coupled with Lagrangian particle tracking software Parcels, to track coral larvae transportation to inform connectivity analysis. Results showed that as sea level increased from 9 ka to 8 ka, tidal strength increased to levels higher than experienced in the present day. The southern GBR experienced a lag in the effects of SLR, so the peak of tidal strength was found in 7 ka. As sea levels rose, the amount of self-seeding reefs was found to increase. There were several reasons for this: sea level increased enough to create more locations for reefs to establish, larger reefs were able to grow, and tidal dynamics such as increased eddies and tidal oscillation assisted with larvae retention. To explore these findings in greater detail, more simulations need to

be ran around 8 ka, and ideally using a higher resolution.

Chapter 5

Future Sea-level shaping coral reef connectivity

This chapter predicts changes to Great Barrier Reef (GBR) tidal dynamics generated by rising sea levels from three Shared Socioeconomic Pathways (SSP) for the year 2100 (Riahi et al. 2017; O'Neill et al. 2017). Three future models are generated based on conversions from SSP to sea level rise (SLR) by IPCC AR6 (Garner et al. 2021; Intergovernmental Panel on Climate Change (IPCC) 2023; Kopp et al. 2023): best case scenario SSP 1 1.9, corresponding to 0.45 m mean SLR; mid case scenario SSP 2 4.5, corresponding to 0.6 m mean SLR; and SSP 5 8.5, corresponding to 0.87 m mean sea level. However, the SLR is spatially varying; making this the first future tidal prediction to incorporate this. These models were then used for tidal analysis and integrated with Lagrangian Particle Tracking in order to answer how changes to tidal dynamics affect coral reef self-seeding behaviour. Self-seeding reefs are defined as reefs which receive the larvae it produces and levels of self-seeding are assessed using the connectivity matrices produced by each of the three models. Throughout, three representative sections in the south, central and northern GBR, particles representing coral larvae are released from reef polygons and tracked for calculating connectivity matrices.This information

is extracted from connectivity matrices using diagonal analysis and used to assess changes to self-seeding behaviour. The findings of this chapter will be used to answer three key questions "How does using a higher resolution model of the entire GBR and relative SLR improve predictions to tidal dynamics?", "How are tidal dynamics affected in 2100 by difference SLR scenarios, based on Shared Socioeconomic Pathways?" and "How is self-seeding behaviour affected by future SLR across difference Shared Socioeconomic Pathways?". Finally, findings from this chapter will be used to highlight implications of future tidal dynamics for coral reef management across the GBR.

5.1 Introduction

5.1.1 Climate Change

Predicting the impacts to our most delicate coral reef systems, such as the Great Barrier Reef (GBR), is of paramount importance. Global sea level has already increased throughout the twentieth Century by 1.7 ± 0.3 mm yr^{-1} (Church and White 2006; Priya et al. 2023; Thompson et al. 2018), linked to the melting of ice sheets and glaciers, and ocean thermal expansion as global temperature increases (Hay et al. 2015; Vermeer and Rahmstorf 2009). Global temperature has increased by $\sim 0.2°$ C per decade over the last 30 years (Goreau and Hayes 2024; McCulloch et al. 2024).

The trajectory of global temperature and sea-level rise (SLR) rely heavily upon on our socioeconomic decisions. Predicting the impact of these decisions has been termed Socioeconomic Pathways (SSP) (O'Neill et al. 2014) and have been used to develop climate scenario predictions (Ebi et al. 2014; Vuuren et al. 2014; Kriegler et al. 2014). The pathways range from the ideal green route, cutting all greenhouse emissions, prioritising human health and education and accepting a slower economic growth (SSP 1), to a middle ground where there is no marked

shift from historic patterns but a slow movement towards a more sustainable future (SSP 2) and then SSP 5 which sees no action being taken to shift towards sustainability, prioritising capital over health and well-being (O'Neill et al. 2017). A study modelling temperature flux according to SSPs found that even under the highly optimistic SSP119, a global temperature increase of 1.5° by 2080 will trigger 3 mass bleaching events per decade in the GBR and the SSP 585 will see bleaching events occurring annually (McWhorter et al. 2022b).

The GBR has already suffered large reductions in coral cover over the last decade as global temperatures have increased and marine heatwaves became more common and intense (De'ath et al. 2012). The threat of rising sea level is a slower and more subtle threat to the reef (Munday et al. 2009). One aspect of the threat is that tropical corals have to remain near the surface in order to obtain enough light, therefore reefs grow to match the pace of SLR (Woodroffe and Webster 2013). However, if the rate of sea-level outpaces the rate of coral growth (between 10 - 100 mm yr^{-1} (Buddemeier and Smith 1988)), then the reefs eventually lose access to light and "drown". Examples of this have been seen in studies looking thousands of years ago when there were large pulses in sea level from ice-cap and glacial melt during the Last Glacial Maximum (LGM), such as between 10.31 - 10.14 ka, where reefs slowed accretion to 4.2- 1.4 mm yr^{-1}, in response to increased sediment flux, leading to an inability to keep up with the rising sea level and a mass death from drowning (Woodroffe and Webster 2013; Webster et al. 2018).

It is predicted that changes to ocean currents will affect coral connectivity in terms of supply and survival rate (Munday et al. 2009). Coral reef populations greatly depend upon connectivity for growth and resilience, so it is important that we are able to predict what will happen with rising sea levels (Caley et al. 1996; Armsworth 2002). On a global scale, changes to poleward-flowing currents may continue to strengthen, such as the South Equatorial Current and the East Australian Current, with the potential of effecting population connectivity in the GBR through impacting local current patterns (Steinberg 2007; Cai et al. 2005).

However, modelling of projected climate changes of large-scale currents have shown a limited effect in the southern GBR, as changes to large-scale currents were found to only have a very small effect on currents passing through the GBR (Figueiredo et al. 2021). Gradual sea-level rise can lead to flooding of shallow reef flats, affecting local current patterns; this is especially likely to happen around enclosed or semi-enclosed lagoons and will lead to more larvae being retained in these areas (Munday et al. 2009). Previous work modelled 100 cm of SLR across the GBR to study changes to tidal dynamics (Mawson, Lee, and Hill 2022). Findings were that the dominant tidal constituent M2 decreases with SLR, whereas the second dominant tidal constituent S2 increases, tidal range changes by ± 10% depending on location. Another study on SLR around Australia also found changes to tidal constituents, particularly M2 increasing in amplitude by 10 mm with 1 m SLR of the Coral Sea (Harker et al. 2019). The impacts of increased M2 is increased turbulence and benthic velocity (Harris, Vila-Concejo, and Webster 2014), this is beneficial up to a limit, assisting with recovery from thermal stress, nutrient influx and waste removal (Sandin et al. 2022; Page et al. 2019; Page et al. 2021; Nakamura, Yamasaki, and Woesik 2003; Sebens et al. 1998; Sebens et al. 2003). So far, studies have not looked at how tidal dynamics will respond to SSP sea-level projections for 2100, nor on the effects on coral larvae dispersal of the GBR.

Here, a detailed study into the effects of SLR from Shared Socioeconomic Pathways in 2100 on coral reef connectivity in the GBR will be carried out. High resolution tidal models of the entire GBR were developed across different SSPs and coupled to particle tracking software to simulate annual mass spawning events. The outputs were then used to study changes in connectivity driven by changes to tidal dynamics. From this, three areas across the GBR will be looked at in detail in order to capture fine scale reef connectivity.

5.1.2 Research Questions

The key questions of this study are:

1. How does using a higher resolution model of the entire GBR and relative SLR improve previous 500 m resolution predictions to tidal dynamics?
2. How are tidal dynamics affected in 2100 by each SSP SLR scenario?
3. How is self-seeding behaviour affected by future SLR across difference Shared Socioeconomic Pathways?

5.2 Methods

Chapter 2 contains all general information on creating and running numerical models along with integrating Lagrangian particle tracking to simulate the movement of coral larvae.

5.2.1 Study Site

The study sites in this chapter are the same as chapters 3 and 4: the entire GBR is modelled using Thetis (Kärnä et al. 2018) to simulate tidal dynamics of future sea level predictions, analysis of changing tidal dynamics are studied across this entire domain. Particle tracking simulations are only conducted on three sectors of the GBR: Cape Grenville (Grenville), Cairns (Cairns) and Swain Area (Swain). For each model, configurations are as follows: viscosity was set to 1.0, mannings drag was set as 0.025 and the wetting and drying alpha was set to minimum of 0.5 and maximum of 75.0. The selected timestep was 90 seconds, with outputs generated every 900 seconds. The models were forced with tidal forcing from TPXO (Egbert and Erofeeva 2002) and no atmospheric forcings were used.

5.2.2 Future Sea-Level Constructions

Three future sea-level projections are taken from Shared Socioeconomic Pathways (SSP) (Riahi et al. 2017; O'Neill et al. 2017) for the year 2100 (McWhorter et al. 2022a; McWhorter et al. 2024), which have been converted to mean SLR by IPCC AR6 (Garner et al. 2021; Intergovernmental Panel on Climate Change (IPCC) 2023; Kopp et al. 2023): best case scenario SSP 1 1.9 (referred to henceforth as SSP119), corresponding to 0.45 m mean SLR; mid case scenario SSP 2 4.5 (referred to henceforth as SSP245), corresponding to 0.6 m mean SLR; and SSP 5 8.5 (referred to henceforth as SSP585), corresponding to 0.87 m mean sea level. For each of the three SSP scenarios, medium confidence values of the 50% quantile of SLR across global oceans at 1 degree resolution were extracted from IPCC AR6 data, converted to raster format and resampled to 250 m resolution. Using QGIS 3.12 (QGIS.org, 2020), IPCC AR6 sea level projections are cropped to the GBR, and subtracted from the present day bathymetry, producing bathymetric data of relative SLR across the GBR to account for spatial variability. Once the three SSP 250 m resolution bathymetries were created, models were generated using the same mesh used for the modern simulations created in chapter 3. This was possible because the modern mesh had been created with a +10 m contour, meaning that there was 10 m of space between the present day 0 m sea level and the model domain. As all SSP sea level scenarios are less than 1 metre above the present day sea level, the modern mesh is able to simulate them, including any possible increases in tidal range. All present day reef locations from the eAtlas Great Barrier Reef Features (Hammerton and Lawrey 2024), were used for each of the SSP scenarios. Here, the assumption is that less than 1 m of SLR is not anticipated to have an effect on the position of the reefs, though may drown individual corals within each reef.

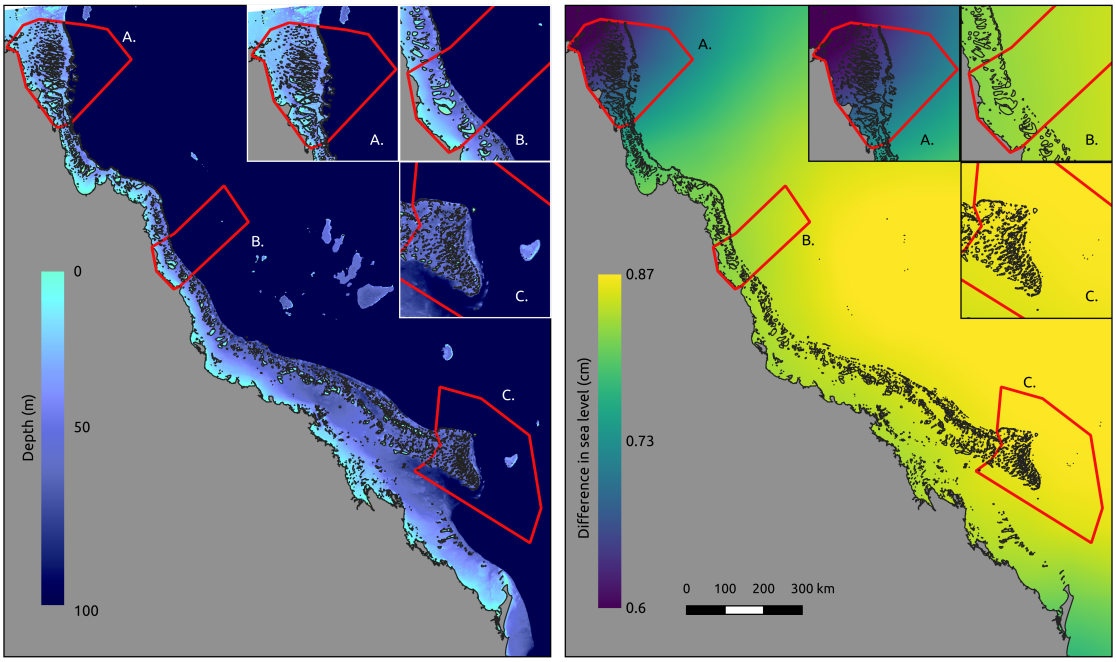


Figure 5.1: Maps displaying differences in sea level between present day and SSP 585 in 2100. Left: map of present day bathymetry with zoomed in plots of the three sectors of interest. A is Grenville, B is Cairns and C is Swain. Right: map of relative sea level from SSP 585 (0.87 cm) change showing that the increase is not uniform. Grey is the continent of Australia and black outlines are reef locations.

5.2.3 Model Setup

The model setup of Thetis will be the similar to chapter 3's tide-only model. Wind is excluded from these models as localised wind predictions are not known for 2100. Although present day wind could have been included in these models, it would introduce a degree of unnecessary uncertainty into the models as global temperature changes have been shown to affect local trade winds in the Great Barrier Reef (Richards et al. 2024). Chapter 3 demonstrated that tide-only models produce maximum connectivity, therefore this study will investigate changes to maximum connectivity from rising sea levels. The validation of present day models in chapter 2 is used as validation for these future SSP scenario models. Simulations in this chapter were run for 14 days (after spin-up) with a time step of 900 seconds are used to the neap tide was present, models were run from the same date as present day models (12/11/2000) using TPXO tidal data. The dominant tidal constituent on the GBR is M2, which creates the spring-neap cycles. To

ensure this was captured by the model therefore models of 14 days will capture a full spring-neap cycle.

5.2.4 Larvae Transport

In order to compare connectivity changes, it is assumed that corals will continue to participate in an annual mass spawning event following the November/December full moon during 2100, therefore particles will be released on the same day as the 2000 annual mass spawning event – in order to be released with the same tidal cycle point – and will be tracked for 48 hours. As the reef shapefile polygons has not been changed, the same number of particles per km^2 will be used, resulting in the same number of particles released as the present day tide-only model.

5.2.5 Tidal Dynamics

To understand the future changes differences between the present day and SSP scenarios for M2 amplitude, tidal range, average velocity and average bed shear stress (BSS) will be analysed. Changes to BSS and velocity will have a direct impact on fluid transportation over reefs (Harris, Vila-Concejo, and Webster 2014). Vorticity and sinuosity will also be analysed for changes across the SSP scenarios in the same way they were analysed and compared in chapter 4. Changes in vorticity will indicate whether higher sea levels produce a difference in the presence of eddies, and changes in sinuosity will illustrate changes to tidal ellipses and the distance that particles are covering during dispersal.

5.2.6 Connectivity

Methods of analysing connectivity will follow the same steps as chapter 2. From the particle tracking data, connectivity matrices will be created from the final position of particles following 48 hours of tracking. To extract self-seeding in-

formation from the connectivity matrices, diagonal analysis was performed by extracting all values on the diagonal and comparing each model within each sector (e.g. Cairns 9 ka was only compared against Cairns 8 ka and Cairns 7 ka), using Kruskal-Wallis tests to check if there were statistical differences between the amount of self-seeding created by each forcing model. Following this, a post-hoc Dunn's test was run on each sector to identify which groups are significantly different from each other.

As well as looking at changes to self-seeding behaviour, Constant Potts Model (CPM) with the Leiden Algorithm will be employed here to explore whether rising sea-level affects community structure, this will be conducted in the same way as chapter 3. The same γ parameter of 0.005, as used in chapter 3, will be used in order to be able to compare differences of community structure and this parameter will be checked to ensure it produces sensible community structure.

Another analysis for exploring network change is using a Principal Component Analysis (PCA) using Python package Networkx (Hagberg, Swart, and Schult 2008) to show simply and clearly whether change in community structure has taken place. Connectivity matrices were converted to directed graphs before the PCA was conducted on eight standardised network metrics: centrality, closeness centrality, betweenness centrality, eigenvector centrality, harmonic centrality, clustering coefficient, graph density, and transitivity. Metrics were then averaged over nodes before carrying out the PCA and the first two components were visualised to assess changes of network within each sector for each SSP scenario.

5.3 Results

Here, results of changes to tidal dynamics will be explored. This will begin by addressing any differences between the work here compared with a previous study by Mawson, Lee, and Hill (2022) from using higher resolution and spatially varying SLR, this will address research question 1. The study will then cover results from

tidal dynamic changes to answer research question 2, analysing how each SSP scenario differs in 2100. Finally, results of connectivity change will be addressed to answer the third research question, how do rising sea levels effect coral reef connectivity.

5.3.1 Tidal Changes

Changes to tidal dynamics are analysed from each of the future sea level models and differences are compared with the modern day M2 amplitude, tidal range, average velocity and average BSS (see fig. 5.2). A summary figure of mean tidal dynamic changes across sectors and SL scenarios can be seen in figure 5.3.

5.3.1.1 Changes in M2 and Tidal Range

Change across the model domain for M2 amplitude is not uniform in location, magnitude or direction (fig. 5.4). In SSP119, the majority of the domain remains consistent to M2 amplitude recorded in the present day. The Capricorn Channel (CC) undergoes a reduction by ∼0.02 m in amplitude and the barrier reefs on the outside of the CC increase in M2 amplitude by 0.01 m. These changes become more pronounced across each SSP scenario: the CC in SSP245 decreases in M2 amplitude by ∼0.03 m, the barrier reefs increase to 0.03 m; the CC in SSP585 decreases from the modern by ∼0.045 m and the barrier reefs increase by ∼0.04 m. M2 amplitude changes in other locations of the GBR are not observed in SSP119 or SSP245. In SSP585 Grenville experiences a small increase in amplitude (∼0.01 m) in the north between the barrier reefs and the mid-shelf reefs. A decrease in amplitude is also seen here along the northern coast.

Future changes to tidal range are also not uniform along the coast (fig. 5.5). In SSP119, tidal range decreases within the southern CC by a maximum of 0.03 m, a reduction of 0.01 m is also observed in the northern GBR below Grenville. The Capricorn Channel north of the Whitsundays and northern GBR both increase

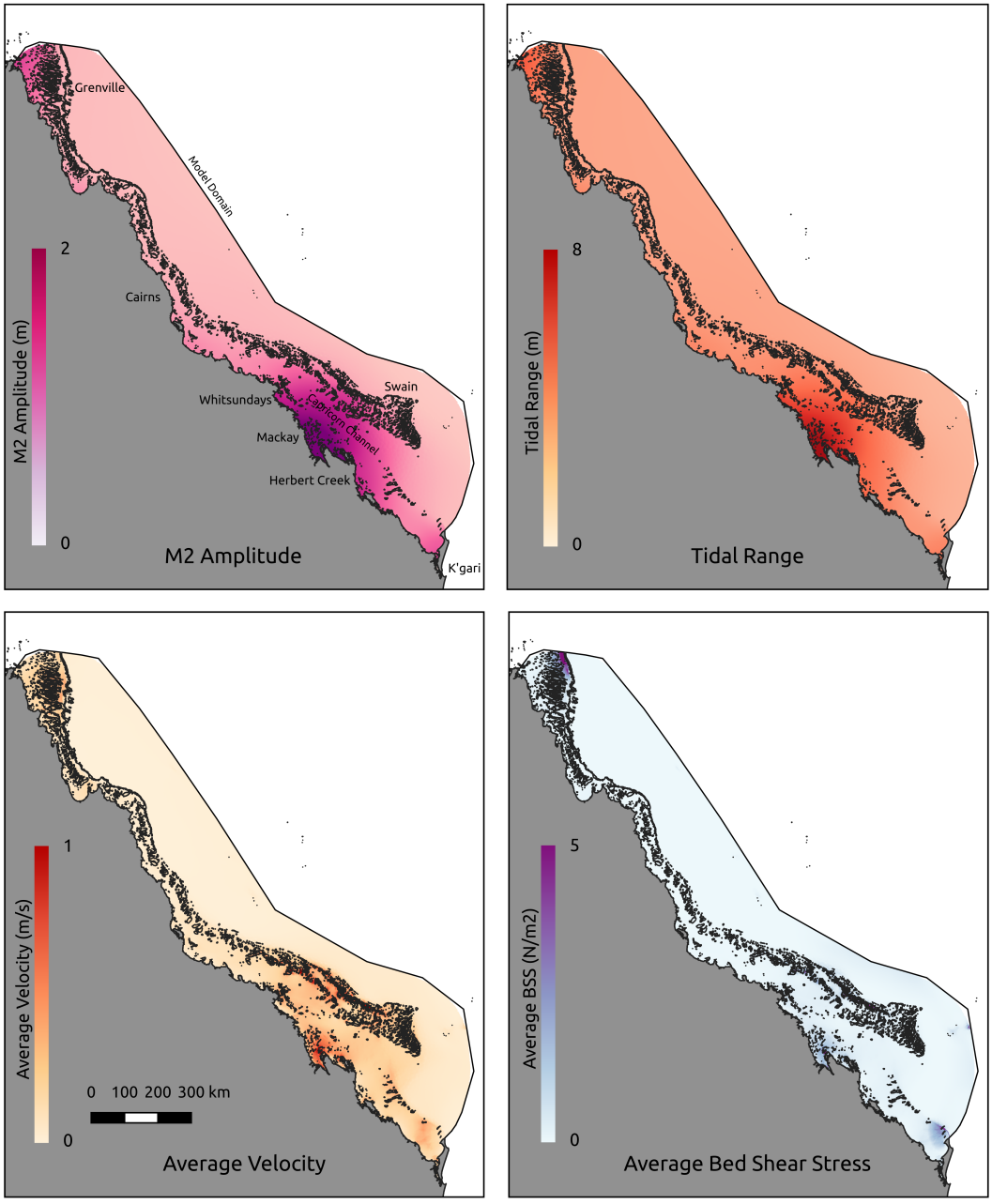


Figure 5.2: Tidal metrics of the modern day for M2 amplitude (top left), tidal range (top right), tidally-averaged velocity magnitude (bottom left) and tidally-average bed shear stress (bottom right). Grey indicates the modern coastline, the black lines indicate the modelled domain and the location of reefs. Colour scales are given for each quantity represented.

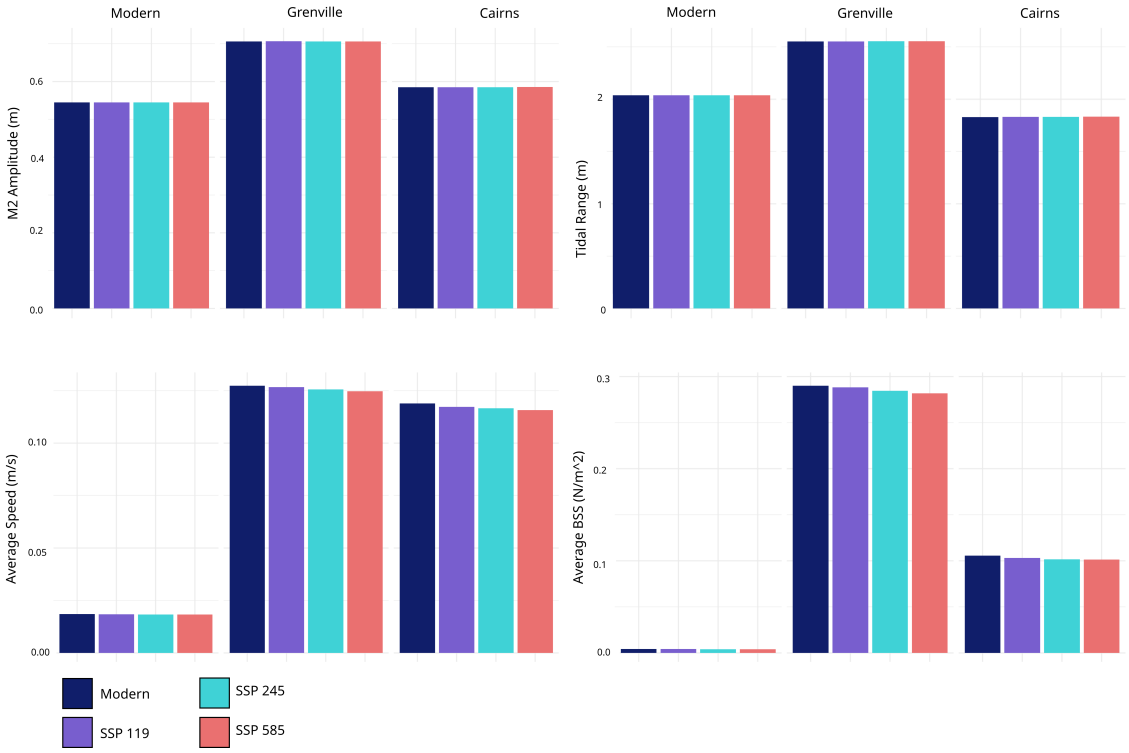


Figure 5.3: Mean measurements of tidal dynamic variables: M2 amplitude, tidal range, average BSS and average speed for each sector across the four sea level scenarios.

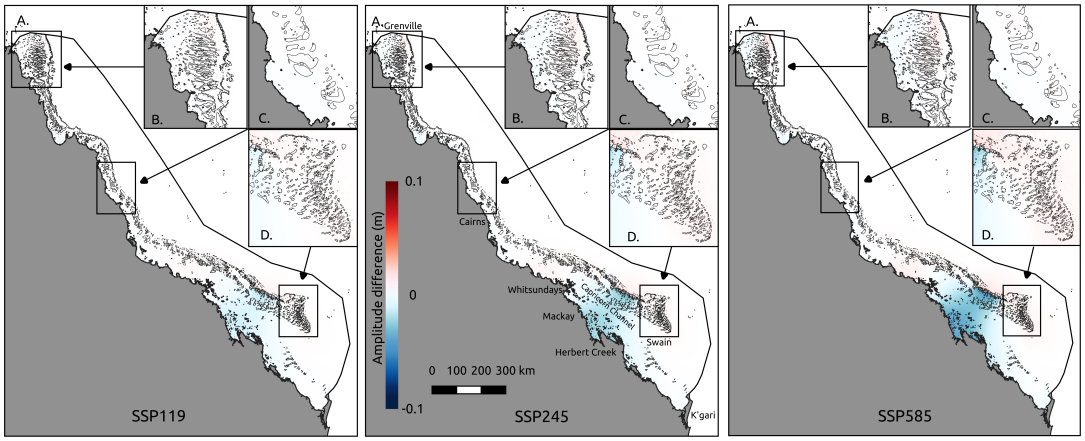


Figure 5.4: Differences between modern day M2 amplitude and each SSP scenario in 2100 (from left to right SSP119, SSP245, SSP585). As in Fig. 5.2 the grey shows the present day coastline and black shows the model domain and reef locations. Insets for each SSP show the three main areas of interest; Grenville (B), Cairns (C) and Swain (D).

by 0.03 m. The central GBR does not change. A convergence zone (white space between the red and blue sections) is present near the Whitsundays, where tidal range does not alter from the present day. Swain increases in tidal range by 0.03 m uniformly except for the north east and south west, which do not change in tidal range. Cairns is observed to have a small reduction of 0.01 m in a small area of the coast in the south of the sector, the rest does not change. Grenville increases in tidal range by ∼0.01 m along the northern mid shelf, and decreases by ∼0.2 m along the south coast.

In SSP245, the CC increases in tidal range by a maximum of ∼0.1 m, particularly along the coast and within the reef area, also expanding further towards the middle of the channel. Swain, the shelf edge of the CC, north of the Whitsundays and Grenville increase in tidal range by ∼0.02 m. Increased tidal amplitude of ∼0.04 m is uniform across Swain, except again for the north east and south west, which do not change in tidal range. Changes to Cairns is the same as SSP119. Grenville increases in tidal range by ∼0.03 m in the north on the mid-shelf but reduces by ∼0.03 m along the south coast.

In SSP585, a reduction of over 0.1 m of tidal range is now observed across the majority of the CC up to the Whitsundays. Increased tidal range in Swain, the shelf edge of the CC, north of the Whitsundays and Grenville reaches ∼0.06 m. A small decrease of tidal range (∼0.02 m) can be observed in the central GBR, further decrease of ∼0.05 m is displayed in the northern GBR, as well as an increase of 0.06 m at the northernmost point of the GBR. Increased tidal range in Swain follows the same pattern as previous SSPs but reaches an increase of ∼0.06 m. Increased tidal range of 0.01 m can be seen on the larger reefs of Cairns, whilst tidal range reduces by 0.01 m along more of the coastline. Grenville increases in tidal amplitude across the northern mid-shelf by 0.06 m, whilst a reduction of 0.06 m is observed along the south coast as well as a small decrease of 0.01 m along the northern coast. The barrier reefs on the shelf edge do not experience any change in tidal range.

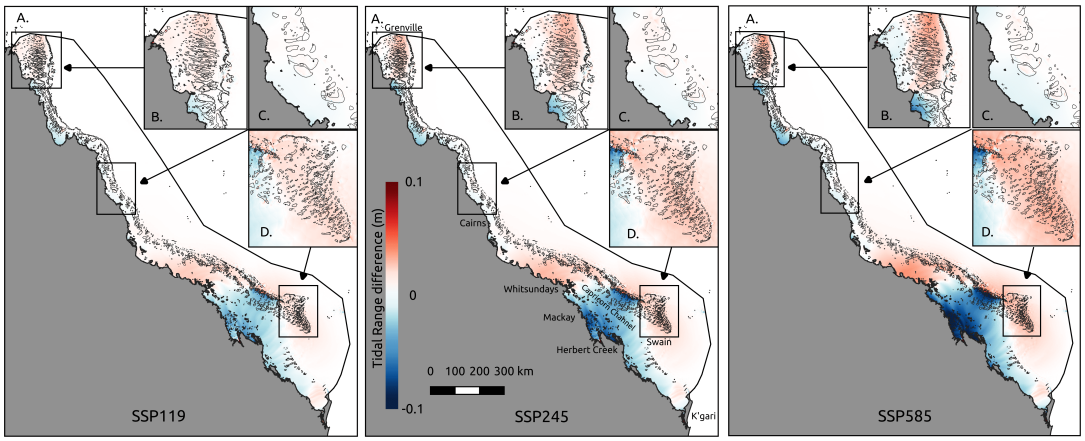


Figure 5.5: Difference between modern day tidal range and each SSP scenario in 2100 (from left to right SSP119, SSP245, SSP585). Blue indicates an increase of tidal range in the future, red a decrease. As in Fig. 5.2 the grey shows the present day coastline and black shows the model domain and reef locations. Insets for each SSP show the three main areas of interest; Grenville (B), Cairns (C) and Swain (D).

5.3.1.2 Changes in Velocity and Bed Shear Stress

Changes in average velocity are studied to look at long-term shifts to velocity across the tidal cycle. Modified average velocity will affect flushing times and long term tidal drift. Changes to velocity are most pronounced in the southern GBR above Swain area across all SSP scenarios (fig. 5.6). In SSP119 the densest regions of reef, such as the barrier reefs along the shelf edge of the CC and the northern GBR, increase in velocity by 0.1 m/s and 0.02 m/s. The region of dense reef opposite the Whitsundays decreases in average velocity by 0.05 m/s, as do reefs north of Swain. Herbert Creek decreases in velocity by ∼0.01 m/s. Swain undergoes a small increase of velocity (0.05 m/s) on reefs in the south, as well as some small areas of decreased velocity (0.03 m/s) between reefs. Cairns increases in velocity by 0.02 m/s on large reefs and Grenville also increases on reefs from the mid-shelf to the coast by 0.03 m/s.

In SSP245, changes in velocity have intensified. Decreases of velocity within the reefs bordering the CC have decreased by 0.1 m/s, and areas of increased velocity have increased by 0.1 m/s. More reefs throughout the central GBR have increased in velocity by 0.02 m/s and the northern GBR reefs have increased in

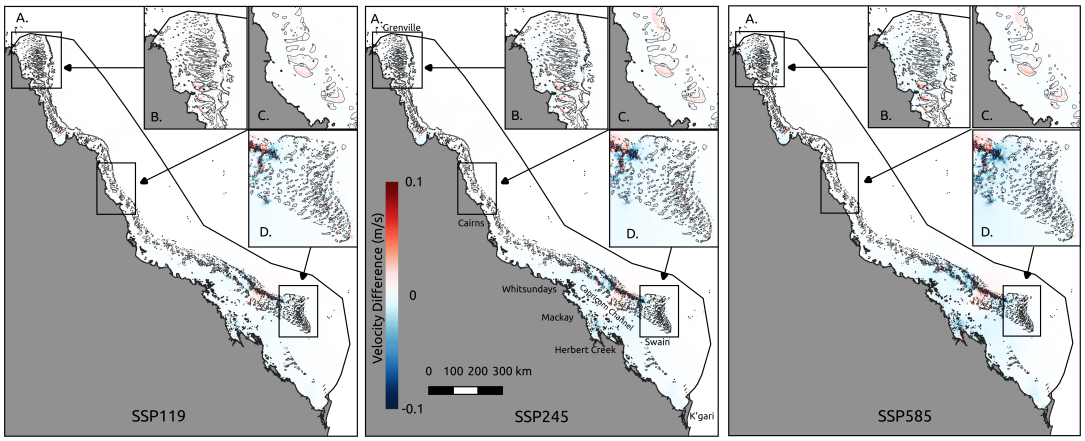


Figure 5.6: Difference between modern day average velocity and each SSP scenario in 2100 (from left to right SSP119, SSP245, SSP585). As in Fig. 5.2 the grey shows the present day coastline and black shows the model domain and reef locations. Insets for each SSP show the three main areas of interest; Grenville (B), Cairns (C) and Swain (D).

velocity by 0.03 m/s. Areas of increased velocity in Swain are 0.06 m/s higher than the present day, while areas of decreased velocity are 0.04 m/s lower than the present day. Reef areas in Cairns have increased in velocity by 0.03 m/s, velocity is also increasing by 0.02 m/s behind some reefs. Reef areas of increased velocity in Grenville are 0.04 m/s higher than the present day, increase in velocity within Grenville is primarily limited to the southern large reefs close to the coast. Average velocity remains the same as the present day within the mid-shelf and along the shelf-edge.

In SSP585, distribution of velocity change is similar to SSP245 but with increased intensity. More areas of decreased velocity within the CC are 0.1 m/s lower than the present day, and more areas of increased velocity within the CC are 0.1 m/s faster than the present day. Reefs in the central GBR have reached a difference of 0.03 m/s, some areas of the northern GBR have increased by 0.09 m/s. Swain experiences a decrease in velocity by 0.01 m/s across the majority of the shelf, some areas of dense reefs still increase in velocity by 0.07 m/s. Cairns large reefs increase by 0.05 m/s, increased areas of velocity behind reefs are the same as SSP245. Reefs in the south of Grenville increase in velocity by 0.09 m/s but the majority of the mid shelf reduces by 0.01 m/s.

Average bed shear stress (BSS) changes across the GBR were measured to explore how transport may change with future sea level scenarios. Overall, average BSS decreases across each SSP scenario from the present day. In SSP119, areas of BSS reduction are observed around the CC, this is particularly within Herbert Creek and the outside reefs of the CC. Reduction of BSS is $\sim$0.2 N/m^2. The barrier reefs along the CC increase in BSS by 0.5 N/m^2. BSS is also seen to decrease by 0.07 N/m^2 near K'gari. Northern Grenville reduces in BSS by $\sim$0.2 N/m^2 between the mid-shelf and the barrier reefs. Swain undergoes a slight reduction of 0.1 N/m^2 within the centre. Cairns experiences very slight reduction of 0.05 N/m^2 in BSS on the larger reefs.

In SSP245, areas that undergo BSS change are the same as in SSP119, however the magnitude of change is different. Decrease of BSS in the CC is by 0.3 N/m^2 and BSS around the barrier reefs has is the same as SSP119. K'gari has decreased by 0.1 N/m^2. BSS has decreased in Swain by 0.2 N/m^2 but a large area across Swain has reduced slightly by 0.05 N/m^2. BSS in Cairns is the same in reduction as SSP119. The north east of Grenville has reduced in BSS by $\sim$0.5 N/m^2 and the area of reduction has spread across more of the mid-shelf. Small areas of the very north east increase is BSS by 0.5 N/m^2.

In SSP585, magnitude of BSS change has continued to grow. The CC experiences reductions of $\sim$0.5 N/m^2 within Herbert Creek and the outside reefs, the barrier reefs still increase in BSS by $\sim$1 N/m^2. K'gari decreases in BSS by 0.2 N/m^2. The centre of Swain reduces in BSS by $\sim$0.3 N/m^2 and the rest of Swain reduces by 0.1 N/m^2. The north east reduction in BSS in Grenville is the same as SSP245, however the area of reduction has spread across the entire mid-shelf. Large reefs in Cairns reduce in BSS by 0.1 N/m^2.

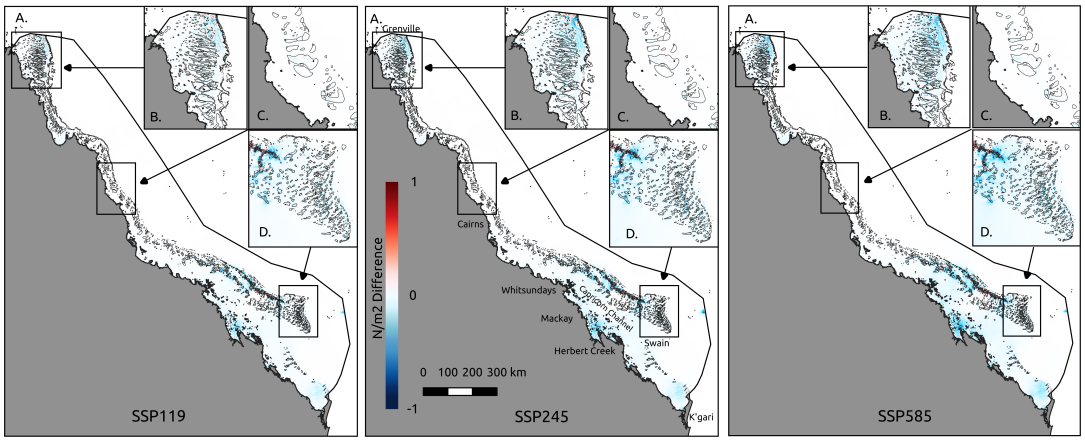


Figure 5.7: Difference between modern day average bed shear stress and each SSP scenario in 2100 (from left to right SSP119, SSP245, SSP585). As in Fig. 5.2 the grey shows the present day coastline and black shows the model domain and reef locations. Insets for each SSP show the three main areas of interest; Grenville (B), Cairns (C) and Swain (D).

5.3.1.3 Vorticity and Sinuosity

Average L_2 Norm Vorticity was calculated for each SSP model across each sector and plotted, see figure 5.8. Average L_2 Norm for each sector shows that vorticity is expected to reduce between the modern day and SSP119, followed by a slight reduction with SLR corresponding to SSP245 and 585. Grenville experiences the largest reduction from the present day, dropping around 1×10^{-4} L_2 Norm to SSP119, Cairns experiences the smallest reduction. Grenville also experiences the largest shift of the sectors between SSP119 and SSP245, whereas the other sectors undergo very little change throughout the other SSP scenarios. Vorticity is shown to continue following the tidal cycle trends as seen in the present day: Grenville's mixed semi-diurnal tides, Swain's diurnal-tides and Cairn's convergence zone of diurnal and mixed semi-diurnal tides.

Sinuosity measurements were calculated from the particle trajectories following the methods used in chapter 2 with lower values representing straighter paths (1 represents a straight path). Mean sinuosity values were then calculated for each sector and SSP scenario. Grenville and Cairns follow the same trend of increasing in sinuosity values as sea level increases. For example, Cairns has a mean sinuosity of 8.51 in the present day, this increases gradually to 9.26 for

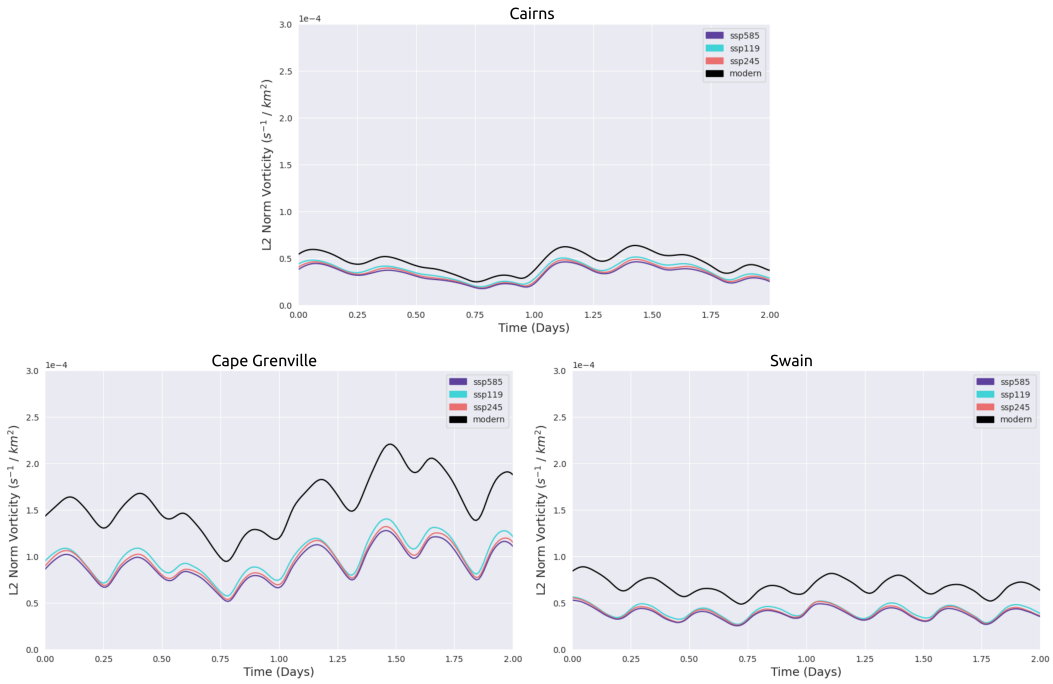


Figure 5.8: Average L_2 Norm vorticity measurements plotted across the anticipated 48 hour window of annual mass spawning events for each SSP model.

SSP585. Grenville also increases in mean sinuosity with each SSP scenario, for example, the present day has a mean sinuosity of 30.8 and this increases to 32.0 by SSP585. Swain has a different trend, sinuosity values decrease from 18.6 to 18.2 between the present day and SSP119, remaining the same for SSP245 before reducing to 17.7 at SSP585. The highest sinuosity values are found in Grenville (30.8 - 32.0) and the lowest sinuosity values are found in Cairns (8.51 - 9.26).

To investigate the significance of changes in sinuosity within each sector, non-parametric Kruskal-Wallis tests were run to detect significant differences across the SSP scenarios. Significant differences were found for all sectors (p = < 0.001). To determine whether the significant differences can be considered practically different in the large datasets, effect size was calculated using eta-squared (η^2). Effect size showed that the practical significance of the differences between sinuosity values are small and therefore, the statistically significant differences observed are simply attributed to the size of the data sets (Cairns, Grenville and Swain $\eta^2 \geq 0.003$) (Peeters 2016).

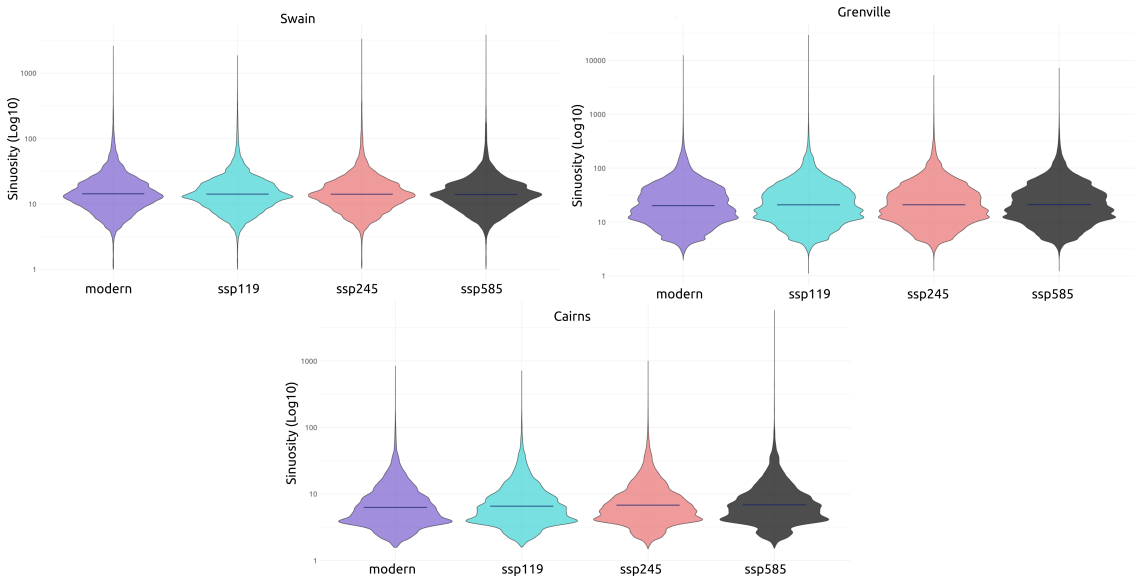


Figure 5.9: Violin plot of subsampled sinuosity data from each sector (top left: Cairns, top right: Grenville, bottom: Swain) and model (purple: modern, green: SSP119, red: SSP245 and black: SSP585).

5.3.2 Connectivity

5.3.2.1 Self-seeding

Following 48 hours of particle tracking, three connectivity matrices were generated. From each of these matrices, diagonal values were extracted for diagonal analysis to calculate the diagonal mean as a measure of self-recruitment strength for each SSP. Table 5.1 shows how increasing sea-levels impact the proportion of particles self-seeding in each sector. The results showed that as sea-level increases, self-seeding generally increases. Swain reduces in mean diagonal value between SSP245 and SSP585. However, this is only a small reduction in mean value and this is not seen across any of the other sectors. The smallest increases in mean value are found in Swain, the biggest increase is a difference in mean value of 5 particles, Where sea level and tidal dynamic measurement changes remain stable. The largest increases are found in Cairns, the difference in diagonal mean value of Cairns between modern and SSP585 is 94 and the largest difference takes place between modern and SSP585. This is the same trend for

Model	Swain	Grenville	Cairns
Modern	188	1763	2623
SSP119	190	1793	2680
SSP245	195	1794	2708
SSP585	193	1811	2717

Table 5.1: Diagonal mean values of particles self-seeding for the present day (Modern) and the three future scenarios for each sector. A total of 256 particles per km^2 from each reef were released for 48 hours: 1,813,504 particles released in Grenville, 269,312 in Cairns and 580,352 in Swain

Grenville, which also sees a large difference between modern and SSP585 (48). The smallest differences are for modern and SSP119. Kruskal-Wallis tests on each sector (Cairns: modern, SSP119, SSP245 and SSP585 etc.) determined there are no significant differences between the diagonal mean of each future sea-level rise (p > 0.9 for each sector).

5.3.2.2 Network Analysis

CPM network analysis was conducted on each sector within each model. Across all models and sectors, change in community structure is not observed. The number of communities recorded for Grenville and Swain increased slightly with sea-level rise from the present day, Grenville increased from 206 to 214, and Swain increased from 224 to 236. Cairns reduced from 44 in the present day, to 37 with SSP119, increased to 46 with SSP245 and reduced again to 35 for SSP585. Cluster maps show clusters remaining similar across the entire shelf, small differences can be observed in small reefs (see fig. 5.10).

A PCA was run on each of the sector networks for each SSP sea level scenario to show network changes (see fig. 5.11). The first two principle components (PC1 and PC2) explained 77.39 % and 10.56 % of the total variance, accounting for 87.94 % cumulatively. PC1 is associated with metrics reflecting overall network connectivity strength (e.g. centrality measures: degree, closeness, eigenvector centrality), and PC2 indicates variation in local network modularity from clustering coefficient and transitivity metrics. Figure 5.11 shows clear separation of SSP scenarios

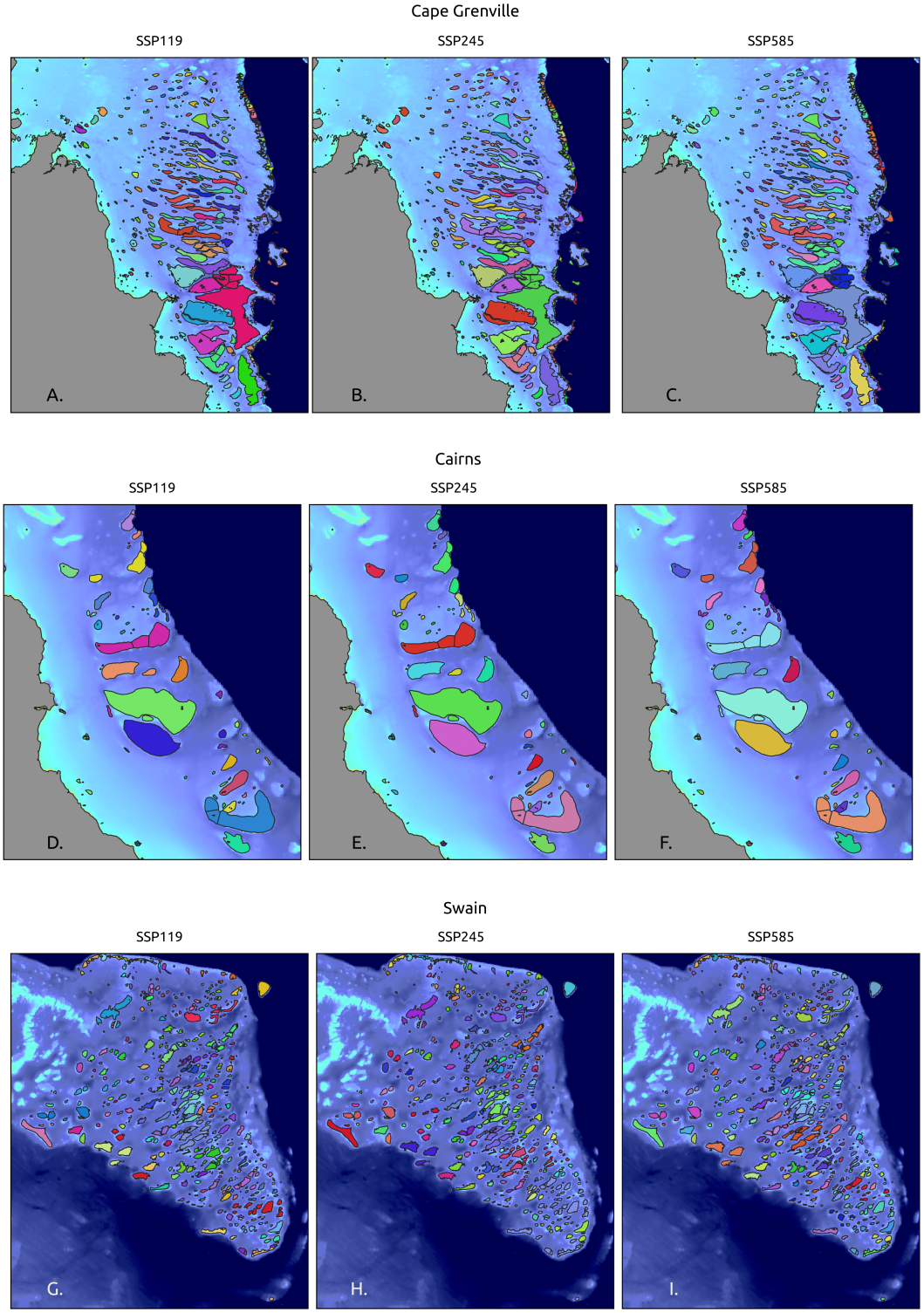


Figure 5.10: Maps of reef community clusters from CPM model for each model and sector. Colours of clusters do not correlate to each other across maps: only shape and size of clusters should be compared.

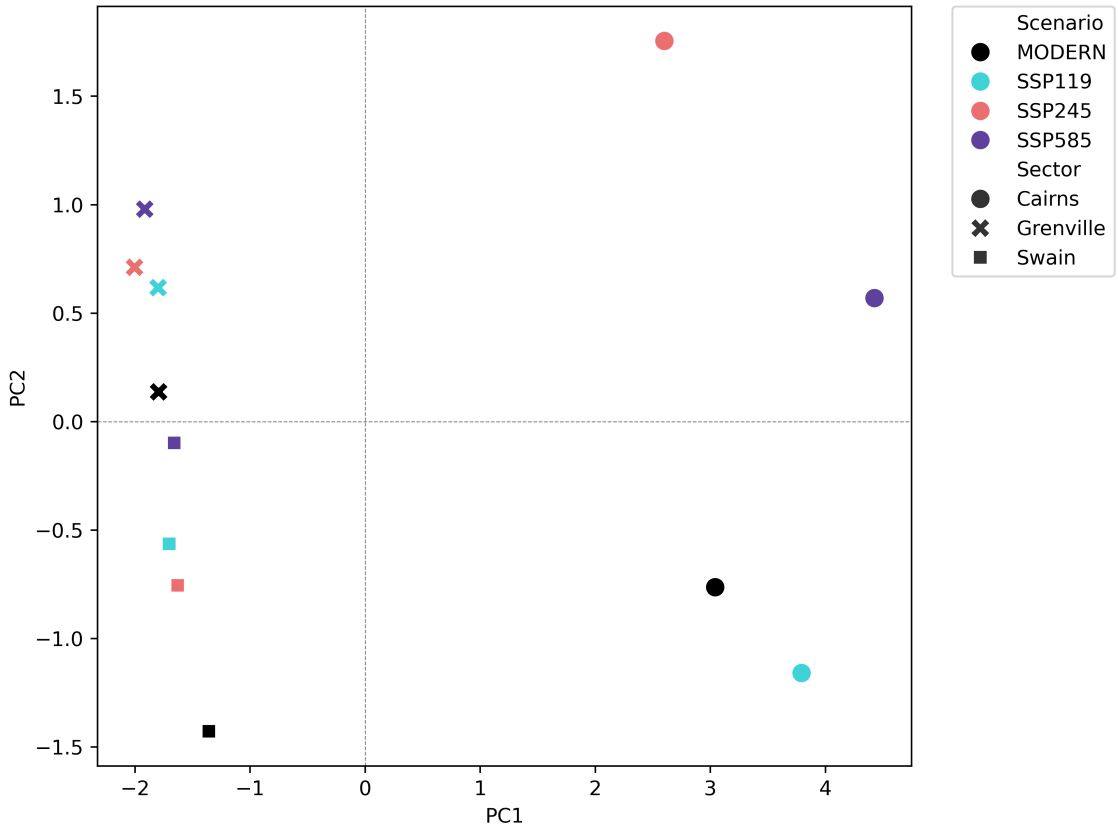


Figure 5.11: PCA figure demonstrating network style changes across sea-level projections. PC1 (X axis) is associated metrics reflecting overall network connectivity strength (e.g. centrality measures: degree, closeness, eigenvector centrality), and PC2 (Y axis)indicates variation in local network modularity from clustering coefficient and transitivity metrics.

along PC2, with modern showing the lowest levels of modularity in Swain and Grenville, and SSP585 producing highest levels of modularity. Both Cairns and Grenville show similarity along PC1, showing an overall weak network strength. Cairns follows a different pattern and experiences separation along both axis, more so in PC2: modularity reduces between modern and SSP119, but increases in SSP245 to the highest modularity level before reducing to SSP585. Cairns increases in overall network strength in SSP119 and SSP585 but weakens slightly in SSP245, however PC1 results are much stronger in Cairns than Grenville and Swain, showing a different network style.

5.4 Discussion

5.4.1 Summary of key results

Here, the results of each study will be combined to give a comprehensive answer to the two research questions (5.1.2). The key findings were:

- Overall, tidal dynamic results were very similar to the study conducted by Mawson, Lee, and Hill (2022).
- As SLR rises, a bottleneck effect is created along the barrier reefs of the CC, reducing tidal dynamic strength behind.
- Tidal range and M2 amplitude increase with SLR but reduces in the CC due to bottleneck effect.
- Average velocity and BSS change with sea level depending on locations of dense reef areas.
- Vorticity and sinuosity differ as sea levels rise, vorticity reduces as eddies decrease, but increased tidal range increases sinuosity.
- Lagoons of low tidal energy will be created which are likely to fragment reefs and retain higher temperatures.
- As sea levels rise, reefs increase in the amount of self-seeding behaviour, complicating management strategies.

5.4.2 Tidal dynamics

5.4.2.1 M2 amplitude and Tidal range

SSP119: as SLR of 0.45 m causes a small reduction in M2 amplitude across the CC, the area of this reduction is inside the barrier reefs along the edge of the shelf, suggesting that they block tidal amplitude from entering the CC from that area

due to a bottleneck effect – increased tidal energy becomes more limited by the narrow channels between dense reefs (Wolanski et al. 2024b). A well known example of tidal dynamic bottleneck effect is in the Sylt-Rømø Bight in the south-eastern North Sea, where secondary rotations of the M4 and M2 tidal ellipsis become trapped in the inlet (Fofonova et al. 2019). M2 amplitude is seen to increase on the CC external reefs, suggesting increased tidal interaction. The area on the inside of these reefs becomes protected from tidal energy, as suggested by Munday et al. (2009) as sea levels increased. The convergence zone near the Whitsundays (where there is no change observed) may be because the area is protected from redirected tides by dense reefs. Changes in energy in areas either side of the Whitsundays has dissipated northwards (increased energy) and southwards (decreased energy), therefore not effecting tidal range in this area. The impact of the convergence zone may be greater coral larvae retention (Munday et al. 2009). M2 amplitude across the rest of the GBR is not impacted by 0.45 m of SLR, but tidal range does show a significant impact on SSP119, again the CC between Herbert Creek and the barrier reefs reduce in amplitude due to the reefs blocking tidal movement. Swain and the northern CC both also increase in tidal range, possibly due to redirected tides from restricted barrier reefs. Tides in the present day around Herbert Creek (Broad Sound) are due to the wide shelf and the barrier reefs forcing tidal flow around the reefs to the south and the north of the CC (Steinberg 2007). The tidal redirection to the north through sparse reef matrix in the Central GBR where they form a macro-tidal standing wave (Steinberg 2007) (a large tidal range but the phase is almost constant (Bowers and Lennon 1990)). The lower northern GBR reduces in tidal range in areas of inlets which are being blocked by large dense reefs, suggesting that reefs are also redirecting tides in this area. Tidal range increases in northern Grenville across the mid-shelf, this may be due to sea level being able to flood over the shelf edge reefs and enter the mid shelf. Cairns and the central GBR does not undergo change in tidal range.

SSP245: M2 amplitude changes are contained to the CC, as in SSP119. There is a larger reduction in amplitude as tides are redirected away from the barrier reefs to less dense areas of the shelf edge. Grenville begins to increase in M2 amplitude, supporting the earlier idea that sea level is coming over the shelf edge reefs and flooding the mid shelf. The central GBR is still unaffected by changes to M2 amplitude from 0.6 m of SLR. The magnitude in changes of tidal range continues from SSP119, suggesting that trends will continue of areas altering in tidal amplitude due to tides being redirected as increased volumes of water generate a bottleneck effect whilst passing through dense areas of reefs.

SSP585: SLR of 0.85 m drives larger changes to M2 amplitude and tidal range than observed in SSP119 or SSP245. The CC continues to reduce as tides are still redirected away from the CC between the barrier reefs and Herbert Creek, the difference of reduction between 0.45 m and 0.6 is much smaller than the difference between 0.6 m and 0.85 m, suggesting a tipping point was reached for acceleration of tidal change. The same conclusion is reached for the jump in tidal range change across the GBR. The central GBR remains very similar in both tidal range and M2 amplitude, only undergoing a small reduction in tidal range along some areas of coast. This suggests that this much narrower section of the shelf has much more stable tidal dynamics than wider sections of shelf further from the coast, as found in palaeo tide studies (Hopley 2006). As the central reef begins to reduce in tidal range, it suggests that tidal range is generally reduced by SLR. Areas with increased tidal range are due to tidal waves being exaggerated from redirected water from barrier reefs.

Overall, even the best case scenario of SSP119 will cause changes in M2 amplitude and tidal range, however changes in M2 amplitude are much smaller than changes to tidal range. There is a complex interaction between rising sea level and dense areas of reef, barrier reefs along the shelf edge of the CC create a bottleneck effect as sea levels rise, causing a reduction in M2 amplitude and tidal range within the channel. However, tides become redirected away from these

dense reefs and increase tidal dynamics to the south and north of the area. Grenville increases in M2 amplitude and tidal range due to higher sea levels being able to flood the shelf area easier than the present sea level. Implications of this are likely to be that small lagoons of low energy water are generated behind dense areas of reefs, potentially leading to greater levels of larvae retention, whilst areas either side of dense reefs will increase in tidal energy, effecting larvae retention and dispersal. The central GBR is unlikely to undergo noticeable changes in tidal range and M2 amplitude even with 0.85 m of SLR.

5.4.2.2 Velocity and Bed Shear Stress

Average velocity and BSS are observed to change in the same areas that recorded changes in tidal range and M2 amplitude. This is to be expected as increased tidal range will provide higher energy waters which will be travelling faster, as well as areas becoming lower energy from reduced tidal range.

In SSP119, velocity changes are highest in the barrier reefs along the CC, where the suggestion that higher sea levels are being bottlenecked in this area. The finding supports this proposal, as velocity increases in the squeezed tidal jets between reefs and will be pushed faster across reefs. High velocity tidal jets can be seen behind reefs in Figure 5.6. Areas in the CC where velocity has reduced are in areas of the convergence zone mentioned earlier across from the Whitsundays, were tidal energy has dissipated due to redirected tides. Velocity increases across large reefs in Cairns, this may be that high sea level submerges more of the reef, either areas which were not submerged now are, or that there is a larger difference between sea surface and the tops of reefs, generating less drag and increasing velocity (Green, Lowe, and Buckley 2018).

BSS is driven by velocity, therefore it is not surprising that BSS follows the same trends as velocity within the CC. However BSS is also driven by shallow water, and as such, increased BSS can be seen within the CC where tidal range has

decreased, reducing how submerged reefs will be during spring tides and driving higher levels of BSS. As shallow waters increase BSS, deeper water decreases BSS as seen in Grenville: as tidal propagation increases across the mid-shelf, BSS is reduced. Cairns experiences slight reduction in BSS on large reefs, as velocity increased in these areas it suggests that the reason behind increased velocity is that the difference between reefs and the sea surface has increased, generating less stress.

SSP245: Areas of change in average velocity expand in size and magnitude of change. SLR of 0.6 m generates increased velocity on reefs and reduced BSS on the substrate behind reefs along the CC and within Swain. The reason for this will be that higher levels of velocity passing over reefs will be generating larger lees which did not previously exist to the same extent (Stammer 1998). Large reefs in Cairns experience similar changes in velocity as SSP119, suggesting that although there is a change, the central GBR is fairly stable during SLR. Grenville reduces in

BSS across the mid-shelf as SLRs however reefs along the coast increase in velocity, this may be from increased tidal energy rebounding off the coast as sea levels increase. BSS across the GBR reduces further with 0.6 m of SLR, particularly in Grenville where tidal range has increased and higher levels of water are being experienced, as well as along the CC where redirected tides have increased tidal elevation. Swain also reduces in BSS amongst the densest areas of reefs, a reason may be tides becoming trapped by the dense reefs in the Sticky Water Effect (Wolanski and Spangnol 2000).

SSP585: The same trends seen in SSP245 average velocity continue with 0.85 m of sea level with increasing intensity, however the area of increased velocity surrounding the barrier reefs of the CC has reduced slightly. This suggests that tidal energy coming through the barrier reefs is beginning to reduce at this sea level and will eventually, as sea level continues to rise past this point, overcome the bottleneck effect and tidal dynamics will become more uniform across the GBR.

Velocity reduces across Swain, suggesting that deeper water submerges reefs further, reducing velocity. The mid-shelf of Grenville decreases in velocity as SLRs to this point, suggesting a new lagoon is forming where the effect of tides is smaller. Coastal reefs in Grenville and Cairns increase in velocity, this may be an effect of the increased tidal range. At this sea level, BSS has reduced further, indicating a higher difference between reefs and the sea surface.

Overall, changes in velocity and BSS are not uniform as sea-level rises but changes are seen from 0.45 m of SLR. The results suggest that as sea-level rises, low tidal-energy lagoons are formed on the shelf near dense reefs, such as in northern Grenville and within the CC. Reefs along the coast will increase in tidal energy from the increased tidal range, such as reefs in the south of Grenville and Cairns. The implication of this is that reefs in different areas of the GBR will experience different shifts in tidal dynamics, reefs in areas which form new lagoons will be more likely to retain their larvae, but will become more isolated from reefs outside of the lagoon (Camp et al. 2019); while coastal reefs in areas with increased tidal energy will be more likely to disperse their larvae.

The changes in tidal energy may also have implications on reef health, for example lagoons have much longer flushing times: during marine heatwaves, the warm water will be trapped for longer and the area will experience less flow of cooler water and temperature increase will be amplified (McCabe et al. 2010). However, reefs in areas of increased tidal energy may have a better chance to avoid bleaching (Lowe et al. 2016) and being buried by increasing levels of sediment (Storlazzi et al. 2011), as higher levels of velocity will increase flushing times and wash away sediment. The downside of increased turbidity is that water clarity can be reduced from more sediment influx and retention, limiting light available for photosynthesis (Kleypas 1996).

5.4.2.3 Vorticity and Sinuosity

Vorticity measurements of L_2 Norm shows that as sea-levels rise, vorticity will reduce. Vorticity of the future sea level scenarios are all very similar to each other, however there is a clear difference between them and the modern vorticity in each of the sectors. The smallest difference between modern and future is in Cairns, in earlier analysis tidal dynamics were found to change very little with increase sea level in Cairns. However, the magnitude of difference between modern and SSP119, verses the magnitude of difference between each future scenario is surprising. The difference suggests that Cairns is more sensitive to the next 0.45 m of sea level, than sea level continuing above 0.45 m. A reason may be that the amount of eddies generated in Cairns are sensitive to the difference in height between the top of reefs and sea surface height: sea level reduces BSS, as shown, which will reduce the amount of eddies. The largest difference in vorticity between modern and future scenarios is found in Grenville, tidal dynamics in this area has been shown to be extremely sensitive to SLR. The sector in the present day is fairly shallow and well protected by the barrier reefs, however 0.45 m of SLR is able to infiltrate the dense reefs and flood this sector, increasing the difference in height between the top of reefs and the sea surface: reducing BSS, drag and therefore the amount of eddies generated.

With reduced vorticity as sea levels rise, sinuosity was expected to also reduce however it was found to only reduce in Swain while it increased slightly in Cairns and Grenville, suggesting that vorticity is not the dominant driver of sinuosity. A reason why sinuosity increased in Cairns and Grenville may be because of increased tidal range: larger tidal oscillations may be generated and this will transport particles back and forth, generating high sinuosity trajectories. Larger tidal oscillations may be less effective at keeping larvae close enough to the parent reef to settle, than eddies or smaller tidal oscillations, explaining why self seeding decreases whilst sinuosity increases. Swain decreasing in sinuosity with rising

sea levels may be that velocity reduces with rising sea levels in this area, whilst velocity increases in Grenville and Cairns. The impact of this in Swain is that although tidal range increases, the speed is reduced, and thereby trajectories are not being washed back and forth within 48 hours as quickly as they are in the present day.

Overall, vorticity decreases with SLR, particularly within the next 0.45 m and this is thought to be due to eddies reducing as sea level increases the height difference between tops of reefs and the sea surface. Following 0.45 m of sea level, vorticity reduces at a slower rate, suggesting that the critical point of drag was lost during 0.45 m of SLR. It is important to note that coral additional coral growth was not accounted for in the bathymetry, therefore drag coefficients affected by height difference may not be exact. If an absolute maximum of 10 mm yr^{-1} vertical accretion is used, taken from coral cores across the GBR (Davies 1985; Buddemeier and Smith 1988), (much lower accretion rates between 2 - 7.5 mm are often suggested in studies (Perris et al. 2024; Ryan et al. 2016; Rodriguez-Ruano et al. 2023)), by 2100 corals will have vertically accreted by a maximum of 0.75 mm and reefs will have been outpaced by SLR in SSP585. However, vertical accretion will not be uniform across the GBR and adding reef growth would require an additional model which was out of the scope of this project based on the spatial scale (Masselink, Beetham, and Kench 2020; Salles et al. 2018).

5.4.3 Connectivity

The diagonal analysis showed self-seeding behaviour does not undergo large change from the present day; although there is a trend of increasing in self-seeding as sea levels rise, there was not a significant difference. The lack of significance is surprising, as SLR of 0.87 cm is a drastic difference for affecting large scale tidal dynamics (Mawson, Lee, and Hill 2022). The increased self-seeding behaviour correlates with predictions made by Munday et al. (2009), that rising sea levels could lead to higher levels of local retention, however the scope of

this work has not looked at whether the increase of self-seeding reefs is due to an increasing amount of newly established lagoons retaining coral larvae.

Network analysis from the CPM showed a trend of reef clusters fragmenting as sea levels rise. This suggests that as sea levels rise, reefs increase in self-seeding and so inter-connectivity reduces. The impact is that reef management in the future is going to become more challenging: as each reef becomes more isolated, in terms of larval exchange, from its neighbours. The impact of SLR is also not uniform, as some regions of the reef will decrease in tidal strength whilst other regions increase, preventing blanket assumptions for management. The GBR will not benefit from only some areas being protected as gene flow will not be travelling between reefs which in turn affects resilience and revival.

The PCA indicated that for all sectors PC2, relating to local network modularity, will change across different SSP scenarios: Grenville and Swain increase in modularity linearly whereas Cairns is not linear and peaks in SSP245, suggesting that Swain and Grenville's networks increase in modularity as SLRs but Cairns may have a tipping point of sea level decreasing modularity. Grenville and Swain are also very similar in overall network strength, which is much weaker than Cairns. This shows a similarity in network within Grenville and Swain, which are on wide sections of the shelf, whereas Cairns is on one the narrowest sections. These findings in modularity mirror the findings of the CPM (reef clusters will become smaller and more fragmented) but highlighted a difference in network style between the central narrow shelf and the widest sections of the shelf.

5.4.4 Summary

Research question 1: Using a model with improved resolution by 50 % and localised SLR generates similar overall results to the study conducted by Mawson, Lee, and Hill (2022). However the improved resolution generates higher detail in reef areas and allows the impact of barrier and dense reefs interacting with

SLR to be shown. This enabled an answer to be given for why the CC around the Whitsundays is not observed to change in tidal dynamics from the present day whilst surrounding areas drastically increase and decrease.

Research question 2: Even the best case scenario SLR from SSP119 will effect tidal dynamics. As sea level rises, tidal dynamics will change in different areas of the GBR depending upon the density of reefs and locality to the coastline. For example, areas protected by dense barrier reefs, such as Grenville and the CC will slowly form lagoons protected from high tidal energy. Other areas of the GBR will also reduce in strength of tidal dynamics despite increased tidal range. This is due to drag decreasing in reef areas as reefs are outpaced by SLR. Tidal range and M2 amplitude are observed to increase across the GBR, apart from in areas protected by barrier reefs. Barrier reefs are found to produce a bottleneck effect as sea level rises, preventing tidal waves from passing to areas behind. Grenville has been protected by barrier reefs up to the present day, but increase SLR has been shown to intrude into the sector over reefs and from less dense reef areas. Cairns undergoes very little change throughout the sea level scenarios. Swain undergoes small changes in tidal dynamics.

Research question 3: SLR by even 0.45 m will increase the amount of self-seeding behaviour across the GBR. Although vorticity reduces as eddies stop being generated, increased tidal range will continue to return larvae to parent reefs.

5.4.5 Implications and Limitations

This work has improved upon previous future GBR sea level studies such as Mawson, Lee, and Hill (2022) because it uses higher resolution and spatially varying sea-level rise scenarios. Producing detailed analysis of tidal dynamic changes, has allows better explanations to phenomena such as why tidal dynamics in the CC increase and decrease, as well why a convergence zone appears near the Whitsundays. The implications of this work is that the number of lagoons will increase,

fracturing reef communities: reefs within an enclosed lagoon will be separated from external genetics. Flushing times will also be affected by reduced tidal dynamics: lagoon areas will increase in and retain temperature longer than previously experienced, as flow in and out of the area is restricted. Areas of low tidal energy will also become more susceptible to wind, as shown by chapter 3 which means that larvae will be more freely dispersed away from reef areas by wind, lowering the chances of settlement. Areas of increased tidal energy will fare better for temperature regulation than in the present day, as temperature regulation will be improved by increased flushing. Self-seeding increases slightly with SLR, this will have negative management consequences as fragmented reefs are harder to protect: a blanket protection is needed and reefs will also become less resilient if they are not able to obtain larvae from neighbouring healthy reefs.

A limitation of the CPM model work is that it is possible that the resolution parameter used across all models was not the optimal resolution for the later SSP scenarios. However the CPM with the Leiden algorithm should be robust-enough to keep consistencies across small variations of reef connectivity across models. If the resolution parameter had been adjusted for each model, comparison would be inappropriate.

Balancing resolution and computational power is a constant battle for modellers. This study uses one of the highest resolution so-far used for the entire GBR, yet 250 m will still be missing small scale tidal dynamics which operate at 10's of m scale, such as the "sticky water phenomenon" (Wolanski et al. 2024a), which requires models below 100 meters. Predicting changes to connectivity across the entire GBR requires higher resolution in order to be more robust and account for changes to the small but important dynamics at play for recruitment. For example, the discrepancy in this study over what is driving the changes in self-seeding would most likely be answered by producing higher resolution models, however the computational cost of doing ~50 m resolution for even sectors of the GBR is large and not possible at this point. My proposed middle ground would be

to continue to use the coarse GBR scale models but compare with more high resolution small scale models to build an idea of what is being missed by the coarse resolution. A study by Saint-Amand et al. (2023) showed that within a 48 hour window, resolution does not make a significant difference to larvae dispersal. therefore dispersal of particles is robust. The difference higher resolution would make is to capturing the tidal mechanisms behind larvae dispersal, such as leading to vorticity and sinuosity discrepancies. A further limitation is not accounting for any coral reef vertical accretion by 2100. This will have an effect on tidal dynamics affected by drag, such as velocity and BSS. Future work should also include a model for simulating reef vertical accretion across the entire GBR so that tidal dynamics can be modelled more precisely for the future.

5.5 Conclusion

In this study, three models were built simulating future SLR based on three SSP scenarios: best case scenario SSP 1 1.9, corresponding to 0.45 m mean SLR; mid case scenario SSP 2 4.5, corresponding to 0.6 m mean SLR; and SSP 5 8.5, corresponding to 0.87 m mean sea level. These models were used to investigate three questions: whether increasing model resolution by 50% and using relative SLR alters predictions made to future tidal dynamics, how tidal dynamics have changed in 2100 from the modern day based on each SSP, and finally how do the difference SSPs affect self-seeding behaviour of reefs. Findings showed that improved resolution and relative sea level generated the same trends and magnitude of change as a study done by Mawson, Lee, and Hill (2022). However more detail in reef areas was able to be extracted and showed the interaction between barrier reefs and SLR. Tidal range and M2 amplitude were shown to increase across most of the GBR, but a bottleneck effect is created by barrier reefs, where tidal dynamics are reduced to levels below the present day behind the reefs. Tidal dynamic changes are not observed on the narrowest sections of the

continental shelf, such as around Cairns. SLR also causes lagoons to begin to form which will have consequences on coral networks and flushing times. Self-seeding is shown to increase with SLR, impacting future management plans by reefs becoming more fragmented.

Chapter 6

Discussion

This chapter provides a summary of what has been covered in this thesis. The chapter begins with a synthesis of the research gap and a recap of the questions that are being addressed in each of the previous chapters. Following on from that, a summary of each chapter is provided with the key findings from each and an explanation on how each chapter builds on from the previous ones. Implications of the individual findings and findings as a whole are then highlighted, before covering limitations of the work presented and how future work should be directed to combat limitations and build upon the work presented here.

6.1 Synthesis

The overall aim of this thesis was to explore the interaction between sea-level and tidal dynamics on the Great Barrier Reef (GBR), and the role they have on shaping coral connectivity across the GBR. The work presented here aims to provide contributions to (i) understanding the physical drivers behind coral larvae dispersal and retention, (ii) how tidal dynamics may have been responsible for the initiation of the modern day GBR around 8,000 years ago and (iii) how future sea-level rise will impact coral connectivity on the GBR, depending on which

shared socioeconomic pathway (SSP) the world takes.

The GBR is a heavily studied area of the world; researchers have been able to make full use of extensive high resolution bathymetry and well established research stations across the GBR, yet due to its size and complexity, much still remains unknown (Wolanski et al. 2024b). It is well established that tidal dynamics on the GBR are highly sensitive to bathymetric changes, including water depth influenced by sea-level (Seifi, Deng, and Andersen 2019), and that coral larvae dispersal is impacted by both winds and tides (Wolanski et al. 1988). However, the different roles and interaction between tides and wind on coral larvae retention is not well understood – particularly as drivers of larval retention. Understanding the relationships between sea level, tidal dynamics and connectivity, by investigating how tidal dynamics initiated growth of the modern GBR will be vital for predicting what will happen as sea level continues to rise in the future.

This thesis focuses on the role tidal dynamics play in coral larvae self-seeding following the annual mass spawning event, and how the relationship is impacted by sea level. Self-seeding reefs are defined as a reef which receives the larvae it produces. Unlike other studies, the work conducted in this thesis has examined the different effects wind and tides have on connectivity within the GBR, and also explores the impact of sea-level across a large temporal range, encompassing three main questions and their sub questions, as outlined in chapter 1. To review, these are as follows:

1. **What are the differing effects of wind and tides on coral larvae transportation?**
    1.1. What is the mechanism behind self-seeding behaviour?
2. **What tidal dynamics were present during the Holocene GBR initiation around 8 ka and how are they different to the present day?**
    2.1. How has connectivity changed throughout the Holocene initiation?

2.2. How did tidal dynamics affect coral connectivity during the Holocene initiation?

3. **How is self-seeding behaviour affected by future sea level rise across different Shared Socioeconomic Pathways?**

3.1. How are tidal dynamics affected in 2100 by each SSP sea level rise scenario?

3.2. How does using a higher resolution model of the entire GBR and relative sea level rise improve predictions to tidal dynamics?

6.1.1 Summary of key research findings

Chapter 3 investigated the difference physical drivers make to the transportation of coral larvae and self-seeding behaviour on the GBR. Three numerical models were developed of the GBR to simulate tidal and wind dynamics, both separately and together, using the unstructured mesh model, Thetis. The output of which were then used for tidal analysis and integrating with the Lagrangian particle tracking software, Parcels (Delandmeter and Sebille 2019). Throughout three sections analysed (south, central and northern GBR) particles representing coral larvae are released from reef polygons and tracked for developing connectivity matrices. Levels of self-seeding are assessed using connectivity matrices produced by each of the three models. The importance of this chapter was to establish the role of tides on connectivity: when models are created for palaeo and future predictions, generating wind predictions is out of the scope of this thesis, whereas tides are much more predictable and will be used in subsequent chapters without wind forcing.

Results showed tide only (TO) models exhibited the highest levels of self-seeding behaviour, along with the highest levels of vorticity and particle trajectory sinuosity through tidal ellipses. In contrast, weak tides – such as those observed at Cairns (central GBR), produce minimal vorticity, allowing larvae to be more read-

ily transported away from parent reefs by wind. The particle trajectories in tidal models revealed that tidal ellipses, rather than sporadic tidal eddies as previously conjectured to drive self-seeding behaviour, are primarily responsible for larvae retention. Trajectories caught in tidal ellipses are symmetrical in their transport, tend to move east-west rather than north-south and also move much further than a tidal eddy generated in the lee of a reef. Wind only (WO) models produced minimal self-seeding, low vorticity and trajectory sinuosity of particle trajectories. In these scenarios, larvae were carried away from parent reefs, and any observed self-seeding occurred only because some parent reefs were too large for the larvae to clear before settling or little to no wind was present. Wind and tide (WT) models resulted in intermediate levels of self-seeding – less than TO models but more than WO models – indicating that tides promote self-seeding while wind tends to disrupt it.

Chapter 4 followed on from the work of chapter 3, the tidal dynamics present during initiation of the GBR around 8,000 years ago (8 ka), during the early Holocene (Hopley, Smithers, and Parnell 2007), were investigated for the first time. Three numerical models were developed of the Great Barrier Reef across three thousand years using Thetis: representing 7 ka (1.7 m below present sea level), 8 ka (7 m below present sea level) and 9 ka (17 m below present sea level). For each of these models, bespoke bathymetry and reef location reconstructions were created for each palaeo-sea level taking into account depth change and position of reefs. These models were then used for tidal analysis, and integrated with Lagrangian particle tracking software, Parcels, in order to investigate whether tidal dynamics at 8 ka were responsible for increased larvae retention that may have contributed to regional reef initiation. Throughout, the same three sectors as used in chapter 3 were selected to study, as well as the same analysis methods to allow comparison against modern sea level.

Results showed that as sea level rose from 9 ka to 8 ka, tidal strength increased to levels higher than experienced in the present day. The southern GBR experienced

a lag in the effects of sea level rise (SLR), so the peak of tidal strength was found in 7 ka. Coinciding with the rise in sea levels, the amount of self-seeding reefs was found to increase. There were several reasons for this: sea level increased enough to create more locations for reefs to establish, larger reefs were able to grow making self-seeding more likely, and tidal dynamics such as increased eddies and tidal ellipses, led to higher levels of larvae retention.

Finally, chapter 5 builds on chapter 4 and chapter 3 to predicts changes to GBR tidal dynamics generated by rising sea levels predicted from three Shared Socioeconomic Pathways (SSP) for the year 2100 (Riahi et al. 2017; O'Neill et al. 2017). Three future models using Thetis are generated based on conversions from SSP to SLR by IPCC AR6 (Garner et al. 2021; Intergovernmental Panel on Climate Change (IPCC) 2023; Kopp et al. 2023): a best case scenario SSP 1 1.9, corresponding to 0.45 m mean SLR; mid case scenario SSP 2 4.5, corresponding to 0.6 m mean SLR; and SSP 5 8.5, corresponding to 0.87 m mean sea level. The models created are the first tidal models to use spatially varying sea-level rise predictions to simulate future tides on the GBR. These models were then used for tidal analysis and again integrated with Lagrangian particle tracking, Parcels, in order to answer how changes to tidal dynamics affect coral reef self-seeding behaviour. The same three sections in the south, central and northern GBR were used for tracking particles representing coral larvae. Findings from this chapter are important for highlighting implications of future tidal dynamics for coral reef management across the GBR, as well as investigating changes derived from using both a higher resolution model and integrating spatially varying sea-level rise than a previous study by Mawson, Lee, and Hill (2022).

Results showed that self-seeding increases with SLR, causing reef larval networks to become more fragmented. Improved resolution and spatially-varying sea level generated the same trends and magnitude of change as a study carried out by Mawson, Lee, and Hill (2022), however the detail obtained in this chapter of reef areas was able to be extracted and showed the interaction between barrier reefs

and SLR. Tidal range and M2 amplitude were shown to increase across the GBR but a bottleneck effect is created by barrier reefs, blocking and redirecting tides around the region, reducing tidal dynamics to levels below the present day behind the reefs. Sea-level rise also causes more atoll lagoons to begin to form, which will have consequences on coral networks and flushing times.

6.2 Wider Implications

The main implication from chapter 3 is that less larvae will be retained near the parent reef if rising sea level reduces the strength of tides across the GBR as wind will disrupt retention with greater effect. The negative consequence of this is that more larvae may be lost, leading to a decline in population growth on the GBR. Both chapter 5 and chapter 4 have shown tides weakening in the future and self-seeding reducing. However, chapter 3 implies that the reduction of self-seeding will be higher than predicted, as wind will serve as additional disruption. The benefit of more larvae being carried away from parent reefs is that it may increase genetic connectivity. Tides have been shown to lead to maximum connectivity, which is a useful metric to use when considering future management implementations, when it is understood that winds will disrupt connectivity.

The most important implication from chapter 4 is that the relationship between sea level, tidal dynamics and coral reef connectivity, is of such importance that it may have led to the initiation of the Holocene GBR (the modern day reef). Self-seeding means greater chance of surviving, therefore reefs establish more quickly. It was shown that self-seeding levels increased with SLR, however there was a point in time where both tidal dynamic strength and self-seeding reduced, indicating that the relationship between sea level and tidal dynamics is not linear or straight forward. However, the relationship between tidal dynamics and self-seeding is more predictable - increased tidal strength results in more asymmetric tidal ellipses and hence greater self-seeding. Further work needs to be carried

out to establish the tipping point of sea level, as it should not be assumed that as sea levels continue to rise, tidal dynamic strength and self-seeding will increase.

The primary consequence of chapter 5 is that self-seeding increases slightly with SLR and this will have negative management consequences as fragmented reefs are harder to protect: a blanket protection is needed and reefs will also become less resilient if all larvae are a result of self-seeding; larvae may also be required from neighbouring healthy reefs. However areas of increased tidal energy will fair better for temperature regulation than in the present day by increased flushing of lagoons and greater tidally driven mixing. Areas of low tidal energy will also become more susceptible to wind dispersal, as shown by chapter 3 which means that coral larvae will be dispersed rather than retained in reef areas. This may increase genetic diversity, but may also reduce total amount of larvae settling as more are lost to areas where the benthos is not suitable for coral growth.

The primary benefit of self-seeding is that it provides the highest chances of settling and survival of recruits, as larvae is not lost to areas of unsuitable substrate. The main implication from this work is that more larvae will be retained near the parent reef if rising sea level increases the strength of tides across the GBR Mawson, Lee, and Hill 2022; Harker et al. 2019. Self-seeding is thought to have enabled quick recovery for some reefs following bleaching events if there are surviving resilient coral species Adjeroud et al. 2018. The negative consequence of this is that although less larvae may be lost, networks will become more fragmented, following destructive disturbances this may lead to further decline in population growth on the GBR. Another negative of strong self-seeding is that residency of disease and COTS may increase in areas of slow flushing Pratchett et al. 2014. With environmental stressors impacting coral reefs, larvae needs to be carried away from parent reefs to increase genetic connectivity. Stronger networks have the potential to develop from larvae dispersal, this will have the benefit of damaged reefs being able to receive new recruits from healthy reefs within the network Greiner et al. 2022 and is the primary driver of reef recovery Gouezo et al. 2019.

Larvae dispersal may also lead to migration of corals to cooler waters, increasing chances of survival of the GBR Davis et al. 2023. Management strategies will also be made easier if reefs are less fragmented, as key networks can be identified and protected Botsford et al. 2009; Roberts et al. 2021.

6.3 Limitations

Balancing resolution and computational power is a constant battle for modellers, this study uses one of the highest resolution so-far used for the entire GBR, yet 250 m will still miss small scale tidal dynamics which operate at 10's of m scale, such as the "sticky water phenomenon" (Wolanski et al. 2024a). However the computational cost of doing ∼50 m resolution for a sector of the GBR is large and not feasible at this point in time. My proposed middle ground would be to continue to use the ∼250 m GBR scale models but compare with small scale higher resolution models of small groups of reefs to build an idea of what is being missed by the coarse resolution. However, in this study, despite 250 m resolution missing fine-scale tidal dynamics, dispersal of particles is considered robust, as a study by (Saint-Amand et al. 2023) showed that within a 48 hour window, resolution does not make a significant difference to larvae dispersal on the GBR.

Another limitation is that wind is not included in the models of chapter 4 and chapter 5. Chapter 3 showed that a combination of tides and wind drive dispersal on the GBR, therefore connectivity driven only by tides will not capture a realistic result. However, although wind data is available for pre-Holocene and the future predictions, this work was focusing solely on the changes of tidal dynamics driven by sea-level change and the consequences on coral connectivity. Including wind data for the palaeo and future studies would have altered the studies far beyond the research questions. Chapter 3 showed that using tides only to model larvae dispersal resulted in maximum connectivity, therefore it was deemed best to only

model maximum connectivity of palaeo and future reefs, with the understanding that wind would, in reality, disrupt local retention and self-seeding. The EAC was also not included in these models, which may be expected to have an effect on dispersal in the southern section of the GBR, however as this thesis was focusing on tidal dynamics, including current forcing would have distorted the results, especially in chapter 3, which was focusing solely on tides and wind. Having not been included in that chapter, it would have been inappropriate to then include it in the subsequent chapters as comparisons would have been difficult, as well as future and palaeo EAC projections for the specific time and sea-level steps do not exist.

Ideally waves would also be included in larvae transportation models, as they play a key role in transporting larvae in and out of enclosed atoll lagoons (Grimaldi et al. 2024), as well as dispersing larvae which have congregated together on the surface (Oliver and Willis 1987). However, including waves at this spatial scale and resolution was not possible for this study, but running smaller models at finer resolution, integrated with wave models such as SWAN (Simulating WAves Nearshore) (Booij, Ris, and Holthuijsen 1999) in the future would be highly beneficial to understanding small-scale transportation of larvae amongst groups of atolls.

A further limitation for future tidal dynamic predictions is that coral reef vertical accretion by 2100 was not modelled. If an absolute maximum of 10 mm/yr vertical accretion is used (Davies 1985; Buddemeier and Smith 1988), by 2100 corals will have vertically accreted by a maximum of 0.75 m and reefs will have been outpaced by SLR in SSP585. This will have an effect on tidal dynamics affected by drag, such as velocity and BSS as the GBR tidal dynamics are sensitive to bathymetry (Seifi, Deng, and Andersen 2019). However, this would have required a stratigraphic forward model to be developed, similar to one developed for removing the Holocene reef growth from the bathymetry used in the palaeo chapter (Salles et al. 2018), which is outside the scope of this project.

6.4 Directions for future research

In this final discussion, recommendations for future research are advocated, based on the wider findings, implications and limitations discussed throughout this Chapter. Questions which still remain unanswered or have been generated by the research conducted throughout this thesis:

- Using a high resolution (< 100 m) model of the entire GBR to detect fine scale tidal phenomena across the entire GBR, and how this affects dispersal/retention
- How does the wind vs tides debate perform for larvae which takes longer than 48 hours from release to settle?
- As well as wind vs tides, how does including currents such as the East Australian Current (EAC) or South Equatorial Current (SEC) affect dispersal?
- Investigate tidal dynamic changes during the Holocene GBR initiation using finer temporal steps - what is the sea level tipping point on tidal dynamics?
- The palaeo-tidal work should form a strong platform for further geological work on age, community structure and geochemical proxies for the GBR initiation
- Adding ecological population models to the model pipeline to see how changes to connectivity affects population growth
- Adding wind and a coral accretion model for more realistic results of dispersal and tidal dynamics

For future research, as specified in the limitations, it would firstly be beneficial to conduct the work carried out in this thesis with even higher resolution in order to capture more tidal phenomena generated by fine scale bathymetry, such as the "sticky water" effect, which has found to not be detectable in models coarser than 100 m resolution (Wolanski et al. 2024a). It would also be useful to choose small

areas of the GBR to model in extremely fine resolution (< 10 metres) in order to resolve the intra-reef scale tidal dynamic changes and capture how coral larvae and gametes exit enclosed atoll lagoons.

Running the biophysical simulations for longer periods of time would also be beneficial, as this would allow larvae which take longer than 48 hours to settle to be captured and traced. This was irrelevant to the questions being asked in this thesis, which focuses on self-seeding. However many GBR modelling studies have released coral larvae for weeks and months at a time (Thomas et al. 2014; Cresswell et al. 2024) and although this ignores the short-term processes of the annual mass spawning event, it captures network dynamics of corals which do not partake in the annual mass spawning event, or do, but their larvae has longer competency periods. These types of studies would benefit from investigating the independent roles wind and tides have on long term dispersed larvae to understand the mechanisms behind network connectivity and what management implications may arise.

The SEC and the EAC could also be implemented into this study, to investigate the effect they have on coral dispersal. The EAC is fed by the SEC and flows polewards along the outer edge of the continental shelf in the southern Coral Sea (Ridgway and Dunn 2003), although the majority of the EAC remains outside of the GBR, separated by the continental shelf, a lagoonal current flows from the EAC onto the narrow central GBR ($\sim$ 18-19°S) and exits from the CC (Benthuysen et al. 2022), and the EAC is thought to be responsible for generating the Capricorn Eddy (Weeks et al. 2010). Therefore the GBR is influenced by the SEC and the EAC, so the EAC will have some effect on the dispersal of larvae.

Further studies investigating timesteps closer to the Holocene initiation around 8 ka would also be encouraged, as the tipping point of sea level driving such high levels of tidal dynamics could be pinpointed. The work conducted in this thesis highlights that there were different tidal dynamic regimes around this time, but

exact timing and sea level have not been found. However, the work carried out does form a strong platform for further systematic geological investigations on coral reef ages, community structure and geochemical proxies which will further point to why and how the GBR initiated from the tidal dynamics present at the time.

Developing the models into full biophysical models by coupling with ecological growth models such as (Mumby et al. 2007; Greiner et al. 2022; Fung, Seymour, and Johnson 2011) would be highly beneficial to investigate what the ecological implication of increased or reduced self-seeding is, in regarding to population dynamics. This work would add weight to the findings of the biophysical model work as it stands, developing a better picture of implications of SLR and also allowing management strategies to be tested. To also add further strength to the findings of future sea level, a further study integrating Thetis with a climate model for future wind would be highly valuable in exploring how changing tidal dynamics will interact with wind forcing, and what the consequence on larvae dispersal will be. This would be important as future dynamical showed that corals will become more reliant on self-seeding, leading to fragmentation of coral networks. However if wind is able to drive dispersal, networks may be less fragmented as currently predicted. Also developing and integrating a coral accretion model for future coral growth would be vital for realistic tidal dynamic predictions. The study conducted in this thesis shows that the widening gap between coral height and the sea surface has an effect on tidal dynamics, however there is no account for coral growth over the duration. It is well known that the GBR tidal dynamics are highly sensitive to bathymetry, meaning that to get accurate predictions of tidal dynamic changes with rising sea level, coral vertical accretion needs to be modelled.

6.5 Conclusions

In conclusion, this thesis has demonstrated that sea-level and tidal dynamics are dominant drivers of coral larvae retention and local connectivity of the GBR. By isolating the effects of wind and tides, and projecting tidal simulations into the past and future, this work identified tidal ellipses as a primary driver of larval retention and self-seeding. Wind was found to disrupt this, and drive dispersal, especially in areas of weak tidal strength. During the early Holocene, rising sea levels increased tidal strength and self-seeding potential, likely facilitating the initiation of the modern GBR. By 2100, SLR projections under all SSP scenarios will increase tidal strength, leading to enhanced self-seeding and fragmentation of coral reef networks across all three studied sectors.

Together, these findings provide new insight into the physical processes underpinning driving coral connectivity, with clear implications for understanding reef resilience, predicting future connectivity and informing management strategies. This work highlights the essential role tides have in coral connectivity on the GBR, and will continue to have as sea level rises. This work also emphasises the need to incorporate realistic, high-resolution numerical models of tidal dynamics – both past and future – in coral reef connectivity modelling and management planning.

Bibliography

Adjeroud, Mehdi et al. (June 2018). “Recovery of coral assemblages despite acute and recurrent disturbances on a South Central Pacific reef”. en. In: *Sci. Rep.* 8.1, p. 9680.

Aldyan, Rizal Akbar et al. (2023). “Impact of coral reef damage due to tourism activities in Karimunjawa National Park”. en. In: *E3S Web Conf.* 448, p. 03063.

Allison, Mead A et al. (July 2017). “Observational and numerical particle tracking to examine sediment dynamics in a Mississippi River delta diversion”. In: *Estuar. Coast. Shelf Sci.* 194, pp. 97–108.

Almany, G R et al. (June 2009). “Connectivity, biodiversity conservation and the design of marine reserve networks for coral reefs”. en. In: *Coral Reefs* 28.2, pp. 339–351.

Amores, Angel et al. (Mar. 2022). “Numerical simulation of atmospheric lamb waves generated by the 2022 Hunga-Tonga volcanic eruption”. en. In: *Geophys. Res. Lett.* 49.6, e2022GL098240.

Andersen, Ole B et al. (Dec. 2006). “Mapping nonlinear shallow-water tides: a look at the past and future”. en. In: *Ocean Dyn.* 56.5-6, pp. 416–429.

Andrews, John C and Lance Bode (Sept. 1988). “The tides of the central Great Barrier Reef”. In: *Cont. Shelf Res.* 8.9, pp. 1057–1085.

Andutta, Fernando P, Michael J Kingsford, and Eric Wolanski (Apr. 2012). “‘Sticky water’ enables the retention of larvae in a reef mosaic”. In: *Estuar. Coast. Shelf Sci.* 101.0, pp. 54–63.

Andutta, Fernando P, Peter V Ridd, and Eric Wolanski (Feb. 2013). “The age and the flushing time of the Great Barrier Reef waters”. In: *Cont. Shelf Res.* 53, pp. 11–19.

Ani, Chinenye J et al. (June 2024). “Connectivity modelling identifies sources and sinks of coral recruitment within reef clusters”. en. In: *Sci. Rep.* 14.1, p. 13564.

Arbic, Brian K, Richard H Karsten, and Chris Garrett (Dec. 2009). “On tidal resonance in the global ocean and the back-effect of coastal tides upon open-ocean tides”. In: *Atmosphere-Ocean* 47.4, pp. 239–266.

Armsworth, Paul R (Apr. 2002). “Recruitment limitation, population regulation, and larval connectivity in reef fish metapopulations”. en. In: *Ecology* 83.4, pp. 1092–1104.

Assis, Jorge et al. (May 2025). “Coastal oceanographic connectivity at the global scale: a dataset of pairwise probabilities and travel times derived from biophysical modeling”. en. In: *Sci. Data* 12.1, p. 737.

Avdis, Alexandros et al. (Feb. 2018). “Efficient unstructured mesh generation for marine renewable energy applications”. In: *Renewable Energy* 116, pp. 842–856.

Babcock, Russell C et al. (1986). “Synchronous spawnings of 105 scleractinian coral species on the Great Barrier Reef”. In: *Mar. Biol.* 90.3, pp. 379–394.

Baird, Andrew H et al. (Nov. 2014). “Comment on “Chemically mediated behavior of recruiting corals and fishes: A tipping point that may limit reef recovery””. en. In: *PeerJ* e628v1.

Baird, Mark Edward et al. (Oct. 2020). “Optimising cool-water injections to reduce thermal stress on coral reefs of the Great Barrier Reef”. en. In: *PLoS One* 15.10, e0239978.

Bak, Rolf P M (Jan. 1978). “Lethal and sublethal effects of dredging on reef corals”. en. In: *Mar. Pollut. Bull.* 9.1, pp. 14–16.

Baker, Amy L et al. (Aug. 2020). “Modelling the impact of tidal range energy on species communities”. en. In: *Ocean Coast. Manag.* 193.105221, p. 105221.

Baker, Andrew C, Peter W Glynn, and Bernhard Riegl (Dec. 2008). “Climate change and coral reef bleaching: An ecological assessment of long-term impacts, re-

covery trends and future outlook". en. In: *Estuar. Coast. Shelf Sci.* 80.4, pp. 435–471.

Ballantine, Bill (Aug. 2014). "Fifty years on: Lessons from marine reserves in New Zealand and principles for a worldwide network". en. In: *Biol. Conserv.* 176, pp. 297–307.

Ban, Natalie C et al. (June 2019). "Well-being outcomes of marine protected areas". en. In: *Nat. Sustain.* 2.6, pp. 524–532.

Bartelet, Henry A, Michele L Barnes, and Graeme S Cumming (Jan. 2024). "Estimating and comparing the direct economic contributions of reef fisheries and tourism in the Asia-Pacific". en. In: *Mar. Policy* 159.105939, p. 105939.

Bateman, Mark D et al. (Oct. 2021). "Detailing the impact of the Storegga Tsunami at Montrose, Scotland". en. In: *Boreas* 50.4, pp. 1059–1078.

Beaman, Robin (Nov. 2023). *AusBathyTopo 250m 2023 grid - Deepreef Explorer*. en. https://www.deepreef.org/2023/11/01/ausbathytopo-250m-2023-grid/. Accessed: 2025-3-18.

Beaurepaire, Max et al. (Oct. 2021). "Microplastics in the atmospheric compartment: a comprehensive review on methods, results on their occurrence and determining factors". en. In: *Curr. Opin. Food Sci.* 41, pp. 159–168.

Benthuysen, Jessica A et al. (Nov. 2022). "Oceanographic influences on reef fish assemblages along the Great Barrier Reef". In: *Prog. Oceanogr.* 208, p. 102901.

Berkelmans, Ray et al. (Apr. 2004). "A comparison of the 1998 and 2002 coral bleaching events on the Great Barrier Reef: spatial correlation, patterns, and predictions". en. In: *Coral Reefs* 23.1, pp. 74–83.

Bianucci, Laura et al. (Jan. 2018). "Sensitivity of the regional ocean acidification and carbonate system in Puget Sound to ocean and freshwater inputs". en. In: *Elementa (Wash., DC)* 6.1, p. 22.

Birkeland, C et al. (2013). "Substratum stability and coral reef resilience: insights from 90 years of disturbances on a reef in American Samoa". In: *Micronesica*.

Black, Kerry P (Mar. 1993). “The relative importance of local retention and inter-reef dispersal of neutrally buoyant material on coral reefs”. In: *Coral Reefs* 12.1, pp. 43–53.

Black, Kerry P and S L Gay (Aug. 1987). “Eddy formation in unsteady flows”. en. In: *Journal of Geophysical Research: Oceans* 92.C9, pp. 9514–9522.

Bode, L and K P Stark (1983). *Simulation of Tides and Currents in the Mackay Region*. en. https://search.informit.org/doi/abs/10.3316/informit.916270082179355. Accessed: 2025-6-23.

Boland, F M and J A Church (Sept. 1981). “The east Australian current 1978”. en. In: *Deep Sea Res. A* 28.9, pp. 937–957.

Booij, N, R C Ris, and L H Holthuijsen (Apr. 1999). “A third-generation wave model for coastal regions: 1. Model description and validation”. en. In: *J. Geophys. Res.* 104.C4, pp. 7649–7666.

Boström-Einarsson, Lisa et al. (Jan. 2020). “Coral restoration - A systematic review of current methods, successes, failures and future directions”. en. In: *PLoS One* 15.1, e0226631.

Botsford, L W et al. (June 2009). “Connectivity and resilience of coral reef metapopulations in marine protected areas: matching empirical efforts to predictive needs”. en. In: *Coral Reefs* 28.2, pp. 327–337.

Bowers, D G and G W Lennon (Jan. 1990). “Tidal progression in a near-resonant system—A case study from South Australia”. en. In: *Estuar. Coast. Shelf Sci.* 30.1, pp. 17–34.

Bozec, Yves-Marie, Lorenzo Alvarez-Filip, and Peter J Mumby (Jan. 2015). “The dynamics of architectural complexity on coral reefs under climate change”. en. In: *Glob. Chang. Biol.* 21.1, pp. 223–235.

Braithwaite, C J R et al. (Mar. 2004). “The great barrier reef: The chronological record from a new borehole”. en. In: *J. Sediment. Res.* 74.2, pp. 298–310.

Bray, Nancy A et al. (May 1996). “Large-scale sea level, thermocline, and wind variations in the Indonesian throughflow region”. en. In: *J. Geophys. Res.* 101.C5, pp. 12239–12254.

Bricheno, Lucy M, Judith Wolf, and Saiful Islam (Dec. 2016). “Tidal intrusion within a mega delta: An unstructured grid modelling approach”. In: *Estuar. Coast. Shelf Sci.* 182, pp. 12–26.

Briggs, John C (Dec. 1961). “The east pacific barrier and the distribution of marine shore fishes”. en. In: *Evolution* 15.4, p. 545.

Brodie, Jon and Richard G Pearson (Dec. 2016). “Ecosystem health of the Great Barrier Reef: Time for effective management action based on evidence”. In: *Estuar. Coast. Shelf Sci.* 183, pp. 438–451.

Brodie, Jon and Jane Waterhouse (June 2012). “A critical review of environmental management of the ‘not so Great’ Barrier Reef”. en. In: *Estuar. Coast. Shelf Sci.* 104-105, pp. 1–22.

Bruno, John F and Abel Valdivia (July 2016). “Coral reef degradation is not correlated with local human population density”. en. In: *Sci. Rep.* 6.1, p. 29778.

Bryant, Edward (Oct. 1992). “Last interglacial and Holocene trends in sea-level maxima around Australia: Implications for modern rates”. en. In: *Mar. Geol.* 108.2, pp. 209–217.

Buddemeier, R W and S V Smith (May 1988). “Coral reef growth in an era of rapidly rising sea level: predictions and suggestions for long-term research”. en. In: *Coral Reefs* 7.1, pp. 51–56.

Burgess, S C, M J Kingsford, and Kerry P Black (July 2007). “Influence of tidal eddies and wind on the distribution of presettlement fishes around One Tree Island, Great Barrier Reef”. In: *Mar. Ecol. Prog. Ser.* 341, pp. 233–242.

Cai, W et al. (Dec. 2005). “The response of the Southern Annular Mode, the East Australian Current, and the southern mid-latitude ocean circulation to global warming”. en. In: *Geophys. Res. Lett.* 32.23.

Caley, M J et al. (1996). “Recruitment and the Local Dynamics of Open Marine Populations”. In: *Annu. Rev. Ecol. Syst.* 27, pp. 477–500.

Camp, E F et al. (Aug. 2019). “Mangrove lagoons of the Great Barrier Reef support coral populations persisting under extreme environmental conditions”. en. In: *Mar. Ecol. Prog. Ser.* 625, pp. 1–14.

Carlon, David B and Richard Randolph Olson (Nov. 1993). “Larval dispersal distance as an explanation for adult spatial pattern in two Caribbean reef corals”. In: *J. Exp. Mar. Bio. Ecol.* 173.2, pp. 247–263.

Carruthers, Lucy et al. (Nov. 2024). “Sea-level rise and extreme Indian Ocean Dipole explain mangrove dieback in the Maldives”. en. In: *Sci. Rep.* 14.1, p. 27012.

Carter, Amber L et al. (May 2022). “Cyclone impacts on coral reef communities in southwest Madagascar”. en. In: *Front. Mar. Sci.* 9, p. 753325.

Cartwright, D E (2000). “Tides: a scientific history”. In.

Ceccarelli, Daniela M et al. (Oct. 2020). “Substrate stabilisation and small structures in coral restoration: State of knowledge, and considerations for management and implementation”. en. In: *PLoS One* 15.10, e0240846.

Cesar, H, L Burke, and L Pet-Soede (2003). “The economics of worldwide coral reef degradation”. In.

Chalker, B E (July 1981). “Simulating light-saturation curves for photosynthesis and calcification by reef-building corals”. In: *Mar. Biol.* 63.2, pp. 135–141.

Chalker, Bruce E et al. (Sept. 1988). “Light and Reef-Building Corals”. In: *Interdiscip. Sci. Rev.* 13.3, pp. 222–237.

Chandra, Rohitash et al. (June 2019). “Bayeslands: A Bayesian inference approach for parameter uncertainty quantification in Badlands”. In: *Comput. Geosci.*

Chappell, John et al. (June 1996). “Reconciliaion of late Quaternary sea levels derived from coral terraces at Huon Peninsula with deep sea oxygen isotope records”. In: *Earth Planet. Sci. Lett.* 141.1, pp. 227–236.

Chassignet, Eric P et al. (Mar. 2007). “The HYCOM (HYbrid Coordinate Ocean Model) data assimilative system”. en. In: *J. Mar. Syst.* 65.1-4, pp. 60–83.

Cheal, A J et al. (Jan. 2007). “Spatial synchrony in coral reef fish populations and the influence of climate”. en. In: *Ecology* 88.1, pp. 158–169.

Chen, Changsheng et al. (2006). “An unstructured grid, finite-volume coastal ocean model: FVCOM user manual”. In: *SMAST/UMASSD* 6, p. 78.

Cheung, Mandy W M et al. (Dec. 2021). “Cumulative bleaching undermines systemic resilience of the Great Barrier Reef”. en. In: *Curr. Biol.* 31.23, 5385–5392.e4.

Chia, Fu-Shiang, John Buckland-Nicks, and Craig M Young (July 1984). “Locomotion of marine invertebrate larvae: a review”. en. In: *Can. J. Zool.* 62.7, pp. 1205–1222.

Choukroun, Severine et al. (Dec. 2024). “Larval dispersal predictions are highly sensitive to hydrodynamic modelling choices”. en. In: *Coral Reefs*, pp. 1–13.

Church, J A, John C Andrews, and F M Boland (Jan. 1985). “Tidal currents in the central Great Barrier Reef”. In: *Cont. Shelf Res.* 4.5, pp. 515–531.

Church, John A and Neil J White (Jan. 2006). “A 20th century acceleration in global sea-level rise: AN ACCELERATION IN GLOBAL SEA-LEVEL RISE”. en. In: *Geophys. Res. Lett.* 33.1.

Clark, Peter U et al. (Aug. 2009). “The Last Glacial Maximum”. en. In: *Science* 325.5941, pp. 710–714.

Cmems, E U (2023). “Global ocean physics reanalysis”. In: *Marine Data Store (MDS)[data set]*.

Colberg, Frank et al. (Nov. 2019). “High and medium resolution ocean models for the Great Barrier Reef”. In: *Ocean Model.*, p. 101507.

Coles, Stephen L and Yusef H Fadlallah (Jan. 1991). “Reef coral survival and mortality at low temperatures in the Arabian Gulf: new species-specific lower temperature limits”. en. In: *Coral Reefs* 9.4, pp. 231–237.

Coles, Stephen L and Paul L Jokiel (May 2018). “Effects of salinity on coral reefs”. In: *Pollution in Tropical Aquatic Systems*. 1st Edition. CRC Press, pp. 147–166.

Colosi, John A and Walter Munk (June 2006). “Tales of the venerable Honolulu tide gauge”. en. In: *J. Phys. Oceanogr.* 36.6, pp. 967–996.

Cong, Shuai et al. (Nov. 2023). “Intermittent migration of mixing front driven by typhoon events on the inner shelf of the East China Sea: A FVCOM modeling study”. en. In: *Mar. Geol.* 465.107161, p. 107161.

Corrège, Thierry (Mar. 2006). “Sea surface temperature and salinity reconstruction from coral geochemical tracers”. en. In: *Palaeogeogr. Palaeoclimatol. Palaeoecol.* 232.2-4, pp. 408–428.

Cowen, Robert K, C B Paris, and A Srinivasan (Jan. 2006). “Scaling of connectivity in marine populations”. en. In: *Science* 311.5760, pp. 522–527.

Cowen, Robert K and Su Sponaugle (Jan. 2009). “Larval dispersal and marine population connectivity”. en. In: *Ann. Rev. Mar. Sci.* 1.1, pp. 443–466.

Crain, Caitlin M et al. (Apr. 2009). “Understanding and managing human threats to the coastal marine environment”. en. In: *Ann. N. Y. Acad. Sci.* 1162.1, pp. 39–62.

Cresswell, Anna K et al. (Oct. 2024). “Capturing fine-scale coral dynamics with a metacommunity modelling framework”. en. In: *Sci. Rep.* 14.1, p. 24733.

Crimp, O N and R D Braddock (Mar. 1993). “Simulation of coral reefs and crown-of-thorns starfish”. en. In: *Environmetrics* 4.1, pp. 53–74.

Csárdi, Gábor et al. (2025). *igraph: Network Analysis and Visualization in R*.

Danilov, S (Sept. 2013). “Ocean modeling on unstructured meshes”. en. In: *Ocean Model. (Oxf.)* 69, pp. 195–210.

Davies, P J (1985). “Relationships between reef growth and sea level in the Great Barrier Reef”. In: *Proc. 5th Int. Coral Reef Congr.*

Davies, Thomas W et al. (May 2023). “Global disruption of coral broadcast spawning associated with artificial light at night”. en. In: *Nat. Commun.* 14.1, p. 2511.

Davis, Tom R et al. (Aug. 2023). “Are corals coming to a reef near you? Projected extension of suitable thermal conditions for hard coral communities along the east Australian coast”. en. In: *Austral Ecol.* 48.5, pp. 885–892.

Day, Jon C (2002). “Marine park management and monitoring–lessons for adaptive management from the Great Barrier Reef”. In: *Soren Bondrup-Nielsen, Neil WP*.

Day, Jon C et al. (Oct. 2019). “Marine zoning revisited: How decades of zoning the Great Barrier Reef has evolved as an effective spatial planning approach for marine ecosystem-based management”. en. In: *Aquat. Conserv.* 29.S2, pp. 9–32.

De Valck, Jeremy and John Rolfe (Feb. 2022). “Reviewing the use of proxies to value coastal and marine biodiversity protection: The Great Barrier Reef in Australia”. en. In: *Mar. Policy* 136.104890, p. 104890.

De’ath, Glenn et al. (Oct. 2012). “The 27-year decline of coral cover on the Great Barrier Reef and its causes”. en. In: *Proc. Natl. Acad. Sci. U. S. A.* 109.44, pp. 17995–17999.

Dechnik, Belinda et al. (May 2015). “Holocene “turn-on” and evolution of the Southern Great Barrier Reef: Revisiting reef cores from the Capricorn Bunker Group”. In: *Mar. Geol.* 363, pp. 174–190.

DeFilippo, Lukas B et al. (May 2022). “Assessing the potential for demographic restoration and assisted evolution to build climate resilience in coral reefs”. en. In: *Ecol. Appl.*, e2650.

Defne, Zafer and Neil K Ganju (Sept. 2015). “Quantifying the residence time and flushing characteristics of a shallow, back-barrier estuary: Application of hydrodynamic and particle tracking models”. en. In: *Estuaries Coast.* 38.5, pp. 1719–1734.

Delandmeter, Philippe and Erik van Sebille (Aug. 2019). “The Parcels v2.0 Lagrangian framework: new field interpolation schemes”. en. In: *Geoscientific Model Development* 12.8, pp. 3571–3584.

Deshpande, Koumudhi et al. (Mar. 2025). “Direct observation and quantitative characterization of chemotactic behaviors in Caribbean coral larvae exposed to organic and inorganic settlement cues”. en. In: *Sci. Rep.* 15.1, p. 10173.

Devlin, Michelle and Jon Brodie (2023). “Nutrients and eutrophication”. en. In: *Marine Pollution – Monitoring, Management and Mitigation*. Springer Textbooks in Earth Sciences, Geography and Environment. Cham: Springer Nature Switzerland, pp. 75–100.

Dixon, Adele M et al. (Aug. 2022). “Coral reef exposure to damaging tropical cyclone waves in a warming climate”. en. In: *Earths Future* 10.8, e2021EF002600.

Drake, Matilde A et al. (Mar. 2025). “Current velocity, water quality, and benthic taxa as predictors for coral recruitment rates on the Great Barrier Reef”. en. In: *PLoS One* 20.3, e0319521.

Duan, Dongli et al. (July 2023). “Effect of network nestedness on stability, diversity, and resilience of ecosystems”. en. In: *Chaos* 33.7, p. 073113.

Dubinsky, Zvy and Noga Stambler (Dec. 1996). “Marine pollution and coral reefs”. en. In: *Glob. Chang. Biol.* 2.6, pp. 511–526.

Dumas, F et al. (July 2012). “Tidal flushing and wind driven circulation of Ahe atoll lagoon (Tuamotu Archipelago, French Polynesia) from in situ observations and numerical modelling”. en. In: *Mar. Pollut. Bull.* 65.10-12, pp. 425–440.

Dutton, Andrea et al. (Jan. 2015). “Tropical tales of polar ice: evidence of Last Interglacial polar ice sheet retreat recorded by fossil reefs of the granitic Seychelles islands”. In: *Quat. Sci. Rev.* 107, pp. 182–196.

Ebi, Kristie L et al. (Feb. 2014). “A new scenario framework for climate change research: background, process, and future directions”. en. In: *Clim. Change* 122.3, pp. 363–372.

Egbert, Gary D and Svetlana Y Erofeeva (Feb. 2002). “Efficient Inverse Modeling of Barotropic Ocean Tides”. In: *J. Atmos. Ocean. Technol.* 19.2, pp. 183–204.

Egbert, Gary D, Richard D Ray, and Bruce G Bills (Mar. 2004). “Numerical modeling of the global semidiurnal tide in the present day and in the last glacial maximum: GLOBAL TIDAL MODELING”. en. In: *J. Geophys. Res.* 109.C3.

Elahi, M W E et al. (Nov. 2020). “Influence of seasonal river discharge on tidal propagation in the Ganges-Brahmaputra-Meghna delta, Bangladesh”. en. In: *J. Geophys. Res. Oceans* 125.11, e2020JC016417.

Enfield, David B (Feb. 1989). “El Niño, past and present”. en. In: *Reviews of Geophysics* 27.1, pp. 159–187.

Fabricius, Katharina E et al. (Jan. 2023). “Macroalgal cover on coral reefs: Spatial and environmental predictors, and decadal trends in the Great Barrier Reef”. en. In: *PLoS One* 18.1, e0279699.

Fadlallah, Y H and J S Pearse (Nov. 1982). “Sexual reproduction in solitary corals: Overlapping oogenic and brooding cycles, and benthic planulas in Balanophyllia elegans”. In: *Mar. Biol.* 71.3, pp. 223–231.

Fairbanks, Richard G (Dec. 1989). “A 17,000-year glacio-eustatic sea level record: influence of glacial melting rates on the Younger Dryas event and deep-ocean circulation”. In: *Nature* 342.6250, pp. 637–642.

Fairbridge, Rhodes W (July 1950). “Recent and Pleistocene Coral Reefs of Australia”. In: *J. Geol.* 58.4, pp. 330–401.

Faryuni, Irfana Diah et al. (Feb. 2024). “Assessing coral reef conservation planning in Wakatobi National Park (Indonesia) from larval connectivity networks”. en. In: *Coral Reefs* 43.1, pp. 19–33.

Felis, Thomas et al. (June 2014). “Intensification of the meridional temperature gradient in the Great Barrier Reef following the Last Glacial Maximum”. en. In: *Nat. Commun.* 5.1, p. 4102.

Feng, Ming et al. (Dec. 2016). “Ocean circulation drives heterogeneous recruitments and connectivity among coral populations on the North West Shelf of Australia”. In: *J. Mar. Syst.* 164, pp. 1–12.

Fennel, Katja et al. (Sept. 2022). “Ocean biogeochemical modelling”. en. In: *Nat. Rev. Methods Primers* 2.1, pp. 1–21.

Figueiredo, Joana et al. (Dec. 2021). “Global warming decreases connectivity among coral populations”. en. In: *Nat. Clim. Chang.* 12.1, pp. 83–87.

Fofonova, Vera et al. (Dec. 2019). “Non-linear aspects of the tidal dynamics in the Sylt-Rømø Bight, south-eastern North Sea”. en. In: *Ocean Sci.* 15.6, pp. 1761–1782.

Fox, Helen E and Roy L Caldwell (Oct. 2006). “Recovery from blast fishing on coral reefs: a tale of two scales”. en. In: *Ecol. Appl.* 16.5, pp. 1631–1635.

Fox, Helen E et al. (July 2019). “Rebuilding coral reefs: success (and failure) 16 years after low-cost, low-tech restoration”. en. In: *Restor. Ecol.* 27.4, pp. 862–869.

Fraser, Kerrie A et al. (Oct. 2019). “Impact evaluation and conservation outcomes in marine protected areas: A case study of the Great Barrier Reef Marine Park”. en. In: *Biol. Conserv.* 238.108185, p. 108185.

Friedrichs, Carl T, David G Aubrey, and Paul E Speer (1990). “Impacts of relative sea-level rise on evolution of shallow estuaries”. en. In: *Residual Currents and Long-term Transport*. New York, NY: Springer New York, pp. 105–122.

Frost, Adam et al. (June 2012). “Functional repurposing revealed by comparing S. pombe and S. cerevisiae genetic interactions”. en. In: *Cell* 149.6, pp. 1339–1352.

Fung, Tak, Robert M Seymour, and Craig R Johnson (Apr. 2011). “Alternative stable states and phase shifts in coral reefs under anthropogenic stress”. en. In: *Ecology* 92.4, pp. 967–982.

Gaonkar, Chetan A et al. (June 2012). “Numerical simulations of barnacle larval dispersion coupled with field observations on larval abundance, settlement and recruitment in a tropical monsoon influenced coastal marine environment”. en. In: *J. Mar. Syst.* 94, pp. 218–231.

Garner, G G et al. (2021). *IPCC AR6 Sea Level Projections*.

Garrard, Samantha L et al. (Apr. 2024). “Identifying potential high-risk zones for land-derived plastic litter to marine megafauna and key habitats within the North Atlantic”. en. In: *Sci. Total Environ.* 922.171282, p. 171282.

Gehrels, W Roland et al. (May 1995). “Modeling the contribution of M2 tidal amplification to the Holocene rise of mean high water in the Gulf of Maine and the Bay of Fundy”. en. In: *Mar. Geol.* 124.1-4, pp. 71–85.

Geuzaine, Christophe and Jean-François Remacle (Sept. 2009). “Gmsh: A 3-D finite element mesh generator with built-in pre- and post-processing facilities: THE GMSH PAPER”. en. In: *Int. J. Numer. Methods Eng.* 79.11, pp. 1309–1331.

Gissi, Elena et al. (Feb. 2021). “A review of the combined effects of climate change and other local human stressors on the marine environment”. en. In: *Sci. Total Environ.* 755.Pt 1, p. 142564.

Gleason, D F and G M Wellington (Oct. 1995). “Variation in UVB sensitivity of planula larvae of the coral Agaricia agaricites along a depth gradient”. In: *Mar. Biol.* 123.4, pp. 693–703.

Gleason, Daniel F and Dietrich K Hofmann (Nov. 2011). “Coral larvae: From gametes to recruits”. In: *J. Exp. Mar. Bio. Ecol.* 408.1, pp. 42–57.

Glynn, Peter W (1984). “Widespread coral mortality and the 1982–83 El Niño warming event”. en. In: *Environ. Conserv.* 11.2, pp. 133–146.

Godin, Gabriel (Jan. 1993). “On tidal resonance”. en. In: *Cont. Shelf Res.* 13.1, pp. 89–107.

Good, Alexandra M and Keisha D Bahr (Mar. 2021). “The coral conservation crisis: interacting local and global stressors reduce reef resiliency and create challenges for conservation solutions”. en. In: *SN Appl. Sci.* 3.3, pp. 1–14.

Gordon, Arnold L and Rana A Fine (Jan. 1996). “Pathways of water between the Pacific and Indian oceans in the Indonesian seas”. en. In: *Nature* 379.6561, pp. 146–149.

Goreau, Thomas J F and Raymond L Hayes (1994). “Coral bleaching and ocean“ hot spots””. In: *Ambio-Journal of Human Environment Research and Management* 23.3, pp. 176–180.

— (June 2021). “Global warming triggers coral reef bleaching tipping point : This article belongs to Ambio’s 50th Anniversary Collection. Theme: Climate change impacts”. en. In: *Ambio* 50.6, pp. 1137–1140.

— (Jan. 2024). “2023 Record marine heat waves: coral reef bleaching HotSpot maps reveal global sea surface temperature extremes, coral mortality, and ocean circulation changes”. en. In: *Oxford Open Climate Change* 4.1, kgae005.

Goss, Z et al. (2019). “Tidal modelling with Thetis: preliminary English Channel benchmarking”. In.

Goss, Z et al. (Aug. 2021). “Efficient economic optimisation of large-scale tidal stream arrays”. en. In: *Appl. Energy* 295.116975, p. 116975.

Gouezo, Marine et al. (Feb. 2019). “Drivers of recovery and reassembly of coral reef communities”. en. In: *Proc. Biol. Sci.* 286.1897, p. 20182908.

Grech, Alana et al. (July 2018). “Predicting the cumulative effect of multiple disturbances on seagrass connectivity”. en. In: *Glob. Chang. Biol.* 24.7, pp. 3093–3104.

Green, Alison L et al. (Nov. 2015). “Larval dispersal and movement patterns of coral reef fishes, and implications for marine reserve network design: Connectivity and marine reserves”. en. In: *Biol. Rev. Camb. Philos. Soc.* 90.4, pp. 1215–1247.

Green, J A M et al. (Aug. 2009). “Tidal mixing and the Meridional Overturning Circulation from the Last Glacial Maximum”. en. In: *Geophysical Research Letters* 36.15.

Green, Johan A M (Oct. 2010). “Ocean tides and resonance”. In: *Ocean Dyn.* 60.5, pp. 1243–1253.

Green, Rebecca H, Ryan J Lowe, and Mark L Buckley (Oct. 2018). “Hydrodynamics of a tidally forced coral reef atoll”. en. In: *J. Geophys. Res. Oceans* 123.10, pp. 7084–7101.

Greenwood, Jim et al. (May 2025). “Passive retention of simulated larvae on coral reefs”. en. In: *R. Soc. Open Sci.* 12.5, p. 241708.

Greiner, Ariel et al. (Dec. 2022). “The combined effects of dispersal and herbivores on stable states in coral reefs”. In: *Theor. Ecol.* 15.4, pp. 321–335.

Griffiths, Stephen D and W Richard Peltier (June 2009). “Modeling of polar ocean tides at the Last Glacial Maximum: Amplification, sensitivity, and climatological implications”. en. In: *J. Clim.* 22.11, pp. 2905–2924.

Grimaldi, Camille M et al. (Oct. 2022). “Hydrodynamic drivers of fine-scale connectivity within a coral reef atoll”. en. In: *Limnol. Oceanogr.* 67.10, pp. 2204–2217.

Grimaldi, Camille M et al. (Dec. 2024). “Local coral connections within an atoll reef system underlie reef resilience and persistence”. en. In: *Limnol. Oceanogr.* 69.12, pp. 3020–3032.

Grottoli, Andréa G, Lisa J Rodrigues, and James E Palardy (Apr. 2006). “Heterotrophic plasticity and resilience in bleached corals”. en. In: *Nature* 440.7088, pp. 1186–1189.

Gurvan, Madec et al. (Oct. 2017). *NEMO ocean engine*. en.

Hagberg, Aric, Pieter J Swart, and Daniel A Schult (Jan. 2008). *Exploring network structure, dynamics, and function using NetworkX*. en. Tech. rep. LA-UR-08-05495; LA-UR-08-5495. Los Alamos National Laboratory (LANL), Los Alamos, NM (United States).

Haigh, Ivan D et al. (Mar. 2020). “The Tides they are A-changin’: A comprehensive review of past and future nonastronomical changes in tides, their driving mechanisms, and future implications”. en. In: *Rev. Geophys.* 58.1, e2018RG000636.

Hammerton, M and E Lawrey (2024). *North Australia Sentinel 2 Satellite Composite Imagery - 15th percentile true colour (NESP MaC 3)*. Vol. 17. AIMS.

Hanert, Emmanuel et al. (Mar. 2023). “A multiscale ocean modelling system for the central Arabian/Persian Gulf: From regional to structure scale circulation patterns”. en. In: *Estuar. Coast. Shelf Sci.* 282.108230, p. 108230.

Harii et al. (July 2002). “Larval survivorship, competency periods and settlement of two brooding corals, Heliopora coerulea and Pocillopora damicornis”. en. In: *Mar. Biol.* 141.1, pp. 39–46.

Harker, Alexander et al. (Feb. 2019). *The impact of sea-level rise on tidal characteristics around Australia*.

Harris, Daniel L, Ana Vila-Concejo, and Jody M Webster (Oct. 2014). “Geomorphology and sediment transport on a submerged back-reef sand apron: One Tree Reef, Great Barrier Reef”. In: *Geomorphology* 222, pp. 132–142.

Harris, Daniel L and Ana Vila-Concejo (2013). “Wave transformation on a coral reef rubble platform”. In: *J. Coast. Res.* 65, pp. 506–510.

Harrison, P L and C Wallace (1990). “Reproduction, dispersal and recruitment of scleractinian corals”. In: *Ecosystems of the world* 25, pp. 133–207.

Harrison, P L et al. (Mar. 1984). “Mass spawning in tropical reef corals”. en. In: *Science* 223.4641, pp. 1186–1189.

Hasson, Audrey et al. (Apr. 2018). “Northward pathway across the tropical north Pacific Ocean revealed by surface salinity: How do El Niño anomalies reach Hawaii?” en. In: *J. Geophys. Res. Oceans* 123.4, pp. 2697–2715.

Hay, Carling C et al. (Jan. 2015). “Probabilistic reanalysis of twentieth-century sea-level rise”. en. In: *Nature* 517.7535, pp. 481–484.

Hays, Graeme C et al. (Nov. 2020). “A review of a decade of lessons from one of the world’s largest MPAs: conservation gains and key challenges”. en. In: *Mar. Biol.* 167.11, pp. 1–22.

Hersbach, H et al. (2023). “ERA5 hourly data on single levels from 1940 to present. Copernicus Climate Change Service (C3S) Climate Data Store (CDS)”. In.

Higgins, Emily, Anna Metaxas, and Robert E Scheibling (Jan. 2022). “A systematic review of artificial reefs as platforms for coral reef research and conservation”. en. In: *PLoS One* 17.1, e0261964.

Highsmith, R (1982). “Reproduction by Fragmentation in Corals”. In: *Marine Ecology Progress Series* 7, pp. 207–226.

Hill, D F et al. (Oct. 2011). “High-resolution numerical modeling of tides in the western Atlantic, Gulf of Mexico, and Caribbean Sea during the Holocene”. en. In: *J. Geophys. Res.* 116.C10.

Hill, Jon et al. (Nov. 2023). “Resolving tsunami wave dynamics: Integrating sedimentology and numerical modelling”. en. In: *Depositional Rec.* 9.4, pp. 1046–1065.

Hinestrosa, Gustavo, Jody M Webster, and Robin J Beaman (Mar. 2016). “Postglacial sediment deposition along a mixed carbonate-siliciclastic margin: New constraints from the drowned shelf-edge reefs of the Great Barrier Reef, Australia”. In: *Palaeogeogr. Palaeoclimatol. Palaeoecol.* 446, pp. 168–185.

Hock, Karlo et al. (Oct. 2014). “Connectivity networks reveal the risks of crown-of-thorns starfish outbreaks on the Great Barrier Reef”. en. In: *J. Appl. Ecol.* 51.5, pp. 1188–1196.

Hock, Karlo et al. (Nov. 2017). “Connectivity and systemic resilience of the Great Barrier Reef”. en. In: *PLoS Biol.* 15.11, e2003355.

Hock, Karlo et al. (Aug. 2019). “Split spawning increases robustness of coral larval supply and inter-reef connectivity”. en. In: *Nat. Commun.* 10.1, p. 3463.

Hoegh-Guldberg, O et al. (Dec. 2007). “Coral reefs under rapid climate change and ocean acidification”. en. In: *Science* 318.5857, pp. 1737–1742.

Hoeksema, Bert W, Giyanto, and Suharsono (Mar. 2019). “The role of maximum shelf depth versus distance from shore in explaining a diversity gradient of mushroom corals (Fungiidae) off Jakarta”. en. In: *Diversity (Basel)* 11.3, p. 46.

Hopley, David (Jan. 2006). “Coral Reef Growth on the Shelf Margin of the Great Barrier Reef with Special Reference to the Pompey Complex”. en. In: *coas* 2006.221, pp. 150–158.

Hopley, David, T L Graham, et al. (1997). “Submerged shelf-edge reefs, coral reefs, great barrier reef australia”. In: *Recent Advances in Marine Science and Technology*.

Hopley, David, Scott G Smithers, and Kevin Parnell (May 2007). *The geomorphology of the Great Barrier Reef: Development, diversity and change*. en. Cambridge, England: Cambridge University Press.

Hori, Nobuyuki (1977). “A morphometrical study on the geographical distribution of coral reefs”. ja. In: *Geographical Reports of Tokyo Metropolitan University* 12, pp. 1–75.

Hu, Dunxin et al. (June 2015). “Pacific western boundary currents and their roles in climate”. en. In: *Nature* 522.7556, pp. 299–308.

Huang, Wen et al. (Dec. 2018). “Genetic diversity and large-scale connectivity of the scleractinian coral Porites lutea in the South China Sea”. en. In: *Coral Reefs* 37.4, pp. 1259–1271.

Hubbard, Dennis K et al. (1991). “The effects of hurricane Hugo on the reefs and associated environments of st. Croix, U.s. virgin Islands?A preliminary assessment”. en. In: *J. Coast. Res.*, pp. 33–48.

Hughes, Terry P et al. (Jan. 1999). “Patterns of recruitment and abundance of corals along the Great Barrier Reef”. en. In: *Nature* 397.6714, pp. 59–63.

Hughes, Terry P et al. (Mar. 2017). “Global warming and recurrent mass bleaching of corals”. en. In: *Nature* 543.7645, pp. 373–377.

Humblet, Marc and Jody M Webster (Apr. 2017). “Coral community changes in the Great Barrier Reef in response to major environmental changes over glacial-interglacial timescales”. In: *Palaeogeogr. Palaeoclimatol. Palaeoecol.* 472, pp. 216–235.

Idier, Déborah et al. (Apr. 2017). “Sea-level rise impacts on the tides of the European Shelf”. In: *Cont. Shelf Res.* 137, pp. 56–71.

Intergovernmental Panel on Climate Change (IPCC) (July 2023). “Ocean, cryosphere and sea level change”. In: *Climate Change 2021 – The Physical Science Basis*. Cambridge University Press, pp. 1211–1362.

Ishida-Castañeda, Jun et al. (Jan. 2020). “Coral reef restoration in the Eastern Tropical Pacific: feasibility of the coral nursery approach: Coral reef restoration: nursery approach”. en. In: *Restor. Ecol.* 28.1, pp. 22–28.

Jackson, J B et al. (July 2001). “Historical overfishing and the recent collapse of coastal ecosystems”. en. In: *Science* 293.5530, pp. 629–637.

Jacobi, Martin Nilsson and Per R Jonsson (July 2011). “Optimal networks of nature reserves can be found through eigenvalue perturbation theory of the connectivity matrix”. en. In: *Ecol. Appl.* 21.5, pp. 1861–1870.

Jiang, Long et al. (July 2015). “Biophysical modeling assessment of the drivers for plankton dynamics in dreissenid-colonized western Lake Erie”. en. In: *Ecol. Modell.* 308, pp. 18–33.

Jiang, Li-Qing et al. (Mar. 2023). “Global surface ocean acidification indicators from 1750 to 2100”. en. In: *J. Adv. Model. Earth Syst.* 15.3, e2022MS003563.

Kärnä, Tuomas et al. (Jan. 2011). “A fully implicit wetting–drying method for DG-FEM shallow water models, with an application to the Scheldt Estuary”. In: *Comput. Methods Appl. Mech. Eng.* 200.5, pp. 509–524.

Kärnä, Tuomas et al. (Oct. 2018). “Thetis coastal ocean model: discontinuous Galerkin discretization for the three-dimensional hydrostatic equations”. en. In: *Geoscientific Model Development* 11.11, pp. 4359–4382.

Keith, Sally A et al. (May 2016). “Coral mass spawning predicted by rapid seasonal rise in ocean temperature”. en. In: *Proc. Biol. Sci.* 283.1830.

Kendrick, Gary A et al. (May 2017). “Demographic and genetic connectivity: the role and consequences of reproduction, dispersal and recruitment in seagrasses: Demographic and genetic connectivity in seagrasses”. en. In: *Biol. Rev. Camb. Philos. Soc.* 92.2, pp. 921–938.

Kennedy, D M and C D Woodroffe (May 2002). “Fringing reef growth and morphology: a review”. In: *Earth-Sci. Rev.* 57.3, pp. 255–277.

Kerry, Colette et al. (Oct. 2016). “Development and evaluation of a high-resolution reanalysis of the East Australian Current region using the Regional Ocean Modelling System (ROMS 3.4) and Incremental Strong-Constraint 4-Dimensional Variational (IS4D-Var) data assimilation”. en. In: *Geosci. Model Dev.* 9.10, pp. 3779–3801.

King, Brian and Eric Wolanski (1992). “Coastal dynamics along a rugged coastline”. In: *Dynamics and Exchanges in Estuaries and the Coastal Zone*. Washington, D. C.: American Geophysical Union, pp. 577–598.

— (Dec. 1996). “Tidal current variability in the Central Great Barrier Reef”. In: *J. Mar. Syst.* 9.3, pp. 187–202.

King, Samantha et al. (Jan. 2023). “Larval dispersal patterns and connectivity of Acropora on Florida’s Coral Reef and its implications for restoration”. en. In: *Front. Mar. Sci.* 9, p. 1038463.

Kingsford, M J, Eric Wolanski, and J H Choat (Feb. 1991). “Influence of tidally induced fronts and Langmuir circulations on distribution and movements of presettlement fishes around a coral reef”. In: *Mar. Biol.* 109.1, pp. 167–180.

Kleypas, J A (Sept. 1996). “Coral reef development under naturally turbid conditions: fringing reefs near Broad Sound, Australia”. en. In: *Coral Reefs* 15.3, pp. 153–167.

Kleypas, Joan A, John W Mcmanus, and Lambert A B Meñez (Feb. 1999). “Environmental limits to coral reef development: Where do we draw the line?” en. In: *Am. Zool.* 39.1, pp. 146–159.

Kool, Johnathan T et al. (Sept. 2011). “Connectivity and the development of population genetic structure in Indo-West Pacific coral reef communities”. en. In: *Glob. Ecol. Biogeogr.* 20.5, pp. 695–706.

Kopp, Robert E et al. (Dec. 2023). “The Framework for Assessing Changes To Sea-level (FACTS) v1.0: a platform for characterizing parametric and structural uncertainty in future global, relative, and extreme sea-level change”. en. In: *Geosci. Model Dev.* 16.24, pp. 7461–7489.

Kriegler, Elmar et al. (Feb. 2014). “A new scenario framework for climate change research: the concept of shared climate policy assumptions”. en. In: *Clim. Change* 122.3, pp. 401–414.

Kyvelou, Pinelopi, Craig Buchanan, and Leroy Gardner (Sept. 2022). “Numerical modelling of the world’s first metal 3D printed bridge”. en. In: *Ce/pap.* 5.4, pp. 59–66.

Ladd, Harry S (2012). “Types of coral reefs and their distribution”. In: *Biology and geology of coral reefs* 4.

Lambrechts, Jonathan et al. (Aug. 2008). “A multi-scale model of the hydrodynamics of the whole Great Barrier Reef”. In: *Estuar. Coast. Shelf Sci.* 79.1, pp. 143–151.

Lange, Michael and Erik van Sebille (Nov. 2017). “Parcels v0.9: prototyping a Lagrangian ocean analysis framework for the petascale age”. en. In: *Geosci. Model Dev.* 10.11, pp. 4175–4186.

Larcombe, P et al. (Sept. 1995). “Factors controlling suspended sediment on inner-shelf coral reefs, Townsville, Australia”. In: *Coral Reefs* 14.3, pp. 163–171.

Large, W G and S G Yeager (Aug. 2009). “The global climatology of an interannually varying air–sea flux data set”. In: *Clim. Dyn.* 33.2, pp. 341–364.

Largier, John L (Feb. 2003). “Considerations in estimating larval dispersal distances from oceanographic data”. en. In: *Ecological Applications* 13.sp1, pp. 71–89.

Larson, Silva et al. (Apr. 2015). “The role the Great Barrier Reef plays in resident wellbeing and implications for its management”. en. In: *Ambio* 44.3, pp. 166–177.

Le, Hoang-Anh et al. (Feb. 2020). “Suspended sediment properties in the Lower Mekong River, from fluvial to estuarine environments”. en. In: *Estuar. Coast. Shelf Sci.* 233.106522, p. 106522.

Lee, Jungeon et al. (Feb. 2021). “Review on quality control methods in metal additive manufacturing”. en. In: *Appl. Sci. (Basel)* 11.4, p. 1966.

Lee, Katherine C et al. (Dec. 2022). “Tidal dynamics drive ooid formation in the Capricorn Channel since the Last Glacial Maximum”. en. In: *Mar. Geol.* 454.106944, p. 106944.

Lesser, G R et al. (Oct. 2004). “Development and validation of a three-dimensional morphological model”. en. In: *Coast. Eng.* 51.8-9, pp. 883–915.

Lesser, Michael P (Dec. 2021). “Eutrophication on coral reefs: What is the evidence for phase shifts, nutrient limitation and coral bleaching”. en. In: *Bioscience* 71.12, pp. 1216–1233.

Lester, S E et al. (May 2009). “Biological effects within no-take marine reserves: a global synthesis”. In: *Mar. Ecol. Prog. Ser.* 384, pp. 33–46.

Lewis, Stephen E et al. (Aug. 2013). “Post-glacial sea-level changes around the Australian margin: a review”. en. In: *Quat. Sci. Rev.* 74, pp. 115–138.

Li, Li et al. (June 2012). “Numerical study of the effects of mangrove areas and tidal flats on tides: A case study of Darwin Harbour, Australia”. en. In: *Journal of Geophysical Research: Oceans* 117.C6.

Li, Yanfang et al. (Mar. 2016). “Influence of rising sea level on tidal dynamics in the Bohai sea”. en. In: *J. Coast. Res.* 74.74 (10074), pp. 22–31.

Li, Yanfang et al. (Dec. 2018). “Trapping of plastics in semi-enclosed seas: Insights from the Bohai Sea, China”. en. In: *Mar. Pollut. Bull.* 137, pp. 509–517.

Limer, Benjamin D, Jeanne Bloomberg, and Daniel M Holstein (May 2020). “The influence of eddies on coral larval retention in the flower garden banks”. In: *Front. Mar. Sci.* 7.

Lin, Yucheng (2019). *Closing the Last Deglacial Global Sea Level Budget by different antarctic deglaciation models*.

Lin, Yucheng et al. (Apr. 2023). “Relative sea level response to mixed carbonate-siliciclastic sediment loading along the Great Barrier Reef margin”. In: *Earth Planet. Sci. Lett.* 607, p. 118066.

Liu, Dongfang, David P Callaghan, and Tom E Baldock (May 2025). “Quantifying the impact of future climate change on the risk of coral rubble instability across the Great Barrier Reef by 2100”. en. In: *J. Environ. Manage.* 386.125716, p. 125716.

Liu, Hongguang et al. (June 2022). “The state of the art for numerical simulations of the effect of the microstructure and its evolution in the metal-cutting processes”. en. In: *Int. J. Mach. Tools Manuf.* 177.103890, p. 103890.

Lowe, Ryan Joseph et al. (Aug. 2016). “Rising sea levels will reduce extreme temperature variations in tide-dominated reef habitats”. en. In: *Sci. Adv.* 2.8, e1600825.

Lu, Jiaying et al. (Mar. 2023). “Larval dispersal modeling reveals low connectivity among national marine protected areas in the Yellow and East China Seas”. en. In: *Biology (Basel)* 12.3, p. 396.

Lyard, Florent et al. (Dec. 2006). “Modelling the global ocean tides: modern insights from FES2004”. In: *Ocean Dyn.* 56.5, pp. 394–415.

M. Lopes, Antonio and Jose Tenreiro Machado (July 2017). “Tidal analysis using time–frequency signal processing and information clustering”. en. In: *Entropy (Basel)* 19.8, p. 390.

Mace, A J and S G Morgan (Aug. 2006). “Larval accumulation in the lee of a small headland: implications for the design of marine reserves”. In: *Mar. Ecol. Prog. Ser.* 318, pp. 19–29.

Macintyre, Ian G (Apr. 1972). “Submerged reefs of eastern Caribbean”. en. In: *Am. Assoc. Pet. Geol. Bull.* 56.4, pp. 720–738.

Mackie, Lucas et al. (Nov. 2021). “Assessing impacts of tidal power lagoons of a consistent design”. en. In: *Ocean Eng.* 240.109879, p. 109879.

Madin, Joshua S et al. (Aug. 2014). “Mechanical vulnerability explains size-dependent mortality of reef corals”. en. In: *Ecol. Lett.* 17.8, pp. 1008–1015.

Mansui, J, A Molcard, and Y Ourmières (Feb. 2015). “Modelling the transport and accumulation of floating marine debris in the Mediterranean basin”. en. In: *Mar. Pollut. Bull.* 91.1, pp. 249–257.

Mao, Yadan and John L Luick (Mar. 2014). “Circulation in the southern Great Barrier Reef studied through an integration of multiple remote sensing and in situ measurements”. en. In: *J. Geophys. Res. Oceans* 119.3, pp. 1621–1643.

Maragos, James E and Gareth J Williams (2011). “Pacific coral reefs: an introduction”. In: *Encyclopedia of Modern Coral Reefs. Springer: New York, NY*, pp. 753–776.

Marcos, Concepción et al. (June 2021). “Reviewing the ecosystem services, societal goods, and benefits of marine protected areas”. en. In: *Front. Mar. Sci.* 8, p. 613819.

Marsaleix, P, F Auclair, and C Estournel (Nov. 2006). “Considerations on open boundary conditions for regional and coastal ocean models”. en. In: *J. Atmos. Ocean. Technol.* 23.11, pp. 1604–1613.

Marshall, John F and P J Davies (June 1982). “Internal structure and Holocene evolution of One Tree Reef, southern Great Barrier Reef”. en. In: *Coral Reefs* 1.1, pp. 21–28.

Marshall, John F and Peter J Davies (Mar. 1988). “Halimeda bioherms of the northern Great Barrier Reef”. en. In: *Coral Reefs* 6.3-4, pp. 139–148.

Marshall, John F and B G Thom (Sept. 1976). “The sea level in the last interglacial”. en. In: *Nature* 263.5573, pp. 120–121.

Marshall, N A et al. (Nov. 2016). “Advances in monitoring the human dimension of natural resource systems: an example from the Great Barrier Reef”. en. In: *Environ. Res. Lett.* 11.11, p. 114020.

Marshall, Nadine et al. (June 2018). “Measuring what matters in the Great Barrier Reef”. en. In: *Front. Ecol. Environ.* 16.5, pp. 271–277.

Marshall, Nadine A et al. (Nov. 2017). “The dependency of people on the great barrier reef, Australia”. en. In: *Coast. Manage.* 45.6, pp. 505–518.

Mascia, Michael B, C Anne Claus, and Robin Naidoo (Oct. 2010). “Impacts of marine protected areas on fishing communities: MPA social impacts”. en. In: *Conserv. Biol.* 24.5, pp. 1424–1429.

Masselink, Gerd, Eddie Beetham, and Paul Kench (June 2020). “Coral reef islands can accrete vertically in response to sea level rise”. en. In: *Sci. Adv.* 6.24, eaay3656.

Matemilola, Saheed, Oluwaseun Fadeyi, and Timothy Sijuade (2023). “Paris Agreement”. en. In: *Encyclopedia of Sustainable Management*. Cham: Springer International Publishing, pp. 2555–2559.

Mawson, Eleanor E, Katherine C Lee, and Jon Hill (Aug. 2022). “Sea level rise and the Great Barrier Reef the future implications on reef tidal dynamics”. en. In: *J. Geophys. Res. C: Oceans*, e2021JC017823.

Maxwell, W G H and Jonathan P Swinchatt (Mar. 1970). “Great Barrier Reef: Regional Variation in a Terrigenous-Carbonate Province”. In: *GSA Bulletin* 81.3, pp. 691–724.

Mayorga-Adame, C Gabriela, Harold P Batchelder, and Yvette H Spitz (2017). “Modeling Larval Connectivity of Coral Reef Organisms in the Kenya-Tanzania Region”. In: *Frontiers in Marine Science* 4.

McCabe, R M et al. (Dec. 2010). “Temperature variability in a shallow, tidally isolated coral reef lagoon”. en. In: *Journal of Geophysical Research: Oceans* 115.C12.

McCormick, Mark I (June 2003). “Consumption of coral propagules after mass spawning enhances larval quality of damselfish through maternal effects”. en. In: *Oecologia* 136.1, pp. 37–45.

McCulloch, Malcolm T et al. (Feb. 2024). “300 years of sclerosponge thermometry shows global warming has exceeded 1.5 °C”. en. In: *Nat. Clim. Chang.* 14.2, pp. 171–177.

McWhorter, Jennifer K et al. (Oct. 2022a). “Climate refugia on the Great Barrier Reef fail when global warming exceeds 3°C”. en. In: *Glob. Chang. Biol.* 28.19, pp. 5768–5780.

McWhorter, Jennifer K et al. (Feb. 2022b). “The importance of 1.5°C warming for the Great Barrier Reef”. en. In: *Glob. Chang. Biol.* 28.4, pp. 1332–1341.

McWhorter, Jennifer K et al. (Apr. 2024). “Climate change impacts on mesophotic regions of the Great Barrier Reef”. en. In: *Proc. Natl. Acad. Sci. U. S. A.* 121.16, e2303336121.

Mellin, Camille et al. (June 2024). “Cumulative risk of future bleaching for the world’s coral reefs”. en. In: *Sci. Adv.* 10.26, eadn9660.

Mengel, Matthias et al. (Feb. 2018). “Committed sea-level rise under the Paris Agreement and the legacy of delayed mitigation action”. en. In: *Nat. Commun.* 9.1, p. 601.

Miller, K and C Mundy (July 2003). “Rapid settlement in broadcast spawning corals: implications for larval dispersal”. In: *Coral Reefs* 22.2, pp. 99–106.

Milne, Russell, Chris T Bauch, and Madhur Anand (Feb. 2022). “Local overfishing patterns have regional effects on health of coral, and economic transitions can promote its recovery”. en. In: *Bull. Math. Biol.* 84.4, p. 46.

Mirdan, Mohamed et al. (Aug. 2024). “Modeling coastal morphological features in proximity to breakwaters using delft 3D”. en. In: *J. Marit. Res.* 21.2, pp. 196–203.

Molen, J van der, J Gerrits, and H E de Swart (Mar. 2004). “Modelling the morphodynamics of a tidal shelf sea”. en. In: *Cont. Shelf Res.* 24.4-5, pp. 483–507.

Montaggioni, Lucien F et al. (June 1997). “Continuous record of reef growth over the past 14 k.y. on the mid-Pacific island of Tahiti”. In: *Geology* 25.6, pp. 555–558.

Mulà, Clelia et al. (May 2025). “Restoration cannot be scaled up globally to save reefs from loss and degradation”. en. In: *Nat. Ecol. Evol.* 9.5, pp. 822–832.

Müller, M (Sept. 2012). “The influence of changing stratification conditions on barotropic tidal transport and its implications for seasonal and secular changes of tides”. en. In: *Cont. Shelf Res.* 47, pp. 107–118.

Müller, M, B K Arbic, and J X Mitrovica (May 2011). “Secular trends in ocean tides: Observations and model results”. en. In: *J. Geophys. Res.* 116.C5.

Mumby, Peter J, Alan Hastings, and Helen J Edwards (Nov. 2007). “Thresholds and the resilience of Caribbean coral reefs”. en. In: *Nature* 450.7166, pp. 98–101.

Mumby, Peter J et al. (May 2007). “Trophic cascade facilitates coral recruitment in a marine reserve”. en. In: *Proc. Natl. Acad. Sci. U. S. A.* 104.20, pp. 8362–8367.

Munday, P L et al. (June 2009). “Climate change and coral reef connectivity”. In: *Coral Reefs* 28.2, pp. 379–395.

Nakamura, T, H Yamasaki, and R van Woesik (July 2003). “Water flow facilitates recovery from bleaching in the coral Stylophora pistillata”. In: *Mar. Ecol. Prog. Ser.* 256, pp. 287–291.

Newman, William A (Nov. 2017). “Origin of the Hawaiian marine fauna: Dispersal and vicariance as indicated by barnacles and other organisms”. In: *Crustacean Biogeography*. 1st Edition. Routledge, pp. 21–49.

Nunn, Brook L et al. (Mar. 2025). “Protein signatures predict coral resilience and survival to thermal bleaching events”. en. In: *Commun. Earth Environ.* 6.1, pp. 1–17.

O'Neill, Brian C et al. (Feb. 2014). "A new scenario framework for climate change research: the concept of shared socioeconomic pathways". en. In: *Clim. Change* 122.3, pp. 387–400.

O'Neill, Brian C et al. (Jan. 2017). "The roads ahead: Narratives for shared socioeconomic pathways describing world futures in the 21st century". en. In: *Glob. Environ. Change* 42, pp. 169–180.

Ogston, Andrea S and Michael E Field (Nov. 2010). "Predictions of turbidity due to enhanced sediment resuspension resulting from sea-level rise on a fringing coral reef: Evidence from Molokai, Hawaii". en. In: *J. Coast. Res.* 26.6, pp. 1027–1037.

Oksanen, Jari et al. (July 2019). "vegan: Community Ecology Package. R package version 2.5-6". In: 9, p. 12489.

Oliver, J K and B L Willis (Dec. 1987). "Coral-spawn slicks in the Great Barrier Reef: preliminary observations". In: *Mar. Biol.* 94.4, pp. 521–529.

Page, Charlotte E et al. (July 2019). "Seeking resistance in coral reef ecosystems: The interplay of biophysical factors and bleaching resistance under a changing climate: The interplay of a reef's biophysical factors can mitigate the coral bleaching response: The interplay of a reef's biophysical factors can mitigate the coral bleaching response". en. In: *Bioessays* 41.7, e1800226.

Page, Charlotte E et al. (June 2021). "High flow conditions mediate damaging impacts of sub-lethal thermal stress on corals' endosymbiotic algae". en. In: *Conserv. Physiol.* 9.1, coab046.

Page, Michael C and Gerald R Dickens (July 2005). "Sediment fluxes to Marion Plateau (southern Great Barrier Reef province) over the last 130 ky: New constraints on 'transgressive-shedding' off northeastern Australia". en. In: *Mar. Geol.* 219.1, pp. 27–45.

Palmer, Karen, Christopher Watson, and Andrew Fischer (Sept. 2019). "Non-linear interactions between sea-level rise, tides, and geomorphic change in the Tamar Estuary, Australia". en. In: *Estuar. Coast. Shelf Sci.* 225.106247, p. 106247.

Pandolfi, John M et al. (July 2011). “Projecting coral reef futures under global warming and ocean acidification”. en. In: *Science* 333.6041, pp. 418–422.

Paris, Claire B et al. (Apr. 2013). “Connectivity Modeling System: A probabilistic modeling tool for the multi-scale tracking of biotic and abiotic variability in the ocean”. In: *Environmental Modelling & Software* 42, pp. 47–54.

Pascolo, Sara, Marco Petti, and Silvia Bosa (Sept. 2018). “On the wave bottom shear stress in shallow depths: The role of wave period and bed roughness”. en. In: *Water (Basel)* 10.10, p. 1348.

Pedersen, Thomas Lin (2024). *ggraph: An Implementation of Grammar of Graphics for Graphs and Networks*.

Peeters, Michael J (Jan. 2016). “Practical significance: Moving beyond statistical significance”. en. In: *Curr. Pharm. Teach. Learn.* 8.1, pp. 83–89.

Pelasula, Daniel D et al. (Feb. 2023). “Key success factors and problems in coral transplantation: A review”. en. In: 16.1, pp. 1–24.

Pelling, Holly E and J A Mattias Green (June 2013). “Sea level rise and tidal power plants in the Gulf of Maine: SLR and TPP in the Gulf of Maine”. en. In: *J. Geophys. Res. Oceans* 118.6, pp. 2863–2873.

Peltier, W R, D F Argus, and R Drummond (Jan. 2015). “Space geodesy constrains ice age terminal deglaciation: The global ICE-6G_C (VM5a) model”. en. In: *J. Geophys. Res. Solid Earth* 120.1, pp. 450–487.

Pennisi, Elizabeth (Feb. 2005). “South Asia tsunami. Powerful tsunami’s impact on coral reefs was hit and miss”. en. In: *Science* 307.5710, p. 657.

Perris, Lachlan et al. (Aug. 2024). “The influence of coral reef spur and groove morphology on wave energy dissipation in contrasting reef environments”. en. In: *J. Geophys. Res. Earth Surf.* 129.8, e2023JF007424.

Piggott, M D et al. (Mar. 2008). “A new computational framework for multi-scale ocean modelling based on adapting unstructured meshes”. In: *Int. J. Numer. Methods Fluids* 56.8, pp. 1003–1015.

Piniak, Gregory A and Curt D Storlazzi (Mar. 2008). “Diurnal variability in turbidity and coral fluorescence on a fringing reef flat: Southern Molokai, Hawaii”. en. In: *Estuar. Coast. Shelf Sci.* 77.1, pp. 56–64.

Power, Scott B and Greg Kociuba (Nov. 2011). “The impact of global warming on the Southern Oscillation Index”. en. In: *Clim. Dyn.* 37.9-10, pp. 1745–1754.

Prandle, D (Jan. 1997). “Tidal currents in shelf seas—their nature and impacts”. en. In: *Prog. Oceanogr.* 40.1-4, pp. 245–261.

Pratchett, Morgan S et al. (Sept. 2014). “Limits to understanding and managing outbreaks of crown- of- thorns starfish (Acanthaster spp.)” In: *Oceanography and Marine Biology*. Oceanography and Marine Biology: An Annual Review. CRC Press, pp. 133–200.

Priya, A et al. (Dec. 2023). “Impact of climate change and anthropogenic activities on aquatic ecosystem - A review”. en. In: *Environ. Res.* 238.Pt 2, p. 117233.

Pugh, D and P L Woodworth (2014). “Sea-level science: understanding tides, surges, tsunamis and mean sea-level changes”. In.

Raitsos, Dionysios E et al. (Aug. 2017). “Sensing coral reef connectivity pathways from space”. en. In: *Sci. Rep.* 7.1, p. 9338.

Ramak, Hossein, Maryam SoyufJahromi, and Parasto Akbari (Jan. 2023). “Investigation of salinity and temperature of Persian Gulf water by FVCOM Model”. en. In: *Journal of Oceanography* 13.52, pp. 106–120.

Randall, Carly J et al. (Jan. 2024). “Larval precompetency and settlement behaviour in 25 Indo-Pacific coral species”. en. In: *Commun. Biol.* 7.1, p. 142.

Rappaz, Michel, Michel Bellet, and Michel Deville (2010). “The Finite Element Method”. en. In: *Numerical Modeling in Materials Science and Engineering*. Springer series in computational mathematics. Berlin, Heidelberg: Springer Berlin Heidelberg, pp. 93–147.

Rasheed, Shuaib et al. (Feb. 2021). “Response of tidal flow regime and sediment transport in North Malé Atoll, Maldives, to coastal modification and sea level rise”. en. In: *Ocean Sci.* 17.1, pp. 319–334.

Reguero, Borja G et al. (Jan. 2018). “Coral reefs for coastal protection: A new methodological approach and engineering case study in Grenada”. en. In: *J. Environ. Manage.* 210, pp. 146–161.

Riahi, Keywan et al. (Jan. 2017). “The Shared Socioeconomic Pathways and their energy, land use, and greenhouse gas emissions implications: An overview”. en. In: *Glob. Environ. Change* 42, pp. 153–168.

Richards, Lara Shania et al. (Oct. 2024). “The meteorological drivers of mass coral bleaching on the central Great Barrier Reef during the 2022 La Niña”. en. In: *Sci. Rep.* 14.1, p. 23867.

Richmond, R H (Jan. 1987). “Energetics, competency, and long-distance dispersal of planula larvae of the coral Pocillopora damicornis”. en. In: *Mar. Biol.* 93.4, pp. 527–533.

— (Jan. 1990). “The effects of the El Niño/southern oscillation on the dispersal of corals and other marine organisms”. In: *Global Ecological Consequences of the 1982–83 El Nino—SouthernOscillation*. Vol. 52. Elsevier oceanography series. Elsevier, pp. 127–140.

— (1997). “Reproduction and recruitment in corals”. In: *Life and death of coral reefs*.

Ridgway, K R and J R Dunn (Feb. 2003). “Mesoscale structure of the mean East Australian Current System and its relationship with topography”. en. In: *Prog. Oceanogr.* 56.2, pp. 189–222.

Riegl, B (Dec. 2003). “Climate change and coral reefs: different effects in two high-latitude areas (Arabian Gulf, South Africa)”. en. In: *Coral Reefs* 22.4, pp. 433–446.

Rinkevich, Baruch (June 2005). “Conservation of coral reefs through active restoration measures: recent approaches and last decade progress”. en. In: *Environ. Sci. Technol.* 39.12, pp. 4333–4342.

Roberts, Callum M (1997). “Connectivity and Management of Caribbean Coral Reefs”. In: *Science* 278.5342, pp. 1454–1457.

Roberts, Kelsey E et al. (Apr. 2021). “Assessing the current state of ecological connectivity in a large marine protected area system”. en. In: *Conserv. Biol.* 35.2, pp. 699–710.

Robins, Peter E et al. (Mar. 2013). “Physical and biological controls on larval dispersal and connectivity in a highly energetic shelf sea”. en. In: *Limnol. Oceanogr.* 58.2, pp. 505–524.

Rodrigues, N et al. (Aug. 2021). “Cost-benefit analysis of tidal energy production in a coastal lagoon: The case of Ria Formosa – Portugal”. In: *Energy* 229, p. 120812.

Rodrigues, Regina R et al. (Mar. 2025). “The severe 2020 coral bleaching event in the tropical Atlantic linked to marine heatwaves”. en. In: *Commun. Earth Environ.* 6.1, pp. 1–9.

Rodriguez-Ruano, Victor et al. (Feb. 2023). “Upwelling, climate change, and the shifting geography of coral reef development”. en. In: *Sci. Rep.* 13.1, p. 1770.

Roff, George et al. (Aug. 2015). “Phase shift facilitation following cyclone disturbance on coral reefs”. en. In: *Oecologia* 178.4, pp. 1193–1203.

Rogers, Caroline S, Thomas H Suchanek, and Frank A Pecora (Apr. 1982). “Effects of hurricanes David and Frederic (1979) on shallow Acropora palmata reef communities: St. Croix, U.s. virgin Islands”. In: *Bull. Mar. Sci.*

Rogers, Justin S et al. (Feb. 2017). “A coupled wave-hydrodynamic model of an atoll with high friction: Mechanisms for flow, connectivity, and ecological implications”. In: *Ocean Model.* 110, pp. 66–82.

Rolfe, John and Jeremy De Valck (Aug. 2021). “Values for protecting the Great Barrier Reef: A review and synthesis of studies over the past 35 years”. en. In: *Mar. Pollut. Bull.* 169.112531, p. 112531.

Romero-Torres, Mauricio et al. (June 2018). “The Eastern Tropical Pacific coral population connectivity and the role of the Eastern Pacific Barrier”. en. In: *Sci. Rep.* 8.1, p. 9354.

Rose, Linta, Rohith, and Prasad K Bhaskaran (Dec. 2022). “Amplification of regional tides in response to sea level”. en. In: *Ocean Eng.* 266.112691, p. 112691.

Ruckelshaus, Mary et al. (Jan. 2008). “Marine Ecosystem-based Management in Practice: Scientific and Governance Challenges”. en. In: *BioScience* 58.1, pp. 53–63.

Ryan, E J et al. (Sept. 2016). “The influence of sea level and cyclones on Holocene reef flat development: Middle Island, central Great Barrier Reef”. In: *Coral Reefs* 35.3, pp. 805–818.

Ryan, Emma J et al. (Oct. 2018). “The Variable Influences of Sea Level, Sedimentation and Exposure on Holocene Reef Development over a Cross-Shelf Transect, Central Great Barrier Reef”. en. In: *Diversity* 10.4, p. 110.

Sadourny, Robert (Apr. 1975). “The dynamics of finite-difference models of the Shallow-Water equations”. en. In: *J. Atmos. Sci.* 32.4, pp. 680–689.

Saila, S B, Vlj Kocic, and J W McManus (Nov. 1993). “Modelling the effects of destructive fishing practices on tropical coral reefs”. en. In: *Oceanogr. Lit. Rev.* 94.1, pp. 51–60.

Saint-Amand, Antoine et al. (Dec. 2023). “How fine is fine enough? Effect of mesh resolution on hydrodynamic simulations in coral reef environments”. en. In: *Ocean Model. (Oxf.)* 186.102254, p. 102254.

Salas-Saavedra, Marcos et al. (Aug. 2022). “Holocene microbialite geochemistry records > 6000 years of secular influence of terrigenous flux on water quality for the southern Great Barrier Reef”. en. In: *Chem. Geol.* 604.120871, p. 120871.

Salles, Tristan et al. (Mar. 2018). “A unified framework for modelling sediment fate from source to sink and its interactions with reef systems over geological times”. en. In: *Sci. Rep.* 8.1, p. 5252.

Sammarco, Paul W (Jan. 1980). “Diadema and its relationship to coral spat mortality: Grazing, competition, and biological disturbance”. In: *J. Exp. Mar. Bio. Ecol.* 45.2, pp. 245–272.

— (1994). “Larval dispersal and recruitment processes in great barrier reef corals: Analysis and synthesis”. en. In: *Coastal and Estuarine Studies*. Washington, D. C.: American Geophysical Union, pp. 35–72.

Sammarco, Paul W and J C Andrews (Mar. 1988). “Localized dispersal and recruitment in great barrier reef corals: the helix experiment”. en. In: *Science* 239.4846, pp. 1422–1424.

Sanborn, Kelsey L et al. (Nov. 2019). “A new model of Holocene reef initiation and growth in response to sea-level rise on the Southern Great Barrier Reef”. In: *Sediment. Geol.*, p. 105556.

Sanborn, Kelsey L et al. (May 2024). “The impact of elevated nutrients on the Holocene evolution of the Great Barrier Reef”. en. In: *Quat. Sci. Rev.* 332.108636, p. 108636.

Sandin, Stuart A et al. (Nov. 2022). “Evidence of biological self-organization in spatial patterns of a common tropical alga”. en. In: *Am. Nat.* 200.5, pp. 722–729.

Schill, Steven R et al. (Dec. 2015). “No Reef Is an Island: Integrating Coral Reef Connectivity Data into the Design of Regional-Scale Marine Protected Area Networks”. en. In: *PLoS One* 10.12, e0144199.

Schindelegger, M et al. (July 2018). “Can we model the effect of observed sea level rise on tides?” en. In: *J. Geophys. Res. Oceans* 123.7, pp. 4593–4609.

Schlaefer, Jodie A et al. (2018). “Wind Conditions on the Great Barrier Reef Influenced the Recruitment of Snapper (Lutjanus carponotatus)”. In: *Frontiers in Marine Science* 5.

Schröder, Andreas and Daniel Schanz (Jan. 2023). “3D Lagrangian particle tracking in Fluid Mechanics”. en. In: *Annu. Rev. Fluid Mech.* 55.1, pp. 511–540.

Scott, David B and David A Greenberg (Oct. 1983). “Relative sea-level rise and tidal development in the Fundy tidal system”. en. In: *Can. J. Earth Sci.* 20.10, pp. 1554–1564.

Sebens, K P and A S Johnson (Nov. 1991). “Effects of water movement on prey capture and distribution of reef corals”. en. In: *Hydrobiologia* 226.2, pp. 91–101.

Sebens, K P et al. (May 1998). “Water flow and prey capture by three scleractinian corals, Madracis mirabilis , Montastrea cavernosa and Porites porites , in a field enclosure”. en. In: *Mar. Biol.* 131.2, pp. 347–360.

Sebens, K P et al. (Apr. 2003). “Effects of water flow on growth and energetics of the scleractinian coral Agaricia tenuifolia in Belize”. en. In: *Coral Reefs* 22.1, pp. 35–47.

Seifi, Fardin, Xiaoli Deng, and Ole Andersen (Sept. 2019). “UoNGBR: A Regional Assimilation Barotropic Tidal Model for the Great Barrier Reef and Coral Sea Based on Satellite, Coastal and Marine Data”. en. In: *Remote Sensing* 11.19, p. 2234.

Seo, Hyodae et al. (Apr. 2023). “Ocean mesoscale and frontal-scale ocean–atmosphere interactions and influence on large-scale climate: A review”. en. In: *J. Clim.* 36.7, pp. 1981–2013.

Shafir, Shai, Jaap Van Rijn, and Baruch Rinkevich (June 2006). “Steps in the construction of underwater coral nursery, an essential component in reef restoration acts”. en. In: *Mar. Biol.* 149.3, pp. 679–687.

Sharrocks, Patrick D and Jon Hill (Apr. 2024). “Evaluating the impact of the Storegga tsunami on Mesolithic communities in Northumberland”. en. In: *J. Quat. Sci.* 39.3, pp. 473–487.

Shi, Fengyan et al. (Jan. 2017). “High-resolution non-hydrostatic modeling of frontal features in the mouth of the Columbia river”. In: *Estuaries Coast.* 40.1, pp. 296–309.

Simmons, Joshua A et al. (July 2017). “Calibrating and assessing uncertainty in coastal numerical models”. en. In: *Coast. Eng.* 125, pp. 28–41.

Simpson, J H and J Sharples (2012). “Introduction to the physical and biological oceanography of shelf seas”. In.

Sloss, Craig R, Colin V Murray-Wallace, and Brian G Jones (Nov. 2007). “Holocene sea-level change on the southeast coast of Australia: a review”. en. In: *Holocene* 17.7, pp. 999–1014.

Soong, K and T Chen (2003). “Coral Transplantation: Regeneration and Growth of Acropora Fragments in a Nursery”. In: *Restor. Ecol.*

Stake, Joel L and Paul W Sammarco (Apr. 2003). “Effects of pressure on swimming behavior in planula larvae of the coral Porites astreoides (Cnidaria, Scleractinia)”. In: *J. Exp. Mar. Bio. Ecol.* 288.2, pp. 181–201.

Stammer, Detlef (Apr. 1998). “On eddy characteristics, eddy transports, and mean flow properties”. en. In: *J. Phys. Oceanogr.* 28.4, pp. 727–739.

Stanford, J D et al. (Dec. 2011). “Sea-level probability for the last deglaciation: A statistical analysis of far-field records”. en. In: *Glob. Planet. Change* 79.3-4, pp. 193–203.

Steinberg, Craig (2007). “Impacts of climate change on the physical oceanography of the Great Barrier Reef”. In.

Stoeckl, Natalie et al. (Dec. 2014). “A new approach to the problem of overlapping values: A case study in Australia?s Great Barrier Reef”. en. In: *Ecosyst. Serv.* 10, pp. 61–78.

Storlazzi, C D et al. (June 2011). “Numerical modeling of the impact of sea-level rise on fringing coral reef hydrodynamics and sediment transport”. en. In: *Coral Reefs* 30.S1, pp. 83–96.

Stumpf, R P and J W Haines (Feb. 1998). “Variations in tidal level in the gulf of Mexico and implications for tidal wetlands”. en. In: *Estuar. Coast. Shelf Sci.* 46.2, pp. 165–173.

Sun, Ruohan, Xinyi Kang, and Meng Xia (Dec. 2024). “The roles of nutrient loading and river discharge on the phytoplankton dynamics in the semi-enclosed sea”. en. In: *J. Geophys. Res. Oceans* 129.12, e2024JC021466.

Suryawan, I Wayan Koko et al. (Mar. 2025). “Importance-performance evaluation of coral reef conservation in advancing the bioeconomy of marine tourism in Bali, Indonesia”. en. In: *Aquat. Conserv.* 35.3, e70085.

Swart, Huib E de and Bing Yuan (Oct. 2019). “Dynamics of offshore tidal sand ridges, a review”. en. In: *Environ. Fluid Mech. (Dordr.)* 19.5, pp. 1047–1071.

Taebi, Soheila et al. (Feb. 2011). “Nearshore circulation in a tropical fringing reef system”. In: *J. Geophys. Res.* 116.C2, p. 40.

Takano, Yohei et al. (Nov. 2023). “Simulations of ocean deoxygenation in the historical era: insights from forced and coupled models”. en. In: *Front. Mar. Sci.* 10, p. 1139917.

Tartinville, B, E Deleersnijder, and J Rancher (July 1997). “The water residence time in the Mururoa atoll lagoon: sensitivity analysis of a three-dimensional model”. en. In: *Coral Reefs* 16.3, pp. 193–203.

Thomas, Christopher J et al. (Jan. 2014). “Numerical modelling and graph theory tools to study ecological connectivity in the Great Barrier Reef”. In: *Ecol. Modell.* 272, pp. 160–174.

Thomas, Christopher J et al. (Oct. 2015). “Connectivity between submerged and near-sea-surface coral reefs: can submerged reef populations act as refuges?” en. In: *Divers. Distrib.* 21.10, pp. 1254–1266.

Thompson, D M et al. (July 2018). “Variability in oceanographic barriers to coral larval dispersal: Do currents shape biodiversity?” In: *Prog. Oceanogr.* 165, pp. 110–122.

Thomson, Richard E and William J Emery (2014). “Time Series Analysis Methods”. en. In: *Data Analysis Methods in Physical Oceanography*. Elsevier, pp. 425–591.

Thorrold, S et al. (Jan. 2002). “Quantifying larval retention and connectivity in marine populations with artificial and natural markers”. In: *Bulletin of Marine Science* 70.1, pp. 291–308.

Toomey, Michael, Andrew D Ashton, and J Taylor Perron (July 2013). “Profiles of ocean island coral reefs controlled by sea-level history and carbonate accumulation rates”. In: *Geology* 41.7, pp. 731–734.

Traag, V A, P Van Dooren, and Y Nesterov (July 2011). “Narrow scope for resolution-limit-free community detection”. en. In: *Phys. Rev. E Stat. Nonlin. Soft Matter Phys.* 84.1 Pt 2, p. 016114.

Traag, V A, L Waltman, and N J van Eck (Mar. 2019). “From Louvain to Leiden: guaranteeing well-connected communities”. en. In: *Sci. Rep.* 9.1, p. 5233.

Uehara, Katsuto et al. (Sept. 2006). “Tidal evolution of the northwest European shelf seas from the Last Glacial Maximum to the present”. en. In: *Journal of Geophysical Research: Oceans* 111.C9.

Underwood, J N et al. (Feb. 2007). “Multiple scales of genetic connectivity in a brooding coral on isolated reefs following catastrophic bleaching: GENETIC CONNECTIVITY IN A BROODING CORAL”. en. In: *Mol. Ecol.* 16.4, pp. 771–784.

Valderrama Ballesteros, Laura, Jennifer L Matthews, and Bert W Hoeksema (Oct. 2018). “Pollution and coral damage caused by derelict fishing gear on coral reefs around Koh Tao, Gulf of Thailand”. en. In: *Mar. Pollut. Bull.* 135, pp. 1107–1116.

Valentine, John F and Kenneth L Heck Jr (June 2005). “Perspective review of the impacts of overfishing on coral reef food web linkages”. en. In: *Coral Reefs* 24.2, pp. 209–213.

Van Dongeren, Ap et al. (Mar. 2013). “Numerical modeling of low-frequency wave dynamics over a fringing coral reef”. In: *Coast. Eng.* 73, pp. 178–190.

Verhofstede, Alex et al. (Nov. 2023). “Seychelles Plateau’s oil spill vulnerability”. en. In: *Mar. Pollut. Bull.* 196.115652, p. 115652.

Vermeer, Martin and Stefan Rahmstorf (Dec. 2009). “Global sea level linked to global temperature”. en. In: *Proc. Natl. Acad. Sci. U. S. A.* 106.51, pp. 21527–21532.

Vermeij, Mark J A et al. (May 2010). “Coral larvae move toward reef sounds”. en. In: *PLoS One* 5.5, e10660.

Viehman, T S et al. (Oct. 2018). “Understanding differential patterns in coral reef recovery: chronic hydrodynamic disturbance as a limiting mechanism for coral colonization”. en. In: *Mar. Ecol. Prog. Ser.* 605, pp. 135–150.

Vila-Concejo, Ana et al. (Jan. 2013). “Coral reef sediment dynamics: evidence of sand-apron evolution on a daily and decadal scale”. In: *J. Coast. Res.*, pp. 606–611.

Vincent, David et al. (Oct. 2019). “Normal modes and resonance in Ontario Lacus: a hydrocarbon lake of Titan”. en. In: *Ocean Dyn.* 69.10, pp. 1121–1132.

Vogt-Vincent, N S and S Mitarai (July 2020). “A persistent kuroshio in the glacial east China sea and implications for coral paleobiogeography”. en. In: *Paleoceanogr. Paleoclimatology* 35.7.

Vogt-Vincent, Noam S, Satoshi Mitarai, and Helen L Johnson (Dec. 2023). “High-frequency variability dominates potential connectivity between remote coral reefs”. en. In: *Limnol. Oceanogr.* 68.12, pp. 2733–2748.

Vogt-Vincent, Noam S et al. (June 2024). “Coral reef potential connectivity in the southwest Indian Ocean”. In: *Coral Reefs*.

Von Prahl, H and A Mejía (1985). “Primer informe de un coral acropórido, Acropora valida (Dana, 1984)(Scleractina: Astrocoeniida: Acroporidae) para el Pacífico americano”. In: *Revista de Biología Tropical* 33.1, pp. 39–43.

Vuuren, Detlef P van et al. (Feb. 2014). “A new scenario framework for Climate Change Research: scenario matrix architecture”. en. In: *Clim. Change* 122.3, pp. 373–386.

Wallwork, Joseph G et al. (Apr. 2022). “Goal-oriented error estimation and mesh adaptation for tracer transport modelling”. en. In: *Comput. Aided Des.* 145.103187, p. 103187.

Wallwork, Joseph G et al. (Feb. 2024). “Tidal turbine array modelling using goal-oriented mesh adaptation”. en. In: *J. Ocean Eng. Mar. Energy* 10.1, pp. 193–216.

Wang, Guihua et al. (Nov. 2022). “Ocean currents show global intensification of weak tropical cyclones”. en. In: *Nature* 611.7936, pp. 496–500.

Ward, Sophie L et al. (Nov. 2016). “Sensitivity of palaeotidal models of the northwest European shelf seas to glacial isostatic adjustment since the Last Glacial Maximum”. In: *Quat. Sci. Rev.* 151, pp. 198–211.

Warder, Simon C, Kevin J Horsburgh, and Matthew D Piggott (Apr. 2021). “Adjoint-based sensitivity analysis for a numerical storm surge model”. en. In: *Ocean Model. (Oxf.)* 160.101766, p. 101766.

Warner, Patricia A, Bette L Willis, and Madeleine J H van Oppen (Mar. 2016). “Sperm dispersal distances estimated by parentage analysis in a brooding scleractinian coral”. en. In: *Mol. Ecol.* 25.6, pp. 1398–1415.

Weaver, Andrew J and E S Sarachik (Sept. 1991). “The role of mixed boundary conditions in numerical models of the ocean’s climate”. en. In: *J. Phys. Oceanogr.* 21.9, pp. 1470–1493.

Webster, Jody M and Peter J Davies (June 2003). “Coral variation in two deep drill cores: significance for the Pleistocene development of the Great Barrier Reef”. In: *Sediment. Geol.* 159.1, pp. 61–80.

Webster, Jody M et al. (May 2018). “Response of the Great Barrier Reef to sea-level and environmental changes over the past 30,000 years”. en. In: *Nat. Geosci.* 11.6, pp. 426–432.

Weeks, S J et al. (Dec. 2010). “The Capricorn Eddy: a prominent driver of the ecology and future of the southern Great Barrier Reef”. In: *Coral Reefs* 29.4, pp. 975–985.

Wildermann, Natalie et al. (May 2017). “Does behaviour affect the dispersal of flatback post-hatchlings in the Great Barrier Reef?” en. In: *R. Soc. Open Sci.* 4.5, p. 170164.

Williams, D Mcb, Eric Wolanski, and J C Andrews (1984). “Transport mechanisms and the potential movement of planktonic larvae in the central region of the Great Barrier Reef”. In: *Coral Reefs* 3.4, pp. 229–236.

Williams, Gareth J (May 2025). “Protecting existing coral reefs must be our priority”. en. In: *Nat. Ecol. Evol.* 9.5, pp. 754–755.

Williamson, David H et al. (Dec. 2016). “Large-scale, multidirectional larval connectivity among coral reef fish populations in the Great Barrier Reef Marine Park”. en. In: *Mol. Ecol.* 25.24, pp. 6039–6054.

Willis, B L and J K Oliver (Jan. 1988). “Inter-reef dispersal of coral larvae following the annual mass spawning on the Great Barrier Reef”. In: *Illumina Biological Content - unstructured*.

Willis, B L and J K Oliver (Oct. 1990). “Direct tracking of coral larvae: Implications for dispersal studies of planktonic larvae in topographically complex environments”. In: *Ophelia* 32.1-2, pp. 145–162.

Willis, B L et al. (1985). “Patterns in the mass spawning of corals on the Great Barrier Reef from 1981 to 1984”. In: Proceedings of the Fifth International Coral Reef Congress. Moorea, French Polynesia: Antenne Museum-EPHE, p. 6.

Wilmes, S-B and J A M Green (July 2014). “The evolution of tides and tidal dissipation over the past 21,000 years”. en. In: *J. Geophys. Res. Oceans* 119.7, pp. 4083–4100.

Wilmes, S-B et al. (Nov. 2023). “Late Pleistocene evolution of tides and tidal dissipation”. en. In: *Paleoceanogr. Paleoclimatology* 38.11, e2023PA004727.

Wilson, N A J Graham, and N V C Polunin (May 2007). “Appraisal of visual assessments of habitat complexity and benthic composition on coral reefs”. en. In: *Mar. Biol.* 151.3, pp. 1069–1076.

Wilson, J R and P L Harrison (May 1998). “Settlement-competency periods of larvae of three species of scleractinian corals”. en. In: *Mar. Biol.* 131.2, pp. 339–345.

Wilson, Shaun K et al. (Feb. 2018). “Climatic forcing and larval dispersal capabilities shape the replenishment of fishes and their habitat-forming biota on a tropical coral reef”. en. In: *Ecol. Evol.* 8.3, pp. 1918–1928.

Woesik, R van (Mar. 2010). “Calm before the spawn: global coral spawning patterns are explained by regional wind fields”. en. In: *Proc. Biol. Sci.* 277.1682, pp. 715–722.

Woesik, R van and T J Done (June 1997). “Coral communities and reef growth in the southern Great Barrier Reef”. en. In: *Coral Reefs* 16.2, pp. 103–115.

Woesik, R van et al. (July 2011). “Revisiting the winners and the losers a decade after coral bleaching”. en. In: *Mar. Ecol. Prog. Ser.* 434, pp. 67–76.

Woesik, R van et al. (July 2022). “Coral-bleaching responses to climate change across biological scales”. en. In: *Glob. Chang. Biol.* 28.14, pp. 4229–4250.

Wolanski, Eric (1983). “Tides on the Northern Great Barrier Reef Continental Shelf”. In: *J. Geophys. Res.* Res. Pap. 88.C10, p. 5953.

— (Jan. 1994). *Physical Oceanographic Processes of the Great Barrier Reef*. en. CRC Press.

Wolanski, Eric, Derek Burrage, and Brian King (May 1989). “Trapping and dispersion of coral eggs around Bowden Reef, Great Barrier Reef, following mass coral spawning”. In: *Cont. Shelf Res.* 9.5, pp. 479–496.

Wolanski, Eric, Peter Doherty, and John Carleton (June 1997). “Directional swimming of fish larvae determines connectivity of fish populations on the great barrier reef”. In: *Sci. Nat.* 84.6, pp. 262–268.

Wolanski, Eric and G L Pickard (Apr. 1985). “Long-term observations of currents on the central Great Barrier Reef continental shelf”. In: *Coral Reefs* 4.1, pp. 47–57.

Wolanski, Eric and S Spangnol (2000). “Sticky Waters in the Great Barrier Reef”. In: *Esturine, Coastal and Shelf Science* 50, pp. 27–32.

Wolanski, Eric et al. (Feb. 1988). “Tidal jets, nutrient upwelling and their influence on the productivity of the alga Halimeda in the Ribbon Reefs, Great Barrier Reef”. In: *Estuar. Coast. Shelf Sci.* 26.2, pp. 169–201.

Wolanski, Eric et al. (July 2017). “The Gulf of Carpentaria heated Torres Strait and the Northern Great Barrier Reef during the 2016 mass coral bleaching event”. In: *Estuar. Coast. Shelf Sci.* 194, pp. 172–181.

Wolanski, Eric et al. (Oct. 2024a). “Mechanisms enabling the self-recruitment of passive larvae in the Great Barrier Reef”. en. In: *Estuar. Coast. Shelf Sci.* 309.108976, p. 108976.

Wolanski, Eric et al. (Jan. 2024b). “The physical oceanography of the great barrier reef:” en. In: *Oceanographic Processes of Coral Reefs*. Boca Raton: CRC Press, pp. 9–34.

Wood, S et al. (Jan. 2014). “Modelling dispersal and connectivity of broadcast spawning corals at the global scale”. en. In: *Glob. Ecol. Biogeogr.* 23.1, pp. 1–11.

Woodley, J D et al. (Nov. 1981). “Hurricane allen’s impact on Jamaican coral reefs”. en. In: *Science* 214.4522, pp. 749–755.

Woodroffe, C and Naomi Biribo (2011). “Atolls”. In: *Encyclopedia of Modern Coral Reefs*. Encyclopedia of earth sciences. Dordrecht: Springer Netherlands, pp. 51–71.

Woodroffe, C D and Jody M Webster (2013). “Coral Reefs and Sea-Level Change”. In: *Mar. Geol.* 0.

Woodroffe, Sarah A et al. (Nov. 2023). “On the varied impact of the Storegga tsunami in northwest Scotland”. en. In: *J. Quat. Sci.* 38.8, pp. 1219–1232.

Woodworth, P L (Sept. 2010). “A survey of recent changes in the main components of the ocean tide”. en. In: *Cont. Shelf Res.* 30.15, pp. 1680–1691.

Yang, Chen et al. (May 2023). “Accelerating the Lagrangian particle tracking in hydrologic modeling to continental-scale”. en. In: *J. Adv. Model. Earth Syst.* 15.5, e2022MS003507.

Yokoyama, Yusuke et al. (Aug. 2006). “Sea-level during the early deglaciation period in the Great Barrier Reef, Australia”. In: *Glob. Planet. Change* 53.1, pp. 147–153.

Yokoyama, Yusuke et al. (Sept. 2011). “IODP expedition 325: The great barrier reefs reveal past sea-level, climate and environmental changes since the last ice age”. en. In: *Sci. Drill.* 12.12, September 2011, pp. 32–45.

Yokoyama, Yusuke et al. (July 2018). “Rapid glaciation and a two-step sea level plunge into the Last Glacial Maximum”. en. In: *Nature* 559.7715, pp. 603–607.

Zahel, Wilfried (2005). “Ocean tides”. en. In: *Tidal Phenomena*. Berlin/Heidelberg: Springer-Verlag, pp. 113–143.

Zalesky, Andrew, Alex Fornito, and Ed Bullmore (May 2012). “On the use of correlation as a measure of network connectivity”. en. In: *Neuroimage* 60.4, pp. 2096–2106.

Zhang, Can et al. (Dec. 2022). “Improving tidal turbine array performance through the optimisation of layout and yaw angles”. en. In: *Int. J. Mar. Ene.* 5.3, pp. 273–280.

Zou, Qingping, Anthony J Bowen, and Alex E Hay (Sept. 2006). “Vertical distribution of wave shear stress in variable water depth: Theory and field observations”. en. In: *Journal of Geophysical Research: Oceans* 111.C9.